Heterophase triblock copolymer networks

Michael Jeschke

Heterophase Triblock Copolymer Networks

September 1997

Michael Jeschke

Department of Chemistry

University of Durham

Supervisor

Professor R.W. Richards

University of Durham

A thesis submitted to the University of Durham in partial fulfilment of the regulations for the Degree of Doctor of Philosophy

Heterophase Triblock Copolymer Networks

Michael Jeschke
PhD Thesis September 1997

Abstract

The investigation of morphological properties of linear triblock copolymers in the strong segregation limit has received much experimental and theoretical interest. Butadiene - Styrene - Butadiene (B-S-B) triblock copolymers have been compared to analogous cross-linked varieties using the techniques of small angle x-ray scattering (SAXS), solid state ^{1}H NMR and stress-strain analysis.

The properties being sought are; the dimensions of domains, the type of packing within copolymer systems, polystyrene : polybutadiene composition, and the mechanical properties of network systems. The evaluation of structural changes in the networks whilst the copolymer is continuously stretched is an important section of the project. A comparison of annealed and unannealed samples has been studied in each case.

A comprehensive description of network mechanical properties has been accomplished by performing numerous force-elongation experiments on the materials. Parameters for the chemical cross-link density, physical entanglements, and network looseness have been extracted from force-elongation data using the Ball-Edwards slip-link model. The Mooney-Rivlin model and swelling data from the network systems have served as comparisons to the Ball-Edwards model.

Details of the structural organisation in these systems have been determined using SAXS. The uncross-linked materials have been compared to the analogous networks and show that structural differences are present due to the effect of cross-linking altering the equilibrium structure. It has been demonstrated that stretching the network systems at room temperature induces variations in the domain distances from affine deformation.

Domain distances have been determined for a set of lamellar morphology uncross-linked copolymers using solid-state ^{1}H NMR experiments. The results obtained show a good agreement to SAXS data and theoretical predictions.

Acknowledgements

I would like to thank the following people, without them, the last three years would not have been as productive as it has turned out to be. Firstly, my indebted thanks goes to Randal, without whom I would have not been able to complete my thesis, especially for his patience with my 'Cumbrian' English. Secondly, the people who have contributed towards helping me with my research throughout the last three years, Dr Nick Terril, Dr John Pople, Dr Phil Klein, Dr Alan Kenwright, Tom Kiff, Terry the computer fixer, Gordon and Ray (The Glass Blowers), Neil in the mechanical workshop, Lian Hutchings and Donald Davison for their time and patience by proof reading chapters of my thesis, and finally everyone in the IRC for the daily craic. Not to mention Hazel, Jean and Sandra for keeping the cups of tea rolling and the constant flow of bad jokes.

My family deserve all the thanks I can possibly give for supporting me throughout the good and the bad times, as well as working for myself I want to say that I have done this for them too. Mum, Dad and Gerald, thank you, you've been great, I love you all.

All the lads from Penrith deserve a mention, Bell, Dave B, Tim Bolly, Richie Leighton, Richie Weiss, Archer Jnr., Eggie, Deallo, Mikie Ware, thanks, you've given me support when I've needed it, the constant encouragement has been invaluable. I can't miss out the fact that the fantastic Carlisle United have taken me to Wembley Stadium this year, the victory was much appreciated, cheers lads.

I'd like to mention my friends in Norge who have visited me or put me up when I have visited Oslo. Thanks loads to Knut the partyman, Kent (Mr Chelsea), Rolf (the sailor) and Harry (the hunter), Ketil and Jan (the footie blokes), and finally to Linda and Lisa for their support, love and friendship over the last three years, I can't thank you enough you've helped me so much. You've all played a part and I'd like to thank you for that.

Lastly, the lads in Durham who have been great company over the past three years when talking about music, football, etc... in the pub, thanks to Paddy for his hospitality, Donny, Runner, Lian, Maccam, Townsy, Steve Hamil, Rich Ainsworth, Foggy, Robin, Andy, Gavin, Reptile, Wee man, Bradford Steve, Mark Roden, Simon Lord, Bob Spink, and the normal people at Hatfield college who didn't go to public school.

Declaration

The work reported in this thesis has been carried out at the Interdisciplinary Research Centre (IRC) in Polymer Science and Technology, Department of Chemistry, Durham University, Department of Physics, Leeds University, and at CLRC Daresbury Laboratory, Warrington between October 1994 and September 1997. This work has not been submitted for any other degree in Durham or elsewhere and, unless otherwise, is the original work of the author.

Statement of Copyright

Financial Support

The provision of an award from the Engineering and Physical Science Research Council (EPSRC) and the IRC in Polymer Science and Technology to support this work is gratefully acknowledged.

Contents

CHAPTER 1

Introduction

1.1 Project Objectives

Block copolymers are materials that have found uses in many commercial applications including to homogenise homopolymer mixtures and to impart increased toughness to engineering polymers. The major feature of their solid state organisation is the formation of microphase separated structures in which domains rich in one component are formed. These domains have a regular structure and moreover are organised on lattices that possess a degree of long-range order. The original materials that displayed this behaviour were block copolymers of polystyrene with either polybutadiene or polyisoprene[1,2,3].

At temperatures up to 373K, the domains formed from the minor component are spherical, cylindrical or lamellar depending on the composition of the block copolymer. The domain size and separation being determined by the molecular weight of the domain forming block and the total molecular weight of the block copolymer. An equilibrium thermodynamic theory of such copolymers in the strong segregation limit was proposed by Helfand[4,5] and many of the predictions have been confirmed using small angle x-ray scattering (SAXS) – sections 1.2-1.3 of this Chapter. At higher temperatures, above 373K or in the presence of solvent, the long-range ordering is destroyed and in the weak segregation limit a disordered structure prevails which can be described by the random phase approximation[6] (section 1.2).

This work covered has now been extended to cross-linked networks prepared from polybutadiene-polystyrene-polybutadiene (B-S-B) triblock copolymers. To obtain equilibrium microphase separated organisation requires mass transport of copolymer to take place within the specimen as phase separation takes place. One way of achieving this is to anneal the samples for 1-2 weeks under high vacuum at 393K. However, by

introducing cross-links the mass transport is hindered, and if the cross-link density is sufficiently high it may be prevented altogether. Reports from the literature have shown that networks cross-linked in the homogeneous state with a variety of cross-link densities possess morphologies that were cross-link density dependent[7]. Consequently in this project, pseudo morphologies may be formed that possess novel mechanical properties.

Triblock copolymers are prepared by anionic polymerisation techniques to give 'living' polybutadiene ends. These are cross-linked by the addition of a tetraethoxysilane to generate networks with tetrafunctional cross-links. The molecular weight and composition of the precursor triblock copolymer is closely controlled by anionic polymerisation methods. These addition polymerisations have received much attention, the counterion and the solvent being important with respect to anionic systems[8,9]. Living polymerisations exist in aprotic solvents. However, they are killed by water, oxygen and a vast number of electrophilic substances. If all impurities that are liable to react with carbanions are excluded from the system then propagation continues until all the monomer has been consumed, leaving the carbanion intact, and still alive with the concentration of active centres remaining constant during the polymerisation process.

The propagating species are anionic ion pairs and free ions with relative concentrations that depend on the reaction media. The rate of the polymerisation process is a pseudo first order process, and therefore the propagation involves consecutive addition of monomeric units to reactive centres. After each addition cycle a new reactive centre is regenerated at the end of the growing molecule. Propagation ceases when all the monomer is consumed.

The mechanism of propagation is based on the metal used in the initiator being strongly electropositive with respect to the carbon atom giving a carbanion at the end of the growing chain. The metal is cationic in the free state, or it can couple with the carbanion. If a group 1 metal is used for this purpose spontaneous termination is avoided, lithium is a common example. The desired molecular weight of the polymer is determined by calculating the ratio of monomer mass to initiator concentration. Termination occurs through transfer of a proton (or positive fragment) from an excess of terminating agent, usually a protic solvent such as MeOH. Anionic polymerisations possess positive reaction enthalpy values so therefore room temperature polymerisation will proceed rapidly and no external heat need be added to the system. The synthesis of the networks in this project will be explained in detail in Chapter 2 of the thesis.

Mechanical properties of the networks have been evaluated by performing stress-strain experiments on the materials. The analysis is focused on the evaluation of structural changes in such networks whilst the copolymer is continuously stretched, using the Ball-Edwards slip-link model (section 1.3 of this Chapter). Experiments are performed at temperatures where both constituents of the block copolymer are above their glass transition temperature so that the networks studied are elastomeric – Chapters 2 and 3 of the thesis.

Morphological properties have been studied using SAXS and solid state ^{1}H NMR techniques. The SAXS has been carried out in Durham using a Kratky camera, and at the Daresbury synchrotron radiation source (SRS) – Chapters 2, 4 and 5 of the thesis.

A discussion of the experimental results covering a summary and project conclusions follows in Chapter 6 of the thesis along with possible future work.

1.2 Block Copolymer Thermodynamics of Microphase Separation

1.2.1 Introduction theory

At equilibrium, monodisperse block copolymer chains will arrange themselves in minimum free energy conformations[10]. Contacts between block sections at the interface of different domains will be reduced if the temperature is reduced, which in turn increases the interaction parameter (χ) between the phases of copolymer, inducing phase separation. Further ordering can be achieved if the overall degree of polymerisation, N is sufficiently large, inducing some loss of translational and configurational entropy. Figure 1.2a shows this effect.

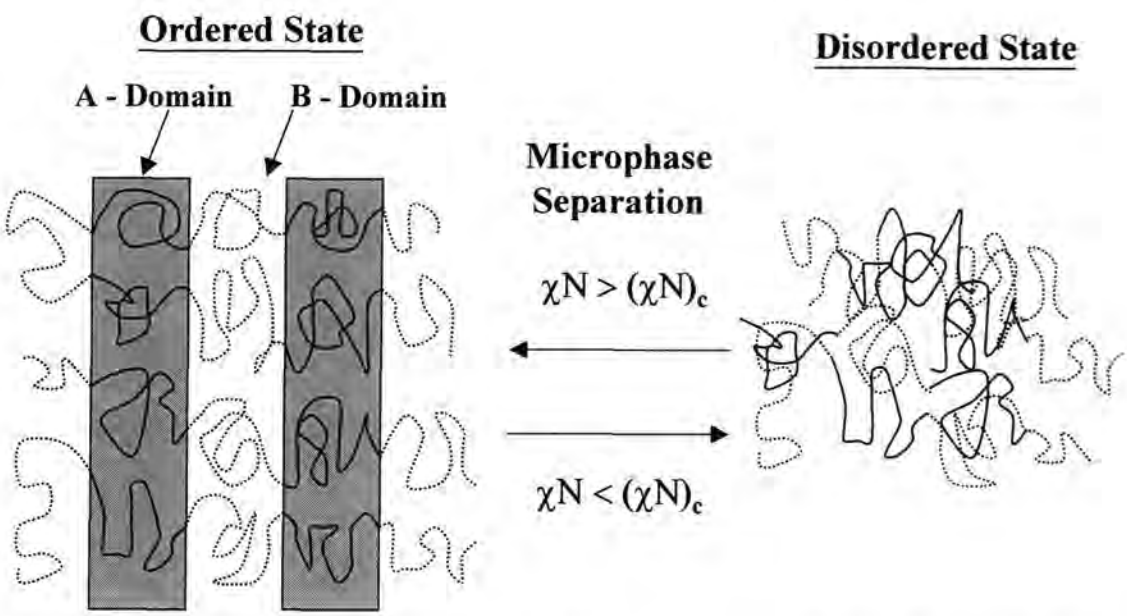

Figure 1.2a Order/disorder in a symmetric block copolymer with lamellar morphology

The term microphase separation is used to describe this effect. If either χ or N is lowered enough, the entropic factors will dominate leading to mixing (disordering) in the system. The parameters χ and N describe the enthalpic and entropic contributions to the free energy density scale, therefore χN dictates the phase state of the block

copolymer. For a composition, f = 0.5 (overall volume fraction of the A-component in an A-B block copolymer), the transition occurs when $\chi N \approx 10.5$. For $\chi N \leq 1.0$ a copolymer melt is disordered, the A-B interactions are sufficiently weak that the individual chain statistics are unchanged (i.e. Gaussian). As χN is increased and approaches 10.5 a delicate balance between energetic and entropic factors produces a disorder to order phase transition. Around this transition the A-B interactions are sufficiently weak that individual copolymers remain largely unchanged and the order composition profile is approximately sinusoidal, this is referred to as the weak segregation limit (WSL).

When $\chi N \geq 10.5$ then a second limiting regime of phase behaviour is used, the strong segregation limit (SSL). Narrow interfaces separate well developed (nearly pure) A and B microdomains. The interaction energy is localised in these interfacial regimes, where the system wants to minimise the total area of such interfaces, but must do under the opposing constraints of incompressibility of the interfacial region, and the entropic penalty of extended chain configurations (i.e. non-Gaussian). The order to disorder transition region is treated as the weak segregation limit, anything more ordered i.e. $\chi N > 10.5$ is treated as the strong segregation limit. In order to carry out experiments over the order-disorder transition (ODT), copolymers of this type are often dissolved in a neutral solvent so as to dilute the A-B contacts. The concentrated solutions behave like the bulk materials but χ is replaced with an effective interaction parameter that is proportional to the copolymer concentration. Bulk materials are difficult to study at this level due to the limited range of χN at experimentally accessible temperatures. A comprehensive review of the strong/weak segregation limits and the ODT, has been carried out by Fredrickson and Bates[10,11].

1.2.2 The Strong Segregation Limit

Originally, five ordered phases appeared in the strong segregation limit, two types of spherical and cylindrical microstructures, and a lamellar morphology. More recently new morphologies have been discovered and are shown in figure 1.2b.

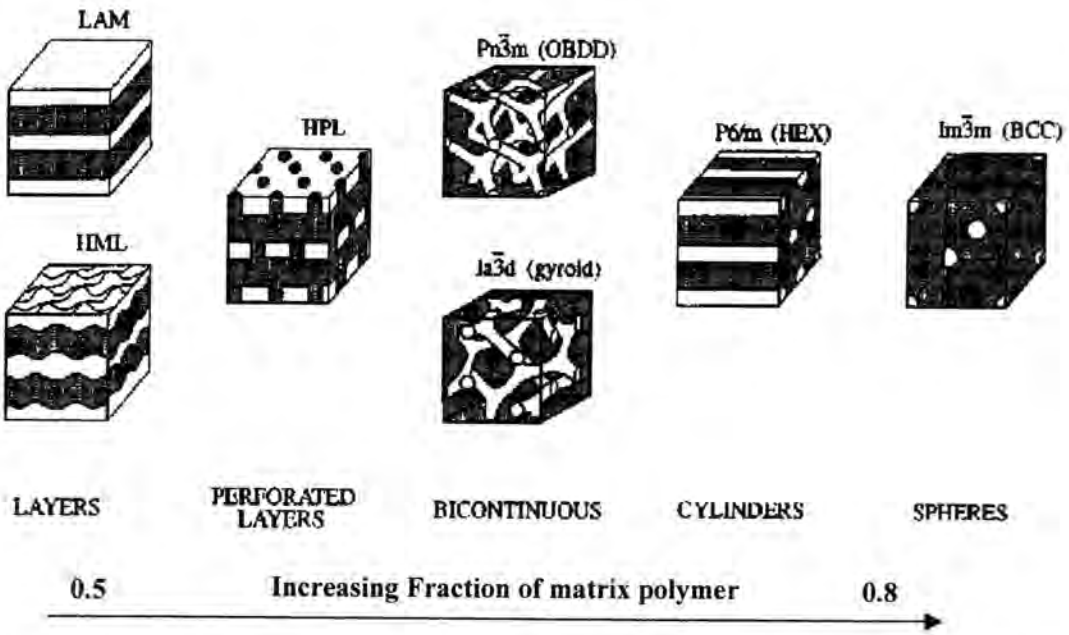

Figure 1.2b Block copolymer morphologies grouped according to microstructure[12]

Phase notation is as follows: Lam = lamellae; HML = hexagonally modulated lamellae; HPL = hexagonally perforated layers; Pn3m (OBDD) = cubic bicontinuous network formed by tetrapod connectors with indicated space group symmetry (also referred to as ordered bicontinuous double diamond); Ia3d (gyroid) = cubic bicontinuous network formed by planar tripod connectors with indicated space group symmetry (also referred to as the 'gyroid' structure); P6/m (HEX) = hexagonally packed cylinders with indicated space group symmetry (commonly denoted HEX); and Im3m (BCC) = body centred cubic packed spheres.

A summary of the three 'classical' morphologies (lamellar, cylindrical and spherical) is given as follows.

Lamellar morphologies are associated with compositionally symmetric block copolymers and are typically found over compositions between 0.4-0.6. As with all the microstructures, increasing molecular weight increases the domain size and spacing. As the composition is increased (or decreased) from the symmetric case, certain lamellar systems become modulated with in-plane hexagonal order, this morphology is referred to as hexagonally modulated lamellae (HML). The HML and lamellar phases are topologically similar.

Cylindrical morphologies along with lamellae and spheres represent one of the 'classical' morphologies. The structure occurs over a relatively wide range of compositions, typically $0.20 \leq f \leq 0.35$ and $0.65 \leq f \leq 0.80$, for essentially all architectures. The cylinders pack in a hexagonal array (P6/m space group).

Spherical morphologies occur at the highest ($f \geq 0.80$) and lowest ($f \leq 0.20$) compositions in the ordered region of the block copolymer phase diagram. The spheres have been found to order on a body centred cubic (BCC) lattice (Im3m space group) in the melt state.

The phases have well defined composition ranges in close agreement with Helfands theory[4,5]. Recent advances over the last 30 years has shown the use of small angle X-ray or Neutron scattering (SAXS or SANS) with the technique of transmission electron microscopy (TEM) as useful techniques for the investigation of block copolymer morphology. Factors such as microdomain size and packing, interfacial mixing and interfacial thickness between microphases can be experimentally measured. Hashimoto *et al*[13,14,15] have matched data to theoretical predictions by Helfand and Wasserman. Studies by Bates *et al*[16] show similar conclusions to Hashimoto. Whilst Roe *et al*[17]

found these factors for PS-PB block copolymer systems over a range of temperatures whilst analysing the domain boundary thickness. Helfand and Wasserman proposed a self-consistent field theory[18] that enables the prediction of many calculations with respect to the strong segregation limit, including free energies, composition profiles and chain conformations. The free energy is calculated from contributions due to the contact enthalpy in the narrow interfaces between the microdomains and the continuous phase of the copolymer. The entropy loss associated with stretching free energy (extended chain conformations) and confinement entropy due to the block copolymer joints at the interface of the microdomain also contributes to the free energy expression.

Numerical techniques for calculating the phase diagram in the SSL were also found to be in good agreement with experimental data already put forward to locate the thermodynamic stability of spheres, cylinders and lamellae. Other work devoted to the calculation of the free energy at the asymptotic limit (χN approaching infinity) was carried out by Semenov *et al*[19] on diblock copolymer melts. In this regime, the block copolymer is in its most probable configuration in the microdomain, and is only legitimate under conditions of strong chain stretching. Inspite of significant chain deformations predicted for the SSL, the domain contribution to the free energy per chain was found in this model to have the same scaling as for a Gaussian chain. In this limit the domain free energy is balanced by the interfacial energy and is asymptotically correct for large incompatibility.

A further strong segregation limit theory was proposed by Ohta and Kawasaki[20] which was field theoretic that used a single scalar field describing the composition patterns. A random phase approximation[6] describes the free energy functional that is only valid for very weak compositional inhomogineities, whilst the SSL is characterised by a volume

fraction of 1.0. Predictions for domain periods and the phase diagram were shown to be able to reduce the calculation of the microdomain energies to a geometric problem.

1.2.3 The Weak Segregation Limit

Bulk block copolymers are brought into the weak segregation limit by decreasing either χ or N. This is done by adding modest amounts of neutral solvent (≤60%) to polystyrene-polydiene materials or increasing the temperature, in order to decrease the order-disorder transition. It was found that there are two regimes in the concentration (C) dependence of domain spacing (d)[13]. Firstly, in the low concentration regime (< 70 wt % polymer), d increases with increasing C. Secondly, in the high concentration regime (> 70 wt % polymer), d tends to decrease with increasing C, consistent with results reported by Skoulios *et al*[21] and Gallot *et al*[22].

Within the WSL the most significant feature is the ODT. A single glass transition is indicative of disorder in a block copolymer system, whilst two separate glass transitions signal microphase separation, i.e. order. The ODT is placed between these two conditions, as well as the WSL. SAXS is a very powerful and important experimental method for investigating the WSL in block copolymer systems. Polystyrene-polydiene systems generally exhibit a sizeable electron density difference between components that provides good X-ray contrast. Roe *et al*[17] illustrated that using SAXS, there exists a broad temperature peak from a polystyrene-polybutadiene diblock copolymer above the ODT temperature. Concluding that a decreasing temperature in the disordered state led to an increase in the peak scattering intensity. Near the ODT the ordered and disordered states differ primarily in the extent of coherence of composition order, this is apparent in direct images of block copolymer where $f > 0.5$.

Developments in the WSL were strongly influenced by a theory developed by Leibler[23], he considered the case of a monodisperse polystyrene-polyisoprene diblock copolymer melt with a degree of polymerisation, N, composition, f, with equal monomer volumes and segment lengths. The findings provide microscopic expressions for the expansion coefficients as functions of the incompatibility, χN and the composition. From work by Bates *et al* a map of the phase diagram of a diblock copolymer melt near the ODT can be drawn, and is shown in figure 1.2c.

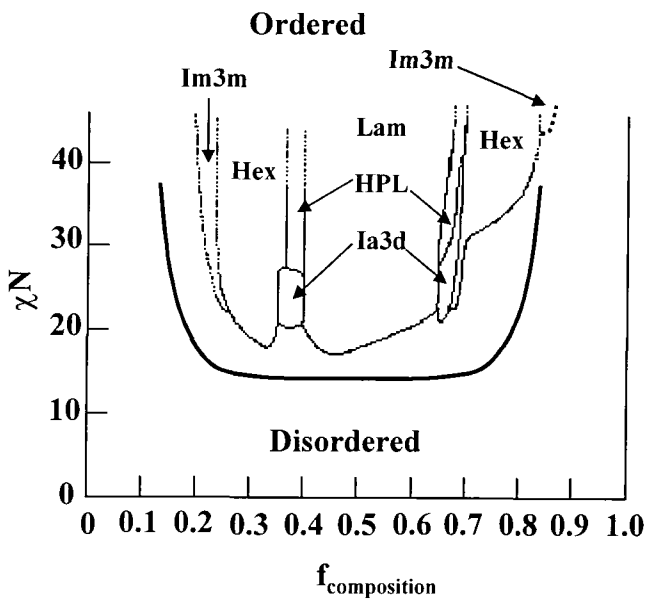

Figure 1.2c Phase behaviour of PS-PI diblock copolymer melts near the order-disorder transition. Microstructures of the copolymers are illustrated in figure 1.2b. Solid curves were drawn based on the experimental results reported by Förster *et al*[24] and Bates *et al*[25]. Dashed curves are extrapolated to include the anticipated morphologies.

The critical point is $(\chi N)_{critical} = 10.5$ where $f_{composition} = 0.5$ when a diblock melt that is compositionally symmetric expects to undergo a second order phase transition from the disordered phase to the lamellar phase. For asymmetric diblock copolymers where $f \neq 0.5$, theory predicts a weak first order transition from the disordered phase to the cylindrical or spherical phase. Fredrickson and Helfand[26] corrected Leiblers mean field

theory in order to control fluctuations in the first order phase transition, where $(\chi N)_c$ = 10.5 is replaced by $(\chi N)_{ODT} = 10.5 + 41.0\ \overline{N}^{-1/3}$ ($\overline{N}$ is proportional to the average molecular weight of the copolymer). Therefore there exists two main theories for the WSL, these are outlined in figure 1.2d, (a) the mean field theory (Leibler) and (b) the fluctuation picture (Fredrickson and Helfand).

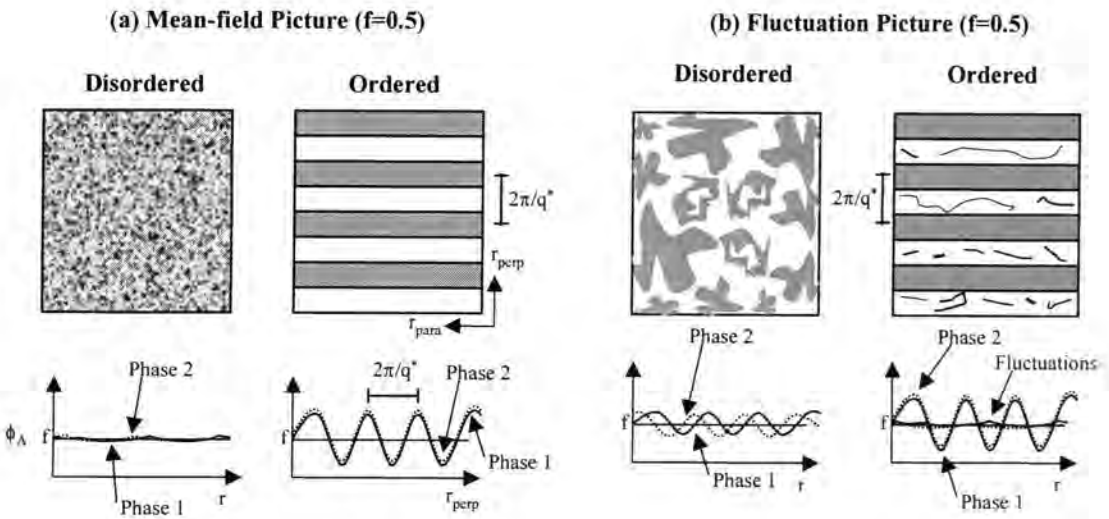

Figure 1.2d Real space composition patterns at the weak segregation limit

The extension of these theories to concentrated and semidilute diblock copolymer solutions swollen using neutral non-selective solvents shows that copolymer solutions have a uniform distribution of ordered microphases. This suggests that in the concentrated regime, where swelling effects are absent, the phase diagram of a copolymer solution is obtained by rescaling χ to $\chi\phi$ in the melt phase diagram, ϕ being the copolymer volume fraction. Solvent was shown to accumulate at the interfaces of the microdomains, which screens the unfavourable A-B monomer contacts with a translational entropy cost that counter balances the loss of contact enthalpy. The choice of the solvent changes the ODT two phase region which is solvent rich in the disordered

part and solvent poor in the ordered part, therefore the region is narrow with good solvents and broadens with a decrease in solvent quality.

Theory predicts that immediately below a well defined transition temperature, the system adopts an ordered structure with domains on a lattice, while above the transition the domains give way to a thermodynamic homogeneous disordered phase.

1.2.4 Theory of microphase separation and domain morphology

Domain size and interfacial thickness can be determined by theory using the confined chain model[27]. If an A-B diblock copolymer of equal volume fractions is used to illustrate this, the morphology will be lamellar. Shown in figure 1.2e is a segmental density profile of a block copolymer with lamellar morphology.

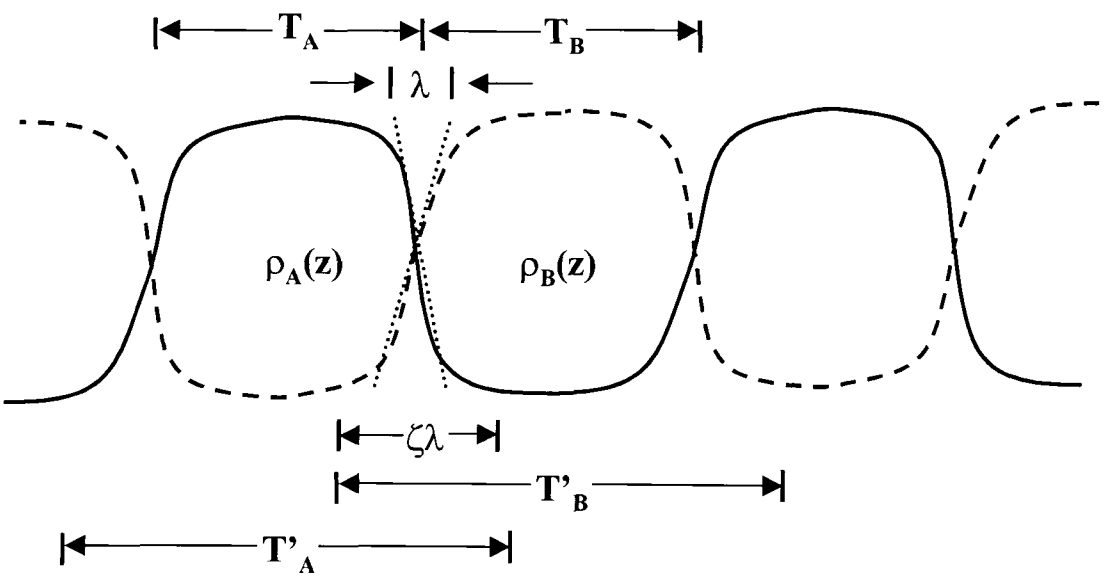

Figure 1.2e Segmental density profile of a block copolymer possessing a lamellar morphology

Interactions of unlike segments in the block copolymer only occur at the interfacial region. Whilst contributions to the free energy change associated with the spatial constraints and interaction energy between the segments are due to the following causes. Firstly, the heat of the mixing of the block components (ΔH_m), secondly, the placement entropy (ΔS_p), and thirdly the volume constrainment entropy (ΔS_c). The heat of mixing in the random state is given by Flory-Huggins theory[27], therefore the derivation of change between the randomly mixed state and the microphase separated state is given as equation 1.2a.

$$\Delta H_m = \frac{N\chi_{AB}k_BT\lambda}{2T_A} - \frac{V\phi_A\phi_B\chi_{AB}k_BT}{\bar{v}_A} \qquad \text{eq.1.2a}$$

ΔH_{int} $\qquad$ ΔH_i

ΔH_{int} is the interfacial energy

ΔH_i is the heat of mixing of segments in the random state

V is the volume of the system

$\bar{v}_A$ is the molecular volume of an A-segment

ϕ_A and ϕ_B are the volume fractions of A- and B- components

χ_{AB} is the interaction parameter between the components

k_B is the Boltzmann constant

T is the temperature

N is the number of A-B molecules

T_A is the thickness of the A-domain

λ is the linear interfacial thickness

Placement entropy (ΔS_p) is the loss of entropy created by placing the A-B junction anywhere within the interfacial region and is given in equation 1.2b.

$$\frac{\Delta S_p}{Nk_B} = \ln\left[\frac{\zeta\lambda}{T_A + T_B}\right] \qquad \text{eq.1.2b}$$

ζ is an adjustable parameter ($\zeta \approx$ 1-2) characterising the greater space available to the junction segments that is given by the interfacial thickness λ

The loss in placement entropy is related to the ratio of volume available to the placement of molecules in the microphase separated state ($\approx \zeta\lambda S$), and that available in the randomly-mixed state ($\approx T_{AB}S$). Where T_{AB} is the repeat spacing of the lamellar domains, i.e. $T_{AB} = (T_A + T_B)$.

Volume constraint entropy (ΔS_c), requires the probability that the chains have one end in the interfacial region and will have all segments within their domain space. The density distribution of segments must be such that space is uniformly filled with segments. This quantity of entropy change associated with constraining the chains to their respective domains while at the same time satisfying the uniform density requirement is given in equation 1.2c.

$$\frac{\Delta S_c}{Nk_B} = \ln P_{AB}(Z_A = T'_A/2; Z_B = T'_B/2: \zeta\lambda) \qquad \text{eq.1.2c}$$

P_{AB} is the joint probability of finding the free ends of the A- and B-chains at positions that satisfy the uniform density requirement

Z_A is the distance between a free end in domain A and the interface edge that borders domain B in the diblock copolymer

T'_A is the distance that borders domain B on either side of domain A

From these three parameters the free energy of A-B domain formation (ΔG_{AB}) associated with microphase separation from a homogeneous state to the domain structured state of an A-B block copolymer can be calculated. The free energy is a function of two independent variables, one associated with domain thickness, d, and the other with interfacial thickness, λ. The relative contributions to the free energy from the three previous contributions are shown in figure 1.2f, as a function of domain thickness.

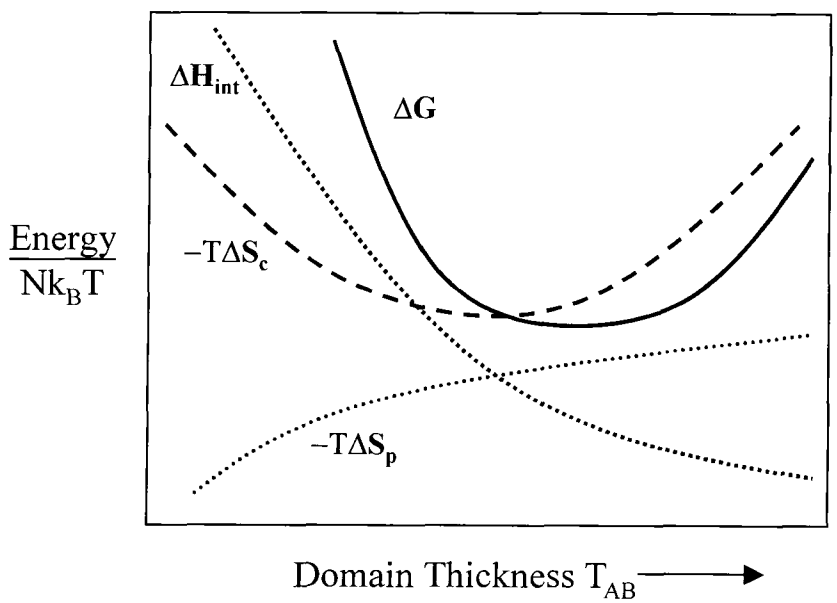

Figure 1.2f Relative contributions to the free energy of domain formation as a function of domain size (redrawn from reference 26)

ΔH_{int} decreases monotonically due to the relative fraction of material in the interface decreasing. The placement entropy increases monotonically with increasing domain size, and the constraint entropy shows a minimum due to the interplay of the boundary constraints (decrease the space available). Therefore an increase in domain thickness

reduces segmental densities in the centre of the domain. The quantity ΔG_{AB} has a minimum and establishes the equilibrium domain size. Theoretical and experimental values for domain size and interfacial thickness can be compared by methods such as SAXS, SANS or NMR techniques.

Conclusions from these comparisons show that there is a no dependence of interfacial thickness on total molecular weight. Theory predicts a slight decrease of the thickness with molecular weight. However, results do not show this behaviour. Helfand theory agrees better with experimental data rather than confined chain theory because molecular weight dependence with interfacial thickness is not predicted by Helfand theory. At infinite molecular weights both theories become identical because the interface has the same properties as a corresponding pair of homopolymers. Critical molecular weights and interaction parameters are calculated for domain formation by setting $\Delta G_{AB} = 0$, but only approximate ranges are possible to show experimentally for the molecular weight.

Domain size and interfacial thickness have been predicted by the mean field model[23] using block copolymer microphases (lamellar, cylindrical and spherical) to include the effects of solvents, using the narrow interface approximation for systems where the interphase represented a small fraction of the total system. This is valid for systems on the verge of becoming homogeneous, i.e. at very high temperatures or diluted with solvent.

The major factor responsible for different composition range transitions is that chain perturbations arise when chains of different molecular volume are coupled and then forced to uniformly fill their respective domain space, so as to maintain a uniform

density of segments. This behaviour occurs when one of the block volumes in an A-B diblock copolymer is reduced, the chains then occupy less space, and a region of low segment density results in between the B chains. This does not occur when the B chains are perturbed (stretched) laterally or the chain junctions are brought closer together (A-chains being perturbed). The mismatch in volume leads to an increase in the free energy of the system, to relieve this (when the energy becomes large enough), the system changes morphology to relieve the space filling problem. Lamellar to cylindrical (curvature in one dimension) to spherical (curvature in two dimensions).

1.2.5 Differences between various Styrene-Butadiene (S-B) block copolymers

The phase structure of the SBS triblock copolymer forming spherical domains has both ends of the structure terminated with polystyrene segments. These segments act as multifunctional junction points to effectively give a cross-linked elastomeric network at room temperature. The cross-linking process is physical not chemical, so when the polymer is heated the domains soften and the network begins to flow and it loses strength. When cooled the domains harden and the network retains the properties originally discovered. This system applies to block copolymers such as SIS, SBS, SISISI... and $(SB)_nx$ (where x is a multifunctional junction point), but has restrictions on the relative phase volume of each block in the copolymer. This applies when the polystyrene phase is a minor part of the total phase volume ($\approx$ 20%).

Block copolymers such as SB and BSB cannot form pseudo-network structures since only one end of each polydiene chain is terminated by a polystyrene segment. These block copolymers are weak materials with no resemblance to conventional vulcanised rubbers. An example of the differences between SBS and BSB triblock copolymers is shown with regards to a comparison of tensile properties[28]. In the study, both polymers

possessed 27% polystyrene content and a total molecular weight of ≈ 75K. The SBS triblock had properties corresponding to a thermoplastic elastomer, however, the BSB copolymer was a weak material that did not develop any strength unless it was vulcanised. The reason for this behaviour is represented in figure 1.2g.

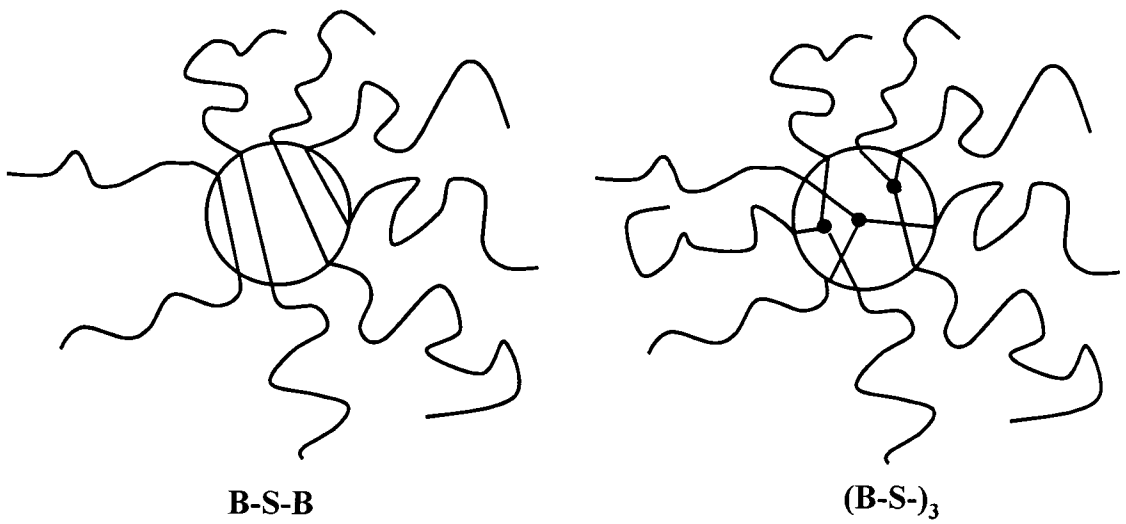

(a)

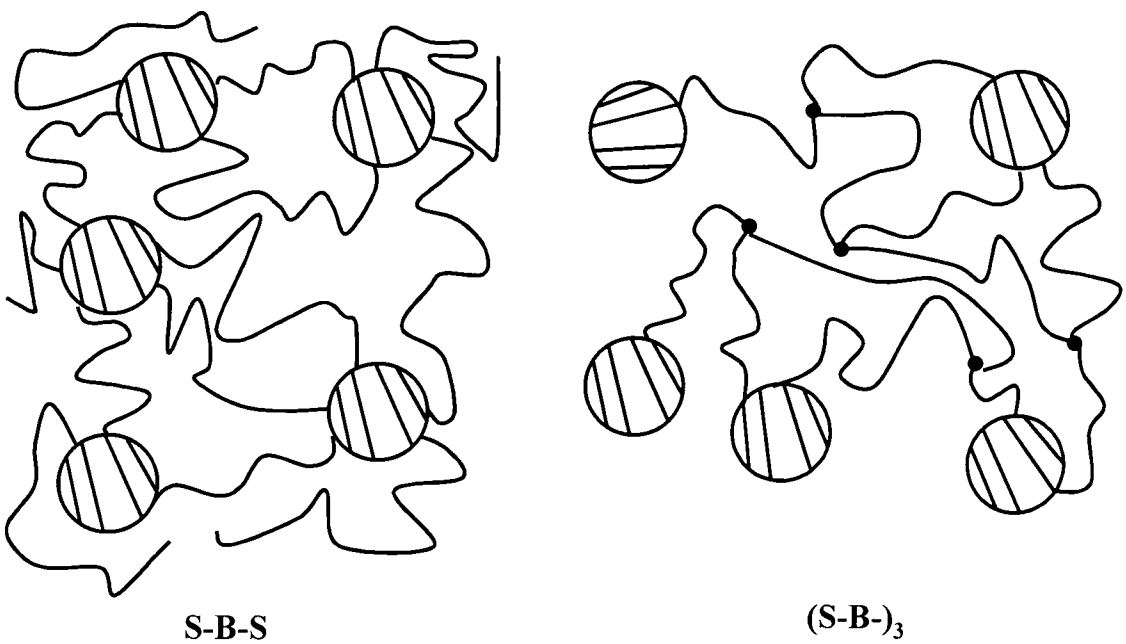

(b)

Figure 1.2g Schematic representation of domain structures; (a) polymers terminating in butadiene blocks; (b) polymers terminating in styrene blocks

1.2.6 Physical property variation with respect to composition variation

If the monomer ratio of a SBS triblock copolymer is varied then a difference of physical properties in the respective polymers is shown to occur. When stretching a number of triblock systems, a range of physical properties was observed with respect to copolymer composition, this is shown in figure 1.2h.

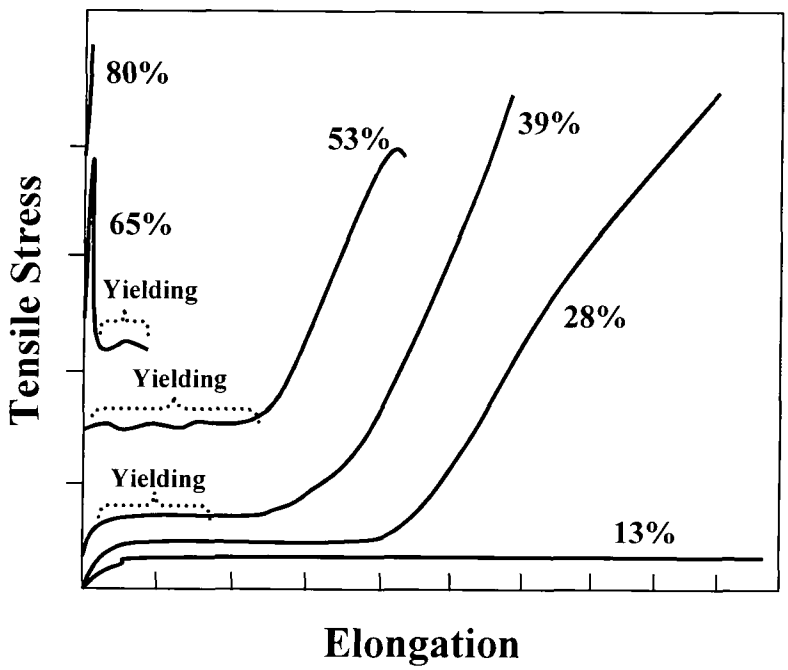

Figure 1.2h Stress-strain curves for a series of SBS triblock copolymers with various polystyrene contents (redrawn from reference 29)

As the PS content in the triblock copolymers increases, the modulus and hardness of the materials steadily increase to very high values typically observed for polystyrene[29]. Flow properties of the range of polymers pass through a maximum and then decrease, due to the viscosities at low shear rates being greater than the viscosities of either the homopolymers of the same molecular weight, even at temperatures well above the glass transition (T_g) of either homopolymer. High viscosities result from a two-phase system existing in the melt. The PS and PB phases are incompatible at high temperatures due to

flow involved that disrupts the fluid PS domains and transfers the PS segments through the thermodynamically incompatible PB phase in to other PS domains. Therefore additional energy is required for flow and a higher viscosity is yielded.

The enhancement of the tensile strength of reinforced elastomers in terms of redistribution of stresses by the filler particle after one or more elastomer chains has broken, is due to the absorption of the energy released in this chain rupture by the relatively large immobile masses of the filler particles. The PS domains prevent individual chain breakages from initiating catastrophic rupture, the requirement being the PS domains to be firmly attached to the elastomeric network by means of covalent bonds.

Viscoelastic behaviour of the PS-PB block copolymers in the melt, show strong non-Newtonian flow between 100-160°C over a range of shear rates. When different block sequences of the PS-PB copolymers are compared, it was shown that the viscosities of the polystyrene terminated polymers (of equal molecular weight) were much greater than polybutadiene terminated copolymers, where branched copolymers have lower viscosities. The trends are similar for dynamic viscosity and steady flow properties.

If polymers of this kind are butadiene terminated the viscosity is a function of the butadiene block length, due to the PS domain size being unaffected by branch points with few disruptions of the PS domains as the polymer flows. Polystyrene terminated polymers do not undergo steady flow without disruption of the domains. The effective molecular weight of the flowing molecules will depend on the ease with which PS blocks are extracted from the domains, and therefore viscosity depends on the length of the PS blocks.

1.3 Small angle X-ray scattering on block copolymers

1.3.1 Introduction

Small angle X-ray scattering data from block copolymer systems has been used to characterise phase separated structures in solution and in the bulk state[18,30,31,32]. When looking at microphase separated systems experimentally in the solid state, samples must be prepared so that an equilibrium state is achieved. Under equilibrium conditions the domains in the phase separated block copolymer can be regularly arranged in lamellar, cylindrical or spherical form. An ordered lattice of domains will be converted to a series of distinct structure factor interference peaks at well defined scattering angles. The structure of the lattice can now be deduced from the angles of the interference peaks.

If the domains are identical, single particle form factor scattering will give rise to several broad peaks at higher scattering angles giving information about the individual particle size within the structure. Data that shows defined peaks both at low and high angles for spherical, cylindrical or lamellar morphology copolymer systems is possible.

Morphological information, representing an average of all features within the scattering volume, is obtained from the scattered intensity data by the use of mathematical analyses based on the theoretical models. The intensity of the scattering is related to the extent of phase separation within the system via the variant. The breadth of the scattering curve is inversely related to the average size of the phases. The correlation function, which is the Fourier transform of the scattering curve, is related to the average phase dimensions and also indicates the average spacing between phases. Finally, the shape of the SAXS curve tail determines the thickness of the interface between the phases.

The X-ray scattering of block copolymer systems involves a number of complicating factors when trying to fit theoretical findings with experimental results. The size distribution of particles that represents a set of monodisperse isolated spheres, having sharp boundaries, differs theoretically compared to experimental results. The measurement of the scattering function from a block copolymer (e.g. spherical morphology) shows deviations from theory due to the spheres possessing a Gaussian distribution and diffuse boundaries. The differences arise from the polymer chains possessing polydispersities between 1.05-1.15, and the effect of the diffuse boundary between the phases in the system. Treating the polymer as having a Gaussian chain distribution with a diffuse boundary produces agreement between experimental and theoretical calculations.

The number of interparticle interference maxima demonstrates the existence of long-range order for isolated spheres in the block copolymer system. The origin of long-range regularity is due to entropic repulsion between the spheres. The average nearest-neighbour distance of the sphere, d is determined using Bragg's equation

$$2d \sin \theta_m = \lambda \qquad \text{eq.1.3a}$$

λ is the wavelength of the x-rays

θ_m is one-half the scattering angle at which the intensity arising from interparticle interference becomes maximum

If the spheres are fairly monodisperse (polydispersities between 1.05-1.15), the domain size can be predicted from the peak position of the i-th intra-particle interference

maxima observed for an isolated sphere. The scattering from a single sphere becomes maximum using equation 1.3b.

$$U_{max,i} = 4\pi(R/\lambda) \sin \theta_{max,i} \qquad \text{eq.1.3b}$$

Calculated results fit better with the experimental data by introducing a Gaussian size distribution, P(R), on the average radius of domain, $\overline{R}$, and the polydispersity of domain size parameter, $\sigma_r / \overline{R}$. The theoretical scattering can now be predicted as shown in equation 1.3c.

$$P(R) = (2\pi\sigma_r^2)^{-1/2} \exp[-(R-\overline{R})^2 / 2\sigma_r^2] \qquad \text{eq.1.3c}$$

SAXS patterns for block copolymers having cylindrical domains usually show a number of scattering maxima indicating structural long-range order of the monodisperse polymer chains. Form factor peaks at higher angles are usually observed arising from the radii of the cylinders in the structure. Lamellar domains produce a number of scattering maxima arising from long-range order of the lamellae.

The relative peak heights of the curves are related to the volume fractions of A and B domains, whilst the number of resolvable scattering maxima are related to the uniformity of domain size within a system. Lamellar and cylindrical domains in solvent cast films have preferred orientation. Lamellar morphology systems exhibit scattering perpendicular to the film surfaces, indicating that the domains are highly oriented with their boundaries parallel to the film surfaces, this effect is shown in figure 1.3a.

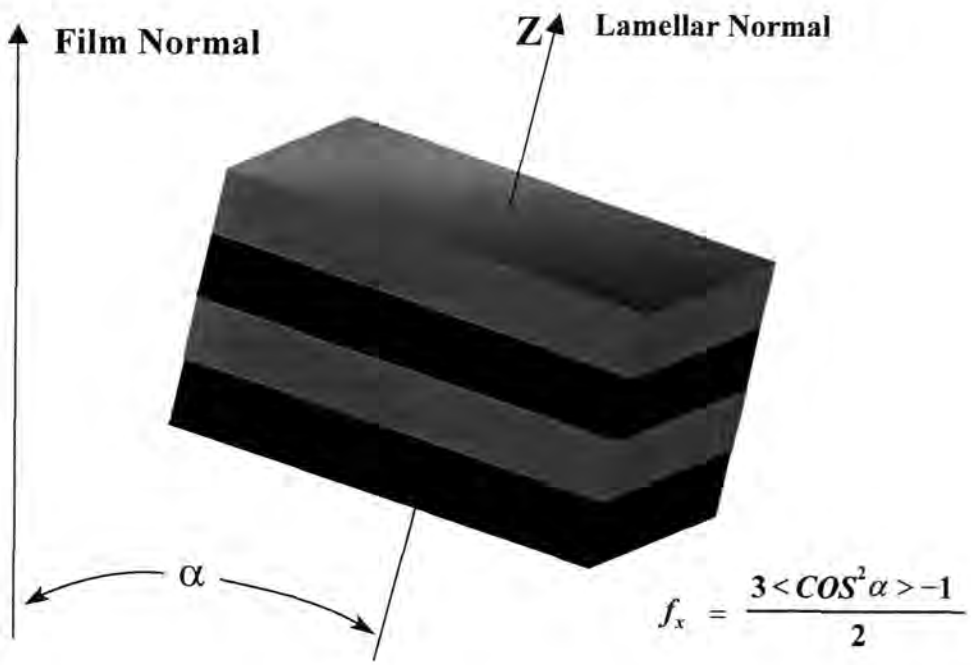

Figure 1.3a The orientation factor of a lamellar normal with respect to the film normal

The factor, f_x has been calculated as 0.95 lamellar orientation[33,34], proving that lamellar stacks predominantly form perpendicular to the film normal. The incident X-ray beam normal to the film surface is circularly symmetric, so the orientation of the lamellar normal is uniaxially symmetric with respect to the film normal. From the measurements using X-rays, the domain thickness, d can be calculated. Figure 1.3b shows that in theory and in practice, domain spacing values of block copolymer systems increase as molecular weight of the monodisperse chains increases.

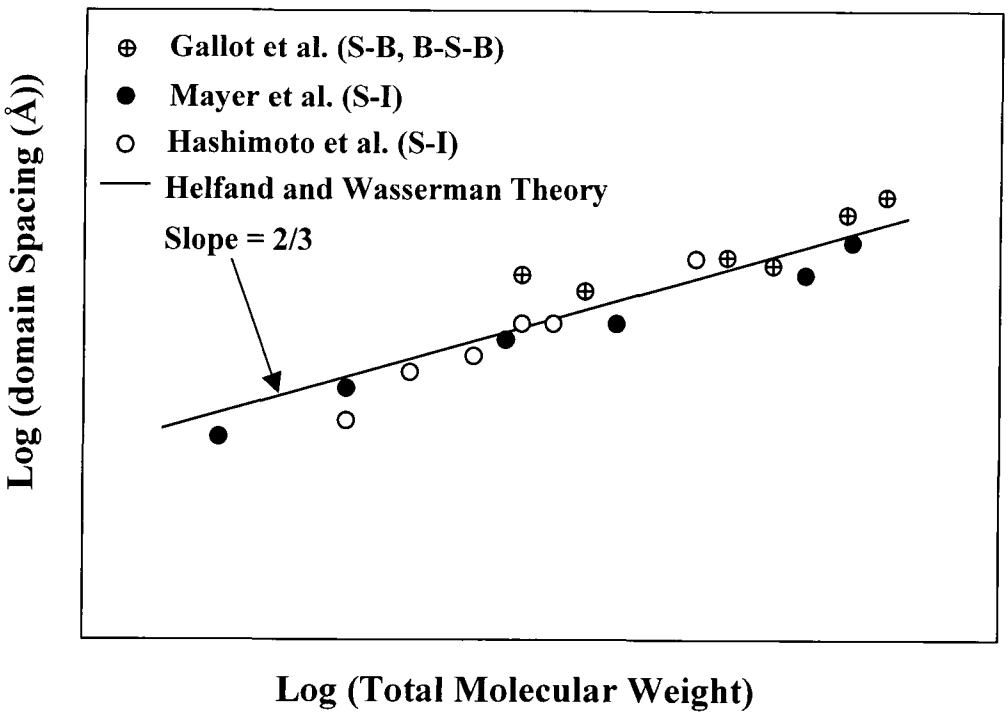

Figure 1.3b Measured domain spacing d, as a function of total molecular weight for a series of block copolymers

Experimental results for polystyrene/polydiene systems have been obtained by many research groups, of which three are featured in the figure above[34,35,36]. The log of the relative intensity can be plotted against the reduced scattering angle, s ($Å^{-1}$) = (2 sinθ)/λ (θ is one half of the scattering angle), to determine the Bragg maxima. The ratios of the relative angular positions describe the arrangement of the domains[37,38].

The first Bragg maximum (s_1) is compared to the other higher order maxima in turn (s_1/s_n), and the ratio of these values in turn indicates a regular spatial arrangement. For spherical domains[39] the ratios of the maxima positions (s_1/s_n) are as follows:

$$1 : 1/(2)^{1/2} : 1/(3)^{1/2} : 1/(4)^{1/2}$$

Indicating that spherical domains have a regular spatial arrangement as simple cubic or body centred cubic packing. For other forms of cubic packing the information is displayed below in the form of their sequential s values:

Face-centred cubic: $1 : 1/(3)^{1/2} : 1/(4)^{1/2} : 1/(8)^{1/2} : 1/(11)^{1/2}$

Diamond cubic: $1 : 1/(3)^{1/2} : 1/(8)^{1/2} : 1/(11)^{1/2} : 1/(16)^{1/2}$

Cylindrical domains are arranged in hexagonally close packed form, their sequential s values are as follows:

$$1 : (3)^{1/2} : (4)^{1/2} : (7)^{1/2} : (9)^{1/2}$$

For lamellar domains the ratios of the maxima positions (s_1/s_n) are as follows:

1 : 0.5 : 0.33 : 0.25 : 0.20 in the direction parallel to the film normal

When analysing lattices of different types, problems arise when calculating the level and nature of lattice distortions within the different polymer phases (or within polymer crystals) and how to measure the coherently diffracting domains. With polymers, it is particularly improbable that the molecular arrangement of linear chains should be ideal, therefore displacement disorder arises. The presence of lattice distortions implies that each cell does not strictly retain the 3-D system of translations a, b, c, which characterise the ideal packing for chain molecules of a given cross-section. The three-dimensional lattice may be preserved but only on an average basis. The two important known classes of lattice distortions are of the first kind and of the second kind[30,37].

Consider a regular system of nodes in a two dimensional lattice with the probability that the position of a given molecule will be displaced from its node. Gradually that probability increases with the increasing separation of the molecules and the

corresponding nodes. The probability distribution is set to be the same for all nodes in the lattice. Therefore each molecule does not strictly lie at each node, and on average the assembly retains crystalline order throughout the volume. The molecules are slightly displaced from their ideal positions. The Q-function (that describes the Bragg maxima) consists of a series of peaks which become diffuse under the influence of distortions of the first kind, whilst the Q-function itself is left periodic. The Bragg maxima lose some of their intensity that is transferred to the background. When molecules forming a crystal are not of the same type and are a mixture of components then distortions of the first kind occur. The imperfections introduce fluctuations in the distances between the corresponding molecules but the long-range order is preserved.

Distortions of the second kind occur when lattice distortions occur and the statistical averages of the positions of the molecules do not form a regular lattice. Successive translation vectors in any given lattice or row line vary in both length and direction, then the long range order in the lattice is lost and the molecules are not placed any longer in their ideal positions over the entire volume. Distortions of the second kind cause the Q-function to produce diffraction patterns that consist of different size peaks that are different shapes that increase in breadth and decrease in intensity with increasing scattering angle. These distortions will possibly effect the structures of the networks being studied in this project. Although these distortions do not affect short-range system order, they reduce long-range order of the structures.

Distortions of the first and second kind will possibly appear in the systems analysed in this project, due to cross-linking that disrupts conventional microphase separation observed in uncross-linked block copolymer systems.

1.3.2 SAXS analysis of di- and triblock copolymer systems

Small angle X-ray scattering (SAXS) of block copolymers in the strong segregation limit yields peaks arising from the microdomain structure present in heterophase systems[311]. Increasing the temperature decreases the 1st order Bragg peak intensity while maintaining its position and shape. Subsidiary peaks disappear much earlier than the main peak but upon disappearance they retain their position and shape. Therefore the basic characteristics of the microdomain structure remain largely unaltered but the contrast between the domains and the surrounding matrix is gradually decreasing with temperature.

The primary set of Bragg peaks arise from the presence of a well defined distance between the nearest neighbour pairs of microdomains (long-range order), the secondary peaks arise from interparticle interference of X-rays scattered from a single spherical microdomain (short-range order). The evaluation of the interdomain distance, d, and the radius, a, of a spherical or cylindrical morphology system is possible. The intensity of the X-ray scattering, I(s), is related to a materials spatial electron density distribution, $\rho(x)$, as follows in equation 1.3d.

$$I(s) = I_e(s) \left[\int_V \rho(x) \exp(-2\pi i s.x)\, dx \right]^2 \qquad \text{eq.1.3d}$$

$I_e(s)$ = intensity scattered by a single electron

$s = 2\sin\theta/\lambda$ = scattering vector magnitude

2θ = scattering angle

V = volume of material exposed to x-rays

The intensity of the scattering observed can be integrated over the entire angular range to evaluate the invariant, Q given by equation 1.3e.

$$Q = \frac{4\pi}{V} \int_0^\infty s^2 \frac{I(s)}{I_e(s)} ds \qquad \text{eq.1.3e}$$

Q represents the mean square deviation $<(\delta\rho)^2>$ of the electron density throughout the sample. If the system is a two-phase one divided by sharp boundaries, the mean square electron density deviation is given by equation 1.3f.

$$<(\delta\rho)^2> = (\rho_1-\rho_2)^2 \phi_1\phi_2 \qquad \text{eq.1.3f}$$

ρ_i are the mean electron densities of each copolymer phase

ϕ_i are the volume fractions of the respective copolymer phases

If the temperature is increased, Q values decrease due to mixing of the two phases and the domain boundaries become more diffuse.

1.3.3 The polymer-polymer interphase in block copolymers

A quantitative method to analyse the thickness of the diffuse boundary is based on an analysis of the systematic deviation of the SAXS intensity distribution at large angles from Porod's rule. This was proposed by Vonk for ideal two phase polymer systems[45]. For spherical domain systems the function related to interfacial thickness depends only on the function variable, but for cylindrical and lamellar domain systems, the boundary exists in a radial direction or in a direction parallel to the lamellar normal. Expressions for the function can be obtained for all domain systems if the function is approximated

by a Gaussian. Using these expressions, the interfacial thickness, t, for domains are minimum estimations because a linear density transition in the interphase is assumed.

If a two phase material is randomly intersected by an infinite number of lines, the average length of all chords lying in phase A will be given by l_A, the phase A inhomogeneity length. The inhomogeneity length in phase A is related to the overall inhomogeneity length, l_P, as follows in equation 1.3g.

$$l_A = \frac{l_P}{1-\phi_A} \qquad \text{eq.1.3g}$$

ϕ_A is the volume fraction of phase A

The overall inhomogeneity length is obtained from the relation to the scattered intensity in equation 1.3h.

$$l_P = \frac{2}{K\pi^2}\int_0^\infty s^2 I(s)\,ds \qquad \text{eq.1.3h}$$

K is the Porod constant

If the system contains density gradients at the interface between phases, the tail of the SAXS curve will fall off more rapidly and theoretically will follow the general form[40,41,42] in equation 1.3i.

$$\lim I(s) = \frac{K}{s^4} \times H^2(s) \qquad \text{eq.1.3i}$$

$H^2(s)$ is a smoothing function related to the shape of the electron density gradient at the interface. For a sharp interface, $H^2(s) = 1$. If the interfacial gradient is assumed to have a sigmoidal shape, then $H^2(s)$ will take the form in equation 1.3j.

$$H^2(s) = \exp(-4\pi^2\sigma^2 s^2) \qquad \text{eq.1.3j}$$

s = the scattering angle in the Porod region (large angles)

σ = the diffuseness of the boundary

The interface in two-phase polymer systems is best approximated by a sigmoidal gradient[43]. However, it is easier to obtain the dimensions of an assumed linear (trapezoidal) interface. The thickness, t, of a linear interface is given in terms of the standard deviation of a sigmoidal gradient, σ, as equation 1.3k.

$$t = \sqrt{12}\,\sigma \qquad \text{eq.1.3k}$$

Hashimoto *et al*[30] and Skoulios *et al*[21] have made analyses on block copolymer systems of the lamellar type to obtain the interfacial thickness based on this method.

1.3.4 The correlation function obtained from two-phase polymer systems

The one-dimensional (1-D) correlation function works on the assumption that the sample under investigation is densely packed with an unoriented distribution of parallel lamellar stacks, where the stacks are normal to the lamellar surfaces under investigation. The 1-D correlation function in the x-direction, $\gamma_1(x)$, is related to the experimental scattering[44,45] by equation 1.3u.

$$\gamma_1(x) = \frac{\int_0^\infty s^2 I(s)\cos(2\pi x s)ds}{\int_0^\infty s^2 I(s)ds} \qquad \text{eq.1.3u}$$

$I(s)$ is the desmeared SAXS intensity

s is the scattering vector ($s = 2\sin\theta/\lambda$)

The two-phase structure studied is made up of two distinct phases, with an electron density that varies gradually (assumed to be linear) from η_1 to η_2, with volume fractions ϕ_1 and ϕ_2. The position of the boundary is in the middle of the transition layer, t. The mean square electron-density gradient in isotropic structures is described in equation 1.3v.

$$<|grad\eta|^2> = \Delta\eta^2 \frac{S}{tV} \qquad \text{eq.1.3v}$$

$\Delta\eta = \eta_1 - \eta_2$

S/V is the specific surface area of the phase boundary

S/V is calculated from the correlation function slope at the origin in equation 1.3w.

$$\left(\frac{d\gamma}{dr}\right)_{r=0} = -\left(\frac{S}{4V}\right)\left(\frac{\Delta\eta^2}{<\eta^2>}\right) \qquad \text{eq.1.3w}$$

Equation 1.3w can be applied to two-phase structures provided the slope is taken at a distance of at least t Å away from the origin. The transition layer t, is described in equation 1.3x.

$$t = -\left(\frac{4}{R}\right)\left(\frac{d\gamma}{dr}\right)_{r=t} \qquad \text{eq1.3x}$$

$$R = \frac{<|grad\,\eta|^2>}{<\eta^2>}$$

$<\eta^2>$ is the average electron density

When looking at pseudo lamellar two-phase structures[46] the electron density variations are represented as $\eta(x) = \eta_2 + P(x)\,\Delta\eta$, where P(x) varies between 0 and 1 between the two phases and is the convolution of the corresponding function in an ideal two-phase system. As the thickness of the two-phases varies from lamellae to lamellae the sharpness of the corner points of the correlation function become smooth. The plotted one-dimensional correlation function shows a number of maxima and minima of constant values and of decreasing height that finally becomes zero at large s, a behaviour suggesting periodicity in the structure. A characteristic 1-D correlation function of a polymer with a relatively broad distribution of long periods is shown in figure 1.3d.

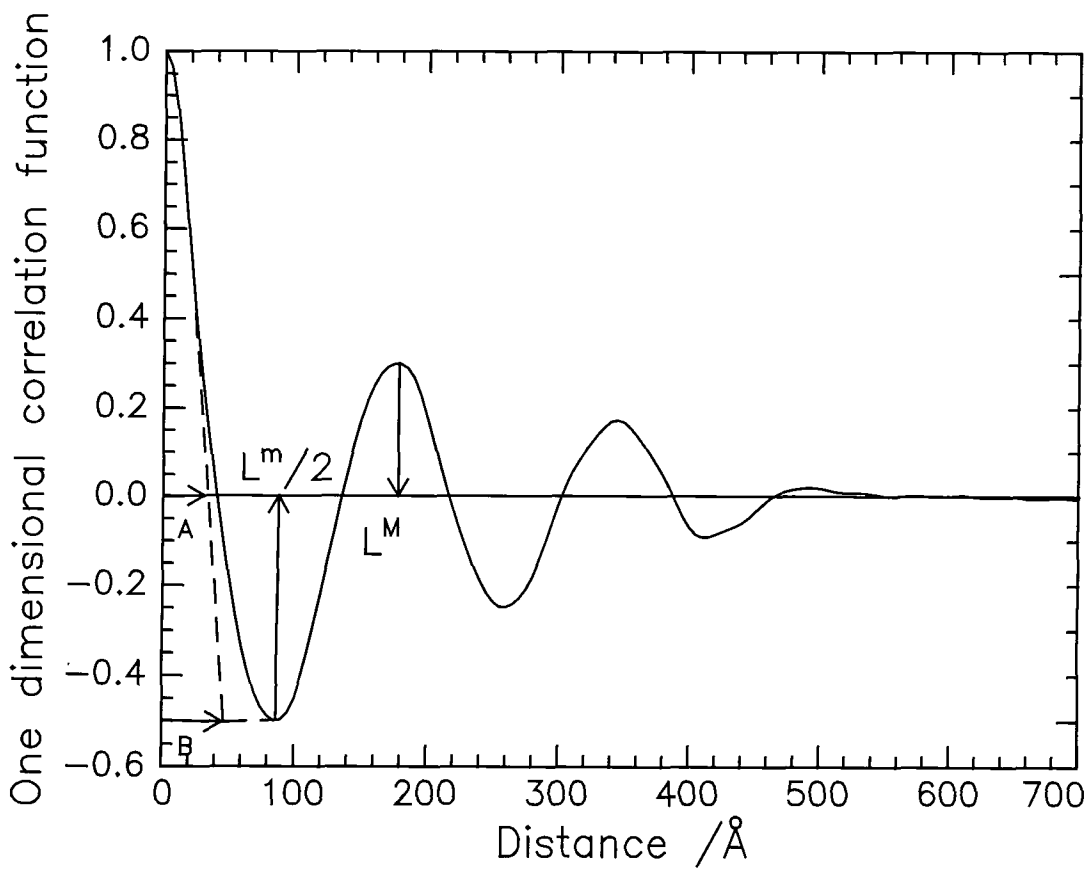

Figure 1.3d 1-D correlation function of an ordered two-phase block copolymer

The positions of the first minimum, $L^m/2$, and maximum L^M, in the function indicates, for $L^m/2$, the most probable distance between the centres of gravity of two lamellar stacks of different compositions, and for L^M, the most probable distance between the centres of gravity of two lamellar stacks. The long periods evaluated from the two different methods are shown in figure 1.3e where electron density distribution is measured along a trajectory normal to the inner surfaces of a lamellar stack. These two values may vary if the lattice is not ideal.

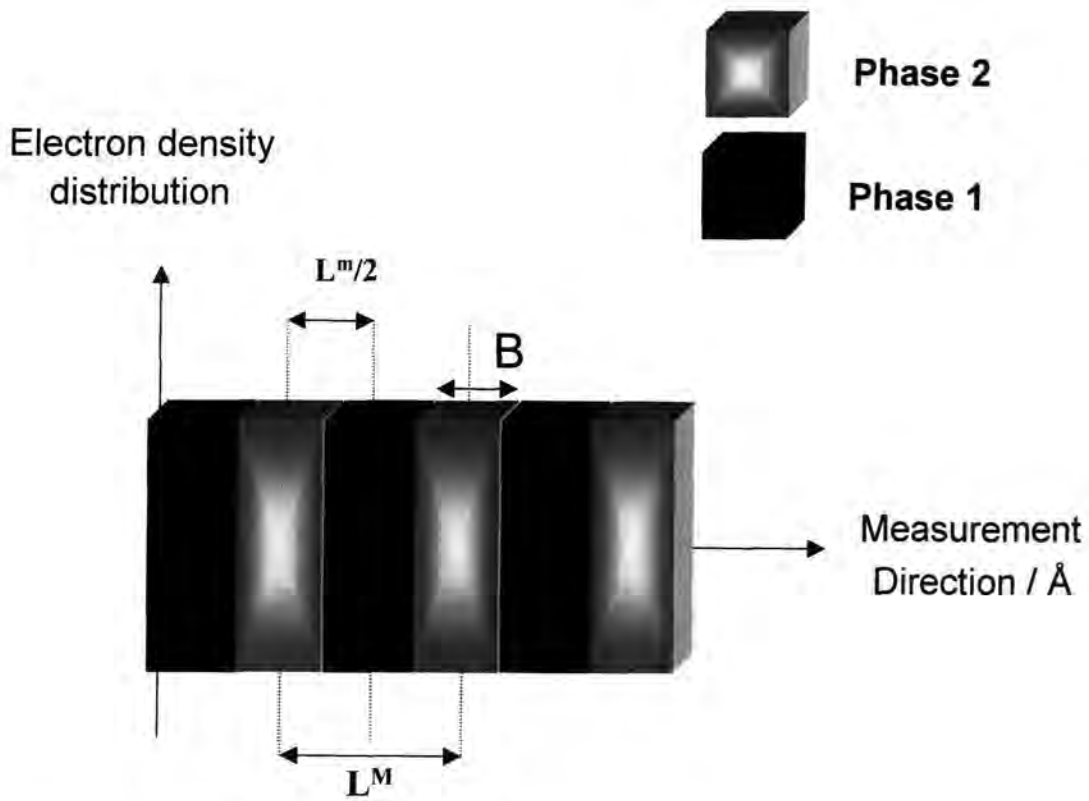

Figure 1.3e Lamellar stacks indicating distances obtained from 1-D correlation functions

1.4 Polymer Networks

1.4.1 Introduction

Methods generally used to synthesise polymeric networks cannot provide adequate control of their internal structures. Radical polymerisation processes are random and the distribution of polymer chain lengths are very broad[47]. Reactions also gel at an early stage, therefore gel points are not easy to define because factors such as segment concentration, chain length, end-to-end distance and functionality cannot be related to it. In some cases the gels are not macroscopically homogeneous, especially when solvent expulsion takes place. Similar problems occur when networks synthesised from polycondensation processes involve a tri- or tetrafunctional component to achieve cross-linking[48].

Useful networks can be obtained when polymers are vulcanised[49], this method cross-links randomly so therefore does not achieve perfect network structures (model networks). A precise knowledge of the total number of branch points formed is impossible because of loops and double connections reducing the number of elastically effective chains. These networks have been used to establish the validity of rubber elasticity theory and equilibrium swelling theory. Ideal networks on the other hand should obey the following requirements:

1. They need to be homogeneous, i.e. no solvent expulsion should occur, with segment density and cross-link density being uniform throughout the sample.
2. Only elastically effective chains should be present. Therefore the gel should not contain defects such as pendant chains, double connections or physical cross-links.

3. The elastically effective network chains should obey Gaussian statistics, i.e. their average degree of polymerisation should be known and the polydispersity of chain-lengths is expected to be narrow.

4. The functionality of the cross-links should be known and constant throughout the gel.

1.4.2 Network characteristics with respect to macromolecules

Mechanical properties of macromolecules are determined by the nature and rate of the configurational changes effected by stress, along with other parameters such as inter-chain couplings, temperature and viscosity. Isolated polymer molecule properties need to be understood in order to understand network characteristics such as the topological behaviour of chains in network polymer systems[50]. The size of a polymer molecule is described using the root mean squared distance between the ends of an unperturbed molecule, given by equation 1.4a.

$$< r^2 >_o = C_\infty n l^2 \qquad \text{eq.1.4a}$$

n represents the number of skeletal bonds

l is the bond length in the polymer chain

C_∞ is the characteristic ratio[51] - an asymptotic value independent of molecular weight

The extensibility of a polymer chain can be calculated and potentially extended many fold, but in practice this is not observed. When polymer elastomeric materials are stretched and then recover, the behaviour is related to the reversible deformability of the long chain molecules. The statistical treatment of chain configurations in real molecules is represented as a freely jointed chain where each link can assume any orientation. This is described using a Gaussian distribution, which is valid for a chain that is sufficiently

long when its end to end separation is significantly less than that of the fully extended chain. The random coil configuration of an unperturbed molecule corresponds to a minimum configuration free energy that is predominantly entropic. If polymer molecular weight is sufficiently high of an amorphous polymer, the number of entanglements per molecule is large and the polymer behaves as a network. For lower molecular weight polymers, cross-linking can be used to implement the same effect, except the chemical cross-links are permanent so therefore flow can not occur due to slippages at elevated temperatures. In order to predict theoretical models for networks, characteristics of linear polymers must be used.

1.4.3 Polymer network chains

A cross-linked polymeric network is a three-dimensional structure of polymeric chains that extends continuously throughout the specimen. The network is a molecule whose weight is that of the macroscopic specimen, provided the sample has no diluent or sol fraction present. During cross-linking many primary molecules become coupled to each other through chemical bonds at the ends of the molecules (using a cross-linking agent)[52], or along the primary molecules (using radiation, vulcanisation, peroxides or any other form of random cross-linking)[53,54,55,56]. Owing to a vast continuity of connecting chains, a network cannot dissolve in a solvent unless skeletal bonds are broken. However, it can imbibe solvent and swell a finite amount. An example of an end cross-linked polymeric network is shown in figure 1.4a.

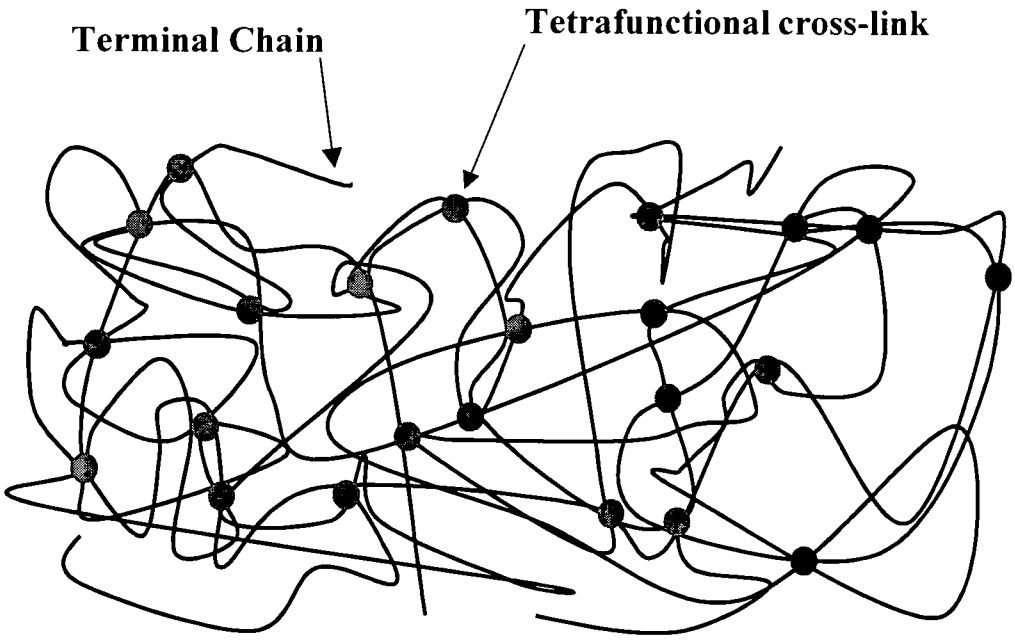

Figure 1.4a Schematic representation of a cross-linked network polymer

The circles show cross-links of a functionality of four. Some chains are attached to the network at one junction only and are called terminal chains that are elastically inactive. If such a network had no terminal or other inactive chains, the number of active chains would equal twice number of junctions (not including trapped entanglements).

To quantify the interpenetration of network chains[57], and the spatial distribution of junctions within a sphere of radius $< r^2 >_i^{1/2}$, the average number of junctions within the sphere, N_j is given by equation 1.4b.

$$N_j = (2\pi / 3M_c)\rho\, N_A < r^2 >_i^{3/2} \qquad \text{eq.1.4b}$$

M_c is the molecular weight of chains between cross-links

ρ is the density of the chains (weight per unit volume)

The end to end separation of a network chain is essentially equal to that of a free unperturbed chain having the same molecular weight. Therefore $\langle r^2 \rangle_i$ can be replaced by $\langle r^2 \rangle_o = (C_\infty M_c/M_o)\, l^2$, (where M_o = the average molecular weight of a skeletal bond) giving equation 1.4c.

$$N_j = \left(\frac{2\pi}{3}\right) \rho\, N_A \left(\frac{C_\infty l^2}{M_o}\right)^{3/2} M_c^{1/2} \qquad \text{eq.1.4c}$$

During the cross-linking of a polymer system, a network structure that extends continuously throughout the specimen becomes insoluble when the average number of cross-links per primary molecule, γ, becomes sufficiently large, this is called the gel fraction. Any polymeric material not part of the network structure including linear or branched molecules of low molecular weight is called the sol fraction, w_s. The amount of sol depends on γ, if all the primary molecules are monodisperse, then γ is given by equation 1.4d.

$$\gamma = -\ln w_s/(1-w_s) \qquad \text{eq.1.4d}$$

The equilibrium modulus of a network is proportional to the concentration of load-bearing/effective chains, it is necessary to consider network imperfections and also permanent or trapped entanglements. The entanglements give rise to elastically effective chains that typically contribute to the modulus, along with the chains terminated solely by cross-links. However, it is not possible to state precisely the number of effective chains that result from each entanglement.

When a stress is applied to a network, the random molecular motions are perturbed and the network chains seek new configurations to compensate for stress. The viscous resistance of the network to these forces is related to intersegmental forces, energy

barriers and its allowable configurations. At high temperatures the chains in many networks rearrange rapidly and equilibrium stress-strain data can be readily obtained. If a network contains a high sol fraction, with highly branched structures, then equilibrium takes a long time to establish. If temperature is lowered then changes in configuration are slow, below the T_g of polymer constituents, configurations are frozen in and only short-range motions are effected by thermal energy.

1.4.4 Structure of polymer networks

In general, network chains exhibit a distribution of molecular weights about an average, which serves as a representative reference quantity in describing network structure. A network may have two or more sets of junctions with different functionalities, it can then be characterised by an average functionality. If a network has no dangling chains or loops with functionality greater than two, it is called a perfect (model) network. This can never be achieved in reality, but forms a reference structure around which molecular theories are constructed.

The topological structure of a perfect network may be described by various parameters[58]. The average molecular weight between cross-links, M_c, the average functionality, ϕ, the number of network chains, υ, the number of junctions, μ, and the cycle rank, ξ, which denotes the number of chains that have to be cut in order to reduce the network to a 'tree' with no closed cycles. For a perfect network, the number of chain ends, 2υ, has to be equal to the number of functional groups, $\phi\mu$, on the end-linking molecules, and equation 1.4e gives:

$$\mu = 2\upsilon/\phi \qquad \text{eq.1.4e}$$

The parameters are also related to each other by using equations 1.4f and 1.4g in the following manner:

$$\xi = (1\text{-}2/\phi)\upsilon \qquad \text{eq.1.4f}$$

$$\xi / V_o = \frac{(1-2/\phi)\rho}{M_c / N_A} \qquad \text{eq.1.4g}$$

V_o is the volume of network in the state of formation

ρ is the corresponding density

N_A is Avogadro's number

The equations require modifications for the case of imperfect networks.

The molecular theory of polymer networks rests on the postulate that the elastic free energy of a network is equal to the sum of the elastic free energies of the individual chains. The chains in a network formed in the amorphous bulk state exhibit unperturbed dimensions identical to that of a single chain in θ solvents. For sufficiently long chains, typically with 100 or more skeletal bonds, the distribution can be approximated by a Gaussian function, $W(r)$, given in equation 1.4h.

$$W(r) = (3/2\pi\langle r^2\rangle_o)^{3/2} \exp(-3r^2/2\langle r^2\rangle_o) \qquad \text{eq.1.4h}$$

$\langle r^2\rangle_o$ denotes the mean-squared value of r for an unperturbed free chain

The total elastic free energy ΔA_{el} of the network relative to the undeformed state is obtained by summing the elastic free energy of one chain over the υ chains of the network to give equation 1.4i.

$$\Delta A_{el} = \frac{3}{2}\upsilon kT\left(\frac{<r^2>}{<r^2>_o} - 1\right) \qquad \text{eq.1.4i}$$

$<r^2> = \sum r^2/\nu$ represents the average of the mean-squared end to end chain vectors in the deformed network

The affine and the phantom network models are the two simplest molecular models employed in relating the deformation of the chains to macroscopic deformation. The affine network model assumes that the junction points are embedded in the network. Therefore relating this to the principal extension ratios, $\lambda_{x,\,y\text{ or }z}$ in the affine system, the elastic free energy of the network in the affine state is given by equation 1.4j

$$\Delta A_{el} = \frac{\nu kT}{2}(\lambda_x^2 + \lambda_y^2 + \lambda_z^2 - 3) \qquad \text{eq.1.4j}$$

The phantom network model has junction points that fluctuate over time without being hindered by the presence of the neighbouring chains. The extent of the fluctuations is not affected by the macroscopic state of deformation. The elastic free energy for the phantom network is given by equation 1.4k.

$$\Delta A_{el} = \frac{\xi kT}{2}(\lambda_x^2 + \lambda_y^2 + \lambda_z^2 - 3) \qquad \text{eq.1.4k}$$

Differences between the two models arise specifically from the nature of transformations of chain dimensions, built in the models of the elementary theory. A real network is expected to exhibit properties that fall between those of the affine and phantom network models, in that junction fluctuations occur but not to the extent present in the phantom limit. A quantitative model of a network with fluctuations of junctions, dependent on the macroscopic state of strain, is given by the constrained junction model of real networks. In this model, a given junction is assumed to be under the joint action of the phantom network and the constraint domains. The elastic free energy of the network is obtained as the sum of the phantom network and constraint free energies, ΔA_{ph} and ΔA_c in equation 1.4l.

$$\Delta A_{el} = \Delta A_{ph} + \Delta A_c \qquad \text{eq.1.4l}$$

The elastic free energy due to constraints is given in terms of the components of the principal extension ratios in equation 1.4m.

$$\Delta A_c = \frac{\mu kT}{2} \sum [B_t + D_t - \ln(B_t + 1) - \ln(D_t + 1)], \qquad t = x, y, z \qquad \text{eq.1.4m}$$

$B_t = \kappa^2(\lambda_t^2 - 1)(\lambda_t^2 + \kappa)^{-2}$

$D_t = \lambda_t^2 \kappa^{-1} B_t$

κ is a quantitative measure of the strength of the constraints, that can be interpreted in terms of the molecular constitution of the network, by assuming it to be proportional to the average number of junctions in the domain, occupied by a network chain. This is given as equation 1.4n.

$$\kappa = I(2/\phi)(N_A d)(\langle r^2\rangle_o/M)^{3/2}M_c^{1/2} \qquad \text{eq.1.4n}$$

I is the constant of proportionality

d is the network density

M is the molecular weight of a chain with end to end mean-square length $\langle r^2\rangle_o$

1.4.5 Mechanical properties and structure of polymer network elastomers

When considering experiment with theory, the three main relationships considered are; equilibrium stress-strain studies, the relationship between network topology and modulus, and thermoelastic properties[57].

In statistical treatments of cross-linking linear polymers, networks are usually treated without any occurrence of chain scission. At the gel point, the concentration of the cross-links in the gel is two-fold greater than in the sol fraction, and the gel fraction approaches unity. Information with regards to the number of cross-links, the terminal chains in the network, the sol fraction, and the number of trapped entanglements all lead to the determination of the cross-link density of the network. This in turn influences the modulus of the network. The swelling of elastomers is a method of calculating the cross-link density of a network, however, an accurate value for the polymer solvent interaction parameter is required for the calculation. According to theory[59], the modulus of the network depends on:

1. The concentration of junctions in the gel and the gel fraction in the sample
2. The fraction of junctions in the gel to which terminal chains or dangling ends are attached

3. The concentration of elastically effective chains that result from trapped entanglements

4. A parameter called the front factor

The molecular theory of rubber elasticity has been proved essential for estimating the concentration of effective chains in a network and thus the average weight associated with each chain. Provided the tensile or shear modulus of a network is known, the elastic behaviour under any type of deformation can be predicted well within the range of Gaussian behaviour.

Methods based on end-linking polymer molecules in order to synthesise model networks, fulfil as much as possible the requirements of ideality[60,61]. Polymers are synthesised so as to possess a narrow molecular weight distribution and reacted with a multifunctional cross-linking agent in stoichiometric amounts. The functionality of the network being that of the cross-linking agent. Networks are produced with precisely known average molecular weight of polymer chains that possess a narrow distribution. The formation of loops in the end-linking reaction is possible, especially when the reaction is carried out at a low polymer concentration or when the molecular weight of the precursor chain is low.

1.4.6 Stretching polymer networks

When a network is subjected to a force, the sample is put under a reduced stress [σ^*] which is independent of deformation in both the phantom or affine network models. The reduced stress can be plotted against the reciprocal extension ratio, λ^{-1} and compared to the two models of a network. The networks are studied at a temperature above the glass transition of the two polymer constituents in the network system. At high deformations,

stress-strain data in elongation are interpreted in terms of the reduced stress given by equation 1.4o

$$[\sigma^*] = \sigma / [A^* (\lambda - \lambda^{-2})] \qquad \text{eq.1.4o}$$

A^* is the cross-sectional area of the sample

σ is the elastic force on the sample

λ is the elongation of the sample

The resulting $[\sigma^*]$ values can then be plotted against reciprocal elongation data and fitted to the Mooney-Rivlin expression[62,63] in equation 1.4p.

$$[\sigma^*] = 2C_1 + 2C_2\lambda^{-1} \qquad \text{eq.1.4p}$$

$2C_1$ and $2C_2$ are constants independent of λ

$2C_1$ is taken as an estimate of the high deformation modulus (phantom model) whilst $2C_1 + 2C_2$ are taken as an estimate for the low deformation modulus (affine model) and is given by equation 1.4q.

$$2C_1 + 2C_2 = \frac{A_\phi' \rho RT \nu_{2C}^{-2/3}}{M_c} \qquad \text{eq.1.4q}$$

A_ϕ' is the structure factor which should be equal to unity at low deformations

ρ is the density of the network

R is the gas constant

T is absolute temperature

$\bar{v}_{2C}$ represents the average value of the volume fraction of polymer present during cross-linking

The elasticity constant $2C_2$ is a measure of the extent to which the elongation changes from the affine to phantom limit with increasing stress. Therefore it is directly related to the looseness with which the cross-links are embedded in the network structure.

The plot below shows a comparison of data for unswollen and swollen networks. Forces are exhibited ranging in values from those close to the affine model in compression and at low extensions, through to values close to the phantom model at high extensions. This behaviour is shown in figure 1.4b.

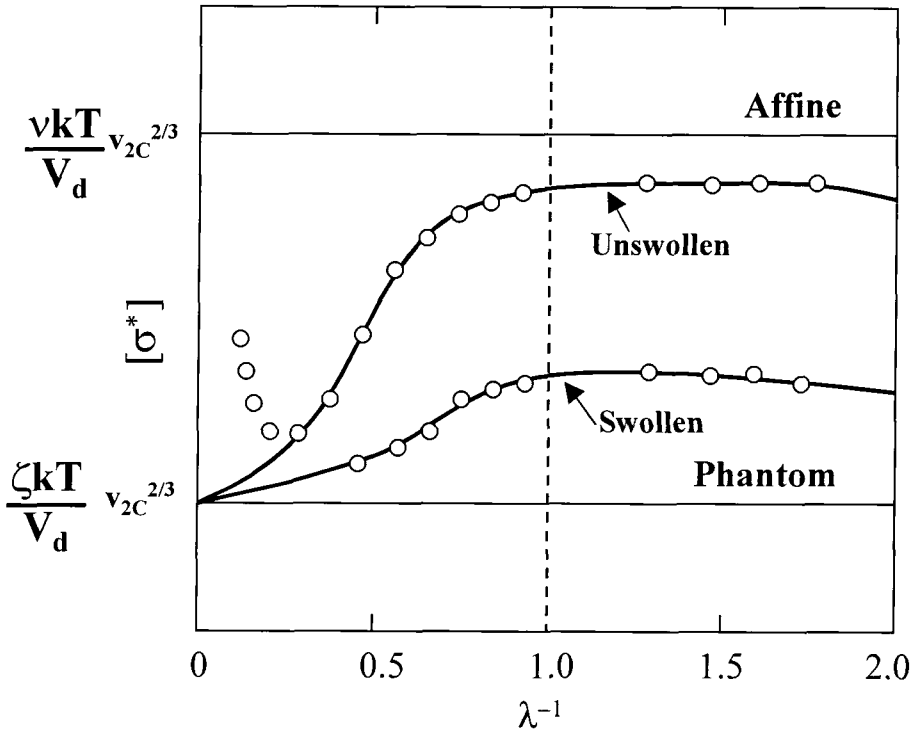

Circles show representitive data from experiments
Curves are from the constrained junction theory

Figure 1.4b Reduced stress as a function of reciprocal extension ratio for a swollen and unswollen polymer network

The effect of cross-link functionality can be analysed by plotting a curve of $2C_2/2C_1$ against network chain molecular weight. The conclusion being that an increase in functionality increases the modulus, $2C_1$. $2C_2$ decreases because if more chains are emanating from a cross-link the more constrained the network is. The ratio $2C_2/2C_1$ decreases with a reduction of network chain molecular weight, due to the decrease in configurational interpenetration in the case of short network chains. This decreases the firmness with which the cross-links are embedded, so the deformation is already affine at small deformations.

Dangling chains acting as network irregularities decrease the ultimate strength of the network. The highest strengths of networks are obtained when the networks are prepared by selectively joining functional groups occurring at chain ends. This is because that these networks possess fewest dangling ends.

Deformation studies show that if a network is dry the chains have unperturbed dimensions. However, swollen networks at equilibrium in good solvents exhibit a radius of gyration of the chain to be equal to that of a corresponding free chain in the same solvent. The molecular deformation induced by strain or swelling is in between that for the affine and phantom network models. Rearrangement of the junctions in the deformation process is strongly dependent on the mesh size of the network. For highly cross-linked bulk networks, few arrangements of the neighbours are allowed, therefore affine behaviour is expected. If the molecular weight between the chains is increased, the spatial rearrangement of the junctions will become more favoured, and the network now behaves more like the phantom model.

1.4.7 Ball-Edwards Slip model analysis of polymer network structures

The deviations from classical statistical elasticity theory for undiluted elastomer networks are currently attributed to the presence of chain entanglements. Theory states that the free energy, $\widetilde{F}$, of single chains between cross-links, N_c, to be proportional to the sum of squares of the principal extension ratios given in equation 1.4r.

$$\frac{\widetilde{F}}{kT} = \frac{N_c}{2}\sum_{i=1}^{3}\lambda_i^2 \qquad \text{eq.1.4r}$$

Stress-strain relations in polymer systems have been analysed using the slip-link model[64]. Complicated entanglements such as those in figure 1.4a are represented by the constraint of a contact through which each chain is free to slide. Physically, the presence of other entanglements due to chemical cross-links will restrict the extent to which the links can slide independently along either of their connecting chains. This will be put in the calculations as the freedom to slide only an arc length ±a in any one direction, shown in figure 1.4c.

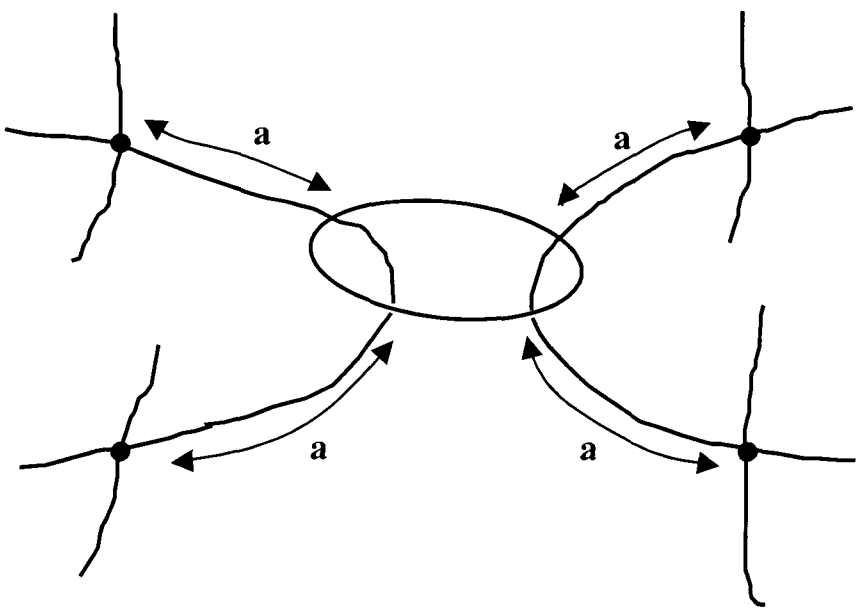

Figure 1.4c Fundamental basis of the slip-link model

The parameter a, will be related to the total number of slip-links, N_s, and the total number of chemical cross-links, N_c. Calculation of the free energy caused by such a link can be made in terms of the two link parameters[65]. The contribution of a sliding link to the strain dependence of the free energy of shear, $\widetilde{F}$ of a Gaussian network leads to a sum of the same functions of each extension ratio $\lambda_1\lambda_2\lambda_3$ shown in equation 1.4s.

$$\frac{\widetilde{F}}{k_B T} = \frac{N_C}{2}\sum\lambda_i^2 + \frac{N_S}{2}\sum\left[\frac{(1+\eta)\lambda_i^2}{1+\eta\lambda_i^2} + \log(1+\eta\lambda_i^2)\right] \qquad \text{eq.1.4s}$$

k_B is the Boltzman constant

T is the temperature

η is a relative measure of the freedom of a link to slide

When $\eta = 0$, the N_s entanglements induce the same strain dependence as the N_c cross-links and equation 1.4r would predict the free energy of a phantom network[66]. An argument minimising $\widetilde{F}$ leads to the conclusion that $\eta = 0.2343$ if each slip-link can on average slide as far as the centres of its topologically neighbouring links[65]. Physical freedom restriction of slip is possibly close to η in this case, however, η is considered as a material parameter, the actual value of which should be determined by comparing equation 1.4s to experimental evidence with N_c and N_s directly related to the networks structure.

An additional problem of finite network extensibility due to the constraints imposed by the topological entanglements was considered by Edwards *et al*[67]. The number of physical entanglements determine the step length of the reptation tube primitive path. The length of a polymer chain within the tube is far greater than the length of the

primitive path, therefore a large proportion of the chain is 'slack'. The chain is considered to be terminated by a cross-link at each end, and therefore no reptation is possible. As the network is deformed, the main consideration is the amount of slack chain between entanglements, which is gradually reduced until the chain is taut. This limits the extensibility of the chains long before the single chain limit is reached. So an additional parameter α, equal to l/a, where l is the Kuhn step length, and a, the step length of the primitive path. The full expression for the free energy is given in equation 1.4t[67].

$$\frac{\tilde{F}}{k_B T} = \frac{N_C}{2}\left[\frac{\sum(1-\alpha^2)\lambda_i^2}{1-\alpha^2\sum\lambda_i^2} + \ln(1-\alpha^2\sum\lambda_i^2)\right] + \frac{N_S}{2}\left[\sum\left\{\frac{(1+\eta)\lambda_i^2(1-\alpha^2)}{(1+\eta\lambda_i^2)(1-\alpha^2\sum\lambda_i^2)} + \log(1+\eta\lambda_i^2)\right\} + \ln(1-\alpha^2\sum\lambda_i^2)\right] \quad \text{eq.1.4t}$$

If the values of α (no extensibility) and η (slip-links as rigid cross-links) are put to zero then the classical result for a phantom network is obtained (equation 1.4r). Thirion and Weil[68] in their study of chemical cross-linked rubbers, determined η experimentally, and found a best fit for η = 0.40. Their work showed η to be independent of N_c and molecular structure.

For uniaxial deformation maintained by a single positive stress, σ, along the direction of extension, λ, the reduced stress $\sigma^* = \sigma/(\lambda-\lambda^{-2})$ of the model is given by equation 1.4u. For uniaxial deformation the incompressibility condition is applied, $\lambda_1=\lambda$, $\lambda_2=\lambda_3=\lambda^{1/2}$.

$$\frac{\sigma}{\lambda-\lambda^{-2}} = kT\left[N_c + N_s H(\eta,\lambda)\right] \quad \text{eq.1.4u}$$

σ is the force per unstrained area, equal to $\mathrm{d}\tilde{F}/\mathrm{d}\lambda$, and $H(\eta,\lambda)$ is given as equation 1.4v.

$$H(\eta,\lambda)=\frac{\lambda^2}{\lambda^2-\lambda+1}\left[\frac{1}{(\lambda+\eta)^2}+\frac{\lambda+1}{\lambda(1+\eta\lambda^2)^2}\right] \qquad \text{eq.1.4v}$$

Thus the reduced stress σ^* plotted against the function H, gives N_c and N_s from the slope and intercept as η is iterated so as to give the best linear fit to data.

The calculated values from the initial fit can now be used as initial guesses to fit all the data to equation 1.4t using a least squares criterion to obtain the best values of N_c, N_s, η and α.

1.5 References

[1] Bailey, J.T.; Bishop, E.T.; Hendricks,W.R.; Holden, G.; Legge, N.R. *Rubber Age* **1966,** *98*, 69

[2] Childers, C.W.; Kraus, G. *Rubber Chem. Technol.* **1967,** *40*, 1183

[3] Hendus, H; Illers, K.H.; Ropte, E. *Kolloid-Z.* **1967,** *110*, 216

[4] Helfand, E. *Acc. Chem. Res.* **1975,** *8*, 295

[5] Helfand, E.; Wasserman, Z.R. *Polym. Eng. Sci.* **1977,** *17*, 535

[6] de Gennes, P.G. *Faraday Discuss. Chem. Soc.* **1979,** *68*, 96

[7] Sakurai, S.; Iwane, K.; Nomura, S. *Macromolecules* **1993,** *26*, 5479

[8] Morton, M.; Fetters, L.J. *Rubber Chem. and Tech.* **1975**, *48*, 359

[9] Odian, G. *Principles of polymerisation,* 2nd Ed. **1981**, 372

[10] Bates, F. S.; Fredrickson, G. H. *Journal. Rev. Phys. Chem.* **1990,** *41*, 525

[11] Fredrickson, G.H.; Bates, F.S. *Annu. Rev. Mater. Sci.* **1996,** *26*, 501

[12] Mark, J.E. *Physical Properties of Polymers Handbook* CD-ROM ISBN, **1996**

[13] Hashimoto, T.; Hasegawa, H.; Kawai, H.; Shibayama, M. *Macromolecules* **1983,** *16*, 1427

[14] Hashimoto, T.; Shibayama, M.; Kawai, H. *Macromolecules* **1983,** *16*, 1093

[15] Shibayama, M.; Hashimoto, T.; Kawai, H. *Macromolecules* **1983,** *16*, 1437

[16] Bates, F. S.; Berney, C. V.; Cohen, R. E. *Macromolecules* **1983,** *16*, 1101

[17] Roe, R. J.; Fishkis, M.; Chang, J. C. *Macromolecules.* **1981,** *14*, 1091

[18] Helfand, E.; Wasserman, Z.R. *Dev. Block Copolym.* **1982,** *1*, 99

[19] Semenov, A. N. *Soviet Phys. JETP* **1985,** *61*, 733

[20] Ohta, T.; Kawasaki, K. *Macromolecules* **1986,** *19*, 2621

[21] Skoulios, A. In *Block and Graft Copolymers*; Burke, J.J., Weiss, V., Eds.; Syracuse University Press: Syracuse, NY, **1973**

[22] Sadron, C.; Gallot, B. *Makromol. Chem.* **1973,** *164*, 301

[23] Leibler, L. *Macromolecules* **1980,** *13*, 1602

[24] Förster, S.; Khandpur, A.K.;Zhao, J. et al *Macromolecules* **1994,** *27*, 6922

[25] Khandpur, A.K.; Förster, S.;Bates, F.S.; Hamly, I.W.; Ryan, A.J.; Bras, W.; Almdal, K.; Mortensen, K. *Macromolecules* **1995,** *28*, 8796

[26] Fredrickson, G. H.; Helfand, E. *J. Chem. Phys.* **1987,** *87*, 697

[27] Legge, N.R.; Holden, G.; Schroeder, H.E. (Eds.) *Thermoplastic Elastomers, Hanser Publishers, New York* **1987.**

[28] Holden, G.; Bishop, E.T.; Legge, N.R. *J. Polym. Sci.* **1969,** Pt.C. *26*, 37

[29] Kraus, G.; Naylor, F.E.; Rollman, K.W. *J. Polym. Sci.* **1971,** Pt.A-2. *9*, 1839

[30] Hashimoto, T.; Fujimura, M.; Kawai, H. *Macromolecules* **1980,** *13*, 1660

[31] Kinning, D.J.; Thomas, E.L. *Macromolecules* **1984,** *17*, 1712

[32] Todo, A.; Uno, H.; Miyoshi, K.; Hashimoto, T.; Kawai, H. *Polym. Eng. Sci.* **1977,** *17*, 587

[33] Keller, A.; Pedemonte, E.; Wilmouth, F.M. *Kolloid Z.* **1970,** *238*, 385

[34] Hashimoto, T.; Shibayama, M.; Kawai, H. *Macromolecules* **1980,** *13*, 1237

[35] Mayer, R. *Polymer* **1974,** *15*, 137

[36] Duoy, A.; Mayer, R.; Rossi, J.; Gallot, B. *Mol. Cryst. Liq. Cryst.* **1969,** *7*, 103

[37] Vonk, C.G.; Balta-Calleja, F.J. *X-ray scattering of synthetic polymers Jenkins, A.D.(Ed.)* **1989**

[38] Howard, R.N. *The Physics of Glassy Polymers, Applied Science Publishers, London* **1973**

[39] Cullity, B.D. *Elements of x-ray diffraction, Addison Wesley, 2nd Edition,* **1978**

[40] Ruland, W *J. Appl. Cryst.* **1971,** *4*, 70

[41] Koberstein, J.T.; Morra, B.; Stein, R.S. *J. Appl. Cryst.* **1980,** *13*, 34

[42] Bonart, R.; Muller, E.H. *J. Macromol. Sci.-Phys.* **1974,** *B10(1)*, 177

[43] Helfand, E. *Accounts of Chemical Research,* **1975,** *8*, 295

[44] Kortleve, G.; Vonk, C.G. *Kolloid-Z.* **1968,** *225*, 124

[45] Vonk, C.G. *J. App. Cryst.* **1973,** *6*, 81

[46] Kratky, O.; Stabinger, H. *Anton paar manual 'Kratky Compact Small Angle System'* **1984**

[47] Flory, P.J. *Principles of Polymer Chemistry, Cornell University Press, Ithaca (N.Y.)* **1953**

[48] Seidl, J. *et al Adv. Polym. Sci.* **1967,** *5*, 113

[49] Chen, R.Y.S.; Yu, C.U.; Mark, J.E. *Macromolecules* **1973,** *6*, 746

[50] Mark, J.E. *Die Angewandte Makromolekulare Chemie* **1992,** *202-203*, 1

[51] Flory, P.J. *Statistical Mechanics of chain molecules, Wiley, New York,* **1969**

[52] Rouf-George, C.; Munch, J.P.; Beinart, G.; Isel, F.; Pouchelon, A.; Palierne, J.F.; Boue, F; Bastide, J. *Polymer Gels and Networks* **1996,** *4*, 435

[53] Sharaf, M.A.; Mark, J.E.; Cesca, S. *Polymer Engineering and Science* **1986,** *26*, 304

[54] Dossin, L.M.; Graessley, W.W. *Macromolecules* **1979,** *12*, 123

[55] Dakin, V. *Radiat. Phys. Chem.* **1995,** *45*, 715

[56] Colo, S.M. *Analitica Chim. Oggi.* **1986,** *9*, 29

[57] Treloar, L.R.G. *The Physics of Rubber Elasticity, 2nd Edition, Oxford Univ. Press (Claendon), London and New York,* **1958**

[58] Mark, J.E.; Erman, B. *Rubberlike Elasticity, A Molecular Primer. Wiley and sons,* **1989**

[59] Mark, J.E. *Advances. Polym. Sci.* **1982,** *44*, 1

[60] Meyers, K.O.; Bye, M.; Merrill, E.W. *Macromolecules* **1980,** *13*, 1045

[61] Gottlieb, M. *et al Macromolecules* **1981,** *14*, 1030

[62] Mooney, M. *J. Appl. Phys.* **1948,** *19*, 434

[63] Rivlin, R.S. *Phil. Trans. Roy. Soc. London Ser. A* **1948,** *241*, 379

[64] Brereton, M.G.; Klein, P.G. *Polymer* **1988,** *29*, 970

[65] Ball, R.C.; Doi, M.; Edwards, S.F.; Warner, M. *Polymer* **1981,** *22*, 1010

[66] Deam, R.T.; Edwards, S.F. *Phil. Trans. Roy. Soc. Lond.* **1976,** *280*, 317

[67] Edwards, S.F.; Vilgis, Th. *Polymer* **1986,** *27*, 483

[68] Thririon, P.; Weil, T. *Polymer* **1984,** *25*, 609

CHAPTER 2

Experimental

2.1 Synthesis of block copolymers and block copolymer networks

2.1.1 Anionic Polymerisation

Polymers unlike small molecules do not have a specific molecular weight, instead they consist of a distribution of chain lengths that can be described by various molecular weight averages[1,2]. As many polymer properties are dependent upon the molecular weight, it is useful to be able to prepare polymers in such a way as to control the molecular weight with a narrow molecular weight distribution. For many monomers containing a vinyl group capable of sustaining a nucleophilic centre, the technique of anionic polymerisation provides a quick and efficient method of preparing polymers of predictable molecular weight and a narrow polydispersity. The reaction is a homogeneous addition polymerisation, which in the absence of compounds containing an active hydrogen has no inherent termination step and is said to be a 'living' polymerisation[3].

There are two steps in anionic polymerisation. Firstly an initiating species adds across the double bond of the monomer to produce a reactive anionic species, which in the second propagation step reacts with a second monomer molecule giving a reactive dimer and so on until all of the monomer is consumed. If the rate of initiation of the chains is relatively fast with respect to the rate of propagation, the chains will all have an equal probability of growth and the molecular weight distribution of the resulting polymer will be narrow, approaching Poisson statistics[4].

Initiator species for anionic polymerisation are frequently organolithium compounds, which are useful as they are soluble in a wide range of organic solvents and initiate

polymerisation by direct anionic attack on the monomer to produce the propagating species[5]. In the anionic polymerisation of styrene, (secondary)-butyllithium has been found to be highly effective in the production of 'monodisperse' polystyrene samples. The initiation step proceeds by nucleophilic attack at the vinyl bond by the (s)-butyllithium shown in figure 2.1a. The resultant anionic species is stabilised by the electron withdrawing effect of the phenyl ring adjacent to the anion.

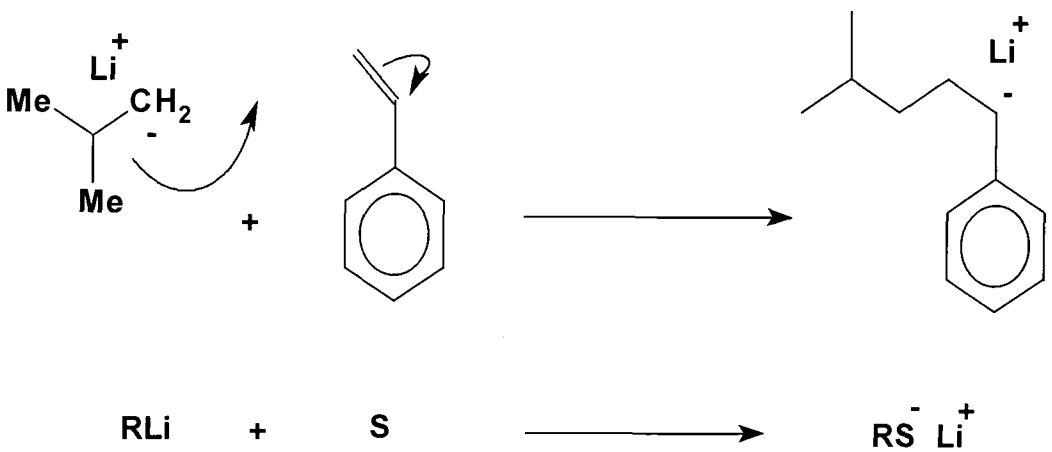

Figure 2.1a Initiation of styrene with s-butyllithium to form poly(stryllithium)

Propagation of the polystyrene chain then proceeds by subsequent addition of monomer to the poly(styryllithium) until there is complete consumption of the monomer by the growing polymer chain.

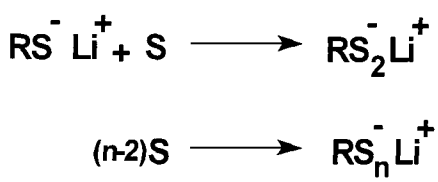

To synthesise a block copolymer, polybutadiene may be introduced into the living system once all the styrene monomer has been consumed. The 1,4 polybutadiene isomer propagates via a concerted four-centre reaction between the incoming monomer and the σ-bonded carbon lithium bond shown in figure 2.1b. Polymers containing a high

proportion of 1,4 isomers are preferred to 1,2 polybutadiene so that end-link network formation is efficient after monomer consumption is complete.

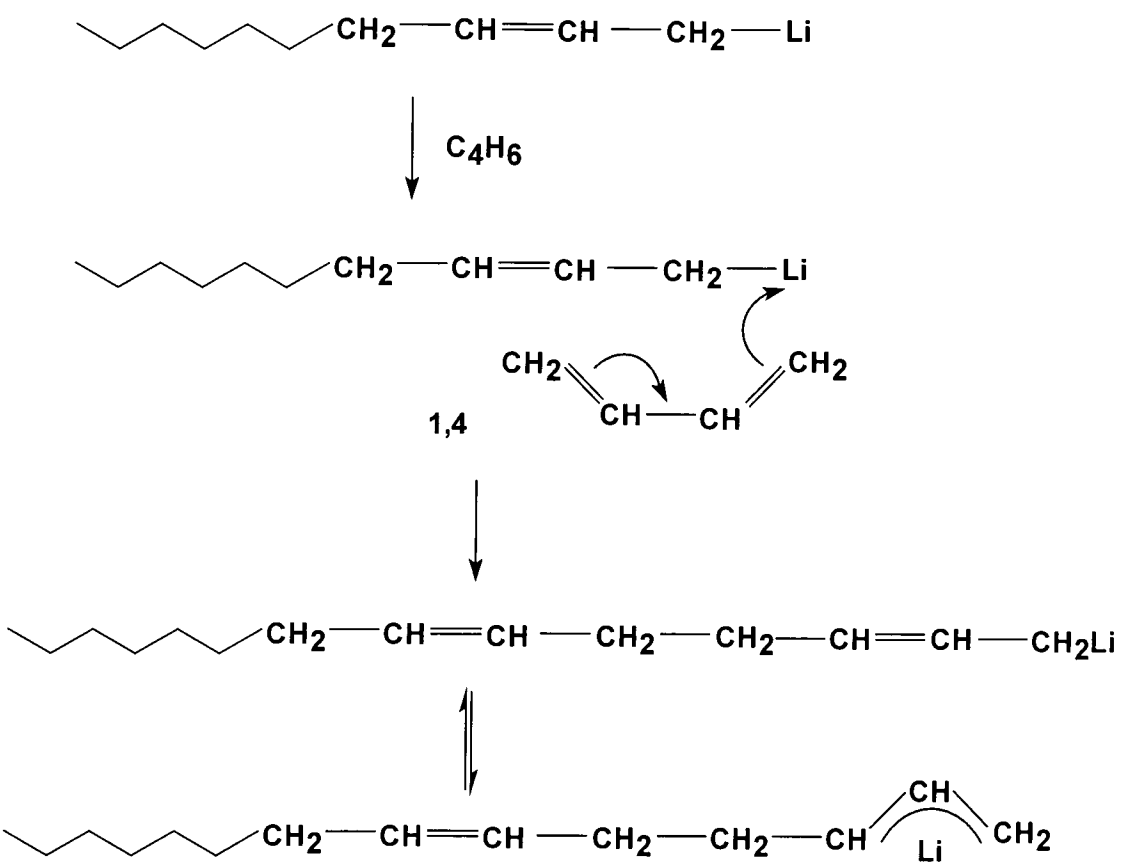

Figure 2.1b Mechanism for 1,4 polybutadiene propagation

The propagating centre of the living polymer will remain intact in the absence of any proton source. Termination of the living chain can then be brought about by the addition of a proton source such as methanol shown in figure 2.1c.

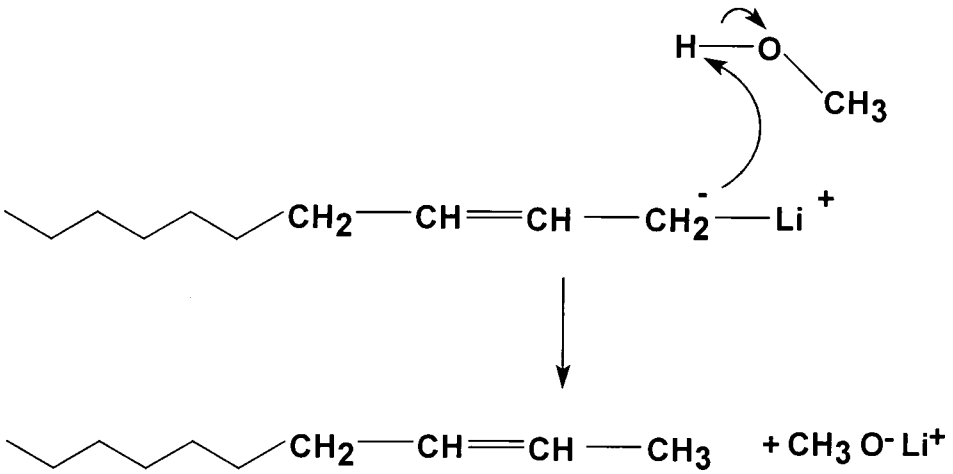

Figure 2.1c Termination of living polybutadiene with methanol

'Monofunctional' initiators such as (s)-butyllithium induce the propagation of the living anion along the growing chain, i.e. from one end of the chain to the other producing monofunctional polystyryl anions, the size of these polymer chains being related to the ratio of monomer and initiator:

$$DP = \frac{\text{mols monomer}}{\text{mols initiator}} \qquad \text{eq.2.1a}$$

Similarly:

$$M_n = \frac{\text{mass monomer (g)}}{\text{mols initiator}} \qquad \text{eq.2.1b}$$

2.1.2 Initiators

In order to prepare polybutadiene-polystyrene-polybutadiene (BSB) networks, it is necessary to prepare a living copolymer with a reactive anionic site at either end of the chain that can then be cross-linked to form a network. This is possible by the use of a difunctional initiator. Propagation of the polymer chain occurs from the centre outwards, as opposed to the monofunctional initiator in which the chain grows from one

end. The type of difunctional initiator available for the preparation of the living triblock copolymer dianion was based on a difunctional organolithium compound.

A series of difunctional dilithium initiators have been prepared which will initiate the polymerisation of styrene[6,7]. One of the most commonly used of these initiators is 1,3-phenylenebis(4-methyl-1-phenylpentylidene)dilithium[8,9] which is prepared by the reaction of a divinyl compound, 1,3-bis(1-phenylethenyl)benzene with two equivalents of s-butyllithium. Self polymerisation of the diolefin is prevented by the large steric bulk of the phenyl rings adjacent to the vinyl groups[8].

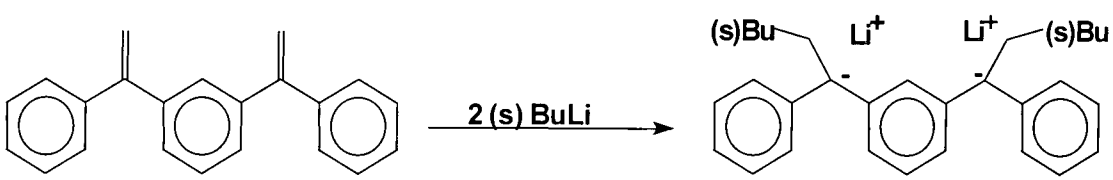

Figure 2.1d Preparation of the difunctional lithium initiator 1,3-phenylenebis(4-methyl-1-phenylpentylidene)dilithium from 1,3-bis(1-phenylethenyl)benzene

The dilithium initiator, soluble in both polar and non-polar solvent initiates the styrene polymerisation by direct anionic attack upon the vinyl group of the styrene. Propagation then proceeds as described earlier.

The molecular weight of a polymer prepared using a difunctional initiator follows the simple relationship:

$$M_n = \frac{\text{mass monomer (g)}}{0.5 \text{ mols initiator}} \qquad \text{eq.2.1c}$$

Polymerisations carried out using the dilithium initiator require the introduction of a polar component to promote initiation and give narrow, monomodal molecular weight distributions for high molecular weight polymers. In the absence of a polar component polymerisation produces systems that possess bimodal molecular weight distributions. Tetrahydrofuran (THF) can be used in order to achieve mondisperse systems, but will result in a higher proportion of the undesired 1,2 isomer of polybutadiene when it polymerises. The 1,2 isomer is produced rather than the desired 1,4 isomer of butadiene, 1,2 addition being preferred in a polar environment because of the attack of incoming monomer at the γ-carbon, π-bonded to the lithium. The mechanism is shown in figure 2.1e.

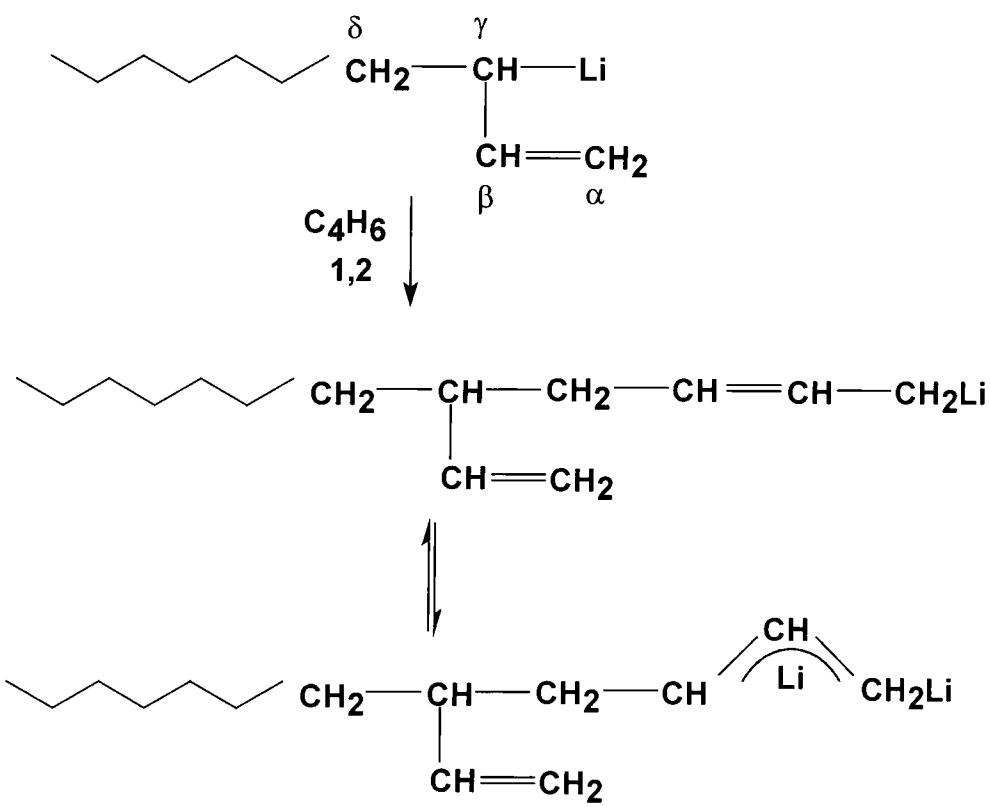

Figure 2.1e Synthetic route of 1,2 polybutadiene propagation

The presence of polar additives leads to an increase in the side-vinyl chain content of the polymer, the formation of side-vinyl units (1,2 or 3,4) relates to the increasing ionic

character of the carbon-metal bond which occurs by solvation of the metal cation. Therefore a suitable polar component is needed to polymerise the styrene efficiently with a monomodal molecular weight distribution whilst not disrupting the microstructure of the butadiene. The polar component used to do this is lithium sec-butoxide (LiOBu), added in a molar ratio of 1.1:1 with respect to lithium in the initiator. The lithium sec-butoxide cross-associates with the dilithium initiator to form a statistical distribution of mixed aggregates, which initiate to give a monomodal molecular weight distribution[8].

2.1.3 Procedure

In order to be able to prepare monodisperse polymers reliably by anionic polymerisation, two experimental criteria must be satisfied. Firstly the rate of initiation should be comparable or preferably faster than the rate of propagation. This can be achieved by a careful choice of initiator and solvent. Secondly the monomers and solvents used must be extremely dry and free from all impurities so as to prevent termination of the polymerisation. This can only be achieved using specially dried and purified monomers and solvents and by polymerising them under either an inert atmosphere or under vacuum.

2.1.3.1 Solvents

Benzene (Aldrich) was freed from thiophene by washing with concentrated sulphuric acid. The sulphur free benzene was then washed with distilled water until all the acid had been removed and was subsequently dried over magnesium sulphate for 24 hours. The benzene was then filtered and distilled under a dry nitrogen atmosphere, the fraction

boiling at 350K was collected and separated into 250 cm^3 portions. The benzene was then further dried by stirring over ground calcium hydride and degassed by repeated freeze-thaw cycles until a pressure of 10^{-2} mbar was maintained above the frozen benzene. The benzene was rapidly stirred in between freeze-thaw cycles and was degassed immediately before use.

THF (laboratory grade, 99+%) was refluxed over sodium wire and benzophenone for around three hours under a dry nitrogen atmosphere until a dark blue-purple coloration dominated showing the absence of moisture. The dried THF was then distilled off under a dry atmosphere and separated into 250 cm^3 portions to which a small amount of benzophenone was added with a slight excess of sodium wire, again a purple coloration dominated. The distillate flask was then connected to the vacuum line and the THF thoroughly degassed by repeated freeze-thaw cycles until a pressure of 10^{-2} mbar was maintained above the frozen solvent.

2.1.3.2 Preparation of monomers

Styrene (99%) was firstly freed from inhibitor (~15 ppm di-tert-butyl catechol) by a thorough washing with a 10% NaOH solution. The inhibitor free styrene was then washed with distilled water until all of the NaOH had been removed and was then dried over magnesium sulphate for 24 hours before vacuum distillation at a pressure of 40 mbar. The fraction boiling at 338 K was collected and was separated into 125 cm^3 portions. Freshly ground calcium hydride was then added to the distillate flask and the flask connected to the high vacuum line. The styrene was then degassed by repeated freeze-thaw cycles until a pressure of 10^{-2} mbar was maintained over the styrene. The styrene was stirred vigorously in between freeze-thaw cycles and was protected from

light between degassing cycles. Despite being wrapped in foil after some time the styrene became viscous due to the formation of small amounts of low molecular weight polymer via photoinitiation. The styrene was always degassed immediately prior to use in a polymerisation.

1:3 butadiene (Aldrich, 99+%) was purified by passing the gas through a column of BDH Carbosorb AS (NaOH supported on silica) dried under vacuum at 413K. This was to remove the p-tertiary butyl catechol inhibitor and was followed by a column containing 3A molecular sieve, to remove water. The monomer is collected as a liquid by cooling the receiver in an acetone/dry ice bath at 195K. The receiver is transferred to an iced water bath, the pressure of the butadiene in the flask is enough to allow distillation of the monomer in to the polymerisation reaction flask and copolymerisation occurs.

2.1.3.3 Preparation of secondary lithium butoxide

The synthesis of LiOBu involves the titration of n-butyl lithium (Aldrich, 2.0M solution in cyclohexane) with sec-butanol (Aldrich, 99.5%) using 1,10 phenanthroline (Aldrich) as an indicator. The chemical formula of the indicator is shown below in figure 2.1f.

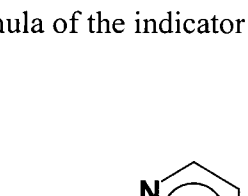

Figure 2.1f Chemical formula of 1,10 phenanthroline

A solution of 1,10 phenanthroline in benzene is prepared under vacuum and let down to atmospheric pressure using nitrogen gas. Upon addition of an aliquot n-butyl lithium, the colour of the solution turned rusty orange. Addition of sec-butanol via a syringe turned the colour to pale yellow/green at the end point, the flask warmed during the addition therefore showing the reaction to be exothermic. The titration is shown below in figure 2.1g.

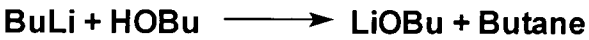

Figure 2.1g Titration that synthesises secondary lithium butoxide

The concentration of lithium sec-butoxide is calculated from the amount of sec-butanol solution used in the synthesis and was determined to be 0.245M in benzene.

2.1.3.4 Preparation of initiator

1,3 phenylenebis(4-methyl-1-phenylpentylidene)dilithium (PBMPPD) was prepared by the reaction of 1,3-bis(1-phenylethenyl)benzene (BPEB) with (s)-butyllithium. BPEB is not commercially available and was prepared by Mr. F. T. Kiff at the I.R.C. in Polymer Science and Technology, University of Durham. The procedure used to prepare BPEB has been outlined in the literature[9] and is shown below in figure 2.1h. The starting material, 1,3 diacetylbenzene (Aldrich) is reacted with two equivalents of phenyl magnesium bromide in a Grignard reaction to produce 1,3-di(1-phenyl-1-hydroxy ethyl) benzene. This is subsequently dehydrated with p-toluene sulphonic acid to prepare BPEB which is then stored under nitrogen to prevent oxidation.

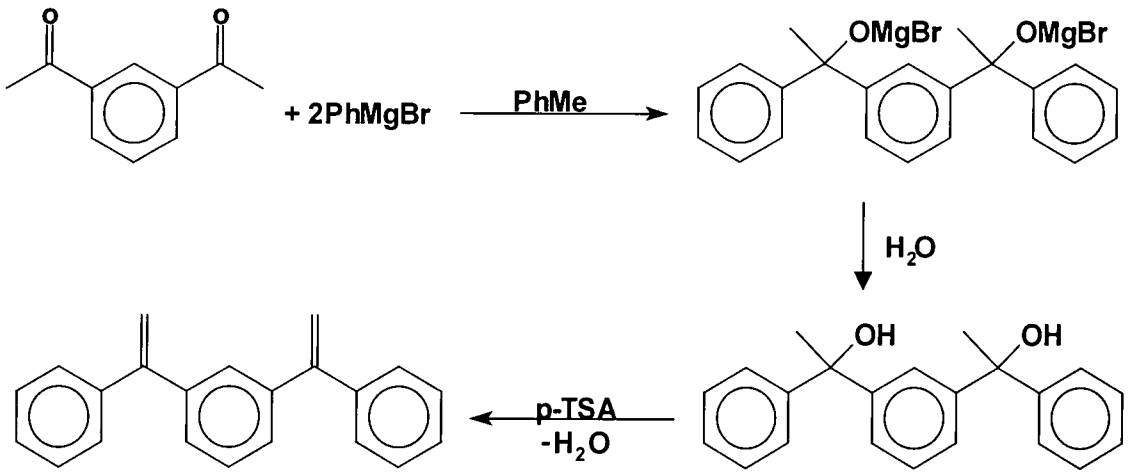

Figure 2.1h Synthetic route to 1,3-bis(1-phenylethenyl)benzene

The addition of s-butyllithium to a solution of BPED produces an intensely red coloured compound which is the difunctional initiator PBMPPD. However the addition of either too much or too little s-butyl lithium will give rise to the presence of a monofunctional initiator in addition to the difunctional product. It is therefore of great importance to attain the correct stoichiometric ratio between BPED and s-butyllithium. Several methods have been developed to achieve this[9], including SEC analysis of the quenched initiator[8], though the technique used here is dependent upon the low solubility of PBMPPD in heptane[7] so that monofunctional initiator and remaining sec-BuLi are left in the solution and difunctional product is the only precipitate to appear in the synthesis.

Apparatus of the type shown in figure 2.1i was used in the preparation of the PBMPPD. A known amount of the BPEB was weighed into the flask and dissolved in approximately 50 cm^3 of anhydrous heptane, transferred into the flask by cannula wire having been dried over calcium hydride on the vacuum line. To this solution was added exactly twice the equivalent of s-butyllithium, producing an intensely dark red solution immediately. However the reaction was allowed to proceed at 333K for 2 hours to ensure completion.

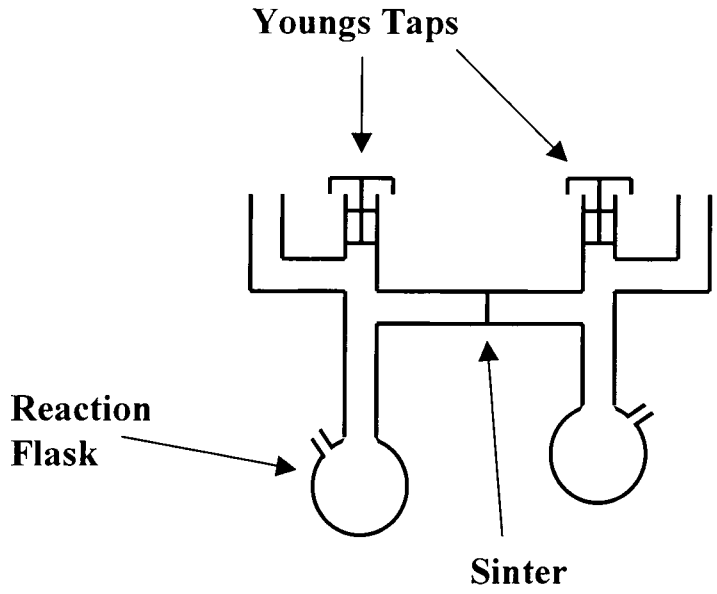

Figure 2.1i Apparatus used for the preparation of initiators under an inert atmosphere

At this point a dark red precipitate (PBMPPD) was observed and the mother liquor removed by filtration. Further heptane was transferred into the flask to wash the precipitate and was again filtered off. The PBMPPD was then dissolved in approximately 80 cm^3 of benzene and was then filtered and transferred into a storage flask by cannular wire. The strength of the initiator was estimated by titration with a solution of (s)-butanol in toluene. The solubility of PBMPPD in benzene is however quite low and the concentration of the initiator is around 0.12 Molar.

2.1.3.5 Preparation of cross-linking agent

The cross-linking agent, tetraethoxysilane (Lancaster, 98+%) was used as dilute solution in benzene. The solution was made up of 1.17g of $Si(OEt)_4$ added to 51.83g of benzene to give a 2.26% w/w solution. The density of the solution is assumed to be that of benzene. One mole of initiator with respect to lithium corresponds to 0.25 moles of

silane. Calculation of the required amount of cross-linking solution to network a living triblock system is as follows :

$$\frac{(Number\ of\ moles\ of\ Li) \times (Formula\ mass\ of\ Si(OEt)_4) \times 100}{4 \times (density\ of\ the\ cross-linking\ agent\ solution) \times (concentration\ of\ cross-linking\ agent)}$$

$$= \textbf{cross-linking agent solution required in } \mu\textbf{l}$$

After preparing the cross-linking agent the solution can be stored at 273K for up to three months.

2.1.3.6 Linear block copolymers

Both linear polymers and triblock networks were prepared using the standard high vacuum techniques required for anionic polymerisation. As noted earlier, one of the main priorities in anionic polymerisation to avoid the presence of impurities and hence there is the need for scrupulously clean equipment and pure reagents.

Here, a high vacuum method has been used to prevent termination by contamination of the polymerisation by reactive impurities. A pressure of 10^{-6} mbar was maintained by the use of rotary (Edwards E2) and oil diffusion pumps (Edwards 63/150 'Diffstack') operated in series. Flasks of the type shown below in figure 2.1j were used to prepare both the polymers and networks.

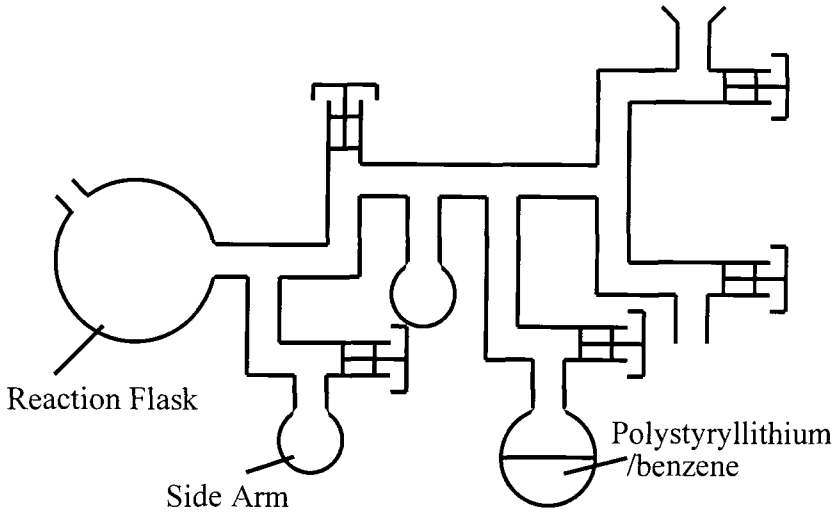

Figure 2.1j Reaction flask of the type used to prepare polymers and networks

The apparatus was cleaned thoroughly by washing with permanganic acid to remove both organic and inorganic residue, followed by rinsing with a large volume of distilled water and methanol. The 'clean' flask was then dried before being attached to one of the secondary manifolds of the vacuum line as shown in figure 2.1k.

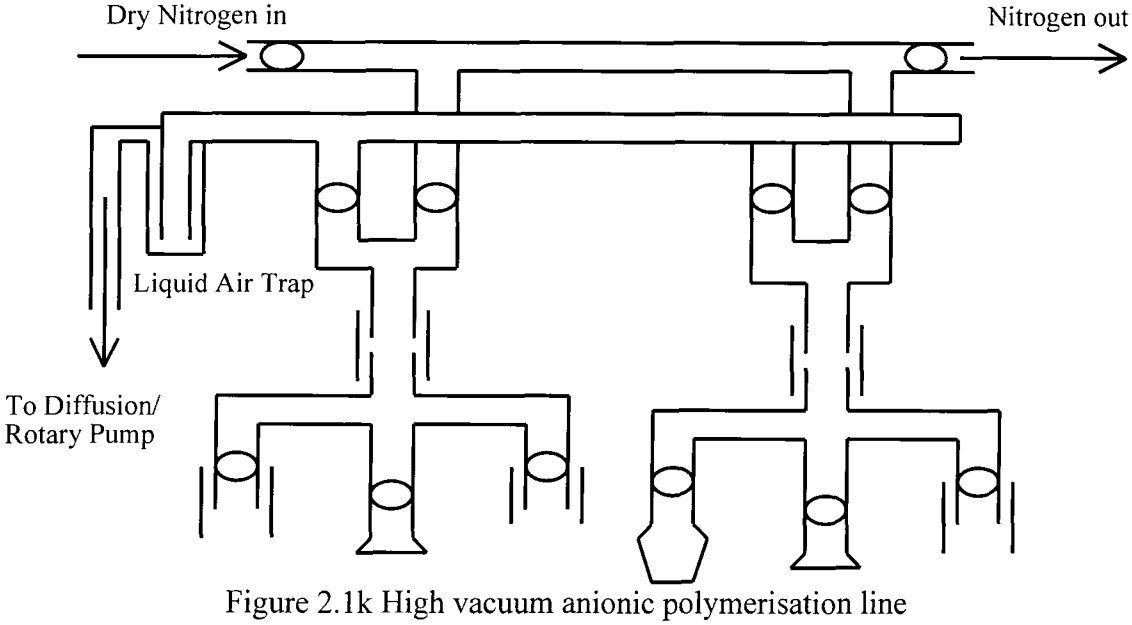

Figure 2.1k High vacuum anionic polymerisation line

The flask was then heated with a hot air gun under vacuum to remove any atmospheric contaminants present upon the inside. A living solution of poly(styryllithium) in

benzene was then introduced into the flask and all surfaces of the glassware and vacuum taps were thoroughly washed to remove any remaining protic impurities. The poly(styryllithium) solution was then returned to the bulb and all traces of the living polymer removed by washing the flask with solvent distilled from the poly(styryllithium) solution. This procedure is particularly important as the poly(styryllithium) is capable of initiating the polymerisation of the monomer to be introduced into the flask. The reaction flask was evacuated once more before the addition of solvent and monomer by vacuum transfer prior to initiation.

Suitable combinations of initiator and solvent for the preparation of linear BSB samples have been described in the literature. One such combination for the polymerisation uses benzene as the solvent and αMeS/K dianion as the initiator[10]. This combination has been shown to produce polymers of predictable molecular weight and low polydispersity but gives a low proportion of 1,4 polybutadiene addition. More recent synthetic methods developed have been shown to overcome this problem and for these reasons were chosen to be used for the synthesis of linear BSB samples to be used in this project[8].

The reaction solvent was distilled by vacuum transfer in to the clean reaction flask followed by a pre-weighed amount of monomer, sufficient to give a polymer concentration of approximately 10% w/v. Addition of the required amount of LiOBu solution by syringe was followed by addition of the appropriate volume of initiator as given by equation 2.1c. A characteristic deep red colouration, indicative of the formation of polystyryl anions was observed and the propagation reaction allowed to proceed for upwards of 2 hours before a sidearm sample was taken for molecular weight

determination and terminated by injection of 50μl of methanol. The desired amount of butadiene monomer was then distilled in to the reaction flask and the polymerisation allowed to proceed overnight to ensure complete polybutadiene propagation. Termination of the reaction was achieved by injection of 1ml of nitrogen sparged methanol.

2.1.3.7 Block copolymer networks

The preparation of the networks differs from that of the linear triblock copolymers only in that the polymer is cross-linked rather than terminated. A small amount of THF is added to the living polymer to disassociate the lithium ions at the end of the chains. A sidearm sample of the linear triblocks was taken for molecular weight determination and terminated with degassed methanol before addition of the required quantity of silane to cross-link the living polymer chain ends.

Parameters considered when cross-linking the living triblock copolymers are listed below:

1. The concentration of the linear polymer in benzene before cross-linking effects the number of network defects and entanglements of chain ends, and also effects how quickly the network reaches the gel point (the point where there is no more motion of polymer chains in the solution and very little further cross-linking can take place).

2. The reactivity of the cross-linking agent effects the structure of the network. A very reactive cross-linker (e.g. a chlorosilane) will result in a non-homogeneous network because the cross-linker is so reactive that reaction will occur before complete mixing between polymer solution and cross-linker solution. Hence there will be a large

concentration of cross-links where the reagent is injected in to the living polymer system, leaving a network with a localised high cross-link density at the point of addition and a low cross-link density in other parts of the network. It is essential that a cross-linking agent has sufficient time to be mixed in to the living polymer solution before complete cross-linking of the chain ends occurs. Using an alkoxy silane achieves better results. Ethoxysilanes are less reactive than chlorosilanes and allow for better mixing. Butoxysilanes however are too unreactive and lead to incomplete cross-linking.

3. The molecular weight of the precursor polymer influences to a small extent how fast the gel point of the network is reached. Therefore an optimum value of molecular weight must be chosen to attain the best network.

4. The homogeneity of cross-linking depends on the concentration of the silane solution before addition to the living linear system. Addition of undiluted cross-linker will result in a non-homogeneous network since reaction will be rapid and localised. Dilution prevents this, a concentration of 2-3% results on addition of 1-2ml of solution, this may be added in a short period of time and therefore good mixing is possible before complete reaction. A solution more dilute than this will require too long an addition time and again inhomogeneities will occur. The solutions of cross-linker and living linear polymer are then mixed by shaking to ensure sufficient dispersion of the cross-linking agent throughout the solution.

The chosen parameters for the networks prepared in this work are a polymer solution concentration of 10% and tetraethoxysilane as a 2.3% w/w solution in benzene as the cross-linking agent, added at a 1:2 stoichiometric ratio to the lithium initiator. When

adding the cross-linking agent to the living triblock copolymer solution, the reaction flask is shaken, the solution swirled around for 30 seconds to mix in the cross-linker thoroughly in the solution, and left to cross-link for five days.

Two series of networks (and their analogous linear triblock copolymers) have been synthesised using well defined anionic polymerisation techniques. The terminology used in the remaining chapters of the thesis for the analysed systems is as follows.

1. Lamellar triblock copolymer – 50% polystyrene, 50% polybutadiene BSB copolymer. Molecular weight range 40-250K.

2. Spherical morphology copolymer – 15% polystyrene, 85% polybutadiene BSB triblock. Molecular weight range 35-240K.

3. Lamellar network – 50% polystyrene, 50% polybutadiene BSB end cross-linked system. Molecular weight range 30-80K.

4. Spherical morphology network – 15% polystyrene, 85% polybutadiene BSB end cross-linked system. Molecular weight range 35-150K.

2.2 Characterisation of block copolymers and block copolymer networks

2.2.1 Size Exclusion Chromatography

Size exclusion chromatography (SEC) was used to determine the molecular weight characteristics of the linear BSB copolymer chains and the network precursor polymers prepared in this project, using tetrahydrofuran (THF) as the solvent. The degree of uncross-linked material was also evaluated by quantitatively measuring the sol fraction of the networks.

Samples for SEC analysis were dissolved in filtered and degassed THF (distilled and degassed GPR grade) and made up to a concentration of 0.1% w/v. Sample solutions (100μl) were filtered through 0.2μm polypropylene backed PTFE membrane filters to remove any dust and particulate matter.

The solutions were analysed with a Viskotek differential refractometer detector/viscometer model 200 fitted with two polymer laboratories PL gel columns 10μl mixed by a Waters model 590 pump operating at 1 cm^3/minute. The SEC detector system has a universal calibration, generated with a range of narrow molecular weight polystyrene standards (162amu-1030000amu) obtained from Polymer Laboratories. Software package used was the Viskotek Unical GPC-Viscometry software version 4.06.

2.2.1.1 Lamellar morphology triblock copolymers

SEC analysis was carried out on the samples of polystyrene blocks and also on the respective triblock copolymers. Table 2.2.1a shows data obtained from SEC traces of

the PS block samples from the lamellar copolymer preparations. Table 2.2.1b shows the data obtained from SEC analysis experiments on the lamellar triblock copolymers.

Table 2.2.1a SEC results from the PS block samples of the lamellar copolymers

Polystyrene block	$\overline{M}_n$	$\overline{M}_w$	Polydispersity
LL1	18 000	25 000	1.43
LL2	18 000	28 000	1.53
LL3	27 000	47 000	1.76
LL4	45 000	81 000	1.81
LL5	81 500	115 000	1.41

Table 2.2.1b SEC results on the BSB lamellar triblock copolymers

BSB Polymer	$\overline{M}_n$	$\overline{M}_w$	Polydispersity
LL1	39 000	46 000	1.19
LL2	57 000	65 000	1.14
LL3	99 000	114 000	1.15
LL4	115 000	144 000	1.26
LL5	240 000	282 000	1.18

Triblock copolymers synthesised with a variety of molecular weights possessing polydispersities between 1.14-1.26 are within the range expected when using the lithium difunctional initiator. A typical copolymer SEC trace in figure 2.2.1a shows that systems are reasonably monodisperse. From the trace it is apparent that there is some low molecular weight polymeric material to the right of the main peak.

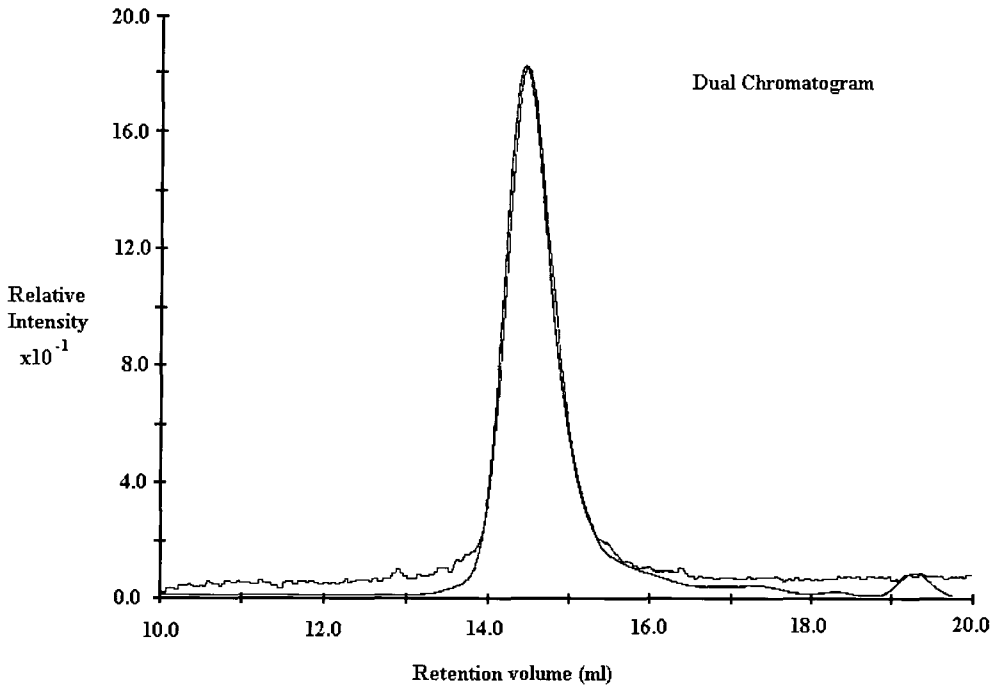

Figure 2.2.1a SEC trace for lamellar copolymer system

2.2.1.2 Lamellar morphology networks

SEC experiments were run on samples of polystyrene blocks and on triblock network precursor samples. Table 2.2.1c shows results from SEC analysis of polystyrene blocks. Table 2.2.1d shows results obtained from SEC analysis of network precursor triblock samples before networking had taken place.

Table 2.2.1c SEC results of the PS blocks of network precursor

Polystyrene block	$\overline{M}_n$	$\overline{M}_w$	Polydispersity
NL1	15 000	20 000	1.35
NL2	14 000	20 000	1.47
NL3	19 500	29 000	1.48
NL4	26 500	43 000	1.61
NL5	31 000	42 000	1.36
NL6	38 500	53 000	1.38

Table 2.2.1d SEC results of the lamellar network precursors

BSB triblock	$\overline{M}_n$	$\overline{M}_w$	Polydispersity
NL1	25 000	32 000	1.28
NL2	35 000	40 000	1.14
NL3	51 000	57 000	1.12
NL4	60 000	64 000	1.08
NL5	66 000	72 000	1.09
NL6	81 000	89 000	1.10

It can be seen from the SEC results that the triblock copolymers were relatively monodisperse before cross-linking. It is generally consistent that PS block polydispersities are higher than triblock ones which is statistically expected. When using sec-BuLi as the initiator (monofunctional) polydispersity values tend to be less than those observed using the difunctional initiator proving that the system is at fault and that results have been produced that are consistent with internal reports from co-workers within the group.

2.2.1.3 Lamellar morphology network sol fraction analysis

The amount of uncross-linked material (sol fraction) in the networks was determined by the extraction of the sol fraction of the networks.

After removing the benzene swollen network from the reaction flask it was placed in a two litre beaker containing one litre of cyclohexane. The sol fraction diffused out of the network in to the cyclohexane, which was decanted out of the beaker and replaced with fresh cyclohexane after 24 hours. The decanted cyclohexane sol solution was reduced in volume to 20-30ml on the rotary evaporator and the sol collected by precipitation in to 20 volumes of methanol and filtered. The sol was dried in vacuo and weighed. This extraction procedure was repeated until no further sol fraction was collected. The results of each extraction for the lamellar networks are given in table 2.2.1e

Table 2.2.1e Sol fraction extractions from lamellar networks

Sol Fraction Weight	**NL1 (g)**	**NL2 (g)**	**NL3 (g)**	**NL4 (g)**	**NL5 (g)**	**NL6 (g)**
Extraction 1	0.38	0.29	0.50	0.44	0.30	0.26
Extraction 2	0.27	0.22	0.28	0.30	0.15	0.25
Extraction 3	0.23	0.14	0.07	0.24	0.14	0.15
Extraction 4	0.15	0.10	0.05	0.16	0.09	0.07
Extraction 5	0.07	0.08	0.03	0.12	0.05	0.06
Extraction 6	0.03	0.08	0.01	0.08	0.01	0.03
Extraction 7	0.01	0.05	0.00	0.06	0.00	0.01
Extraction 8	-	0.01	-	0.03	-	0.00
Extraction 9	-	0.00	-	0.01	-	
Extraction 10	-	-	-	0.00	-	
Sol fraction as % of initial sample weight	**5.7**	**4.9**	**5.6**	**7.5**	**3.8**	**4.2**

As can be seen from the data in table 2.2.1e, a varied amount of sol fraction exists in the series of samples. Measurement of the sol fraction, expressed as a percentage of the initial sample weight, was however subject to several sources of error. In the measurement of the extracted material care was needed to avoid loss of any of material, as the quantities of extracted material were generally small, any loss could be a

significant amount of the sol fraction. In all cases the whole gel was evaluated and sample homogeneity was assumed throughout.

A typical SEC trace for a sol fraction network sample is presented below in figure 2.2.1b.

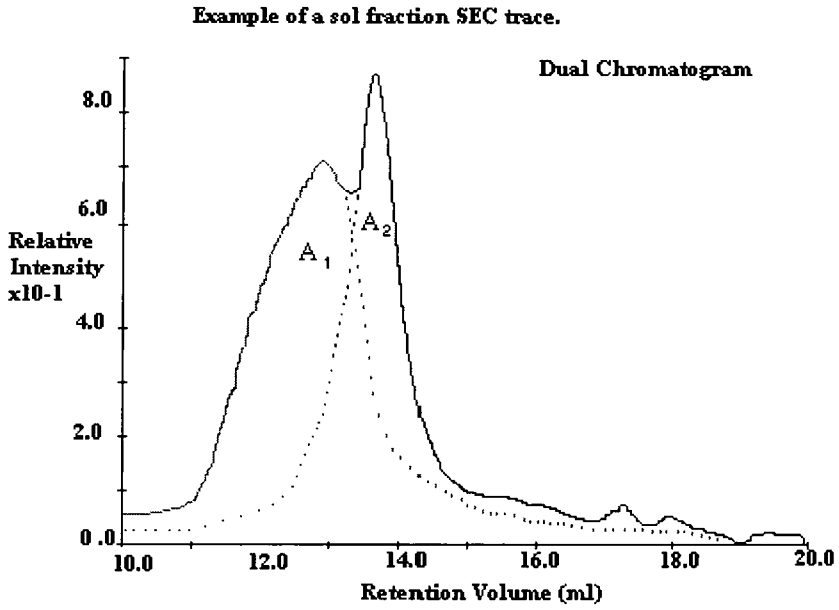

Figure 2.2.1b Sol fraction trace from SEC analysis

SEC results from sol fraction samples are very similar. The SEC trace shows a peak due to the linear BSB triblock copolymer (A_2), and a broader peak of higher molecular weight polymer due to linear chains that are linked together by the cross-linking agent but are not part of the bulk network (A_1). Therefore the polydispersity of the sol fraction samples is greater than the equivalent linear triblock samples. The two peaks can be separated, the ratio of the areas correspond to the weight fractions of components in the trace. The total molecular weight of the sol fraction is proportional to the sum of the two areas. Using equations 2.2.1a–2.2.1c the weight fraction of each peak can be calculated.

$$M_T \propto A_1 + A_2 \qquad \text{eq.2.2.1a}$$

M_T is the molecular weight of the sol fraction, A_1 and A_2 correspond to the areas from the SEC trace of the sol fraction.

$$Weight\ fraction\ of\ the\ triblock\ peak = \frac{A_2}{A_1 + A_2} \qquad \text{eq.2.2.1b}$$

$$Weight\ fraction\ of\ the\ high\ molecular\ weight\ peak = \frac{A_1}{A_1 + A_2} \qquad \text{eq.2.2.1c}$$

Results from SEC traces of sol fraction samples are presented in table 2.2.1f. The masses of the peaks from the SEC traces were weighed on a four decimal place balance.

Table 2.2.1f SEC analysis to calculate weight fractions of sol fraction traces

Network Sol Fraction	Mass of high molecular weight peak, A_1 (mg)	Mass of triblock peak, A_2 (mg)	Weight fraction of high molecular weight peak	Weight fraction of triblock peak
NL1	275.8	288.6	0.49	0.51
NL2	252.7	219.0	0.54	0.46
NL3	312.4	200.9	0.61	0.39
NL4	298.0	138.6	0.62	0.38
NL5	395.6	179.1	0.74	0.26
NL6	354.9	216.3	0.62	0.38

Weight fractions of the respective peaks in the sol fraction traces vary between 0.49 and 0.74. The total molecular weight of the bulk network increases as the weight fraction of the high molecular weight material increases. Increasing the molecular weight of the bulk network increases the yield of high molecular weight material present.

SEC traces were analysed from sol fractions of the lamellar network samples to find $\overline{M}_w$ and polydispersity in the systems. Results from the traces are shown in table 2.2.1g.

Table 2.2.1g SEC results of sol fraction materials from lamellar network systems

Network Sol Fraction	$\overline{M}_w$ of sol fraction	$\overline{M}_n$ of sol fraction	Polydispersity
NL1	37 500	8 500	4.48
NL2	159 000	49 000	3.25
NL3	116 500	59 000	1.98
NL4	120 000	28 500	4.20
NL5	150 000	62 000	2.42
NL6	194 000	84 000	2.32

There are wide variations in the polydispersities of sol fraction materials. No trend is apparent throughout the range of molecular weights in the systems although it is apparent that variations appear to extend either side of the $\overline{M}_w$ value before cross-linking had taken place.

2.2.1.4 Spherical morphology triblock copolymers

Spherical morphology copolymer systems were analysed using the same SEC technique as for the lamellar network samples. Table 2.2.1h shows SEC results from the polystyrene blocks of the linear spherical copolymers. Table 2.2.1i shows information obtained from SEC analysis of the spherical copolymers.

Table 2.2.1h SEC results from the PS blocks of the spherical morphology copolymers

Polystyrene block	$\overline{M}_n$	$\overline{M}_w$	Polydispersity
LS1	5 000	8 000	1.60
LS2	6 000	10 000	1.67
LS3	9 500	13 500	1.42
LS4	21 000	33 000	1.57
LS5	22 000	39 000	1.77

Polystyrene sidearm samples display a narrow range of polydispersity values similar to the lamellar samples.

Table 2.2.1i SEC results for the spherical morphology copolymers

BSB Polymer	$\overline{M}_n$	$\overline{M}_w$	Polydispersity
LS1	34 000	38 500	1.13
LS2	41 500	48 000	1.16
LS3	60 000	67 000	1.12
LS4	120 000	137 000	1.14
LS5	185 000	239 000	1.29

Spherical copolymer molecular weight values are similarly spread as the corresponding lamellar systems with a reasonably narrow spread of polydispersities similar to the uncross-linked lamellar copolymers.

2.2.1.5 Spherical morphology networks

SEC experiments were run on polystyrene blocks and on triblock copolymer precursor samples before the systems were cross-linked. Table 2.2.1j shows results from the SEC traces of the polystyrene blocks. Table 2.2.1k shows data obtained from SEC analysis runs on the network precursor triblock copolymer samples before cross-linking had taken place.

Table 2.2.1j SEC results of the PS blocks of network precursor

Polystyrene blocks	$\overline{M}_n$	$\overline{M}_w$	Polydispersity
NS1	6 000	10 000	1.67
NS2	8 000	13 000	1.63
NS3	9 000	15 500	1.72
NS4	10 500	17 000	1.62
NS5	12 500	20 500	1.64
NS6	15 500	25 000	1.61
NS7	22 000	36 000	1.64

Table 2.2.1k SEC results of the spherical morphology network precursors

BSB triblock	$\overline{M}_n$	$\overline{M}_w$	Polydispersity
NS1	33 000	38 000	1.15
NS2	42 000	47 000	1.12
NS3	49 000	55 000	1.12
NS4	60 000	66 000	1.10
NS5	77 000	88 000	1.14
NS6	95 000	113 000	1.19
NS7	125 000	155 000	1.24

Similar trends are observed for the spherical morphology network precursors as for the lamellar systems. The polystyrene block polydispersities are higher than the network precursor triblocks which is statistically expected. When using sec-BuLi as the initiator (monofunctional) polydispersity values tend to be less than those observed using the difunctional initiator. Spherical morphology copolymer systems possessed low polydispersities before cross-linking commenced with a reasonable spread of molecular weight values so as to detect a variation of domain spacing values in the systems.

2.2.1.6 Spherical morphology network sol fraction analysis

Sol fraction samples from the spherical morphology network systems were analysed using the same method as for the lamellar systems. The results of each extraction for the spherical morphology networks are given in table 2.2.11.

Table 2.2.11 Sol fraction extractions from spherical morphology networks

Sol Fraction Weight	**NS1 (g)**	**NS2 (g)**	**NS3 (g)**	**NS4 (g)**	**NS5 (g)**	**NS6 (g)**	**NS7 (g)**
Extraction 1	0.22	0.70	0.38	0.63	0.38	0.75	0.95
Extraction 2	0.19	0.10	0.24	0.18	0.14	0.26	0.38
Extraction 3	0.07	0.07	0.21	0.15	0.06	0.13	0.23
Extraction 4	0.03	0.02	0.16	0.09	0.05	0.05	0.13
Extraction 5	0.03	0.02	0.12	0.06	0.02	0.03	0.10
Extraction 6	0.02	0.00	0.08	0.06	0.01	0.02	0.09
Extraction 7	0.01	-	0.03	0.05	0.01	0.01	0.08
Extraction 8	0.01	-	0.01	0.04	0.00	0.00	0.05
Extraction 9	0.00	-	0.00	0.02	-	-	0.02
Extraction 10	-	-	-	0.00	-	-	0.00
Sol fraction as % of initial sample weight	**2.8**	**4.5**	**6.2**	**6.4**	**3.4**	**6.3**	**10.2**

Sol fraction percentage values are consistent with lamellar networks and therefore can be analysed using the same techniques. SEC traces were used to calculate weight fraction values and molecular weight variations in the sol fraction samples. Results from SEC traces of sol fraction samples are presented in table 2.2.1m.

Table 2.2.1m SEC analysis to calculate weight fractions of sol fraction traces

Network Sol Fraction	Mass of high molecular weight peak, A_1 (mg)	Mass of triblock peak, A_2 (mg)	Weight fraction of high molecular weight peak	Weight fraction of triblock peak
NS1	245.5	219.0	0.53	0.47
NS2	139.2	292.3	0.32	0.68
NS3	233.6	197.9	0.54	0.46
NS4	301.2	299.0	0.50	0.50
NS5	197.5	243.3	0.45	0.55
NS6	223.0	290.8	0.43	0.57
NS7	306.8	173.1	0.64	0.36

Weight fractions of the respective peaks in the sol fraction traces vary between 0.32 and 0.64 for the high molecular weight peaks. The variation of the high molecular weight fraction is independent of the increase in $\overline{M}_w$ of the bulk spherical morphology network systems and different to that observed for the lamellar systems.

SEC traces were analysed from sol fractions of the lamellar network samples to find $\overline{M}_w$ and polydispersity in the systems. Results from the traces are shown in table 2.2.1n.

Table 2.2.1n SEC results of sol fraction materials from spherical network systems

Network Sol Fraction	$\overline{M}_w$ of sol fraction	$\overline{M}_n$ of sol fraction	Polydispersity
NS1	76 500	15 000	5.10
NS2	93 500	30 500	3.07
NS3	188 000	88 500	2.12
NS4	290 000	123 000	2.35
NS5	238 000	107 000	2.22
NS6	391 000	133 500	2.93
NS7	417 500	173 000	2.41

There is a decrease in the polydispersity of sol fraction materials as the molecular weight of the precursor copolymers before cross-linking increases. The trend is apparent

in the lower molecular weight precursors but steadies out as the molecular weight values in the range increase.

2.2.2 Solution State ^{1}H NMR analysis

Solution state ^{1}H NMR spectroscopy has been used as an analytical technique to calculate the composition of polymer in terms of weight percent PS/PB and the microstructure of the PB i.e. %1,4 content in polybutadiene, and the amount of cis and trans 1,4 polybutadiene in the triblock copolymer samples. The instrument used was a 400 MHz Varian VXR-400(s).

2.2.2.1 Lamellar morphology copolymer analysis

Table 2.2.2a shows data obtained from ^{1}H NMR experiments on the lamellar triblock copolymers.

Table 2.2.2a Information from ^{1}H NMR experiments on lamellar BSB copolymers

BSB Copolymer	Molecular Weight (K)	% 1,4 content of PB in triblock	Weight fraction of polystyrene	Volume fraction of polystyrene
LL1	40	86.9	0.50	0.54
LL2	60	90.6	0.50	0.54
LL3	100	90.4	0.40	0.44
LL4	150	89.6	0.41	0.45
LL5	240	89.8	0.46	0.50

The results show that polymerisation has been completed to a satisfactory extent yielding polybutadiene with a high 1,4 content and compositions that will give lamellar systems in all materials synthesised. Table 2.2.2b shows the polybutadiene microstructure obtained from ^{1}H NMR spectra of the triblock copolymers. Calculations

were obtained by comparing peak heights from the shift values between 5.2-5.4ppm, see figure 2.2.2a. The left peak of the doublet corresponds to trans 1,4 polybutadiene, the right peak is cis 1,4 polybutadiene[11]. The ratio of the peak heights corresponds to the amount of each isomer of polybutadiene in the triblock copolymer. A typical solution state ^{1}H NMR spectrum from a linear BSB copolymer is shown in figure 2.2.2a.

Table 2.2.2b Polybutadiene microstructure of lamellar copolymers obtained by ^{1}H NMR

BSB Copolymer	**% 1,4 trans in polybutadiene**	**% 1,4 cis in polybutadiene**	**% 1,2 in polybutadiene**	**% 1,4 PB in BSB copolymer**
LL1	44.0	42.9	13.1	43.5
LL2	43.3	47.3	9.4	45.3
LL3	44.5	45.9	9.6	36.2
LL4	44.1	45.5	10.4	36.7
LL5	42.9	46.9	10.2	41.3

The results in table 2.2.2b show that each sample has a similar microstructure and differ only in molecular weight. Physical properties differ due to the molecular weight difference of each system.

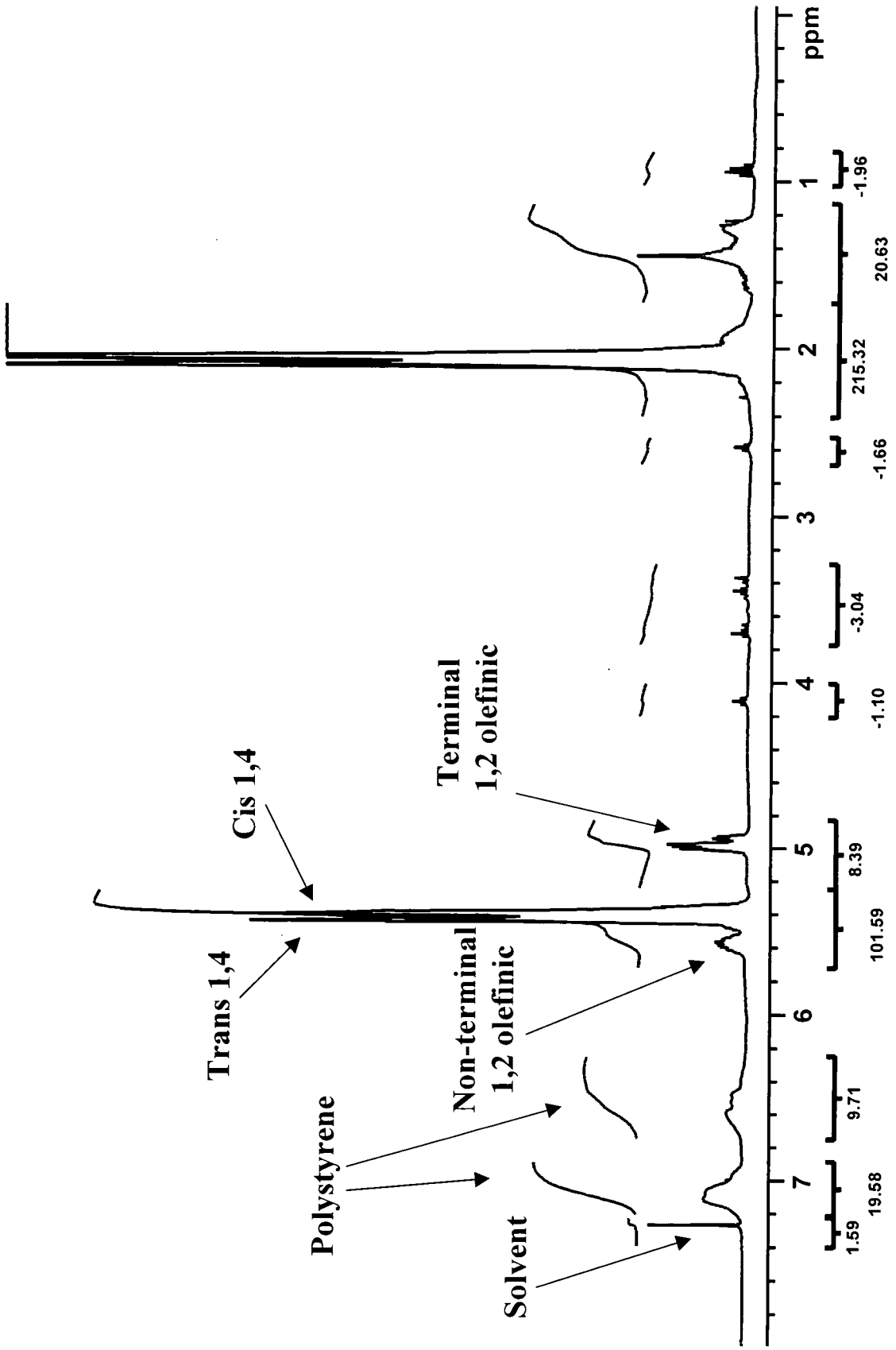

Figure 2.2.2a Solution state ^{1}H NMR spectrum from a linear BSB copolymer

2.2.2.2 Lamellar morphology networks

A series of lamellar networks were synthesised, the range of molecular weights for each triblock copolymer before cross-linking being 30-80K, the composition being about 50:50 polystyrene/polybutadiene. Solution state ^{1}H NMR experiments were run on the network precursor triblock copolymer samples. Information on the composition and the microstructure of the triblocks are shown in table 2.2.2c.

Table 2.2.2c ^{1}H NMR results on precursor triblock samples from lamellar networks

BSB Network	Molecular Weight (K)	% 1,4 content in Polybutadiene	Weight fraction of polystyrene	Volume fraction of polystyrene
NL1	30	86.3	0.55	0.59
NL2	40	87.2	0.55	0.59
NL3	55	87.4	0.54	0.58
NL4	60	86.0	0.55	0.59
NL5	70	88.4	0.57	0.61
NL6	80	79.4	0.59	0.63

Table 2.2.2c shows that composition and microstructure for the network precursor triblocks were very similar to the analogous linear copolymers. Table 2.2.2d shows information obtained from ^{1}H NMR spectra showing the amounts of cis 1,4, trans 1,4 and 1,2 polybutadiene in the network precursor triblocks. Results were obtained using the same method as previously described.

Table 2.2.2d Polybutadiene microstructure of network precursor triblocks obtained by ^{1}H NMR

BSB Network	% 1,4 trans in polybutadiene	% 1,4 cis in polybutadiene	% 1,2 in polybutadiene	% 1,4 PB in BSB precursor
NL1	39.9	46.4	13.7	47.5
NL2	43.6	43.6	12.8	48.0
NL3	43.4	44.0	12.6	47.2
NL4	41.4	44.6	14.0	47.3
NL5	41.3	47.1	11.6	50.3
NL6	39.0	40.4	20.6	46.9

Table 2.2.2d results are very similar to the lamellar uncross-linked materials. Physical properties of the two sets of materials can now be analysed and comparisons made so conclusions can be deduced about the differences within the materials.

2.2.2.3 Spherical morphology copolymer analysis

Solution ^{1}H NMR experiments were carried out on all of the spherical morphology copolymer specimens. Information from the spectra enabled the calculation of 1,4 content in the polybutadiene, the amount of cis 1,4 and trans 1,4 polybutadiene and the weight (and volume) fraction of polystyrene in the copolymer systems. Table 2.2.2e shows data obtained from ^{1}H NMR experiments on the copolymer systems.

Table 2.2.2e Information from ^{1}H NMR experiments on spherical BSB copolymers

BSB Copolymer	Molecular Weight (K)	% 1,4 content in Polybutadiene	Weight fraction of polystyrene	Volume fraction of polystyrene
LS1	35	88.1	0.13	0.15
LS2	40	88.3	0.10	0.12
LS3	60	88.5	0.15	0.17
LS4	120	89.4	0.10	0.12
LS5	240	89.7	0.10	0.12

The data shows that polymerisation has resulted in a satisfactory microstructure and a composition that should give spherical morphologies in all materials synthesised. Table 2.2.2f shows information obtained from ^{1}H NMR spectra on the microstructure of the polybutadiene in the spherical morphology copolymers. Calculations were carried out using the same method as for the lamellar systems. The higher percentage of polybutadiene in the spherical morphology samples increases the elasticity and extensibility of the materials, making the uncross-linked systems very sticky and difficult to analyse, especially at low molecular weights.

Table 2.2.2f Polybutadiene microstructure of spherical morphology copolymers obtained by ^{1}H NMR

BSB Copolymer	% 1,4 trans in polybutadiene	% 1,4 cis in polybutadiene	% 1,2 in polybutadiene	% 1,4 PB in BSB copolymer
LS1	43.3	44.8	11.9	76.6
LS2	43.5	44.8	11.7	79.5
LS3	44.0	44.5	11.5	75.3
LS4	43.4	45.1	11.5	80.4
LS5	44.4	45.3	10.3	80.7

Table 2.2.2f shows similar amounts of each isomeric component exist in the spherical morphology copolymer systems. Physical properties differ due to the molecular weight difference of each system.

2.2.2.4 Spherical morphology networks

A series of spherical morphology network systems were synthesised in which the molecular weight of the precursor polymers varied from 35-150K. The composition being approximately 15:85 polystyrene/polybutadiene. Solution state ^{1}H NMR experiments were run on the network precursor triblock samples with the data shown in table 2.2.2g.

Table 2.2.2g ^{1}H NMR results on precursor triblock samples from spherical networks

BSB Network	Molecular Weight (K)	% 1,4 content in Polybutadiene	Weight fraction of polystyrene	Volume fraction of polystyrene
NS1	35	86.1	0.18	0.20
NS2	45	85.8	0.12	0.13
NS3	50	85.6	0.14	0.16
NS4	60	88.0	0.13	0.15
NS5	80	85.3	0.17	0.20
NS6	100	89.5	0.12	0.14
NS7	150	87.4	0.13	0.15

Table 2.2.2g shows that microstructure and composition of the network precursor polymers was similar to that of the linear triblocks. Table 2.2.2h shows data obtained from ^{1}H NMR spectra showing the microstructure of the polybutadiene in the network precursor triblocks. Results were obtained using the same method previously described.

Table 2.2.2h Polybutadiene microstructure of network precursor triblocks obtained by ^{1}H NMR

BSB Network	% 1,4 trans in polybutadiene	% 1,4 cis in polybutadiene	% 1,2 in polybutadiene	% 1,4 PB in BSB copolymer
NS1	44.8	43.3	11.9	70.6
NS2	42.9	42.9	14.2	75.5
NS3	42.8	42.8	14.4	73.6
NS4	41.6	46.4	12.0	76.6
NS5	41.1	44.2	14.7	70.8
NS6	41.9	46.4	12.0	78.8
NS7	43.7	43.7	12.6	76.0

Table 2.2.2h shows that the microstructure of the polybutadiene is very similar to that of the polybutadiene in the linear. Physical properties of the two sets of materials can now be analysed and compared.

2.2.2.5 Sol fraction analysis of lamellar morphology network systems

Solution state ^{1}H NMR is a useful technique when analysing the microstructure of the sol fraction from the network samples. Table 2.2.2i shows a summary of results from sol fraction amounts taken from the lamellar network systems.

Table 2.2.2i Sol fraction extractions from lamellar network systems

BSB Network	% 1,4 content in polybutadiene	Weight fraction of polystyrene	Volume fraction of polystyrene
NL1	71.0	0.59	0.63
NL2	84.9	0.56	0.60
NL3	79.0	0.62	0.66
NL4	76.0	0.59	0.63
NL5	76.0	0.63	0.67
NL6	72.0	0.64	0.68

Sol fraction polystyrene block weight fractions appear to be slightly higher than polystyrene block samples taken before cross-linking had taken place.

Table 2.2.2j shows data obtained from ^{1}H NMR spectra showing the microstructure of the polybutadiene in the sol fraction samples from lamellar networks. The elasticity in each sample is represented as a percentage of 1,4 polybutadiene in the sol fraction.

Table 2.2.2j Microstructure of polybutadiene in sol fractions from lamellar networks

Sol Fraction	**% 1,4 trans in polybutadiene**	**% 1,4 cis in polybutadiene**	**% 1,2 in polybutadiene**	**% 1,4 PB in the BSB copolymer**
NL1	42.2	42.7	15.1	29.1
NL2	43.4	43.4	13.2	37.3
NL3	39.2	40.0	20.8	30.0
NL4	36.8	38.9	24.3	31.2
NL5	37.0	39.3	23.7	28.1
NL6	32.4	39.8	27.8	25.9

Lamellar sol fraction samples have varied polybutadiene microstructures compared to the copolymer blocks. The higher the molecular weight of the sol fractions the higher the 1,2 polybutadiene content signalling that poorly cross-linked networks form when the precursor polymer has a high molecular weight.

2.2.2.6 Sol fraction analysis of spherical morphology network systems

Solution state ^{1}H NMR experiments were used to analyse the microstructure of the sol fraction from the spherical morphology network samples. Table 2.2.2k shows a summary of results from sol fraction amounts taken from these systems.

Table 2.2.2k Sol fraction extractions from spherical morphology network systems

BSB Network	% 1,4 content in polybutadiene	Weight fraction of polystyrene	Volume fraction of polystyrene
NS1	59.9	0.20	0.23
NS2	47.1	0.22	0.25
NS3	68.7	0.18	0.21
NS4	40.6	0.19	0.22
NS5	47.1	0.24	0.27
NS6	53.1	0.17	0.19
NS7	56.1	0.25	0.28

The trend observed for the spherical morphology network sol fraction materials is similar as for the lamellar sol fractions. More polystyrene is present in the sol extracts indicating a slight decrease in the bulk network. As the mass of sol fraction material is only small the bulk weight fraction of the network should not be affected and will remain the same as before cross-linking.

Table 2.2.2l shows data obtained from ^{1}H NMR spectra showing the polybutadiene microstructure of the sol fraction samples from spherical morphology networks.

Table 2.2.2l Polybutadiene microstructure of sol fraction samples from spherical morphology networks

Sol Fraction	% 1,4 trans in polybutadiene	% 1,4 cis in polybutadiene	% 1,2 in polybutadiene	% 1,4 PB in BSB copolymer
NS1	31.1	34.5	34.4	47.9
NS2	29.7	30.8	39.5	36.7
NS3	32.7	31.2	36.1	56.3
NS4	27.6	42.6	42.6	32.9
NS5	30.0	31.2	38.8	35.8
NS6	31.7	32.4	35.9	44.1
NS7	32.5	31.5	36.0	42.0

Sol fraction samples have increased amounts of bulk 1,2 polybutadiene. The four tables of data presented in this section concerning microstructure and composition of sol fraction from precursor polymers seem to indicate high polystyrene content and lower 1,4 polybutadiene content, the reason being that 1,2 polybutadiene does not cross-link as well as 1,4.

2.2.3 Differential Scanning Calorimetry (DSC)

BSB copolymer and network systems were analysed using a Perkin-Elmer DSC-7 thermal analysis PC. The calibration of the machine was performed using indium (m.p.=429.78K, ΔH_m=28.45 J/g) and zinc (m.p.=692.65K, ΔH_m=108.37 J/g). Samples between 5-10mg were sealed in aluminium pans before analysis. The linear triblock copolymers were heated over a temperature range of 170K to 350K at a rate of 10K per minute and then quenched at 200K per minute back to the starting temperature. A second run was carried out on the same sample using the same conditions. The cooling medium was liquid nitrogen and the purge gas in the sample holder was nitrogen.

2.2.3.1 Lamellar morphology systems

Uncross-linked lamellar copolymer systems show a peak representing the glass transition temperature of cis or trans 1,4 polybutadiene (188K/-85°C) after two DSC scans. A glass transition temperature for the polystyrene phase at 373K/100°C was identified from the traces on runs of the annealed and unannealed samples. Cross-linked samples of the BSB network systems showed similar results to the triblock equivalents. Microphase separation is present in the lamellar copolymer systems because of the distinct polybutadiene T_g values around the 188K mark. Detection of polystyrene glass

transitions were identified between 178-198K (90-110°C). Phase mixing that occurs in the systems would increase T_g values of the polybutadiene towards the value of polystyrene and lower polystyrene glass transition values. Tables 2.2.3a-b show results from the DSC traces of the BSB lamellar systems. Polystyrene values were included in table 2.2.3b when analysis was possible at the onset of the glass transition.

Table 2.2.3a DSC trace results for polybutadiene from the BSB lamellar systems

Polybutadiene T_g (°C)					
Network	**Annealed**	**Unannealed**	**Copolymer**	**Annealed**	**Unannealed**
NL1	-81.1	-81.7	LL1	-86.1	-85.8
NL2	-81.9	-82.0	LL2	-82.8	-82.0
NL3	-81.6	-81.9	LL3	-81.9	-81.6
NL4	-83.2	-82.8	LL4	-82.4	-82.5
NL5	-84.5	-83.6	LL5	-83.6	-83.2
NL6	-84.2	-84.5			

Polybutadiene glass transition results are within the expected range of values expected for systems that are based on cis and trans 1,4 isomers.

Table 2.2.3b DSC trace results for polystyrene from the BSB lamellar systems

Polystyrene T_g (°C)					
Network	**Annealed**	**Unannealed**	**Copolymer**	**Annealed**	**Unannealed**
NL1	104.3	103.3	LL1	103.5	104.5
NL2	102.5	105.3	LL2	104.7	105.6
NL3	103.7	105.3	LL3	104.3	104.7
NL4	102.4	104.3	LL4	102.3	102.3
NL5	104.5	103.8	LL5	105.5	104.9
NL6	104.3	105.3			

Polystyrene glass transitions are within the range of values expected for the lamellar systems analysed. Figures 2.2.3a-c show a typical DSC trace for a lamellar BSB system including the two expected transitions for microphase separated polystyrene and polybutadiene. It is apparent from the set of transitions taken from a DSC trace of a BSB lamellar system that both phases exist separately and that glass transition temperatures are exactly what would be expected for a block copolymer system of this type that is microphase separated.

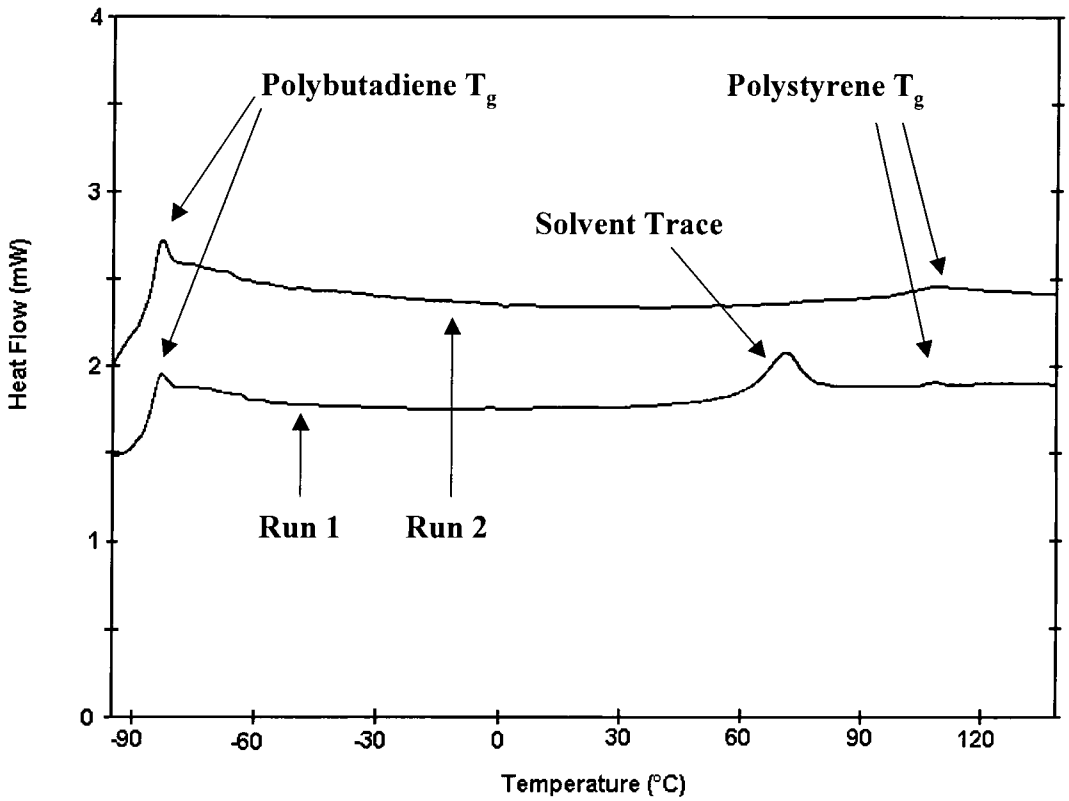

Figure 2.2.3a DSC trace for BSB lamellar system

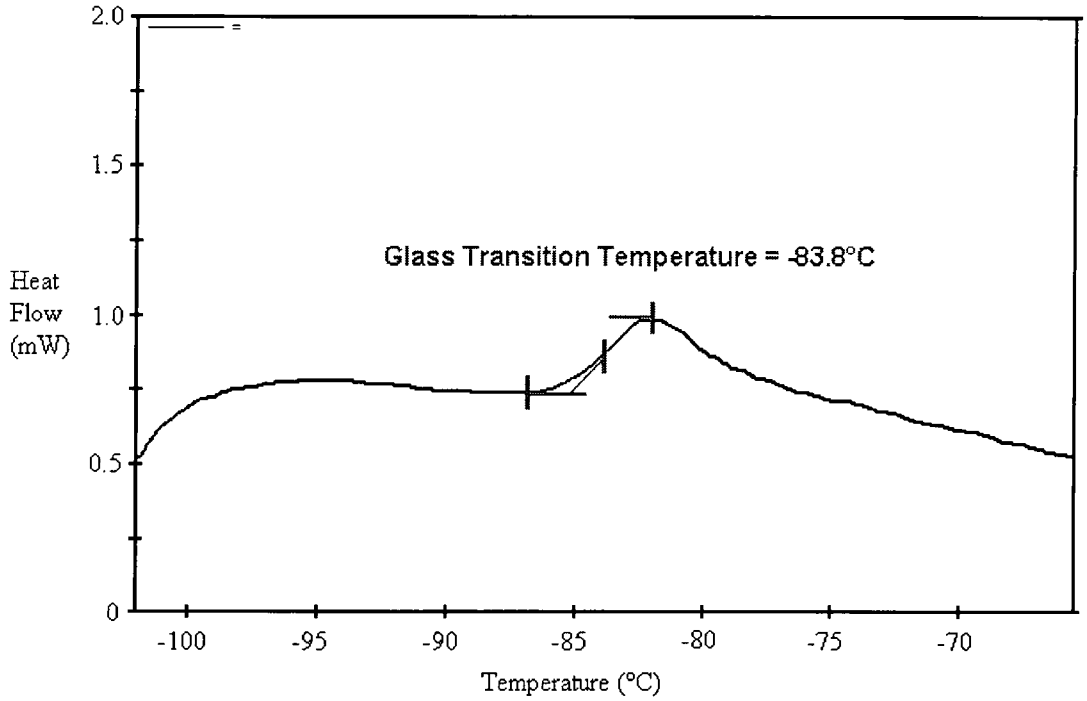

Figure 2.2.3b Polybutadiene glass transition from DSC trace of lamellar system

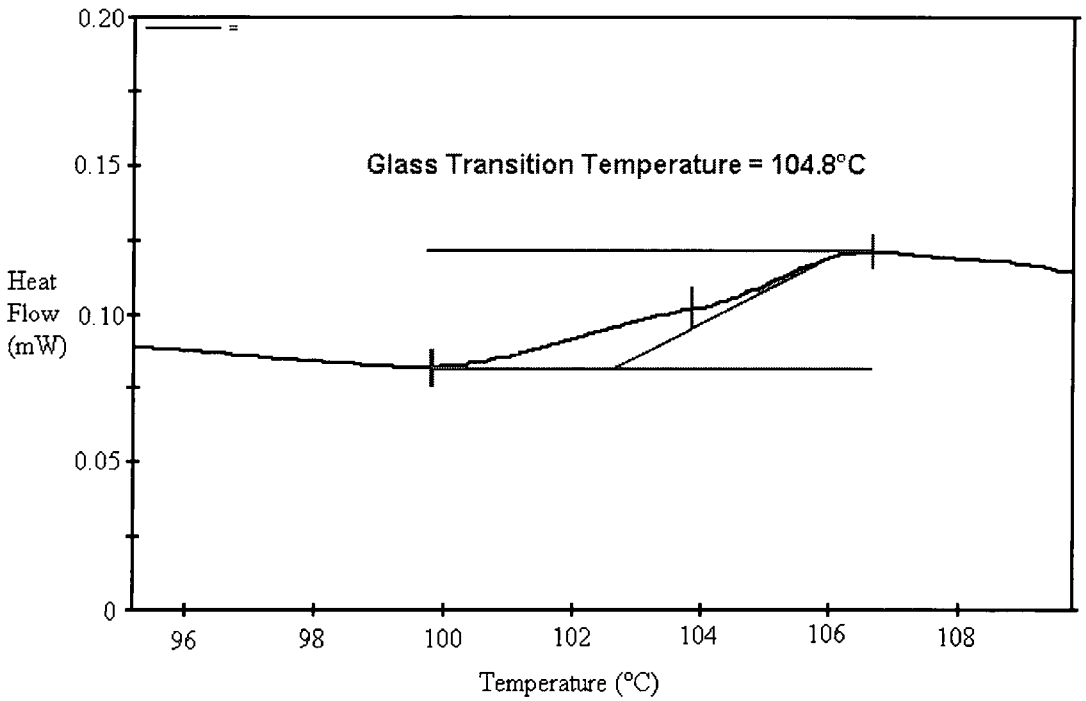

Figure 2.2.3c Polystyrene glass transition from DSC trace of lamellar system

2.2.3.2 Spherical morphology systems

Spherical morphology BSB copolymer and network systems have been analysed using the DSC technique applied to the lamellar samples. The difference from the lamellar systems is the decreased amount of polystyrene in the spherical morphology materials. Scanning traces from the DSC runs of the spherical morphology samples did not show a glass transition for the polystyrene phase in any of the systems. Polybutadiene transitions were observed for all the spherical morphology samples around the 188K/-85°C temperature. Table 2.2.3c shows the DSC results obtained from the spherical morphology copolymer and network systems.

Table 2.2.3c DSC trace results from the spherical morphology systems

Polybutadiene T_g (°C)					
Network	**Annealed**	**Unannealed**	**Copolymer**	**Annealed**	**Unannealed**
NS1	-85.4	-85.7	LS1	-	-88.5
NS2	-84.0	-84.6	LS2	-	-87.3
NS3	-83.5	-83.0	LS3	-85.8	-86.1
NS4	-85.4	-85.9	LS4	-86.9	-87.2
NS5	-86.0	-86.5	LS5	-88.3	-88.5
NS6	-87.1	-86.9			
NS7	-88.6	-88.5			

Glass transitions from the polybutadiene phase are in the same range as for the lamellar systems. The absence of the polystyrene transition in the DSC analysis is because the weight fraction of polystyrene being too low for the transition to be observed. As the polybutadiene transition is observed in the same position it is assumed that phase separation is taking place in the copolymer systems because if mixing between the two phases was taking place the glass transition temperature would shift nearer to that of the polystyrene i.e. it would increase.

2.3 Determination of network M_c values

2.3.1 Stress-strain methods

2.3.1.1 Introduction

Force-extension data was related to the network chain density using the Mooney-Rivlin approach[14,15], the interpretation assisted a qualitative description of the chain entanglement contribution. But the method is known to be suspect and entirely phenomenological. A far more satisfactory approach is the theory of Edwards and co workers[12,13], which addresses the problem of chain entanglements by the slip link model, derived from the theoretical model of reptation. Complicated entanglements are represented by the constraint of a contact through which each chain is free to slide, shown in figure 2.3.1a below.

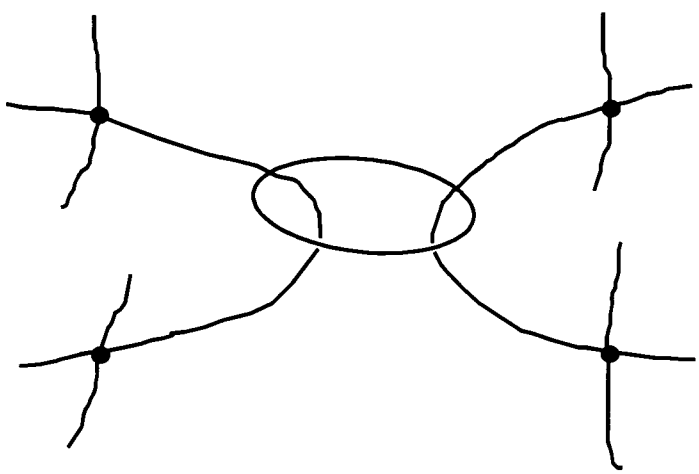

Figure 2.3.1a Diagram that shows a slip-link entanglement

The force-extension data were interpreted in terms of the network structure via two methods:

The Mooney-Rivlin approach and the slip link model of Edwards *et al.*

1. Mooney-Rivlin theory[14,15]

The Mooney-Rivlin equation is an attempt to model the departure from Florys Simple Statistical Theory[16,17] by introducing two empirical constants, C_1 and C_2 shown in equation 2.3.1a.

$$\frac{\sigma}{(\lambda - \lambda^{-2})} = 2C_1 + 2C_2\lambda^{-1} \qquad \text{eq.2.3.1a}$$

A plot of $\sigma/(\lambda-\lambda^{-2})$ versus λ^{-1} should then be linear of slope $2C_2$ and intercept $2C_1$. These parameters are then related to the molecular weight between cross-links, $\overline{M}_c$, via equation 2.3.1b.

$$2C_1 = N_c kT = \frac{\rho RT}{\overline{M}_c} \qquad \text{eq.2.3.1b}$$

where N_C is the number of chemical cross links, k is the Boltzmann constant, T is the experimental temperature, ρ is the density of the network, R is the gas constant and $\overline{M}_c$ the number average molecular weight between cross-links.

2. The Ball-Edwards slip link model[12].

For uniaxial extension, the incompressibility condition was applied, $\lambda_1=\lambda$, $\lambda_2=\lambda_3=\lambda^{1/2}$, and for each sample, the stress-strain data were initially fitted to equation 2.3.1c.

$$\frac{\sigma}{\lambda - \lambda^{-2}} = kT\,[N_c + N_s H\,(\eta, \lambda)] \qquad \text{eq.2.3.1c}$$

where σ is the force per unit unstrained area, N_S is the number of slip links, and $H(\eta,\lambda)$ is the function represented by equation 2.3.1d.

$$H(\eta,\lambda)=\frac{\lambda^2}{\lambda^2+\lambda+1}\left[\frac{1}{(\lambda+\eta)^2}+\frac{\lambda+1}{\lambda(1+\eta\lambda^2)^2}\right] \qquad \text{eq.2.3.1d}$$

where η is a constant that represents the looseness of the network. The reduced stress, $\sigma/(\lambda-\lambda^{-2})$ was plotted against H, and η iterated so as to produce the best linear fit, N_s and N_c being determined from the slope and intercept. The calculated values for N_c, N_s and η were then used to assess the contribution of elasticity from entanglements and chemical cross-links.

2.3.1.2 Procedure

All stress-strain analysis was carried out in the IRC section at the Physics Department of Leeds University. Force-elongation data were obtained for all network samples using an Instron tensile testing machine, equipped with a 2kg load cell (room temp tests) and a 250g cell (high temperature tests), with a circulating air oven. Samples were mounted between clamps, which were fitted with springs to allow for sample softening at higher temperatures. Emery cloth was used between sample and clamp to ensure good contact between the two surfaces. The samples studied were thin sections of network with dimensions approximately 2.1mm wide, between 1-2mm thickness, and 1cm long before extension. The maximum uniaxial extension ratio (λ) obtained was 14. Force-extension experiments were performed at cross-head speeds of 1 cm min^{-1}. Samples of each lamellar and spherical morphology network have been cut so that the physical appearance is void free and uniform.

Unlike chemically uncross-linked materials, samples cannot be prepared as cast films. Occasionally during stretching it was observed that some samples were slightly uneven and contained small voids, weakening part of the material and causing the sample to snap, especially if the void was near the grips on the clamp. Samples that are not uniform increase the error in values of $\overline{M}_c$ due to the inaccuracy of the dimensions used in the slip-link model analysis. Dumb-bell samples were cut out of network strips in an attempt to limit errors caused by using uneven samples, but the problem remained of preparing samples of uniform thickness that were void free.

2.3.2 Swelling measurements

2.3.2.1 Introduction

The purpose of these experiments was to measure the equilibrium swelling ratios, calculate the average molecular weight between cross-links, $\overline{M}_c$, and compare results obtained with stress-strain data from the network systems. The degree of swelling of the network is generally defined in terms of the swelling ratio, Q which relates the mass of the dry network to the mass of the swollen gel shown in equation 2.3.2a.

$$Q = \frac{weight\ of\ swelling\ agent + network}{weight\ of\ dry\ network\ sample} \times \frac{d_r}{d_s} \qquad \text{eq.2.3.2a}$$

d_r is the density of the network sample

d_s is the density of the swelling agent

The polymer network volume fraction, v_p is related to Q in equation 2.3.2b.

$$\nu_p = \frac{1}{1+Q} \qquad \text{eq.2.3.2b}$$

The equilibrium degree of swelling of the network can be related to the cross-link density of the network by the Flory-Rehner model[18] which states that the free energy of mixing is zero at swelling equilibrium.

At swelling equilibrium the Flory-Rehner equation is given by:

$$\frac{1}{\overline{M}_c} = \frac{\nu_p + \chi_{SB}\nu_p^2 + \ln(1-\nu_p)}{-d_r V_o(\nu_p^{1/3} - \nu_p/2)} \qquad \text{eq.2.3.2c}$$

V_O is the molar volume of the solvent

χ_{SB} is the network-swelling agent interaction parameter

The Flory-Rehner equation as discussed above was originally derived for the case of networks cross-linked in the bulk state such as vulcanised rubbers, and as such, is not applicable to the case of model networks prepared by end linking in solution. Since the presence of solvent increases the separation of the cross-links within the network structure and thus the length of the chain and $\overline{M}_c$ will be increased by dilution prior to cross-linking. However, a modified version of the Flory-Rehner equation has been derived by Rotstein and Lodge[19] for the generalised case of networks cross-linked in the presence of low molecular weight solvents and it is this version, equation 2.3.2d which has been used to determine the cross-link density from swelling measurements.

$$\frac{1}{\overline{M}_c} = \left(\frac{c_o}{d_r}\right)^{1/3} \left(\frac{\nu_p + \chi_{SB}\,\nu_p^2 + \ln(1-\nu_p)}{-V_o\,c_o\,(\nu_p^{1/3} - \nu_p/2)}\right) \qquad \text{eq.2.3.2d}$$

c_o is the polymer concentration at cross-linking

2.3.2.2 Procedure

Network samples placed in wire mesh baskets were swollen in toluene at 30°C until no further increase in network mass occurred. The cross-link densities of the lamellar and spherical morphology series of networks were determined from the equilibrium swelling ratio of gels swollen and are shown in the results section of the thesis, Chapter 3, along with the average molecular weights of the precursor chains.

2.4 Small Angle X-ray Scattering (SAXS) analysis

2.4.1 Kratky Camera SAXS analysis

2.4.1.1 Instrumentation

Small angle X-ray scattering experiments were carried out using a Kratky Compact Small Angle System (Anton Paar K.G. A-8054 Graz Austria). The camera parts are built into a cast brass housing which is evacuated to 0.5mbar, using the integrated vacuum system connected to a vacuum pump, during operation. Experimental errors such as thermal fluctuations and air scattering interferences are avoided when the experiments are carried out under vacuum. An XRG 3000 Generator (INEL, Z.A de Courtaboef Av.de.Scandanavie - 91953 LES ULIS) operated at 15mA/25kV generates electrons necessary for the CuKα radiation copper target X-ray tube to create X-rays of wavelength of 1.542Å. The linear, gas tight (90/10% argon/methane) detector, model LPS 50 supplied by INEL, has a beryllium window. A fast analogue-to-digital converter, model 8077 supplied by Canberra Industries, Inc., One State Street, Meriden CT 06450, converts the detected signal and displays the scattering profile on the screen of a PC. The Kratky camera is fitted with a slit collimation system to obtain sufficient scattering intensity. Figure 2.4.1a shows the experimental set-up of the collimating system, sample holder, primary beam stop and detector.

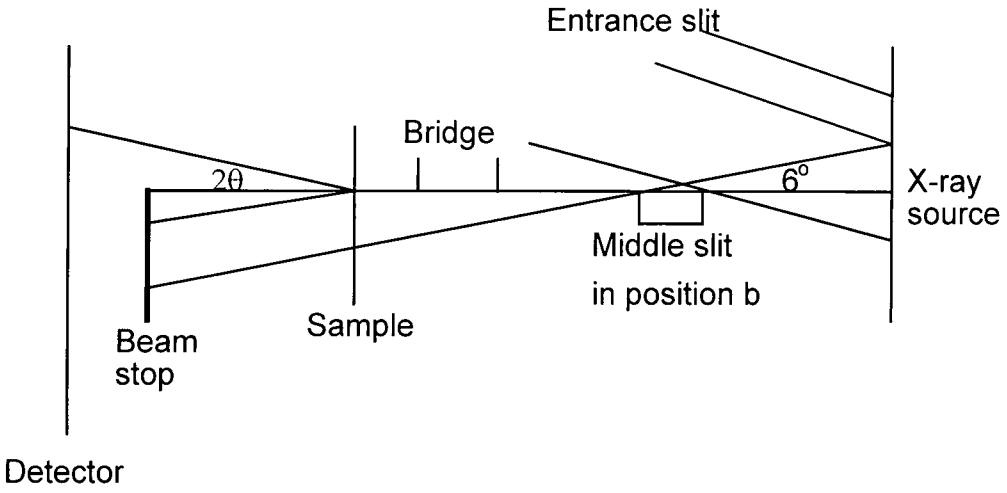

Figure 2.4.1a Schematic cross section of slit collimation geometry seen parallel to the primary beam direction

The middle slit and bridge are fixed in a coplanar position, thus minimising the level of parasitic scattering while forming a horizontal plane. The middle slit is placed in position b and the system is oriented with a projection angle of 6° in all SAXS experiments carried out in this work. The position of the middle slit optimises the set-up in terms of medium to high resolution, medium incident X-ray intensity and an accessible set-up alignment[20]. The width and intensity of the primary beam is regulated by the position of the entrance slit and the radiation entering the counter detector is reduced by the vertical slit. X-rays are directed through the sample (normal to the plane) and radiation is scattered when the beam hits an ordered area of the sample. The resultant readout is plotted as intensity versus scattering vector and referred to as slit smeared data. A moving slit device driven by a sychronous motor attached to the slit holder facility, supplied by Anton Paar, allows measurements of absolute scattering intensity and sample absorption. A Lupolen sample, supplied by Prof. Kratky's laboratory, was used for calibration of intensity values.

2.4.1.2 Sample Preparation

Sample preparation conditions have been employed to promote the system to be driven to thermodynamic equilibrium. Samples of B-S-B triblock copolymers were prepared containing a small amount of anti-oxidant so as to prevent oxidation of the unsaturated polybutadiene, and dissolved in a non-preferential solvent for either block in the copolymer, e.g. toluene, to make a dilute solution (e.g. 10% weight/volume solution). An aliquot of polymer solution is poured on to a covered teflon block which is evaporated at atmospheric pressure at a temperature of 303K so that a polymer film with a quasi-equilibrium state is formed. Network sections were cut from de-swollen bulk material and dried using the same conditions as the block copolymer samples.

A section of each triblock copolymer film/network section (sample dimensions 1cm x 7cm x 1mm) was placed in a glass tube treated with a 10% solution of trimethylchlorosilane in toluene, so as to minimise the polymers sticking to the glass tube after annealing. The glass tubes were evacuated under high vacuum (4×10^{-7} torr) for an hour and then sealed off using a blow torch flame whilst under vacuum. The tubes were placed in a vacuum oven for a week so as to ensure complete annealing at a temperature above the glass transition (T_g) of both polymer constituents (i.e. 393K). Only now can the morphologies of the block copolymers be looked at in a state of thermodynamic equilibrium.

2.4.1.3 Procedure

Four separate SAXS measurements are required to obtain all necessary information for one sample. The background scan measures the parasitic scattering and is obtained by

running the SAXS with no sample present. The background transmission run is carried out without sample with a moving slit going forward and backwards five times and thus passes the primary beam ten times and determines the intensity of the primary beam. The sample transmission run with the sample under investigation present allows a comparison of sample and background intensities. The sample run measures the scattering intensities of the sample.

2.4.1.4 Correction and normalisation of data

The data obtained from the four SAXS runs of each sample were analysed using the two programs SAXFIL and FFSAXS5. The raw data is prepared in SAXFIL, which contains parameters for the routines in FFSAXS5. Initially SAXFIL provides the values of wavelength, sample to detector distance, focus to sample distance, calibration and transmission factors and values to calculate the channel height above the position of the main beam[21]. After this the parameters necessary for FFSAXS5 routines are produced, all summarised below with used values:

SCAL - 1 2 1 0 0 0 : scales the intensity of the parasitic instrumental background intensity in data set 2 to the level of the sample intensity data set in 1.

SUB - 1 2 : subtracts the sample background intensity values in set 2 from the sample data set in 1.

BKGR - 1 3 0 30000 38000 : calculates the sample background (incoherent scattering) and subtracts this from the sample data set 1 and stores the result in the, now smeared background corrected, dataset 1. The curve fitting of the background scattering is

determined by the last two values given to the subroutine for the background range, this determines the quality of the output data.

DESM - 1 3 0 0 0 : the smeared intensities of the background corrected data in set 1 is desmeared according to Vonk[22] and placed in data set 3.

ANAL - 3 0 0 0 0 0 0 0 0 0 0 0 0 : lists the required information in data set 3 in a format necessary for analysis of the scattering curve and includes the channel number distance along the detector, s and H values ($H=2\pi s=(4\pi/\lambda)\sin(\theta/2)$) and the number of counts.

CORL - 3 0 0 5 700 : calculates one and three dimensional correlation functions by Fourier transformations where the intensity curve is extrapolated to x=0 using a Gaussian function, from R=0-700 Å, with an incremental value of 5.

The data has now been organised for the input to FFSAXS5, the 5th update of the FORTRAN routines originally created by Vonk[23]. Great care must be taken when preparing the data in SAXFIL since small changes in the parameter input in FFSAXS5 lead to large differences in the desmeared intensity distributions and correlation functions. The normalisation and correction of the raw data file yields a file of desmeared X-ray scattering intensity distribution as a function of s, which will be used in further analysis.

2.4.2 Time-resolved synchrotron Small Angle X-ray Scattering (SAXS)

Synchrotron radiation is produced at the Synchrotron Radiation Source (SRS) when an electron beam travelling close to the speed of light is accelerated in a magnetic field. The radiation covers a broad area of the electromagnetic spectrum, from infrared through to hard X-rays. Synchrotron X-rays are much more intense than those from a conventional laboratory source, enabling researchers to carry out experiments in a very short time. The radiation from the SRS has other important properties making it different to ordinary radiation; it comes in regular pulses, allowing data to be collected like a movie on samples which vary with time. The radiation is also very highly polarised, linearly in the centre of the beam and circularly above and below centre.

When a charged particle travelling close to the speed of light is accelerated, it emits the broad spectrum of photons known as synchrotron radiation. At the SRS a beam of electrons is accelerated when it passes through a magnetic field, changing its path. The field is produced by sixteen huge 'dipole' electromagnets which constrain the beam to a roughly circular path 96m around with a diameter of 30.56m. Synchrotron radiation is emitted from charged particles in a magnetic field and collected from 12 magnets to feed experiments and test facilities shown in figure 2.4.2a.

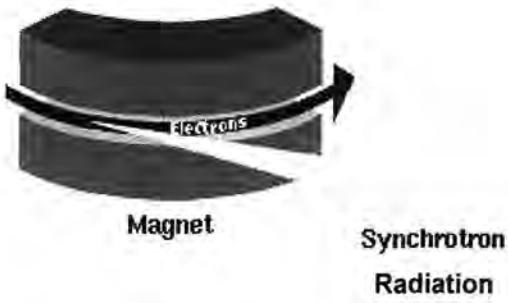

Figure 2.4.2a Synchrotron radiation emitted from magnetic field of Daresbury instrument

The radiation emerges like a searchlight in front of the emitting particle so it appears at a tangent to the bend. Three special magnets known as 'insertion devices' also produce radiation at the SRS. The type of radiation produced at sources like the SRS depends on both the energy of the electron beam and the magnetic fields used to bend the beam. The higher the beam energy, the shorter the wavelength of the radiation produced. Strong magnetic fields will bend the beam more sharply - a greater acceleration which also gives shorter wavelength light. The electron beam loses a great deal of energy emitting synchrotron radiation. To replace this energy, the electron beam bunches are 'pushed along' by radio frequency (RF) waves. The RF is fed into the electron beam in four places as the beam travels around the SRS. This way the same electron beam can emit synchrotron radiation continuously for many hours. Synchrotron experiments at the Daresbury source were performed at work station 16.1.

2.4.2.1 Technical Description of beam station 16.1

Station 16.1 is a fixed wavelength, high intensity diffraction station and has been optimised for low angle scattering studies, but is also capable of some wide angle diffraction. It is used largely by polymer scientists (both biological and non-biological) to study dynamic processes. The station routinely operates in the millisecond time regime, but can operate on the microsecond scale. The data acquisition and motor drive software both operate via a Graphical User Interface.

Wavelength = 1.4Å

Monochromator:

Ge 111 triangle (a=10.5°), bent for horizontal focusing

Cooling system: liquid Ga In Sn

Distance from Tangent Point = 9.74m

Horizontal acceptance: 12 mrad

Mirror:

Pt coated fused quartz (1.2m long)

Distance from Tangent Point = 11.25m

Vertical acceptance from Tangent Point =11.25m

The station presently operates at 6mrad horizontal aperture. Using a standard Daresbury ion chamber (operating in air at 1000V), the user can expect to obtain a reading of 6.5V+/- 0.2V at 250mA. This value is recorded with all post monochromator slits open.

2.4.2.2 Procedure

Samples used at the synchrotron source were the same as the ones used in the Kratky camera. Two separate SAXS measurements are required to obtain necessary information for one static sample. The background scan measures the parasitic scattering and is obtained by running the SAXS with no sample present. The sample transmission run with the sample under investigation present allows a comparison of sample and background intensities. The sample run measures the scattering intensities of the sample. Stretched samples undergo a similar procedure for data acquisition except that frames of data are collected over a time span that incorporates sample stretching to an extension ratio of four ($\lambda = 4$).

2.4.2.3 Data correction and normalisation

Two dimensional raw data was analysed on the Daresbury SUN system computers using the software package BSL. BSL is a 2-D interactive data manipulation package for image data. The program has a wide range of applications even if some of the instructions and options are specific to X-ray applications. BSL was developed by J. Bordas and G. Mant and was based on the OTOKO package sharing the same data format and interface style. This allows data to be reduced to 1-D in BSL and then imported to computer systems in Durham for further processing. The program is available for all major hardware platforms (Sun, HP, DEC, and SG) as BSL and runs on X-windows based workstations. The instruction manual used for data analysis is based on contributions from the original authors, R. Rule (ICI, Runcorn) and I. Dobbie (Kings College).

The following commands were used as operations to transform the two dimensional raw data to one dimensional data analysed on plotting packages in Durham.

.DIN Divide and normalise image using a calibration file

.DIV Weighted division of data file with detector response file

.ADD Weighted subtraction of background data file from sample data file

.SHF Shift an image in x and/or y directions to eliminate bars on the detector

.RMP Remap an image to a given set of remapping points

.HOR Perform a horizontal integration in a selected region

.VER Perform a vertical integration in a selected region

Using the program 'reconv2' the files are subsequently converted to readable ascii files that can be transferred using FTP to the Durham computer systems for analysis.

2.5 Solid State ^1H NMR

2.5.1 Introduction

Information from a number of solid state ^1H NMR experiments can be combined in a numerical model of a heterogeneous polymer system, which can then be optimised by varying a small number of parameters to fully represent the spin diffusion and relaxation behaviour of the system. Useful information can be obtained about the size of the heterogeneities present and also the intrinsic relaxation behaviour of the different regions. All solid state ^1H NMR experiments and data analysis were carried out by Dr. Alan Kenwright at the Chemistry Department, University of Durham.

The Goldman-Shen experiment has been developed to analyse the copolymer and network systems to yield information needed to calculate the repeat lengths (domain spacing values). The experiment is well established and has been used extensively to study the heterogeneity in polymer systems on length scales ranging from a few angstroms to micrometers[24,25]. Information derived using the Goldman-Shen experiment has helped generate a model that fully represents the spin diffusion and relaxation behaviour of the systems giving accurate values for the characteristic diffusion lengths as well as information about the intrinsic relaxation properties of the regions.

2.5.2 Procedure

Measurements were carried out using a custom-built[26] spectrometer operating at a ^1H frequency of 59.95 MHz, and using a 90° pulse duration of 2.0μs. All measurements were carried out at 295K, and samples were stored in a freezer between measurements to prevent oxidation. Samples were prepared by sectioning with a scalpel in to small

strips (≈0.20g) and inserting them in the special solid state NMR tubes for the experiments to be carried out. The orientation of the sample in the tube is not important due to the nature of the experiment performed.

When analysing the systems with a polystyrene weight fraction of 0.15 it was impossible to get reproducible results that matched data obtained from SAXS. The reason being the weight fraction of polystyrene being too low for the rate of spin diffusion transfer to be measured accurately between the two phases. Relaxation and diffusion measurements will not alter when sample orientation is varied. This is different in SAXS analysis when results can be variable if sample orientation is changed.

2.5.3 Data analysis

After acquisition of the data from the experiments the signal was analysed using a non-linear least squares optimisation of the two region numerical model using the Simplex algorithm[27]. The data was then fitted to a model with seven variable parameters and values of the domain spacing were calculated from the effective spin diffusion coefficient[28] and the time taken to reach the magnetisation level appropriate to full mixing (see Chapter 5).

2.6 References

[1] Flory, P.J. *Principles of Polymer Chemistry*, Cornell University Press, Ithaca, N.Y., **1953.**

[2] Cowie, J.M.G. Polymers: Chemistry and Physics of Modern Materials, Blackie, London, **1991.**

[3] Morton, M. *Anionic Polymerisation: Principles and Practice*, Academic Press, New York, **1983.**

[4] Morton, M.; Fetters, L.J. *Macromol. Revs.*, **1967,** *2.*

[5] Morton, M.; Fetters, L.J. *Rubber Chem. and Technol.*, *48*, 359.

[6] Tung, L.H.; Lo, G.Y.S. *Macromolecules*, **1994,** *27*, 2219.

[7] Nugay, T.; Kucukyavuz, S. *Polymer International*, **1992,** *29*, 195.

[8] Quirk, R. P.; Ma J.J. *Polymer International*, **1991,** *24*, 197.

[9] Tung, L.H.; Lo, G.Y.S.; Beyer D.E. U.S. Pat. 4-172190 **1979.**

[10] Douy, A.; Gallot, B. *Die Makromoleculare Chemie* **1971,** *156*, 81.

[11] Morton, M. et al *Polymer Letters Edition* **1973,** *11*, 449.

[12] Ball, R.C.; Doi,M.; Edwards, S.F.; Warner, M. *Polymer,* **1981,** *22*, 1010.

[13] Edwards, S.F.; Vilgis, Th. *Polymer,* **1986,** *27*, 483.

[14] Mooney, M. *J. Appl. Phys.* **1948,** *19*, 434.

[15] Rivlin, R.S. Phil. Trans. Roy. Soc. London Ser. A **1948,** *241*, 379.

[16] Flory, P.J. *Chem. Rev.* **1944,** *35*, 51.

[17] Flory, P.J. *Ind. Eng. Chem.* **1946,** *38*, 417.

[18] Flory, P.J.; Rehner, J. *J. Chem. Phys.* **1943,** *11*, 521.

[19] Rotstein, N.A.; Lodge, T. P. *Macromolecules*, **1992,** *25*, 1316.

[20] Kratky, O.; Stabinger, H. *Anton paar manual Kratky Compact Small Angle System* **1984.**

[21] Richards, R. W. *FFSAXS5 manual Data normalisation and correction for small angle scattering data,* University of Durham.

[22] Vonk, C. G. *J. App. Cryst.* **1971,** *4*, 340.

[23] Kratky, O.; Skala, Z. *Electrochem.* **1958,** *62*, 73.

[24] Kenwright, A.M.; Say, B.J. in Ibbet, R.N. (Ed.), *NMR Spectroscopy of Polymers, Blackie, Glasgow,* **1993** (and references therein).

[25] Demco, D.E.; Johansson, A.; Tegenfeldt, J. *Solid State NMR* **1995,** *4*, 13 (and references therein).

[26] Harris, R.K.; Kenwright, A.M.; Royston, A.; Say, B.J. *Meas. Sci. Technol.* **1990,** *1*, 1304.

[27] Nelder, J.A.; Mead, R. *Computer Journal* **1965,** *7*, 308.

[28] Spiess, H.W.; Schmidt-Rohr, K.; Clauss, J. *Acta Polymer.* **1993,** *44*, 1.

CHAPTER 3

Stress-Strain and Swelling Properties

3.1 Stress-Strain Analysis

3.1.1 Introduction

Chemically cross-linked BSB triblock copolymer networks that comprise tetrafunctional cross-links, free-chain ends, trapped entanglements and closed loops were stretched at room temperature (298K) and at 398K, the latter temperature being above the T_g value of both the constituents of the copolymer. At 398K, the networks display rubber-like elasticity by virtue of the chemical cross-links. There is uncertainty as to how much trapped and non-permanent physical entanglements contribute to this elasticity. Complicated entanglements are represented by the constraint of a contact through which each chain is free to slide. Figure 3.1a shows a typical system that is end cross-linked and the imperfections that such networks tend to possess.

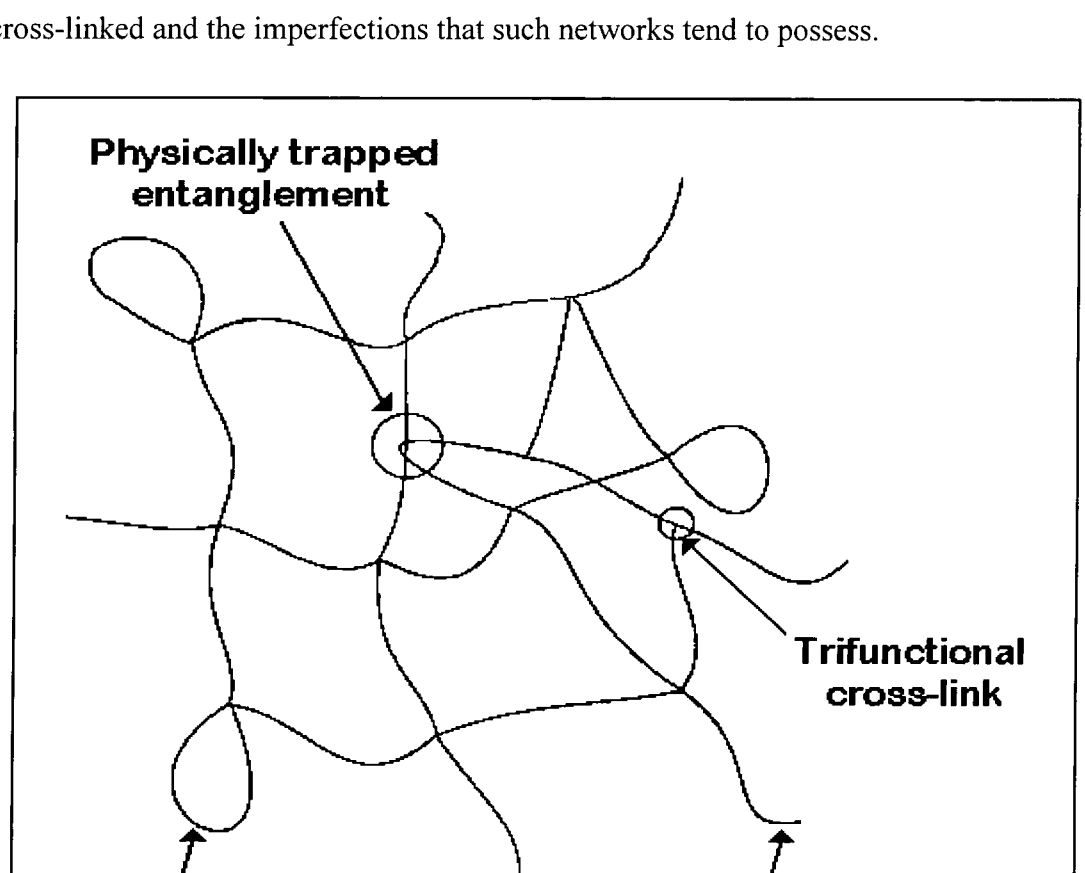

Figure 3.1a End cross-linked network with structural imperfections

The networks were studied over a range of cross-link densities to investigate the effect of physical entanglements as network properties vary. Results were analysed using two separate methods, the Mooney-Rivlin (M-R)[1,2,3] treatment and the Ball-Edwards (B-E) slip link model[4,5]. The results interpreted in terms of apparent molecular weight between cross-links, $\overline{M}_c$, suggest that physical entanglements (N_s) vary in effectiveness over the range of chemical cross-link (N_c) densities used. In the literature, values of N_c and N_s increase with chemical cross-link density implying that the formation of each chemical cross-link 'ties in' a number of entanglements, this renders them elastically effective[6].

3.1.2 Room temperature stress-strain analysis (298K)

Samples investigated at room temperature were analysed using only the B-E slip link model since the M-R model was not suitable for room temperature analysis because of the lack of rubber-like elastic behaviour from the network systems. Glassy polystyrene sections in the samples influenced the stress-strain properties to a dominant extent and the $\overline{M}_c$ values were only apparent ones. The B-E slip link expression was fitted to the data from the stress-strain experiments performed on the samples. Fitting of the data involved selecting a section of data points to be used to obtain values for N_c, N_s, and η so that the reduced stress (σ^*) versus reciprocal extension ratio (λ^{-1}) plot was linear, where reduced stress = $(\sigma/(\lambda-\lambda^{-2}))$. A section of data points from the plot was used to obtain values of a, b, and η by using the data that has a constant linear slope. Where **a** = N_ckT (kPa) = $\frac{\rho RT}{\overline{M}_c}$ and **b** = N_skT (MPa). The parameter η is a representation of the overall looseness of the network structure. A plot of the data needed to create a B-E slip link model fit is shown in figure 3.1b.

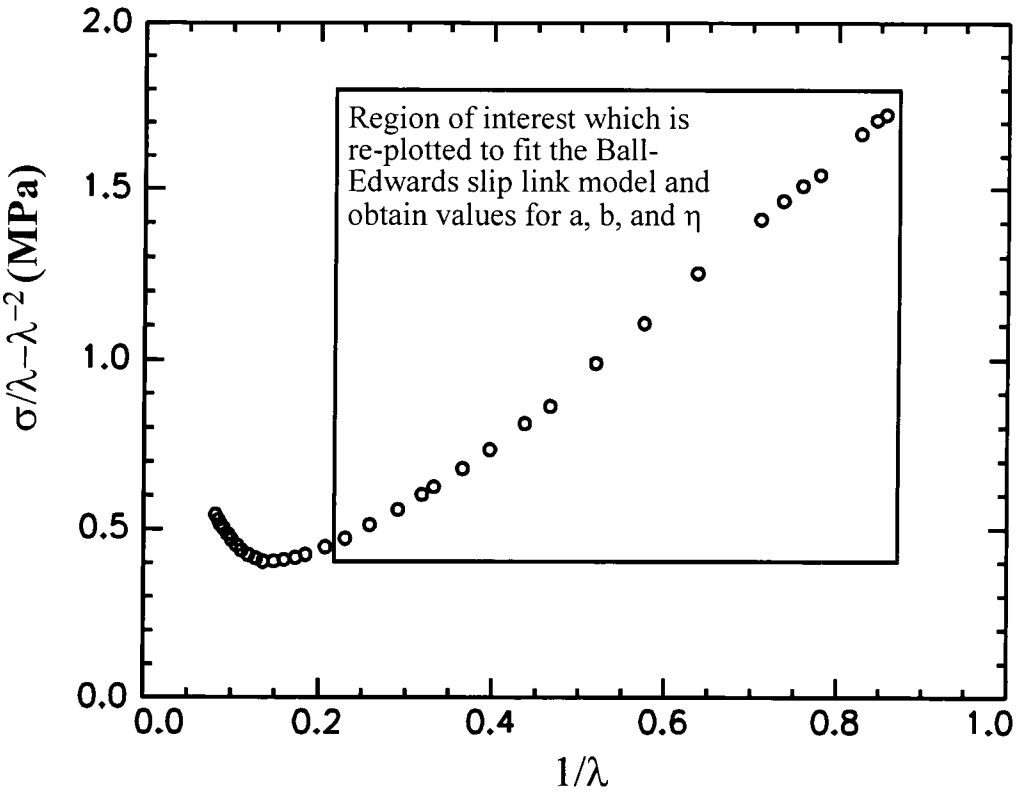

Figure 3.1b Network sample room temperature plot of σ^* versus λ^{-1}

The plot illustrates a sharp upturn in the reduced stress at high deformation. This is a feature of the more highly cross-linked network samples and is accounted for in theory as an inextensibility parameter α, corresponding to a theoretical maximum draw ratio (α^{-1})[6]. The parameter α represents any chemical network chain connectivity capable of imposing a restriction on the finite extensibility of the sample.

Data obtained from the linear plot is then fitted to equation 3.1a and the three variable network parameters (**a**, **b** and η) are obtained from the fit.

$$y = \mathbf{a} + \mathbf{b}*(x^2/(x^2 + x + 1))*((1/(x + \eta)^2)+((x + 1)/(x*(1 + \eta*x^2)^2))) \qquad \text{eq.3.1a}$$

y = reduced stress (σ^*) data point

x = extension ratio (λ) data point

Figure 3.1c shows a B-E fit of a room temperature experiment to obtain the variable parameters a, b, and η.

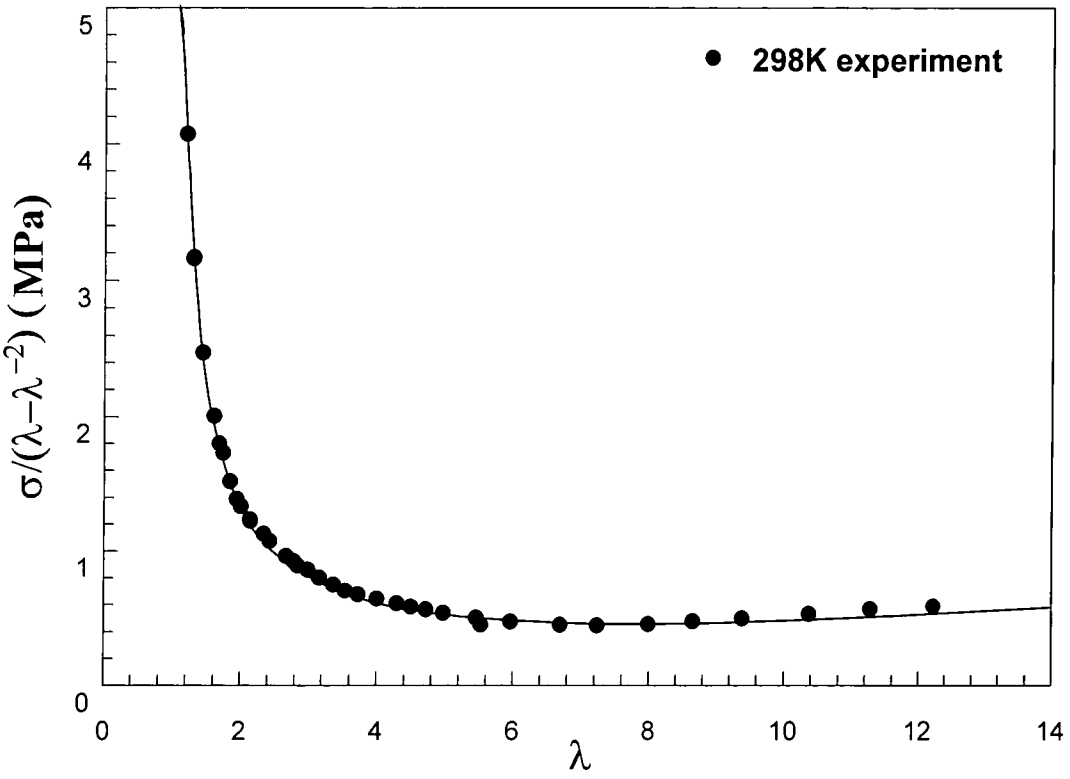

Figure 3.1c Data fit of B-E model to obtain network parameters a, b and η

Table 3.1a shows values of a, b, η, and $\overline{M}_c$ obtained from the B-E slip link model for lamellar network samples at room temperature. The table below, 3.1a shows the effects of annealing and orientation of sample upon values of $\overline{M}_c$ from a set of the lamellar network systems.

Table 3.1a Stress-strain analysis of lamellar network samples at room temperature

Network	a (kPa)	b (MPa)	η	$\overline{M}_c$ (k)	$\overline{M}_c$ of precursor polymer (k)
NL4pe	297	5.59	0.83	11	**60**
NL4pa	302	4.98	0.75	8.5	
NL4pe.an	331	6.40	0.88	7.5	
NL4pa.an	222	11.84	0.96	11	
NL5pe	105	13.82	0.85	24	**70**
NL5pa	174	20.64	1.11	14	
NL5pe.an	220	21.70	1.15	14	
NL5pa.an	318	16.96	1.09	7.8	
NL6pe	89	8.21	0.89	28	**80**
NL6pa	321	7.90	0.72	8	
NL6pe.an	76	24.10	1.21	30	
NL6pa.an	475	6.06	0.51	5.5	

pe is a perpendicular slice of network sample with respect to the surface of evaporation

pa is a parallel section with respect to the surface of evaporation

an denotes if the sample has been annealed

Figure 3.1d is a diagram representing the orientation of samples taken from bulk network with respect to the surface evaporation area.

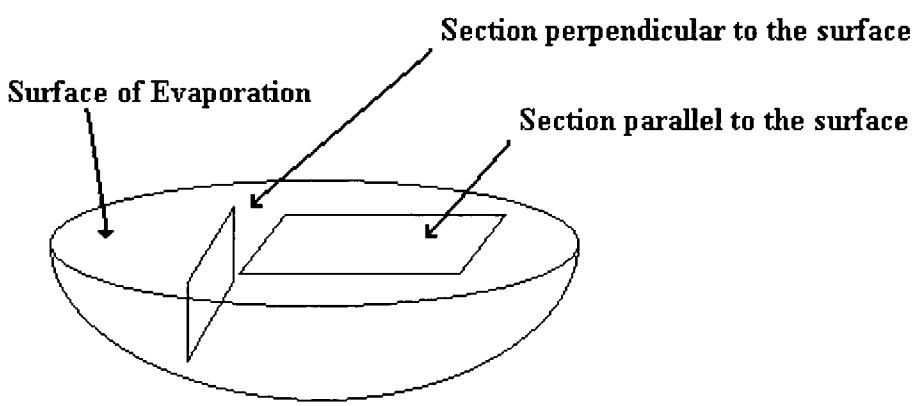

Figure 3.1d Network surface of evaporation area

Results from table 3.1a show that sample orientation is not a factor that influences $\overline{M}_c$ values at room temperature, and is strong evidence that lamellar phase separation does not occur preferentially in one plane, i.e. the distribution of orientations is anisotropic. Values of $\overline{M}_c$ do not seem to vary on annealing network samples meaning that structural stress is created by the cross-links in the sample and not due to any changes in the microstructure of the materials after the treatment. Table 3.1b is a summary of the average $\overline{M}_c$ values obtained from the B-E slip link model analysis of the lamellar network systems.

Table 3.1b Stress-strain analysis on lamellar network samples at room temperature

Network	$\overline{M}_c$ **from chemistry (k)**	**a (kPa)**	**b (MPa)**	η	$\overline{M}_c$ **(k)**
NL1	30	954	17.45	0.86	3.3
NL2	40	476	18.08	1.10	6.7
NL3	55	515	19.47	1.42	6.2
NL4	60	1155	3.38	0.84	2.8
NL5	70	1087	25.03	0.94	2.9
NL6	80	417	5.65	0.83	7.6

Results of $\overline{M}_c$ values for the lamellar network samples stretched at room temperature did not seem to have any correlation with expected values from the chemistry of the network precursor polymers. The influence of the glassy polystyrene blocks caused deviations from the rubber-like elastic behaviour of the polybutadiene jeopardising the accuracy of the B-E slip link fit. Values of $\overline{M}_c$ in table 3.1b are lower than in table 3.1a because samples in table 3.1b were dumb-bell shaped as opposed to thin polymer strips. The thin strips tend to yield and break at point of clamping whilst the dumb-bell shaped samples break in the middle decreasing the error that rectangular strips could introduce in to the analysis.

Table 3.1c shows values of a, b, η, and $\overline{M}_c$ obtained from the B-E model for spherical morphology network samples at room temperature. The analysis involved uses the same method as the lamellar network series with dumb-bell shaped samples.

Table 3.1c Stress-strain results for spherical network samples at room temperature

Network	$\overline{M}_c$ from chemistry (k)	a (kPa)	b (MPa)	η	$\overline{M}_c$ (k)
NS1	35	254.8	1.85	0.90	12.5
NS2	45	80.4	2.10	1.17	30.5
NS3	50	129.1	2.11	1.05	24.7
NS4	60	54.7	4.15	1.56	44.8
NS5	80	87.9	2.00	0.83	27.9
NS6	100	28.7	3.60	1.62	85.5
NS7	150	120.2	3.62	1.39	26.5

Lamellar systems have lower $\overline{M}_c$ values than the spherical systems at room temperature. Physical properties of the dried lamellar network samples are stiffer and stronger than the spherical morphology systems because of the greater PS content and the PS phase is continuous in them. These effects are shown in figure 3.1e.

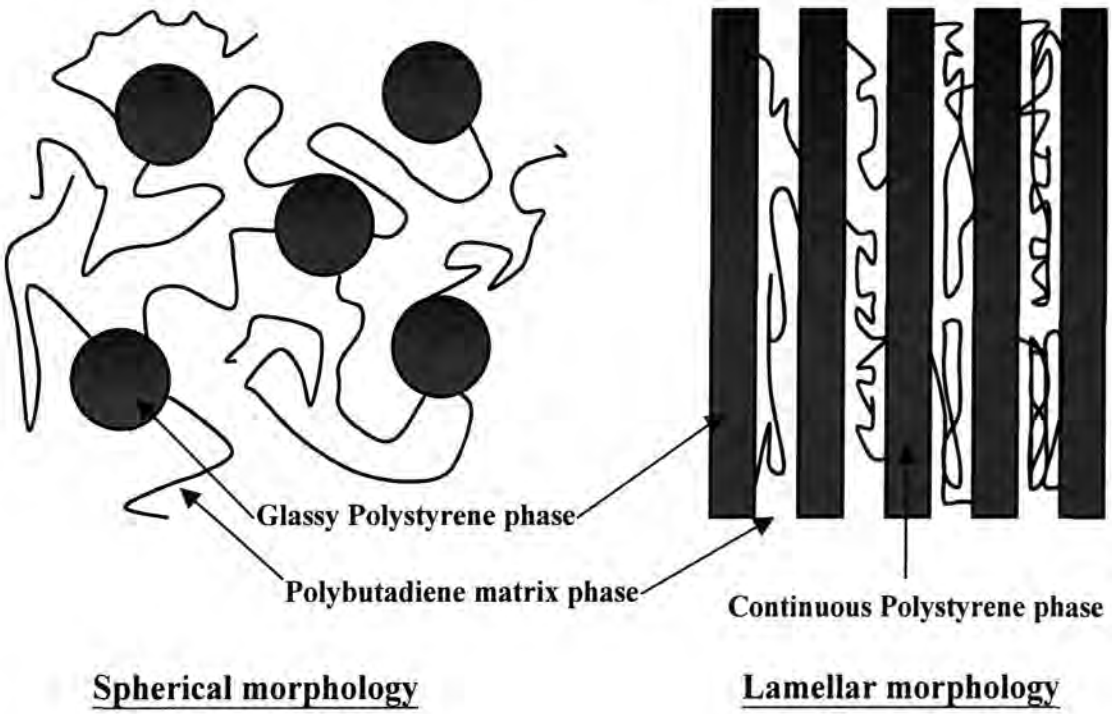

Figure 3.1e Structural differences between spherical and lamellar network systems at room temperature

The differences in physical properties between the two systems have changed the range of experimental $\overline{M}_c$ values in the spherical morphology networks, making it much greater than the lamellar system range. This is due to the spherical morphology samples retaining more rubber-elastic behaviour at room temperature than the lamellar ones. $\overline{M}_c$ values of the spherical morphology systems stretched at room temperature appear to increase in a manner which does not follow the expected trend which is further evidence that this method of analysing polymer networks where one component in the system is below its T_g is not accurate. The B-E model is not a realistic model for room temperature analysis of the network systems due to the ordered phase of polystyrene chains evolved in the melt state. The B-E model is not designed to fit networks that possess ordered phases of polymer chains.

3.1.3 Stress-strain analysis at 398K : Mooney-Rivlin (M-R) Theory

Analysis using the Mooney-Rivlin (M-R) model was initially used on the network systems to obtain an indication of the $\overline{M}_c$ values in question. Samples were stretched at a temperature of 398K in the rubber-like elastic state where only chemical cross-links and physical entanglements contribute to the stress in a force-elongation experiment. Values of $\overline{M}_c$ calculated from M-R data plots were obtained from fits similar to the one shown in figure 3.1f. Results obtained from the lamellar systems that demonstrate the effects of sample preparation are shown in table 3.1d. M-R data compared with Ball-Edwards slip-link model data is presented graphically in section 3.3.3 of the chapter.

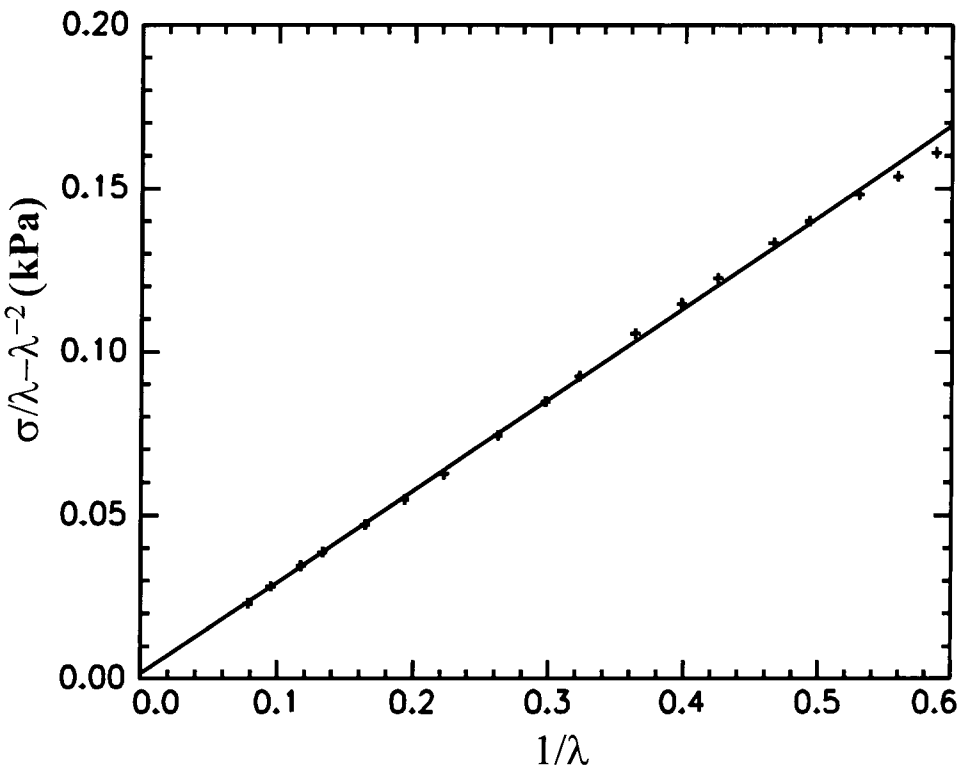

Figure 3.1f M-R plot of reduced stress (σ^*) versus λ^{-1} for a network sample

The intercept obtained from the line of best fit on the M-R plot is taken from extension ratios ranging from 1.5-10.0 and is related to the $\overline{M}_c$ using equation 3.1b.

$$Intercept = \frac{\rho RT}{\overline{M}_c} \qquad \text{eq.3.1b}$$

ρ is density of the network system

R is the gas constant

T is the experimental temperature

Table 3.1d $\overline{M}_c$ values calculated from M-R plots for lamellar systems at 398K

Network	$\overline{M}_c$ **from precursor polymer (k)**	**Strip samples (k)**	**Dumb-bell samples (k)**
NS1	30	250	35
NS2	40	320	95
NS3	55	450	160
NS4	60	650	175
NS5	70	500	160
NS6	80	360	190

Sample strips have dimensions of 1cm × 1cm × 1-2mm after being clamped.

Dumb-bell samples have dimensions 1cm × 2.1mm × 1-2mm after being clamped.

Figure 3.1g shows the two forms of network sample used in the stress-strain experiments. The dumb-bell sample preparation is performed using a dumb-bell punch metal cutter so that every sample has the same dimensions and there is no ambiguity in the results from sample preparation. Variation in sample thickness is accounted for in the analysis of the force elongation curves from the materials.

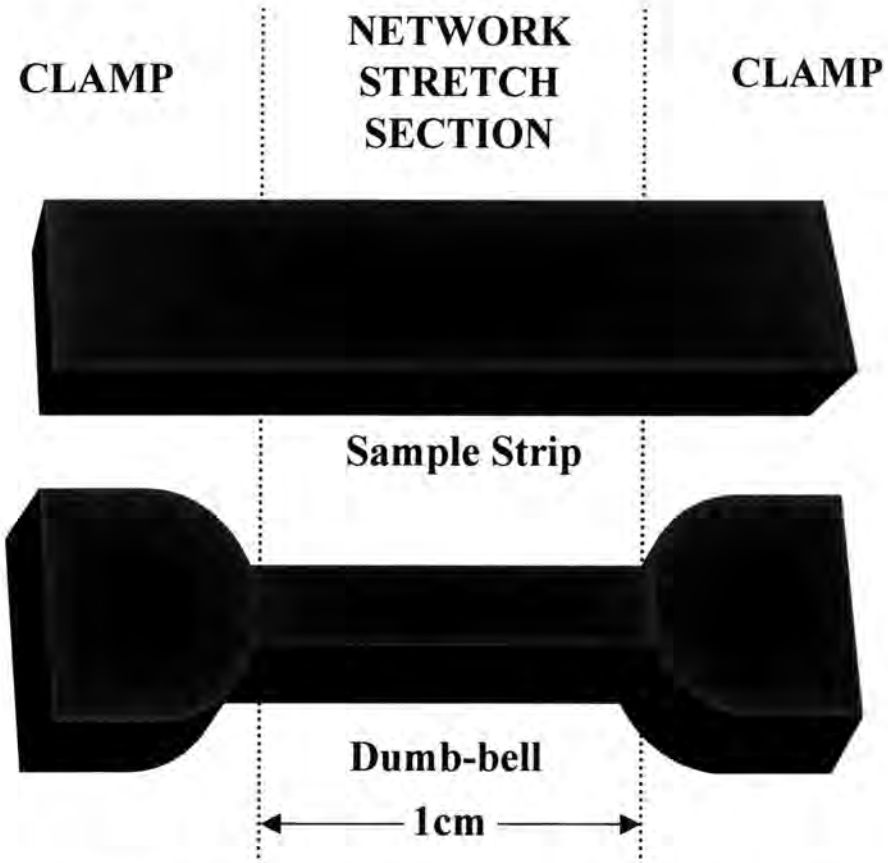

Figure 3.1g Network sample preparation for stress-strain analysis

The lamellar network samples show greater $\overline{M}_c$ values at 398K than at room temperature due to the decreased contribution of stress from the polystyrene segments that are in the rubber-like elastic state at 398K. The values of $\overline{M}_c$ obtained by stress-strain analysis increase with the trend expected from the molecular weights of the precursor polymers. Values of $\overline{M}_c$ increase at a greater rate than might be expected from the differences in actual molecular weight due to the presence of imperfections and physical entanglements in the networks. Comparing the results obtained from the strip samples and dumb-bell specimens, the difference that sample preparation makes to the outcome of the data can be seen. Strip sample values for the $\overline{M}_c$ are variable but increase with increasing precursor molecular weight. Whereas the dumb-bell specimens show the same trend increasing in the direction expected with lower $\overline{M}_c$ values. This comparison shows the unreliability of results obtained from strip sample preparations,

caused by weakening and breakage at clamping points distorting the trend observed using dumb-bell sections for analysis.

Table 3.1e shows results obtained from the analysis at 398K of the spherical morphology network systems using M-R theory. Comparisons to B-E slip link model data are presented in section 3.3.3 later in the chapter.

Table 3.1e Values of $\overline{M}_c$ calculated from M-R plots for spherical morphology systems

Network	$\overline{M}_c$ from precursor polymer (k)	Strip samples (k)	Dumb-bell samples (k)
NS1	35	160	95
NS2	45	130	60
NS3	50	230	85
NS4	60	190	60
NS5	80	500	110
NS6	100	360	600
NS7	150	470	540

Spherical morphology network samples show some correlation with expected trends. The data indicates there is a variable increase of $\overline{M}_c$ when compared to the precursor molecular weight values. Experimental $\overline{M}_c$ values obtained appear to be very high using the M-R theory, therefore rendering the method inaccurate and only useful for estimates of $\overline{M}_c$ when analysing networks of this type. Using low types of bulk sample geometry produce the same kind of pattern for the spherical morphology samples as for the lamellar network analysis. Results were high for both strip and dumb-bell sample analysis but more so for the strip samples. Leading to the conclusion that further comparisons need to be made with the B-E slip link model analysis before further conclusions can be made.

3.1.4 Stress-strain analysis at 398K: Ball-Edwards slip link model

The B-E slip link model is a more rigorous technique when analysing data obtained from force-elongation curves of rubber-like elastic materials. Equation 3.1b was used on data from force-elongation experiments carried out at 398K. An example of a data fit of the reduced stress (σ^*) versus extension ratio (λ) plot used to obtain values of a, b, and η is shown in figure 3.1h.

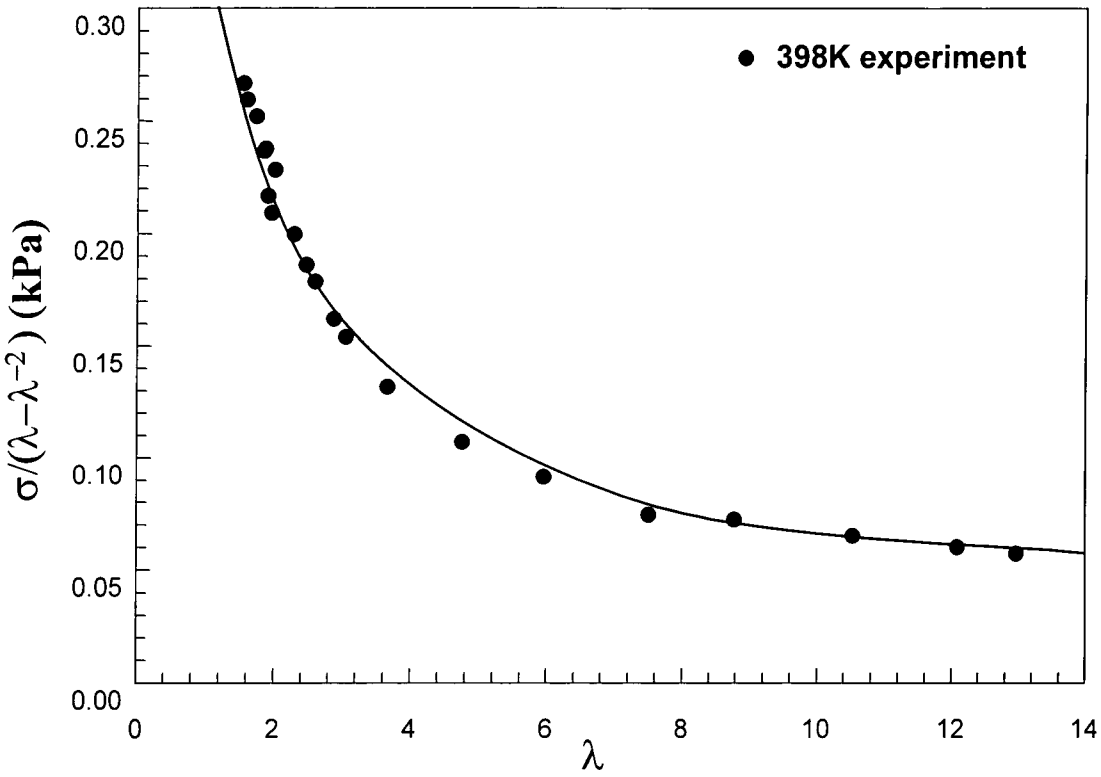

Figure 3.1h Data fit of B-E model to obtain network parameters a, b and η

Values of a, b, η, and $\overline{M}_c$ obtained using the B-E slip link model for the lamellar network samples measured at 398K are shown in table 3.1f. The table looks at the effects of sample orientation and annealing when using the analysis to investigate the $\overline{M}_c$ values of the systems.

Table 3.1f 398K Stress-strain analysis on lamellar network samples

Network	a (kPa)	b (MPa)	η	$\overline{M}_c$ (k)	$\overline{M}_c$ of precursor polymer (k)
NL4pe	14.1	3.12	2.18	235	**60**
NL4pa	8.7	1.82	2.15	380	
NL4pe.an	13.4	2.64	1.94	240	
NL4pa.an	12.8	2.84	2.01	250	
NL5pe	11.9	1.17	1.51	280	**70**
NL5pa	8.1	2.78	1.99	300	
NL5pe.an	8.4	1.90	1.77	380	
NL5pa.an	25.6	3.00	1.63	125	
NL6pe	2.75	2.20	2.29	1 200	**80**
NL6pa	7.8	1.97	1.83	400	
NL6pe.an	10.6	2.95	2.22	300	
NL6pa.an	31.8	1.90	1.63	100	

pe is a perpendicular slice of network sample with respect to the surface of evaporation

pa is a parallel section with respect to the surface of evaporation

an denotes if the sample has been annealed

Results from table 3.1f show a random spread of values for each sample set showing that orientation and annealing have no effect on the eventual $\overline{M}_c$. Although it is apparent that strip samples give higher values of $\overline{M}_c$ than dumb-bell shaped sample results shown in table 3.1g.

Table 3.1g Lamellar dumb-bell samples analysed using the B-E model at 398K

Network	a (kPa)	b (MPa)	η	$\overline{M}_c$ (k)
NL1	127.7	0.368	0.74	25
NL2	69.6	0.233	0.29	46
NL3	54.8	0.526	0.51	58
NL4	31.0	5.60	2.04	103
NL5	36.7	2.81	1.85	87
NL6	31.6	3.63	1.46	100

The B-E model produces $\overline{M}_c$ values nearer the precursor polymer ones than M-R theory, but sample preparation must involve the use of specially cut dumb-bell specimens. Results from table 3.1g show an increase in overall $\overline{M}_c$ values compared to room temperature analysis satisfying the theory of glassy polystyrene lamellae behaving rubber-elastic like at 398K. A typical example of a σ^* versus λ^{-1} plot for the B-E analysis at 398K is shown in figure 3.1i.

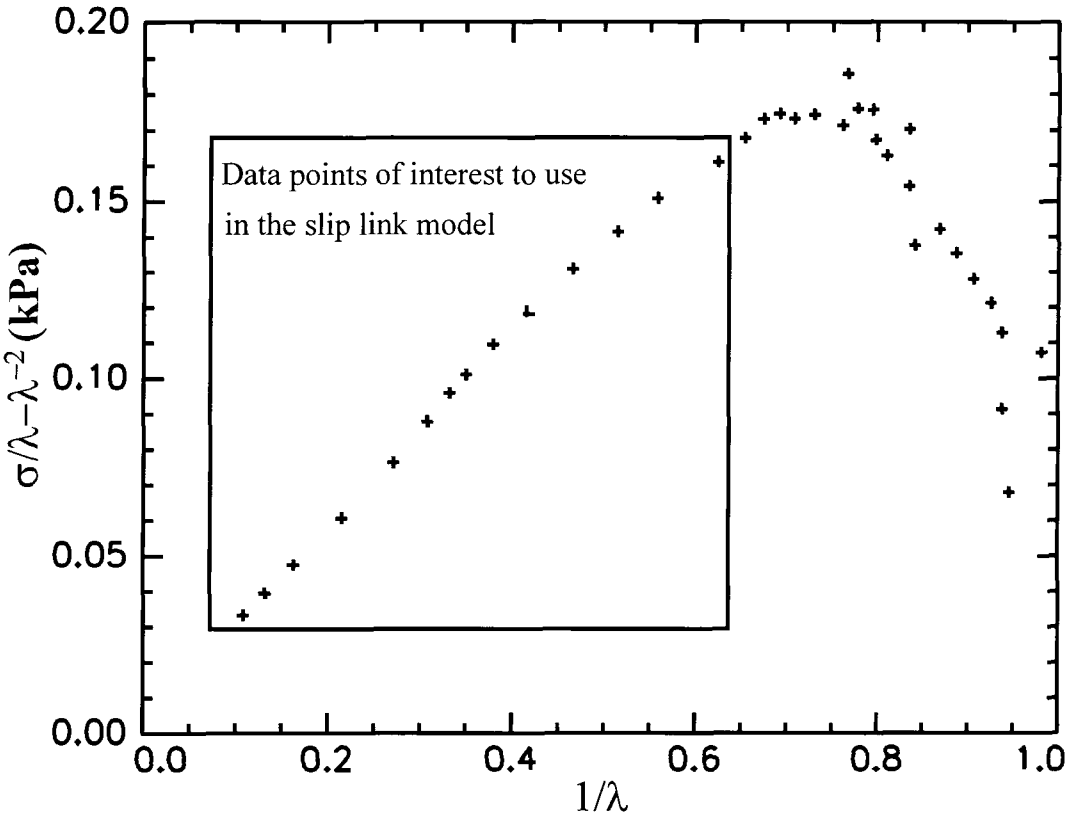

Figure 3.1i Typical reduced stress versus λ^{-1} plot from force-elongation data at 398K

From the plots of σ^* versus λ^{-1} a set of data points from the linear section of the data were chosen to be fitted by equation 3.1a in order to obtain values of a, b and η. Plotting σ^* versus λ then enables the equation to be fitted to the data. The complexity of the function in the B-E model takes in to account parameters involved in more realistic

polymer network behaviour. Figure 3.1j shows a comparison between M-R data and B-E data obtained from dumb-bell samples for the series of lamellar networks. A model network trend refers to a perfectly cross-linked network system.

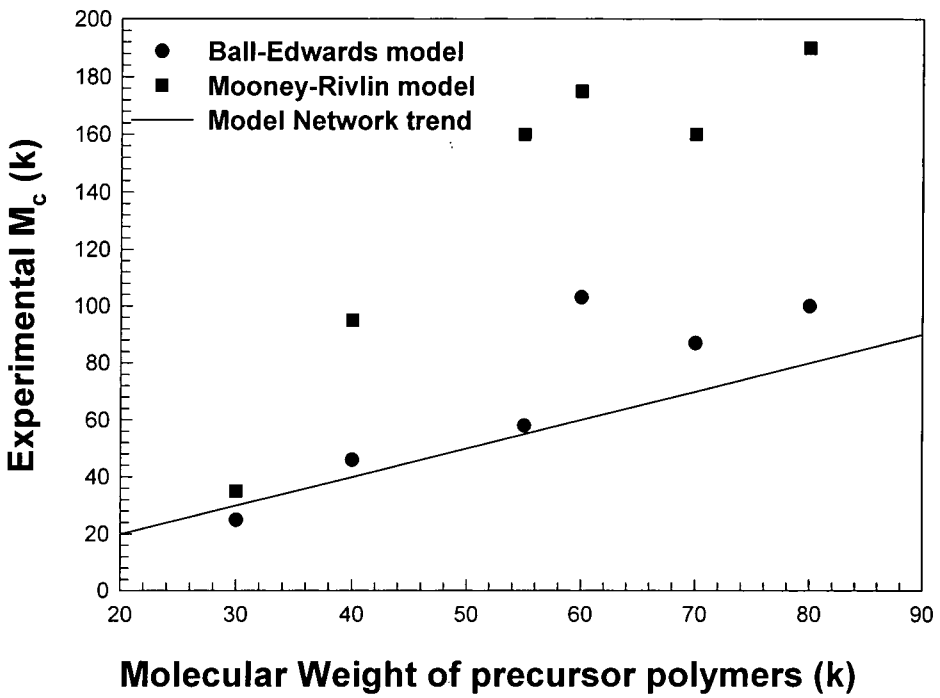

Figure 3.1j A comparison of results from data analysis by B-E and M-R on samples of lamellar networks

Figure 3.1j shows that the B-E model produces $\overline{M}_c$ values close to those expected from the chemistry of the precursor polymers for the lamellar specimens. Whilst the M-R approach over estimates $\overline{M}_c$ values but has the same qualitative features. The slip-link model seems to give a more realistic prediction of the $\overline{M}_c$ values in the systems because it incorporates deliberately the effects of network looseness and physical entanglements. After analysing the lamellar network systems using the B-E model the spherical morphology materials were analysed in the same way. Results for values of a, b, η, and

$\overline{M}_c$ using the slip link model for the spherical morphology network samples at 398K are shown in table 3.1h and figure 3.1k.

Table 3.1h Stress-strain analysis on the spherical morphology network samples at 398K

Network	a (kPa)	b (MPa)	η	$\overline{M}_c$ (k)
NS1 ss				
NS2 ss	36.4	2.06	1.69	85
NS3 ss				
NS4 ss	22.4	4.97	2.67	140
NS5 ss	20.1	3.47	2.00	155
NS6 ss	9.3	5.32	2.89	165
NS7 ss				
NS1 db	93.8	2.35	1.63	35
NS2 db	75.2	2.29	1.46	45
NS3 db	64.1	2.86	1.50	50
NS4 db	120.4	1.19	0.78	30
NS5 db	39.2	4.23	2.18	80
NS6 db	16.6	5.75	2.25	190
NS7 db	30.6	3.84	1.66	105

ss denotes material used in experiment was a **s**ample **s**trip

db denotes material used in experiment was **d**umb-**b**ell shaped

The values of $\overline{M}_c$ obtained from the spherical morphology network samples are much higher when compared with the molecular weight of precursor polymers for samples prepared as rectangular strips (**ss**). Again, values of $\overline{M}_c$ obtained were higher in the sample strip case because these samples tend to break at the clamping point due to stress concentration showing them to give less accurate results than dumb-bell samples. The dumb-bell shaped samples (**db**) show a trend that follows expected values of $\overline{M}_c$ from the chemistry of the precursor polymers. The value of the constant, **a**, (free energy of chemical cross-links) in the dumb-bell samples is much greater than the values obtained from strip samples. Both specimens are from the same bulk sample, therefore they possess the same number of chemical cross-links, but the analytical methods used give

different results. Therefore once again sample preparation is very important in order to obtain results that bear a true representation of network characteristics.

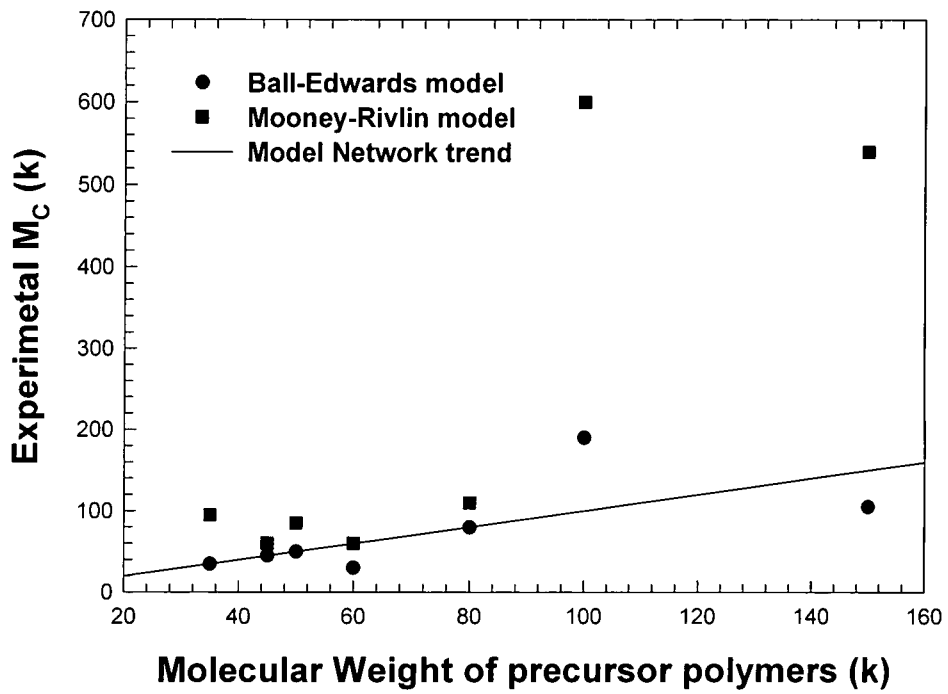

Figure 3.1k A comparison of results from data analysis by B-E and M-R on samples of spherical morphology networks

M-R $\overline{M}_c$ values for the spherical morphology systems are similar to those obtained for the analysis of lamellar systems with similar molecular weight as long as the molecular weight is less than 100,000. At molecular weights greater than 100,000 the values of $\overline{M}_c$ are much higher to a very large degree. Further analysis carried out on the network systems will be in terms of the B-E slip link model, discarding the M-R data as an inaccurate estimate of the network $\overline{M}_c$ parameters. To examine the trends of network properties, N_c is plotted against $\overline{M}_c$ data from the B-E slip-link model and from the network precursor polymers. Figure 3.1l shows an inverse relationship between $\overline{M}_c$

values and the number of chemical cross-links in all network samples (lamellar and spherical), the trend observed is expected to occur. $\overline{M}_c$ values obtained from the B-E method are calculated from N_c values because the inverse function used in the calculation gives results that fall on a curve. N_c values calculated from precursor polymers have been compared to ones obtained from the B-E model.

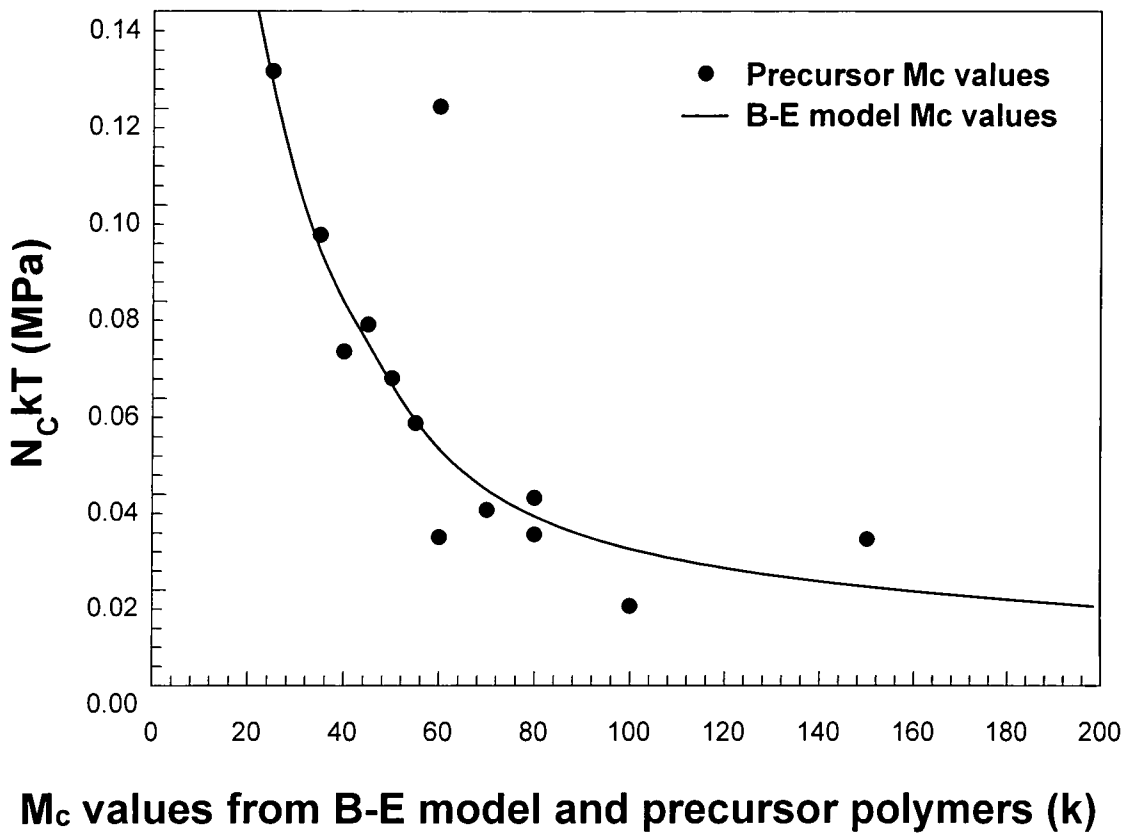

Figure 3.11 Chemical cross-link analysis with respect to $\overline{M}_c$

The molecular weight values of the precursor polymer materials match well with the data obtained from the B-E model showing that reality matches theory quite well. Figure 3.1m shows plots of N_s against $\overline{M}_c$ values obtained from the B-E model and molecular weight values of the precursor polymers. N_s increases linearly with $\overline{M}_c$ values and precursor polymer plots suggesting there is an increase in the number of

physical entanglements as the values of $\overline{M}_c$ increase. It can be observed that the slope of the B-E model is similar to that for the precursor $\overline{M}_c$ values, which suggests that the results obtained for the two sets of data correlate quite well.

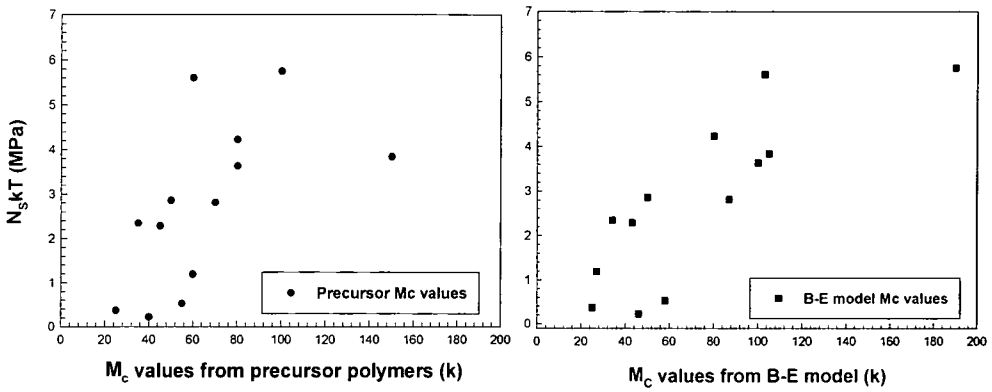

Figure 3.1m N_s values plotted against $\overline{M}_c$ values from different analyses

The plots depicting behaviour of the slip-link values (N_s) suggests that a broad increase of N_s with $\overline{M}_c$ is apparent, the values are distributed over a wide range of molecular weights making any predictions from the plots difficult. It is apparent at low $\overline{M}_c$ that values approaching $N_s = 0$ from the B-E model, approach actual $\overline{M}_c$ precursor molecular weight. Figure 3.1n shows the plot of η versus $\overline{M}_c$, showing η increase systematically as $\overline{M}_c$ increases.

The values of η obtained are not consistent with experimental results from the literature[6]. Experimental values of η that vary between 0.23-2.30 are quite reasonable results from the B-E model and show that the model is valid for the data obtained[7]. Therefore, the networks possess a range of degrees of looseness due to the varying degrees of cross-link density.

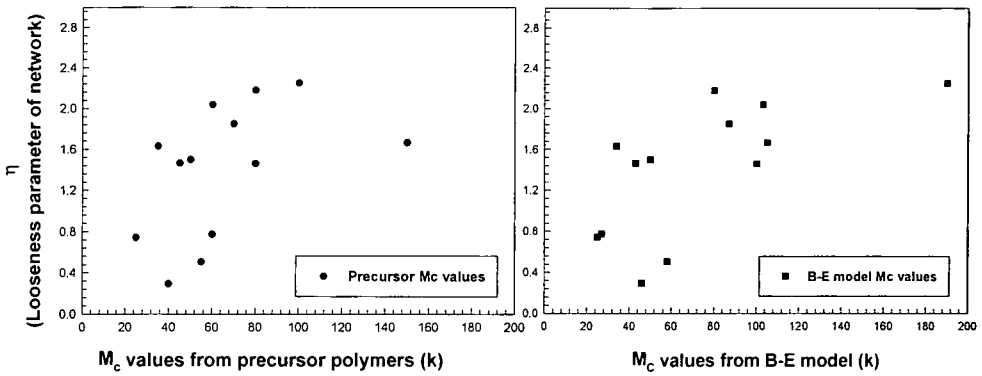

Figure 3.1n Values of η plotted against $\overline{M}_c$ values from different analysis

Values of η vary with $\overline{M}_c$ similarly to that of physical entanglements with $\overline{M}_c$. The general increase in η values signals the increasing looseness of each network as the molecular weight between the cross-links increases and as the number of physical entanglements increase. Again, precursor polymer $\overline{M}_c$ data correlates well with $\overline{M}_c$ values obtained from the B-E model. Figure 3.1o shows the relationship between the ratio of N_s/N_c (physical entanglements : chemical cross-links) against N_ckT.

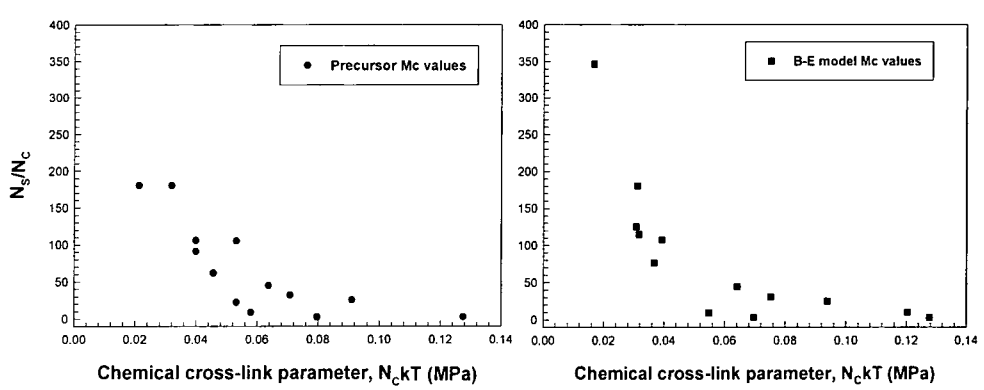

Figure 3.1o N_s/N_c ratio versus chemical cross-link parameter, N_ckT

Values of N_ckT obtained from the B-E model together with precursor polymer values were compared to see which set of results was most consistent with the expected trend. From the graph, both sets of results varied the same amount over the range of chemical cross-link densities obtained. As N_s/N_c increases, values of N_ckT decrease, therefore at higher N_c (lower η) there appears to be less room per physical entanglement. Varying amounts of trapped entanglements in each network alters the effective cross-link density hence varies the conjunction of each network.

Low $\overline{M}_c$ networks have a high cross-link density and therefore physical entanglements are less probable, and η values nearer to the ideal value of 0.23[6] for a model network. High $\overline{M}_c$ gives a lower cross-link density because there are fewer end groups per molecular weight. In an ideal network if the polymer precursor is 10K there will be a very high cross-link density. Whilst if the precursor polymer is 100K there will be a low cross-link density. The lack of chemical cross-links and increased number of loops and trapped chains encourages entanglement formation. A second plot that shows the importance of the N_s/N_c ratio is presented as figure 3.1p.

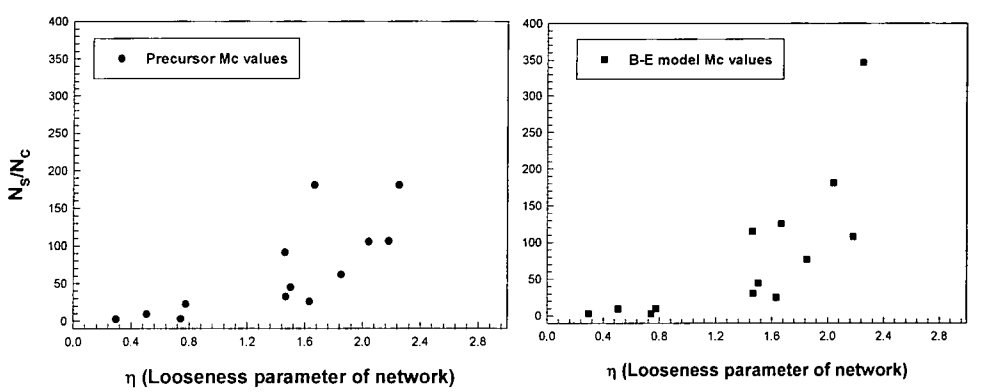

Figure 3.1p Physical entanglement variation with network looseness

The entanglement/cross-link ratio is plotted against the network looseness parameter η, a clear correlation is evident. At low values of η the N_s/N_c ratio is constant suggesting that low $\overline{M}_c$ network systems have a constant number of trapped entanglements that are quite tightly cross-linked. As the values of η increase there is a steady increase in N_s/N_c ratio showing a large increase in the amount of trapped entanglements as the looseness of the network system increases. At high η, values of N_s/N_c are very high, suggesting that networks possess many more physical entanglements than chemical cross-links when the systems are poorly cross-linked.

The B-E model theory was developed for homogeneous network systems. Systems studied in this project are heterophase systems even above the glass transition temperature of both constituents due to chain interactions in the polystyrene phase that can distort true $\overline{M}_c$ values estimated from the model. It is unknown to what amount the systems are ordered or disordered at this temperature.

3.2 Determination of M_c from swelling measurements

3.2.1 Introduction

Values of $\overline{M}_c$ calculated from stress-strain measurements can be compared to values calculated from swelling measurements obtained from network samples. Using toluene as the swelling solvent samples of each network were swollen to equilibrium, i.e. until the weight of the solvent swollen network was constant in excess swelling agent. The interaction parameter, χ_{12} between toluene and copolymers of butadiene and styrene has been calculated to be 0.33 at a temperature of 30°C[8,9].

In order to calculate the average molecular weight between cross-links from swelling measurements the treatment of Rotstein and Lodge[10] was used which is summarised using equation 3.2a which relates $\overline{M}_c$ to the polymer network volume fraction, υ_p.

$$\frac{1}{\overline{M}_c} = \left(\frac{c_o}{d_r}\right)^{1/3} \left(\frac{\nu_p + \chi_{SB}\,\nu_p^2 + \ln(1-\nu_p)}{-V_o\,c_o\,(\nu_p^{1/3} - \nu_p/2)}\right) \qquad \text{eq.3.2a}$$

V_o is the molar volume of the solvent

χ_{SB} is the network-swelling agent interaction parameter

d_r is the density of the network sample

c_o is the polymer concentration at cross-linking

Network samples were swollen to equilibrium (no further change in swollen mass) and a value for $\overline{M}_c$ was calculated for each network. Values of $\overline{M}_c$ calculated from swelling measurements were compared to measurements from stress-strain analysis. Photographs of typical network samples, swollen and unswollen, are presented in figures 3.2a-d.

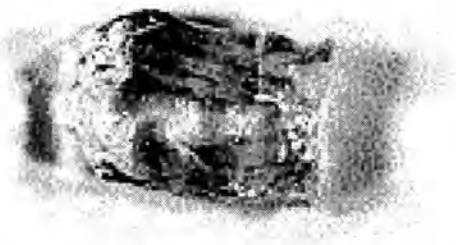

Figure 3.2a Swollen spherical network sample

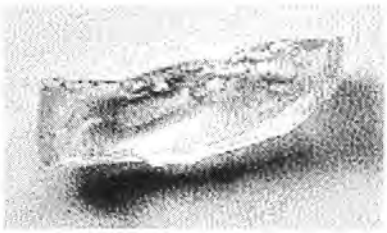

Figure 3.2b Unswollen spherical network sample

Figure 3.2c Swollen lamellar network sample

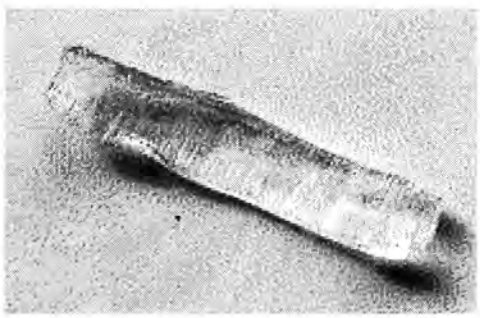

Figure 3.2d Unswollen lamellar network sample

It can be seen that after swelling to equilibrium samples keep their original shapes and weighing is possible in order to estimate $\overline{M}_c$ values. Spherical morphology samples were more difficult to section from bulk material due to their rubber-elastic behaviour at room temperature and therefore appear slightly non-uniform after swelling to equilibrium (figure 3.2a). Lamellar samples sectioned easily due to the combined glassy/rubber-elastic nature due to the 50:50 w/w composition of PS/PB and therefore appear as uniform swollen samples (figure 3.2c).

3.2.2 Results

Table 3.2a and figure 3.2e display $\overline{M}_c$ values calculated from stress-strain analysis and swelling measurements as a comparison to molecular weights from the precursor chains of the network samples.

Table 3.2a $\overline{M}_c$ values calculated using stress-strain analysis and swelling data for all network samples

Network	$\overline{M}_c$ (swelling data) (k)	$\overline{M}_c$ (k) (stress-strain analysis at T=400K)	Expected $\overline{M}_c$ (k)
NL1	33	25	25
NS1	75	34	35
NL2	41	46	40
NS2	115	43	45
NS3	115	50	50
NL3	65	58	55
NL4	130	103	60
NS4	135	30	60
NL5	80	87	70
NL6	85	100	80
NS5	185	80	80
NS6	305	190	100
NS7	475	105	150

Values of swelling $\overline{M}_c$ are compared to stress-strain $\overline{M}_c$ values in section 3.3 of the chapter.

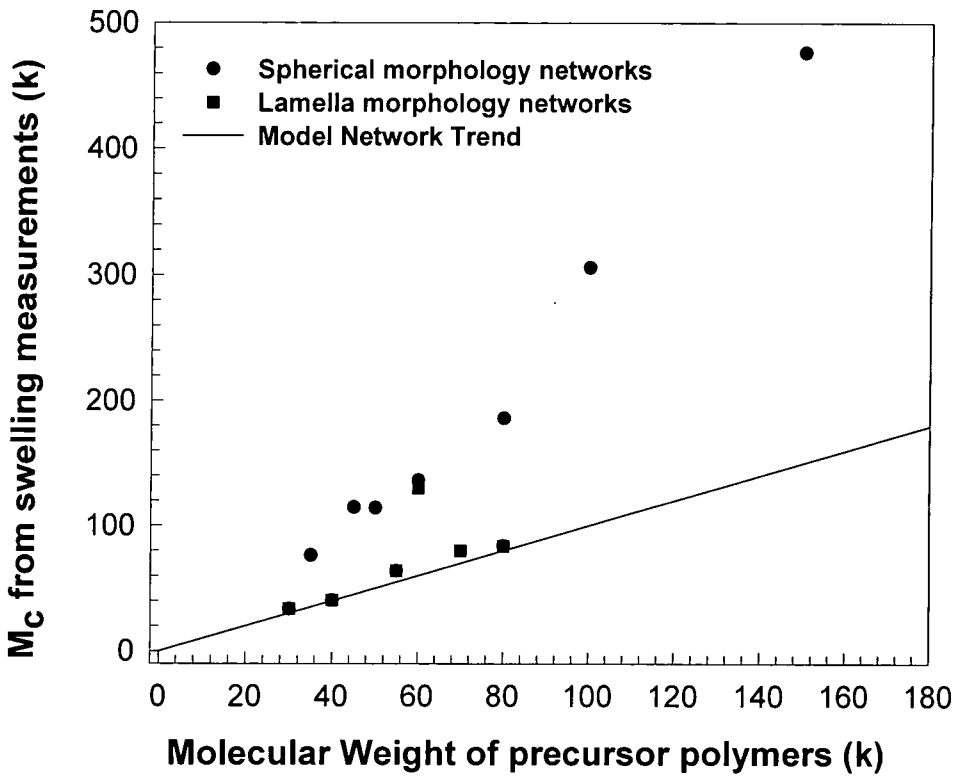

Figure 3.2e $\overline{M}_c$ analysis from swelling measurements

Comparisons of the $\overline{M}_c$ values from swelling measurements with perfectly cross-linked networks (model networks) show good agreement at low $\overline{M}_c$ and poor agreement at high $\overline{M}_c$ between the two forms of analysis. The trend observed indicates a general increase of experimental $\overline{M}_c$ with the increase of precursor polymer molecular weight values. $\overline{M}_c$ values obtained for the lamellar systems appear to match model network trends better than for the spherical morphology systems for which there is no explainable reason. The samples which compare closest to model network behaviour are the lower molecular weight range of the systems studied, which is expected due to the

increased efficiency of cross-linking at low molecular weights. High molecular weight networks possess poor physical properties, many imperfections and inefficient cross-linking potential which is shown from the vast difference from model network trends.

3.3 Discussion

Measurements of $\overline{M}_c$ values using stress-strain and swelling data are summarised in figure 3.3a.

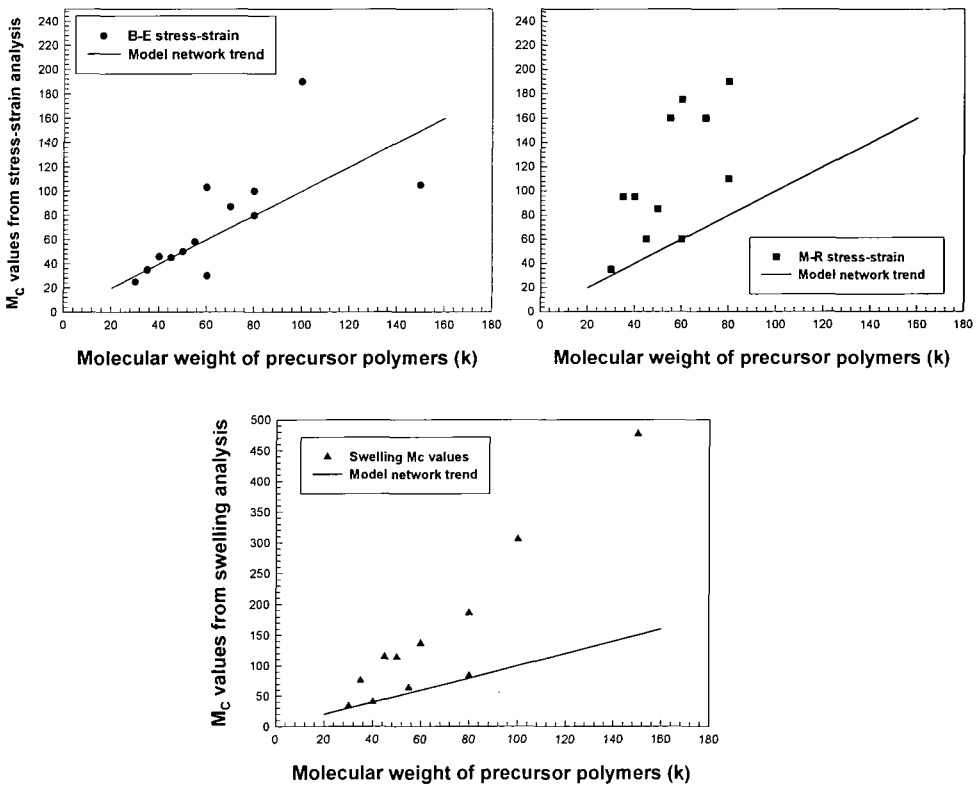

B-E represents the Ball-Edwards slip-link model

M-R represents the Mooney-Rivlin model

Figure 3.3a Summary of data determining $\overline{M}_c$ values

Results obtained from the stress-strain and swelling experiments in figure 3.3a show that there is a wide variation of $\overline{M}_c$ values obtained from the three methods used to calculate them. The results from the B-E model displayed model network behaviour at the lower molecular weight scale whilst M-R and swelling $\overline{M}_c$ values departed from it. M-R data departed furthest from the model network trend because it does not account for network imperfections in the structure. The swelling data takes in to account the end cross-linking of the system but only detects a limited number of the physical entanglements that exist in the swollen network and therefore produces $\overline{M}_c$ values that are slightly lower than the M-R analysis.

The B-E model takes three variable network parameters in to account, so it is not surprising that this method produces data that gives values of $\overline{M}_c$ that differ on a large extent from the other models used. M-R data departed the most from model network trends when analysing high molecular weight systems showing it is inappropriate as a reliable, realistic analytical method. It is debatable to say which of the methods is the most accurate, one can assume the model to believe is the one with most variable parameters that depicts the most realistic network behaviour, this being the B-E model.

3.4 References

[1] Mooney, M. *J. Appl. Phys.* **1948,** *19*, 434

[2] Rivlin, R.S. *Phil. Trans. Roy. Soc. London Ser. A* **1948,** *241*, 379

[3] Klein, P.G.; Ladizesky, N.H. and Ward, I.M. *Polymer,* **1987,** 28, 393

[4] Ball, R.C.; Doi,M.; Edwards, S.F. and Warner, M. *Polymer,* **1981,** *22*, 1010

[5] Edwards, S.F. and Vilgis, Th. *Polymer,* **1986,** 27, 483

[6] Brereton, M.G. and Klein, P.G. *Polymer,* **1988,** 29, 970

[7] Thirion, P.; Weil, T. *Polymer* **1984,** *25*, 609

[8] Joseph, R.; George, K.E.; Francis, D.J.; Thomas, K.T. *Intern. J. Polymeric Mater.* **1987,** *12*, 29

[9] Narasimahan, V.; Huang, R.Y.M.; Burns, C.M. *Journal of Polymer Science: Polymer Physics Edition* **1983,** *21*, 1993

[10] Rotstein N.A.; Lodge T. P. *Macromolecules* **1992,** *25*, 1316

CHAPTER 4

Small Angle X-ray Scattering Results

4.1 Small Angle X-ray Scattering analysis of lamellar morphology systems

4.1.1 Uncross-linked systems

A series of uncross-linked BSB copolymer samples have been studied using time resolved synchrotron SAXS and Kratky camera SAXS techniques. Samples were prepared by casting films from a toluene solution onto PTFE trays which were dried to constant weight under vacuum. Each copolymer film was studied in three ways; un-annealed film, annealed film and edge on film sections. An example of a Lorentz corrected synchrotron scattering curve for copolymer LL4 is shown in figure 4.1a.

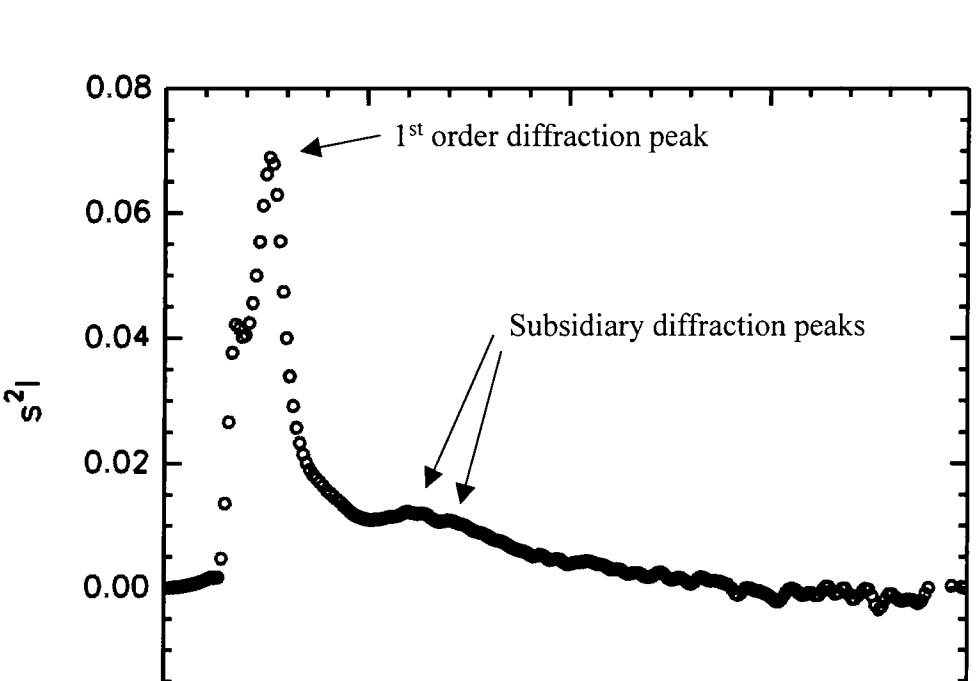

Figure 4.1a Lorentz corrected scattering curve for polymer LL4

Examination of the position of the 1st order diffraction peak in figure 4.1a yields a value for the magnitude of the scattering vector, s. The value of s being the reciprocal of the domain spacing of the system studied. Values of the domain spacing for each film preparation per copolymer sample were constant. Subsidiary diffraction peak positions

are used to determine information about the long-range order of the sample. Intensity scattering profiles from Kratky camera and synchrotron SAXS show that annealed samples possess more resolved peaks than the edge on or unannealed specimens. Figure 4.1b shows a Kratky camera plot for copolymer LL4 using annealed and unannealed sample preparations.

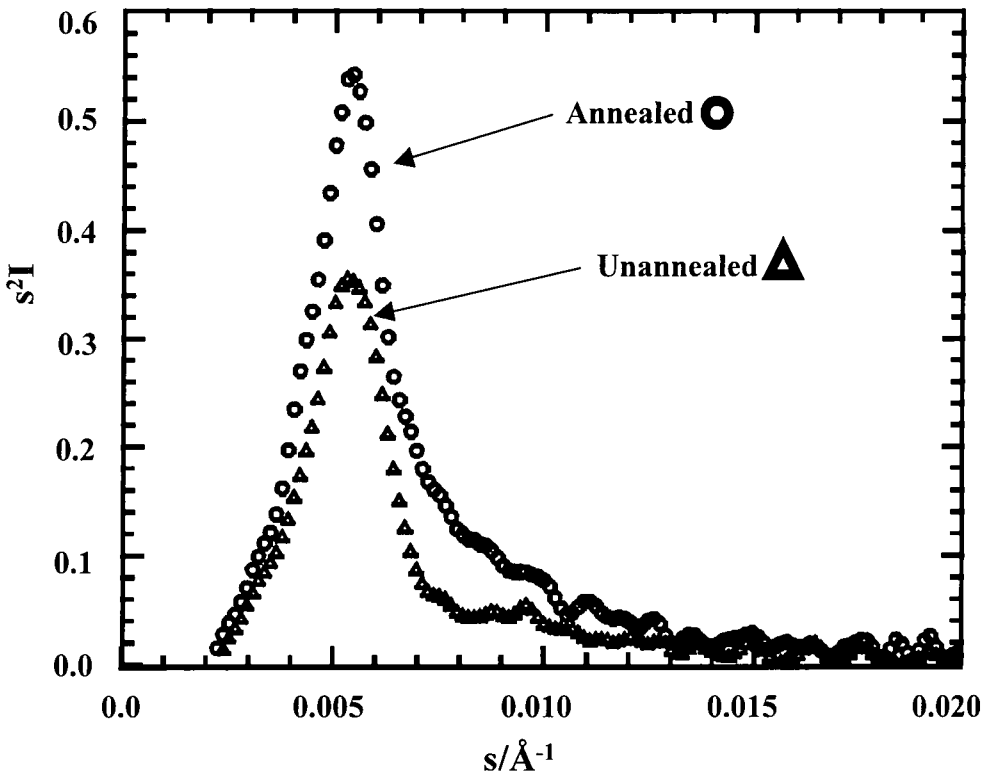

Figure 4.1b Kratky camera plots of LL4 annealed and unannealed

The peaks in figure 4.1b are at the same position on the x-axis, indicating that they possess the same domain spacing value. Edge on samples, (perpendicular to the surface of evaporation of cast film) studied by synchrotron SAXS produced similar profiles as the annealed/unannealed samples. Figure 4.1c shows the method employed to section the 2-D synchrotron SAXS patterns (and the direction of stretch the network samples were subjected to – see section 4.1.2.2). Static uncross-linked systems were analysed

this way in order to establish that scattering was isotropic i.e. domain spacing values were constant in all directions of scattering.

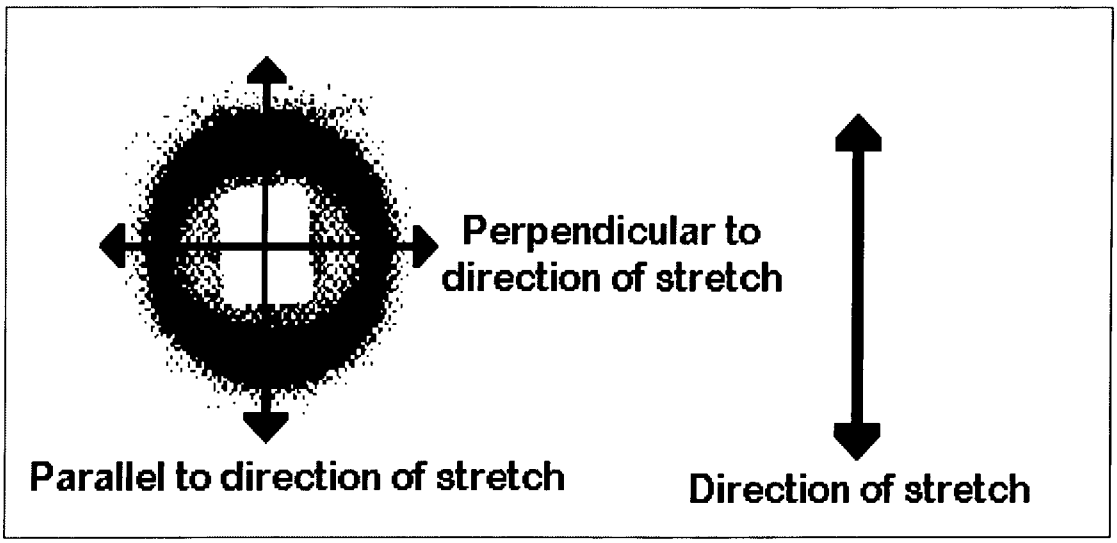

Figure 4.1c Sectioning 2-D synchrotron SAXS patterns

Characteristics of the uncross-linked samples are summarised in table 4.1a where domain spacing values from the Kratky camera analysis are compared to theoretical dimensions predicted using a Fortran computer program by Helfand and Wasserman[1,2]. The theory used was developed by Helfand *et al*[3,4,5,6] and states that domain spacing repeat lengths in block copolymer systems of this kind are proportional to molecular weight raised to the power of 2/3, i.e. $d \alpha M_w^{2/3}$.

If Kratky Camera results are assumed to be from the 1st order diffraction peak, values of theoretical predictions and synchrotron data would not be matched. Therefore Kratky domain spacing values have been assumed to be from the 2nd order diffraction peak, therefore doubling each value obtained from the main visible Bragg peak giving a good match to theoretical and synchrotron data values. The Synchrotron profiles give a large 1st order peak at low s. That range of s is not available from the Kratky camera therefore the 1st order peak will not be visible in Kratky profiles, compare figures 4.1a and 4.1b.

Table 4.1a Lamellar copolymer characteristics obtained from Lorentz corrected curves from the Kratky camera

Copolymer	MW (k)	Unannealed (Å)	Annealed (Å)	Theoretical (Å)
LL1	40	280	280	200
LL2	60	320	340	270
LL3	100	380	380	390
LL4	150	500	520	490
LL5	250	640	680	620

BSB represents butadiene-styrene-butadiene triblock copolymer

MW indicates polymer molecular weight in thousands

Table 4.1b contains domain spacing values measured using time resolved synchrotron SAXS analysis.

Table 4.1b Copolymer domain spacing values from synchrotron analysis

BSB Copolymer	SAXS Lorentz corrected d spacing (Å)					
	Pa Un	Pe Un	Pa An	Pe An	Pa EO	Pe EO
LL1	260	245	275	235	-	-
LL2	260	295	275	295	270	255
LL3	310	300	310	300	305	295
LL4	435	425	405	425	445	425
LL5	610	610	620	620	620	570

Pa indicates parallel to the intended direction of stretch

Pe indicates perpendicular to the intended direction of stretch

Un indicates unannealed sample

An indicates annealed sample

EO indicates an Edge On sample of the as cast material by solvent evaporation

Apparent domain spacing values from table 4.1b for LL4 in the perpendicular direction (see figure 4.1c) were lower than in the parallel direction due to the beam stop

obscuring the 1st order Bragg peak due to the beam stop being rectangular in shape. Figure 4.1d shows the shape of the beam stop to be rectangular when looking at scattering profiles.

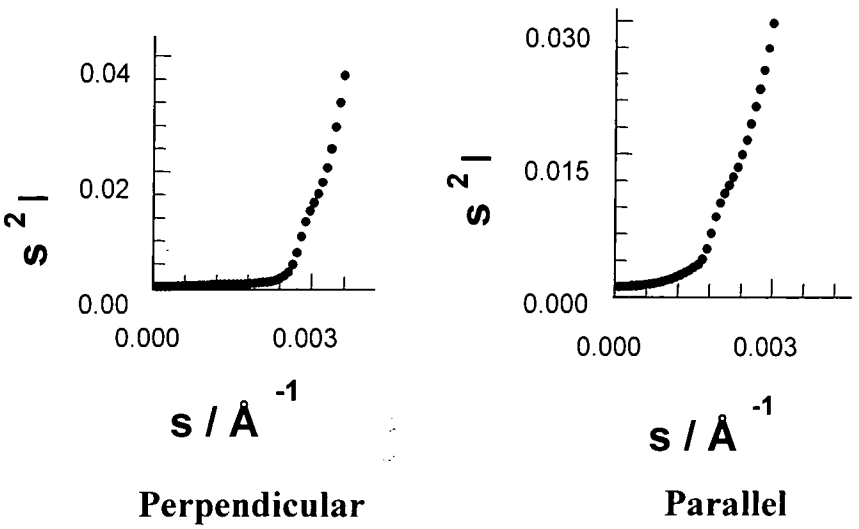

Figure 4.1d Diagramatic representation of scattering from the synchrotron beam stop

Synchrotron data for copolymer LL5, yielded domain spacing values that were interpreted by assuming that the 1st order Bragg peak was obscured behind the beam stop, therefore the first visible diffraction peak is the 2nd order one. Measurement of the domain spacing from the 2nd order diffraction peak was doubled so that the correct domain spacing was obtained. This problem does not occur for copolymer samples LL1-LL4 as the 1st order Bragg peak is visible from the scattering profiles.

Synchrotron and Kratky camera SAXS results are compared to theoretical predictions in figure 4.1e.

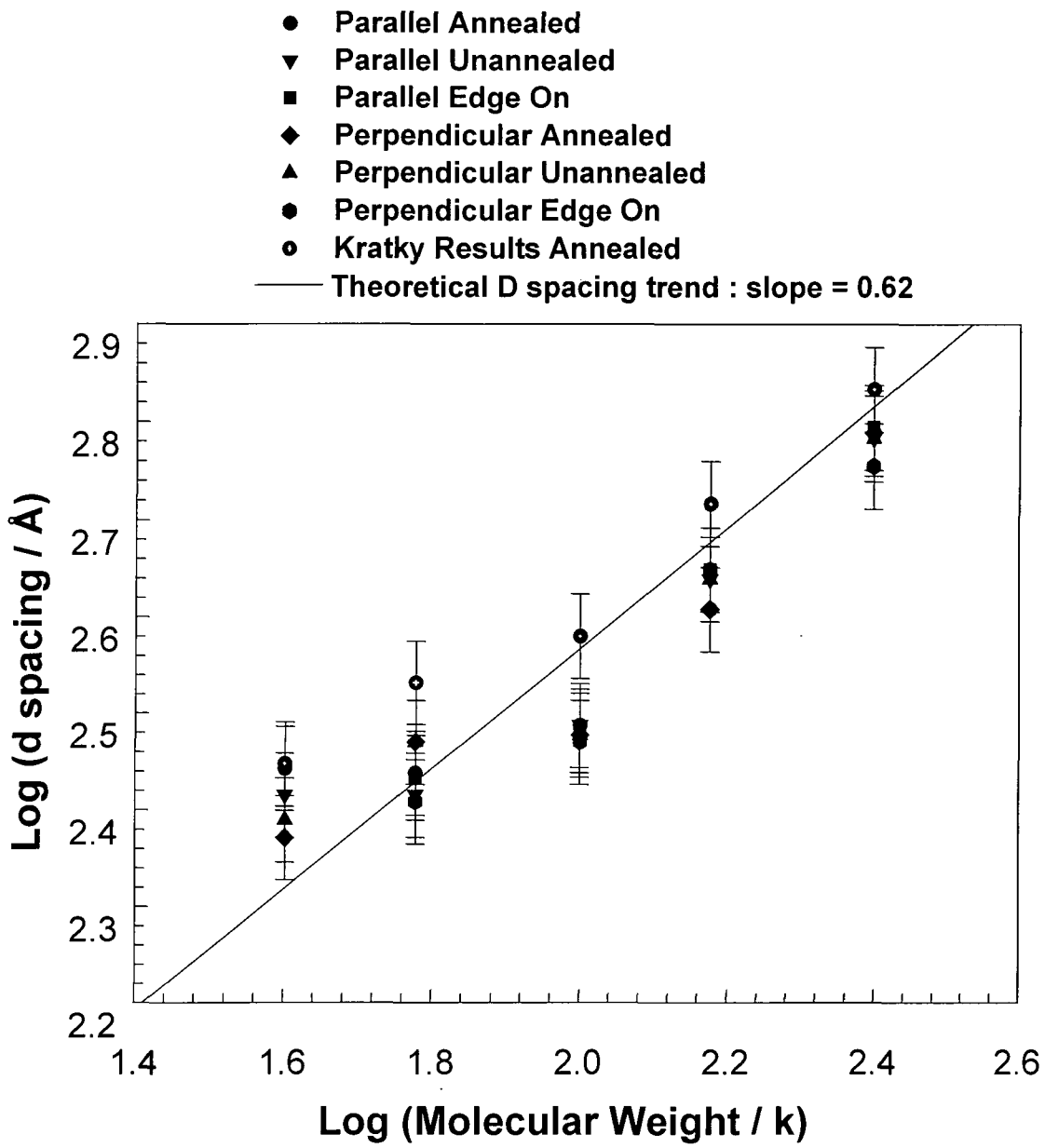

Figure 4.1e Block copolymer SAXS result comparison with theoretical predictions

SAXS results from the lamellar copolymer materials show trends consistent with the theoretical predictions[3,4]. Variations from theoretical predictions are shown in figure 4.1e above and have been calculated using a standard errors treatment of the domain spacing values. The data used was obtained from 2-D scattering patterns after Daresbury synchrotron analysis.

Daresbury SAXS traces from the lamellar systems showed 1st, 2nd and to a lesser extent 3rd order Bragg peaks. The scattering that gives rise to these peak ratios is due to structure of the lamellar system[7], the ratios of these values are shown in table 4.1c

Table 4.1c Bragg peak spacing ratios from lamella uncross-linked materials

	Bragg peak spacing ratio								
Copolymer	**1st Order**			**2nd Order**			**3rd Order**		
BSB	**Un**	**An**	**EO**	**Un**	**An**	**EO**	**Un**	**An**	**EO**
LL1	1.0			-	0.51	-	-	0.44	-
LL2	1.0			0.53	0.51	0.52	0.48	0.47	0.46
LL3	1.0			-	0.56	-	-	0.40	-
LL4	1.0			0.44	0.45	0.44	-	-	-
LL5	1.0			0.50	0.50	0.51	0.33	0.33	0.34
Theoretical	1.0			0.50			0.33		

Results of the Bragg peak ratios from the copolymers are consistent with the theoretical lamellar model[3,4]. Although 2nd and 3rd order peaks are visible, it is not possible to analyse these further in terms of structure factor scattering as peaks from single particle form factor (SPFF) scattering mask the structure factor and prevent identification.

4.1.2 Cross-linked systems

4.1.2.1 Unstretched networks

A series of BSB cross-linked copolymer samples have been studied using both Kratky camera and synchrotron SAXS techniques. Network samples were cut from the swollen bulk and dried under vacuum to produce films 1-2mm in thickness. Homogeneity of the network samples was checked by cutting samples from different sections of the bulk network and performing scattering experiments on them. The position of the 1st order diffraction peak from each sample cut was consistent but no further diffraction peaks were observed, concluding that network sections were homogeneous (see figure 4.1c). An example of a Lorentz corrected synchrotron scattering curve for lamellar network NL2 is shown in figure 4.1f.

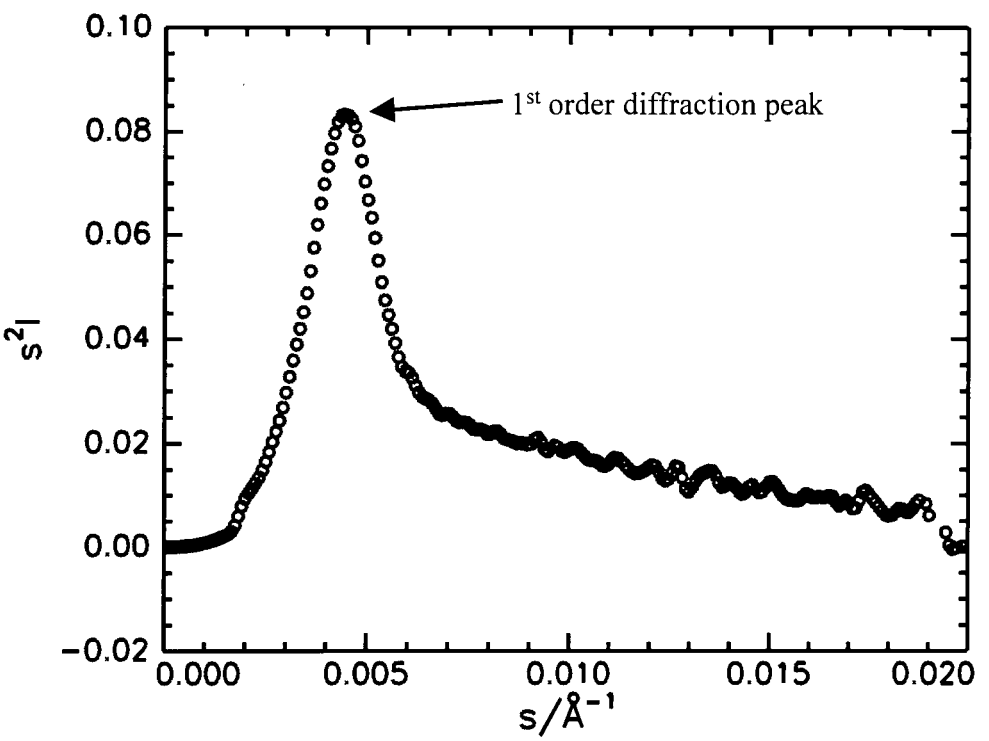

Figure 4.1f Lorentz corrected scattering curve for a lamellar network NL2

Tables 4.1d-e shows characteristics of the lamellar networks obtained from Kratky Camera and synchrotron SAXS analysis. Theoretical domain spacing values are based

on the equivalent uncross-linked copolymer systems calculated using the Helfand and Wasserman computer program[1].

Table 4.1d Lamellar network characteristics obtained from Lorentz corrected curves from the Kratky camera

Network	MW (k)	Unannealed (Å)	Annealed (Å)	Theoretical (Å)
NL1	30	160	160	160
NL2	40	160	160	200
NL3	55	200	180	250
NL4	60	210	205	270
NL5	70	220	220	300
NL6	80	220	225	330

Table 4.1e Network domain spacing values from synchrotron analysis

BSB Network	SAXS Lorentz corrected d spacing (Å)			
	Pa An	**Pa Un**	**Pe An**	**Pe Un**
NL1	228	240	213	195
NL2	200	223	185	195
NL3	260	250	250	240
NL4	240	250	246	250
NL5	237	277	240	259
NL6	237	290	245	280

Irregularity of the microdomain structure affects the broadness of the 1st order Bragg peak. The increase in peak width associated with the network samples is attributed to the cross-linking process. It disrupts the average thickness of lamellae and changes the domain spacings, this widens the 1st order Bragg peak and therefore does not follow block copolymer theory. It is apparent from this behaviour that microphase separation in the polymer networks is significantly different from that in block copolymer systems, due to the existence of random forces from all directions acting on lamellar planes in the networks. These forces are balanced by elastic deformations from the network which destroy the long range order in the microphase separated systems[15]. Therefore only the 1st order Bragg peak appears in the scattering curve describing the short range order

whilst the other lamellar planes are rotated with respect to each other cancelling out the long range order. The scattering from such a structure is spherically symmetric with a peak independent of the direction of the scattering vector indicating further evidence of no long-range order and sample inhomogeniety. A graph depicting network domain spacing values compared to uncross-linked theoretical values is shown in figure 4.1g.

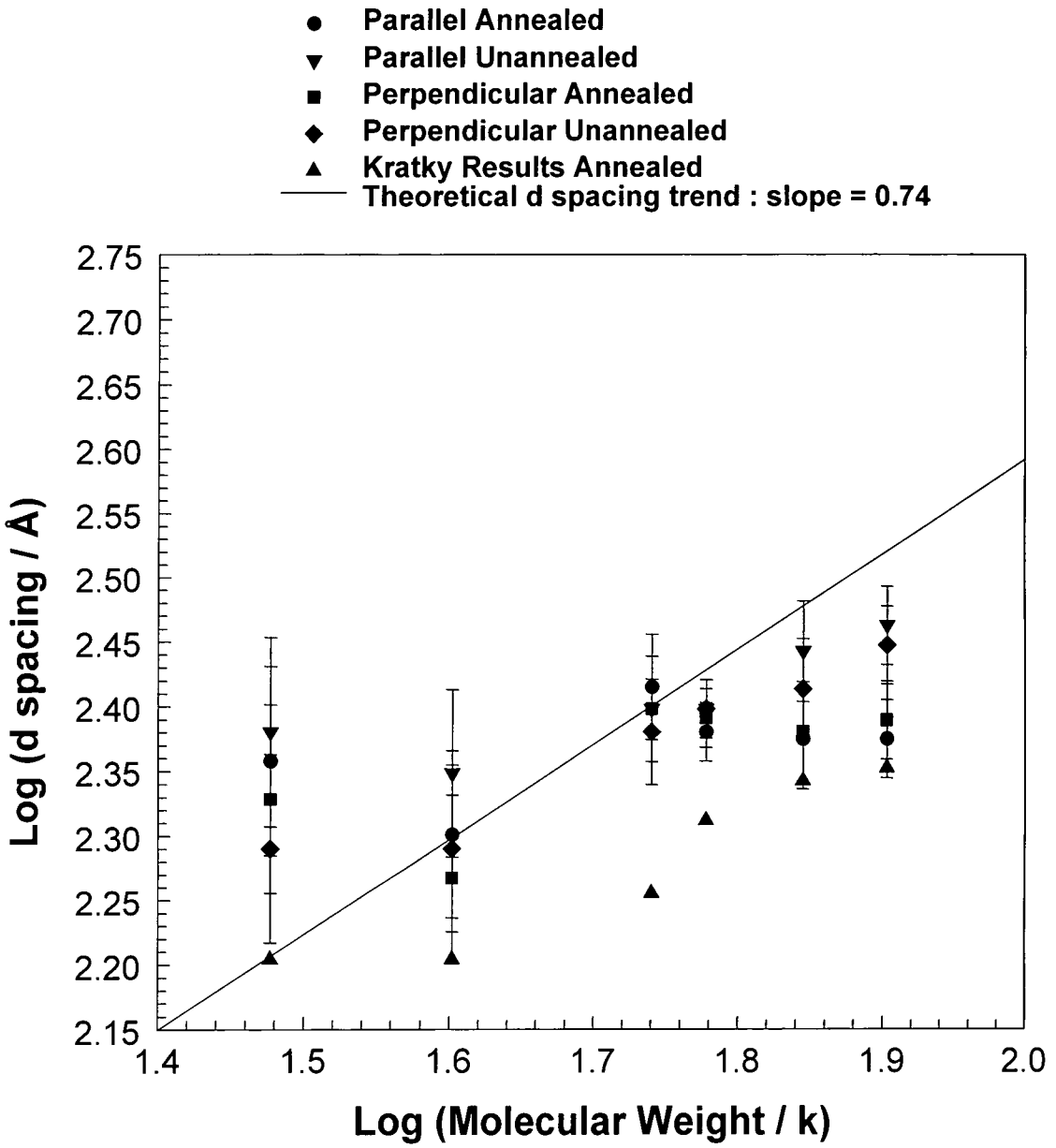

Figure 4.1g Network SAXS result comparison with theoretical predictions

The results shown in figure 4.1g do not compare well to trends from theoretical predictions of the uncross-linked systems. Results not following block copolymer theory are due to the variations of cross-link density in the systems altering the domain spacing in them. Low molecular weight networks appear to possess domain spacing values higher than block copolymer theory would predict. However, high molecular weight networks possess domain spacing values lower than the corresponding uncross-linked precursor polymers. This effect is shown in figure 4.1g. A plot of domain spacing values against the cross-link density of the lamellar networks is shown in figure 4.1h.

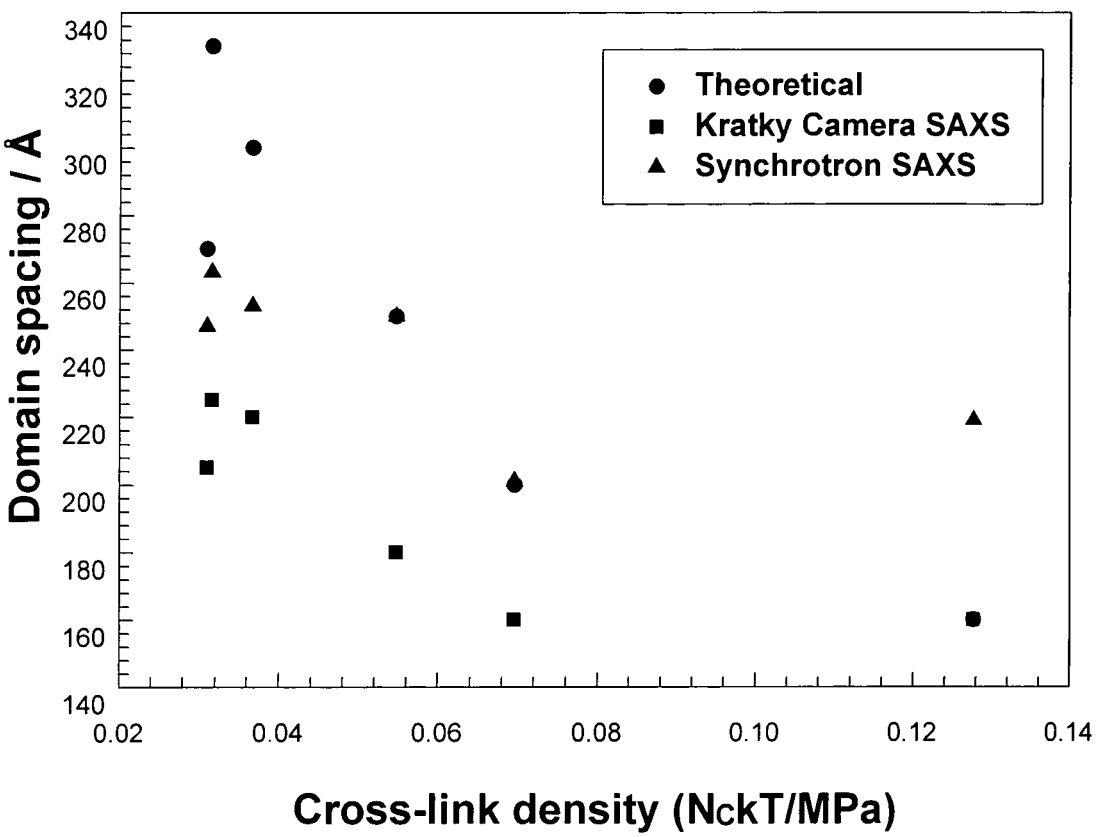

Figure 4.1h Network domain spacing values against cross-link densities

With the exception of sample NL1 the domain spacing values appear to increase as the cross-link density decreases. The domain spacing values also increase with increasing molecular weight, corresponding to the trend that the uncross-linked precursors possess.

Network NL1 has a higher domain spacing than NL2 which can not be explained, there is no logical reason why sample NL1 should have a greater domain spacing value than sample NL2, because sample NL1 possesses the highest cross-link density of all the lamellar networks.

The networks discussed in this project were cross-linked in the homogeneous state but studied in the microphase separated state of the network. Because the networks were cross-linked in a common solvent for both PS and PB, microphase separation was introduced by removing the solvent. These experiments clearly demonstrate that cross-linking leads to the disorder of microphase separated states, hence the variation in domain spacing values in figure 4.1g. Reports in the literature have shown that the presence of cross-links in polymer mixtures, blends or block copolymers also lead to the suppression of microphase separation[8,9,10,11,12].

4.1.2.2 Stretched networks

Synchrotron SAXS data were recorded for the lamellar systems at room temperature using a variety of extension ratios, λ, between 1.0 (un-stretched) and 4.0 (i.e. a maximum extension of 300% of the original un-stretched length). This experiment was to investigate the effect of stretching the sample upon the lamellar network structure. All experiments were carried out at Daresbury laboratories.

Figure 4.1i shows a set of 2-D synchrotron patterns for the homogeneous lamellar network system NL6 demonstrating the increasing anisotropic nature of the scattering as the extension ratio, λ, increases.

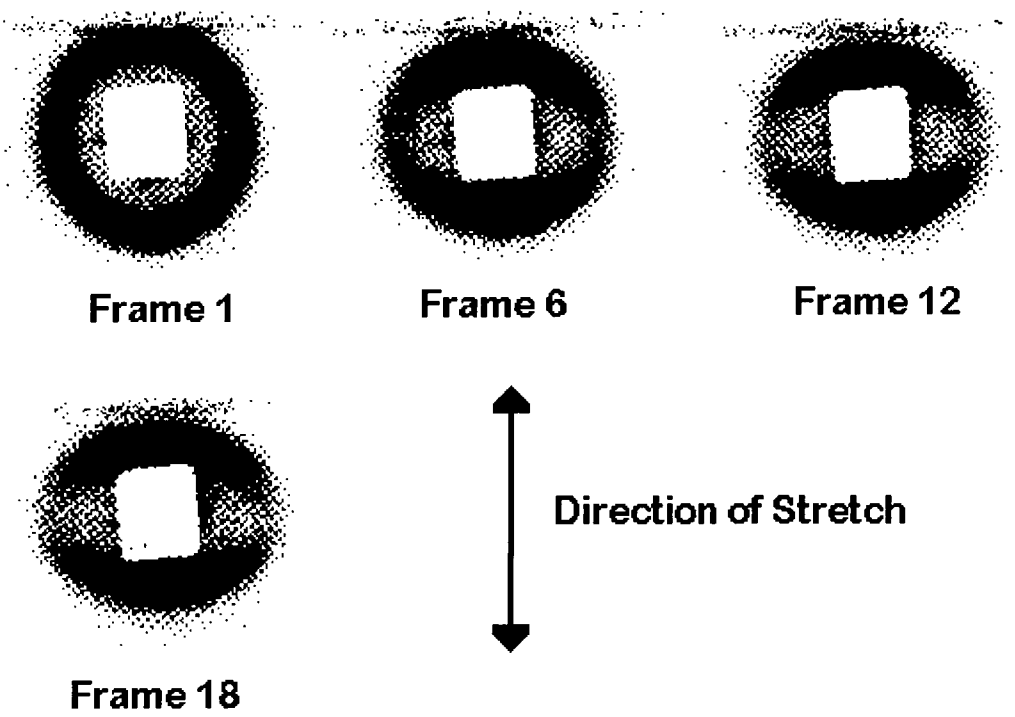

Frame 1 : Static Sample

Frame 6 : Extension ratio = 2.0

Frame 12 : Extension ratio = 3.0

Frame 18 : Extension ratio = 4.0

Figure 4.1i Raw scattering data for NL6 as sample extends

As the sample approaches $\lambda = 4$ the size of the domains increase in the parallel direction of stretch and decrease in the perpendicular direction. No structural changes were observed during the experiment except for the domain spacing alterations, although it was noticeable from the 2-D synchrotron pattern that the scattering intensity decreased in the perpendicular direction as the sample was stretched. Before stretching, lamellae exist isotropically in the network samples (evident from the isotropic scattering observed from the 2-D area detector). Table 4.1f shows the domain spacing values parallel and perpendicular to the direction of stretch for the lamellar network system NL6.

Table 4.1f SAXS analysis of lamellar network sample NL6 stretched

Frame	Extension		Annealed (d/Å)		Unannealed (d/Å)	
	mm	ratio	Parallel	Perpendicular	Parallel	Perpendicular
0	0.00	1.00	237	245	290	280
1	1.66	1.17	240	232	320	274
2	3.33	1.33	277	221	354	267
3	5.00	1.50	295	219	383	261
4	6.66	1.66	303	219	390	256
5	8.33	1.83	307	217	397	261
6	10.00	2.00	315	213	411	253
7	11.66	2.17	307	217	426	261
8	13.33	2.33	300	219	426	261

Figure 4.1j shows scattering curves parallel to the direction of stretch for lamellar network NL6 at various extension ratios between 1.0-4.0 showing the 1st order Bragg peak disappear behind the beam stop as the extension ratio of the sample passes 2.0 (frame 6). The figure described displays results of scattering curves parallel to the direction of stretch.

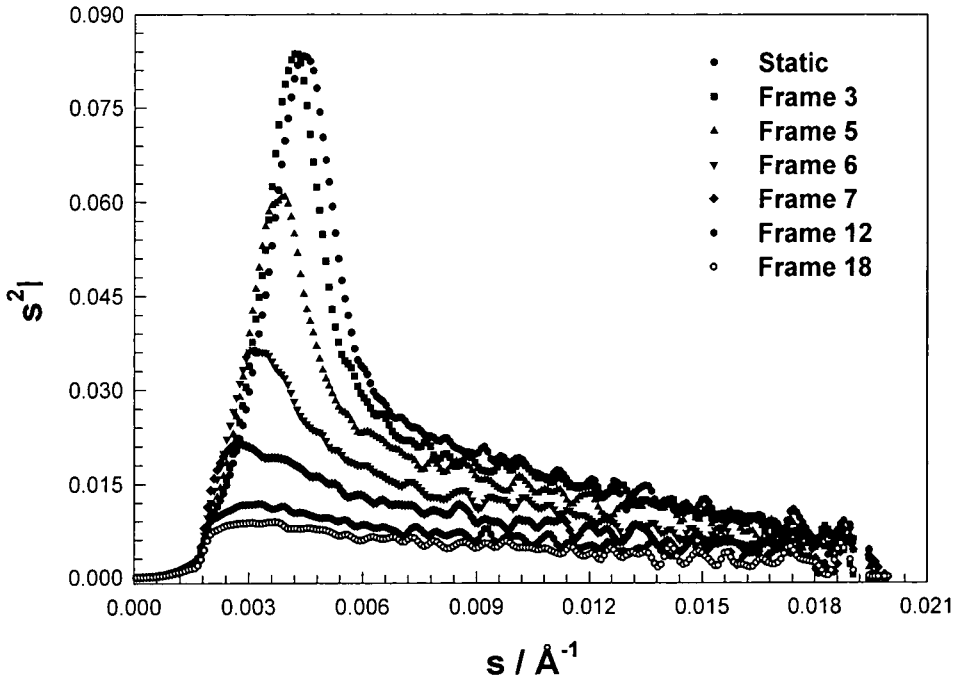

Frame 3 : $\lambda = 1.50$ Frame 5 : $\lambda = 1.83$ Frame 6 : $\lambda = 2.00$

Frame 7 : $\lambda = 2.17$ Frame 12 : $\lambda = 3.00$ Frame 18 : $\lambda = 4.00$

Figure 4.1j Scattering curves for network sample NL6 with uniaxial extension in the parallel direction

At low deformations the scattering maximum parallel to the direction of stretch shifts to smaller angles, indicating an increase in the interdomain distance along the stretching direction. At the same time, the 1st order Bragg peak intensity decreases which can be attributed to either increasing disorder in the interdomain distances or to reorientation of the microdomains from the perpendicular direction to the stretching direction. There is a uniform increase of the mean interdomain distance along the stretching direction as the rubbery matrix is deformed in a homogeneous manner before disordering begins to disrupt the structure after the yield point. Over the whole range of uniaxial extension

ratios parallel to the direction of stretch, the SAXS extension ratio increases in a non-uniform manner, leading to the belief that after maximum extension of the domains, yielding of the polystyrene microdomains follows.

The data in table 4.1f are displayed graphically in figure 4.1k with the stress-strain curve of the network sample at room temperature for comparison, showing how the SAXS extension ratio varies with the nominal stress at a constant drawing rate of 1.0cm per minute. The SAXS extension ratio is defined as the domain spacing when λ is greater than 1.0/initial domain spacing (λ=1.0). Nominal stress is calculated by dividing the drawing force by the cross-sectional area of the undrawn sample. The initial length of the sample before stretching began was 1.0cm.

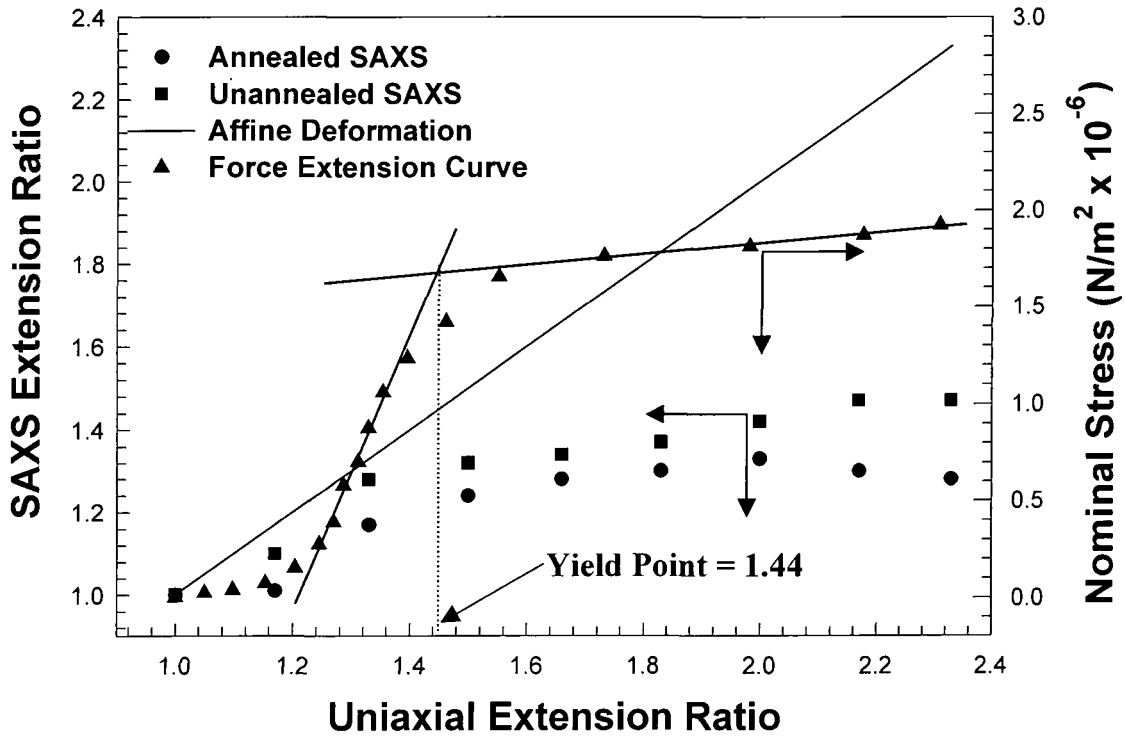

Figure 4.1k Force-elongation curve of network NL6 parallel to the direction of stretch

Data plots of SAXS extension ratios and force-elongation curves in the figure above do not conform to affine deformation, instead they increase and form a plateau after the yield point as stretching occurs. A comparison of the SAXS extension ratio curve shapes with the uniaxial curve shape show similarities to each other. This leads to the conclusion that uniaxial variation in the sample upon stretching is similar to domain spacing variations within the samples.

As the sample approaches the yield point, the domain spacing increases at a slightly lower rate than affine to the uniaxial extension of the sample. For the lamellar system shown in figure 4.1k, the yield point occurs at an extension ratio of 1.44. After the yield point, domain spacing values remain constant as further stretching occurs, proving the existence of sample yielding.

The corresponding synchrotron SAXS scattering curves for the same lamellar network perpendicular to the direction of stretch are shown in figure 4.1l.

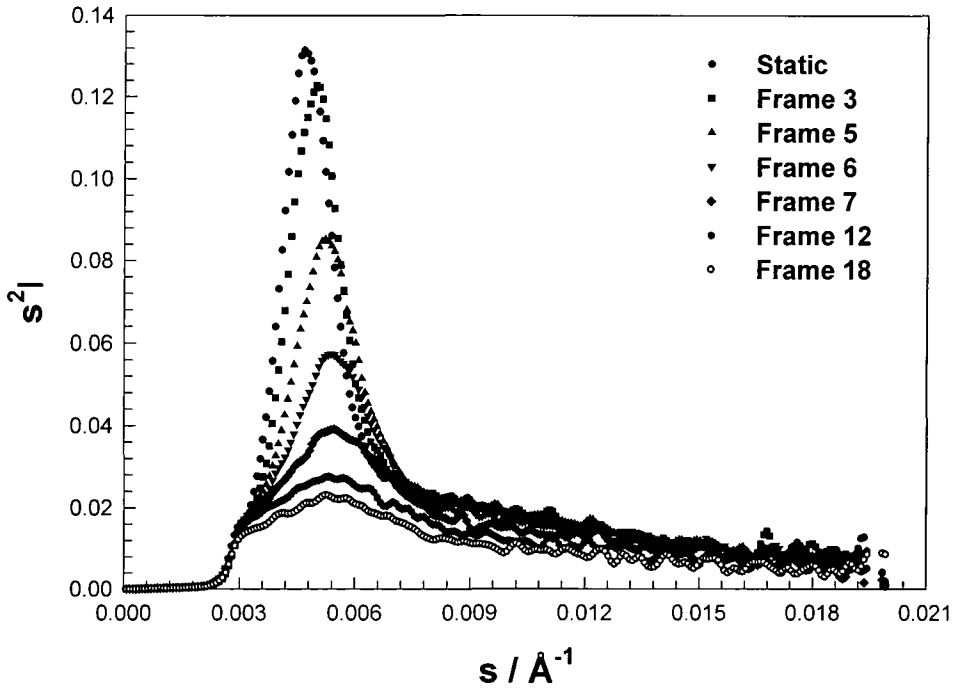

Frame 3 : $\lambda = 1.50$ Frame 5 : $\lambda = 1.83$ Frame 6 : $\lambda = 2.00$

Frame 7 : $\lambda = 2.17$ Frame 12 : $\lambda = 3.00$ Frame 18 : $\lambda = 4.00$

Figure 4.11 Scattering curves for network sample NL6 perpendicular to the direction of stretch

Scattering perpendicular to the direction of stretch behaves in the opposite way to the parallel direction. Domain spacing values decrease at a uniform rate until the sample yields and scattering intensity decreases as structure deformation increases whilst stretching the sample. The peak breadth at half height is an indication of the grain size in the lamellar system. As the sample is stretched the peak breadth at half height increases suggesting that the average lamellar grain size within the system has decreased.

Figure 4.1m shows the domain spacing extension ratios for the isotropic sample of NL6 perpendicular to the direction of stretch, calculated using Poisson's Ratio[13,14]. A generalised definition for Poisson's ratio, μ, is given by equation 4.1a.

$$\lambda_{PERP} = \lambda_{PARA}^{-\mu} \qquad \text{eq.4.1a}$$

λ_i is the extension ratio of the sample in parallel and perpendicular directions

Over the range of uniaxial extension ratios used for the network samples, μ was calculated to be 0.369. From the value of Poisson's ratio it is possible to calculate a range of uniaxial compression ratios to compare with SAXS extension ratios perpendicular to the direction of stretch.

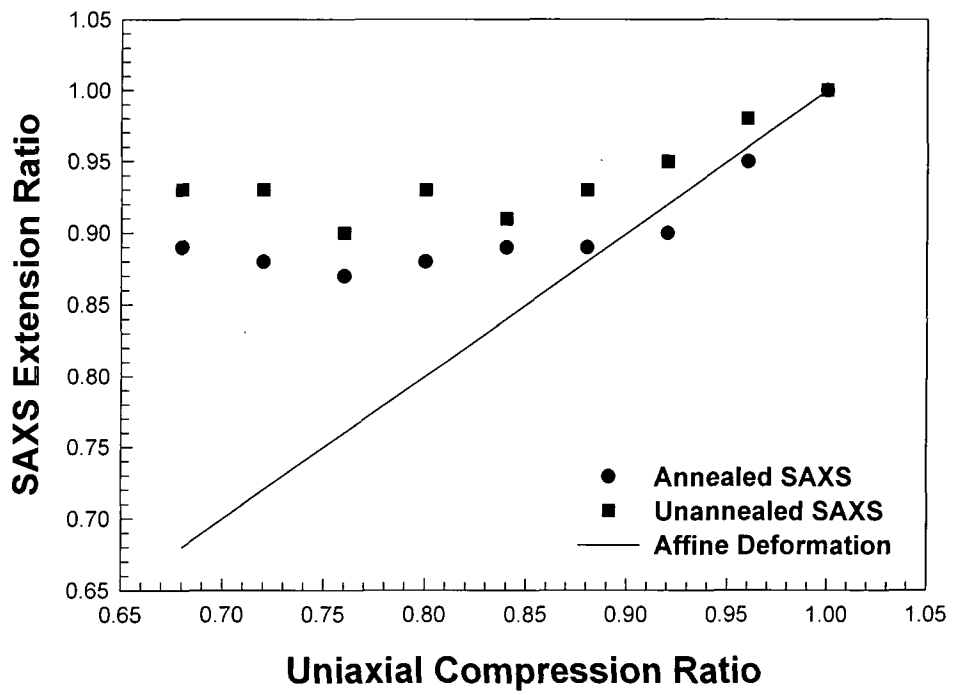

Figure 4.1m Lamellar network characteristics perpendicular to the direction of stretch

Reports of uniaxial deformation of lamellar networks[15] have shown that normals to the lamellar planes tend to turn to the direction of the weakest stretching (ξ^{or}_{perp}). The deviations of the normals from this preferred direction are shown to decrease with increasing deformation. This is shown schematically in figure 4.1n.

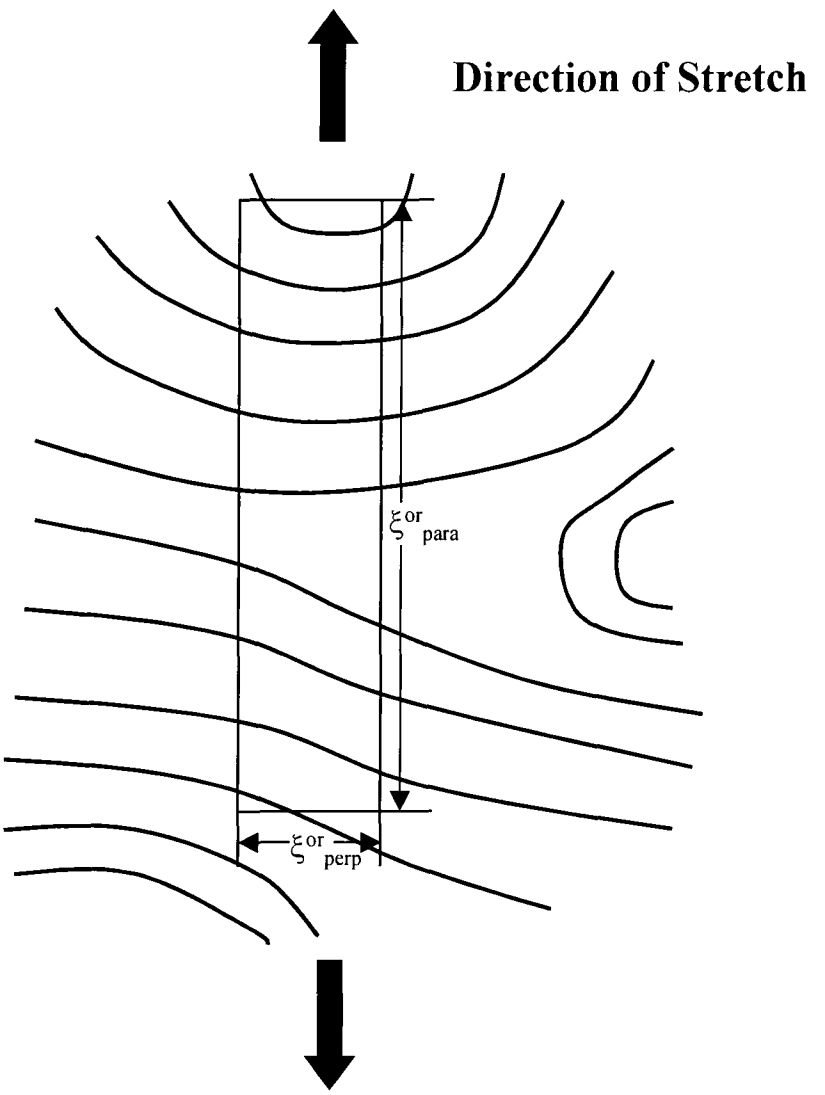

Figure 4.1n Distorted conformation of lamellae under the influence of random forces of the network

The correlation region is sketched by the rectangle with dimensions ξ^{or}_{para} and ξ^{or}_{perp} (the orientational correlation length). During stretching of the network sample, further deformation occurs with the appearance of long-range order in the 2-D scattering pattern.

If the networks studied in this project behaved in this way then the lamellae should change direction by rotation and long-range order would be observed with increasing anisotropy. This does not appear to be so here.

The polybutadiene lamellae extend in the direction of stretch and decrease in size in the direction perpendicular to stretching. Domain spacing variations end when sample yielding begins. Plots for the remaining force-extension curves and SAXS extension ratios of the lamellar samples are listed in appendix 1.

The random forces in polymer networks are a factor influencing domain spacing variations due to the random nature of the cross-linking process before microphase separation has taken place. The maximum SAXS extension ratio depends on the cross-link density in each network sample and at the yield point. If the cross-link density is low then the system is more elastic and the higher the final SAXS extension ratio is before yielding takes place. Figure 4.1o shows the effect of stress-strain on two SBS block copolymers with cylindrical morphology[16], the scattering patterns are taken at individual extension ratios.

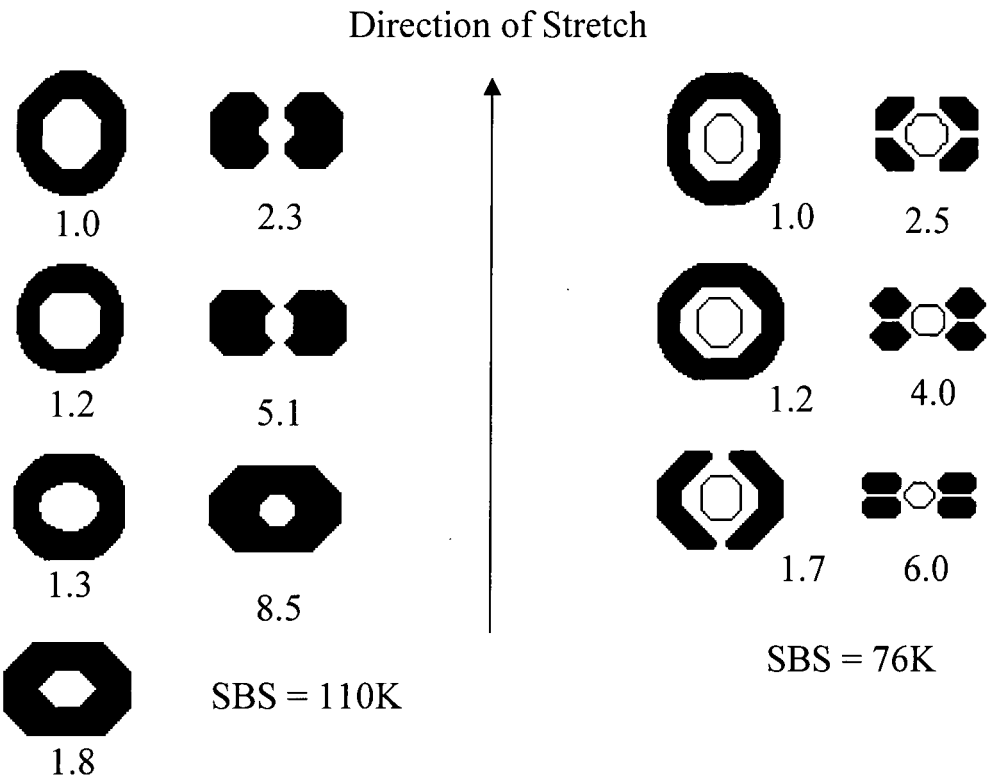

The numbers designate the draw ratios.

Figure 4.1o SAXS patterns at various draw ratios of SBS triblock copolymers

Due to the difference in morphology between the block copolymer and network systems, the behaviour of the uncross-linked materials is different to the networks. At the yield point ($\lambda \approx 1.5$) the scattering maximum for the block copolymers in the direction of stretch disappears, this is not seen in the network systems analysed in this project. Therefore lamellae in the network systems do not change orientation to the direction of stretch. The maxima that appear perpendicular to the direction of stretch decrease as stretching occurs for the triblock systems, the same occurs in the network systems which suggests that interdomain correlation has been destroyed due to sample yielding. Figure 4.1p shows how a lamellar styrene-butadiene network system might react upon extension in the direction of stretching.

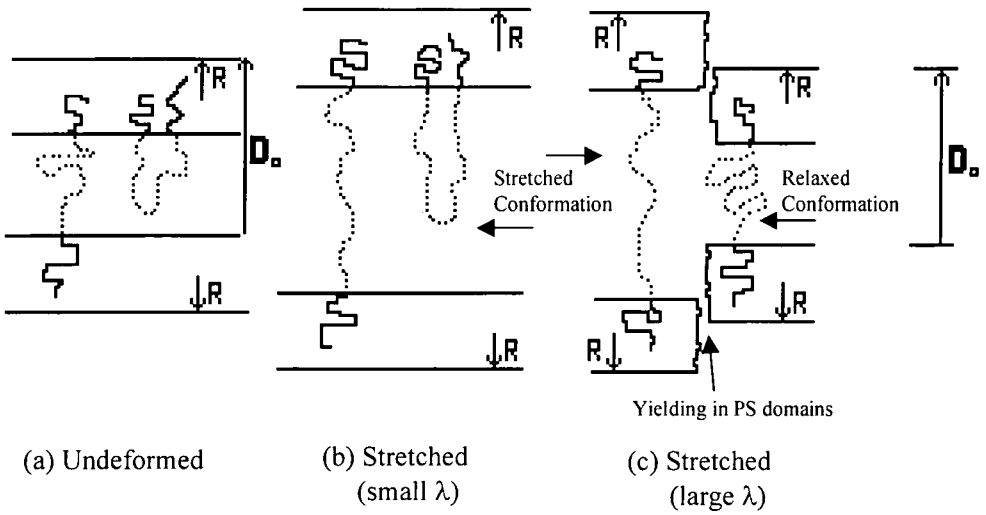

Figure 4.1p Effect of yielding polystyrene domains perpendicular to the direction of stretch

When sample extension passes the yield point, variation in domain spacing values increases causing phase disorder in the system. As the network systems are inhomogeneous there appears to be lamellar disorder in both parallel and perpendicular directions, with the cross-linking preventing complete disorder and rearrangement of the structure. Tables 4.1g-h show domain spacing values of the lamellar networks stretched at extension ratios between 1.0-2.0 parallel and perpendicular to the detector in the Kratky SAXS camera.

Table 4.1g Lamellar networks stretched parallel to the detector

BSB Network	Kratky domain spacing	Predicted domain spacing	Extension Ratio 1.25 (d/Å)	Extension Ratio 1.50 (d/Å)	Extension Ratio 1.75 (d/Å)	Extension Ratio 2.0 (d/Å)
NL1	140 Å	160 Å	195	210	205	205
NL2	160 Å	200 Å	170	180	185	260
NL3	180 Å	250 Å	200	220	250	250
NL4	205 Å	270 Å	230	250	270	320
NL5	225 Å	300 Å	225	240	275	315
NL6	220 Å	330 Å	245	255	265	275

Table 4.1h Lamellar networks stretched perpendicular to the detector

BSB Network	Kratky domain spacing	Predicted domain spacing	Extension Ratio 0.92 (d/Å)	Extension Ratio 0.86 (d/Å)	Extension Ratio 0.81 (d/Å)	Extension Ratio 0.77 (d/Å)
NL1	140 Å	160 Å	-	-	-	-
NL2	160 Å	200 Å	-	-	-	-
NL3	180 Å	250 Å	170	150	150	150
NL4	205 Å	270 Å	180	170	170	170
NL5	225 Å	300 Å	-	-	-	-
NL6	220 Å	330 Å	200	200	200	200

Figure 4.1q shows a set of lamellar network SAXS intensity curves generated from the Kratky camera as network samples are being extended parallel to the direction of stretch.

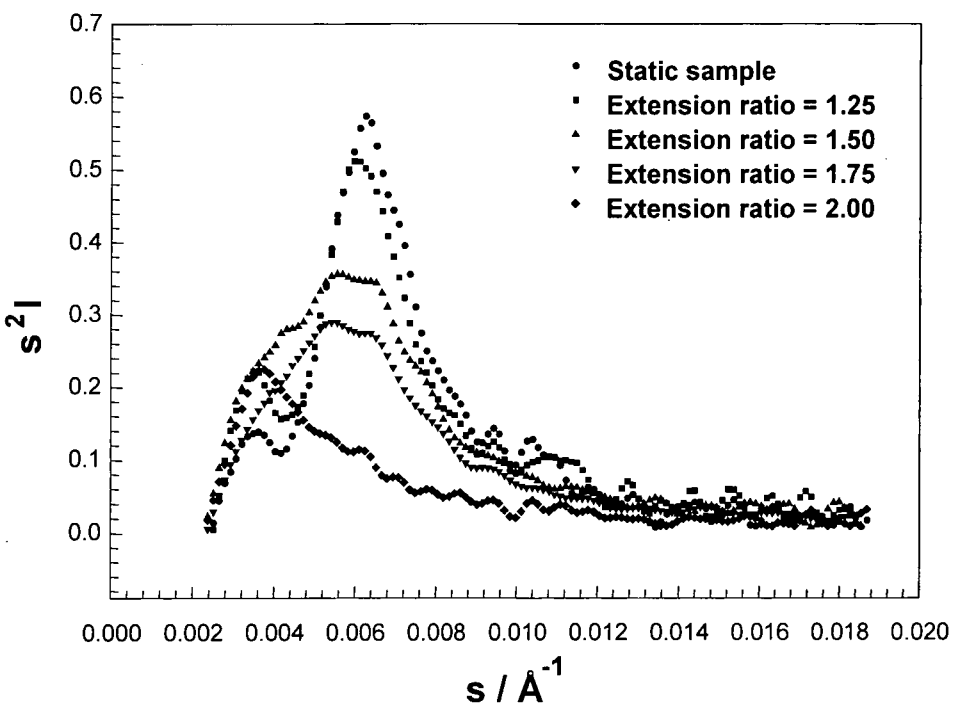

Figure 4.1q Kratky camera SAXS curves of lamellar network extended parallel to the direction of stretch

SAXS intensity curves from the Kratky camera show similar trends to the synchrotron data. Kratky SAXS extension ratios in the parallel direction increase in a similar way to the force elongation curve, with little increase in the SAXS values after the yield point of the materials. Figure 4.1r shows the main visible Bragg peak decrease in intensity and approach the beam stop as sample stretching occurs. As the extension ratio = 2.0 the main Bragg peak with the highest intensity before stretching has been obscured behind the beam stop leaving residual scattering after the beam stop.

Figures 4.1r-s summarise the data in tables 4.1g-h showing similar trends are found when using the Kratky SAXS camera technique. A comparison of the SAXS extension ratio with the stress-stain curve is included in figure 4.1r showing there is some change in the SAXS extension ratio after sample yielding occurs, but which forms a plateau before the extension ratio = 2.0.

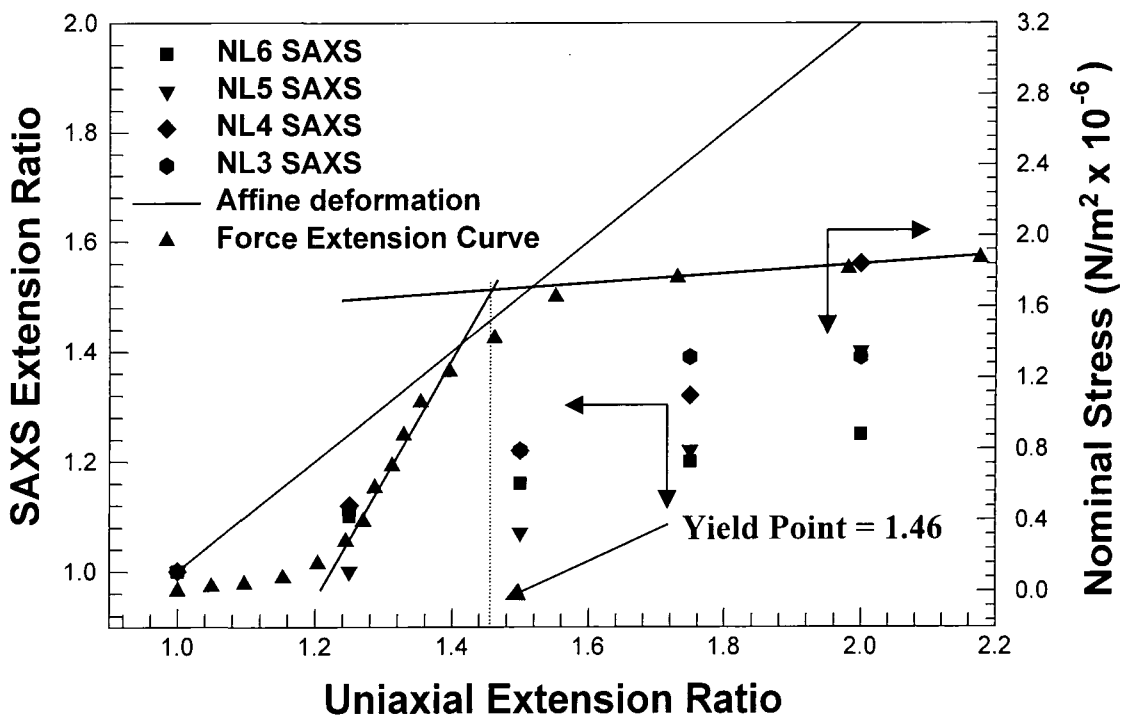

Figure 4.1r Lamellar networks stretched parallel to the SAXS detector

Only limited analysis was possible with samples stretched perpendicular to the detector in figure 4.1s, due to sample properties and the method employed to stretch the materials. Measurements on the more physically elastic samples were pursued due to extensive yielding and sample breakage in the less elastic lamellar samples. A scale describing the uniaxial compression ratio in the perpendicular direction was again calculated using Poisson's ratio[13,14].

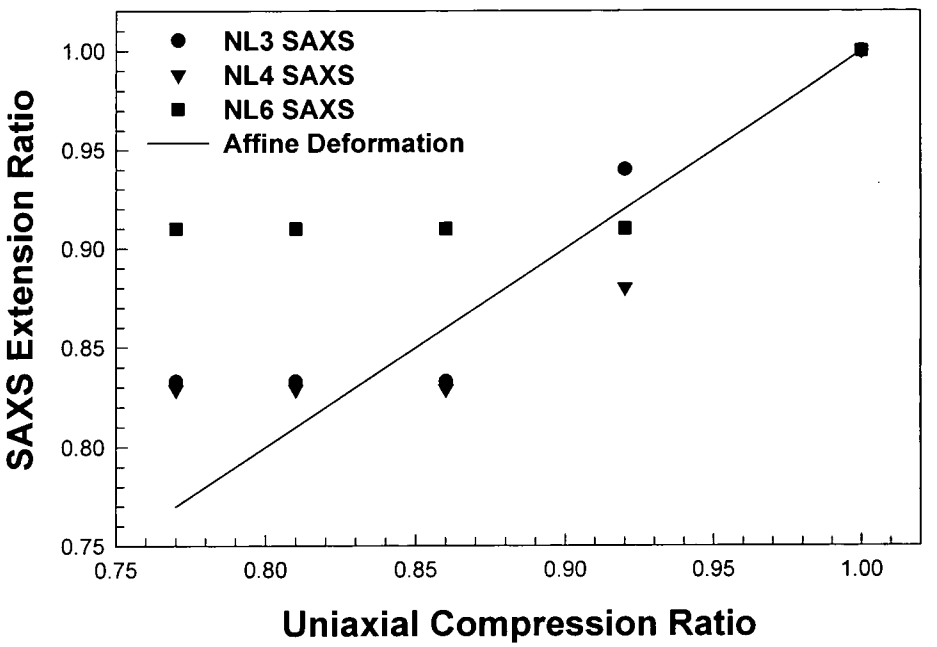

Figure 4.1s Lamellar networks stretched perpendicular to the SAXS detector

Kratky SAXS extension ratios in the perpendicular direction appear to act similarly to results from the synchrotron data by following affine deformation until the yield point of the material.

4.2 Small Angle X-ray Scattering results of spherical morphology systems

4.2.1 Uncross-linked systems

A series of BSB uncross-linked copolymer samples with spherical morphology have been studied using time-resolved synchrotron SAXS and Kratky camera SAXS. Preparation of the sample films involved the same procedure as the lamellar uncross-linked materials. Examination of the 1st order Bragg peak from the scattering curves gave the domain spacing between spheres in each material. Subsequent peaks were used where possible to determine the type of cubic lattice present in the spherical systems. An example of a time resolved Lorentz corrected scattering curve for copolymer LS4 is shown in figure 4.2a.

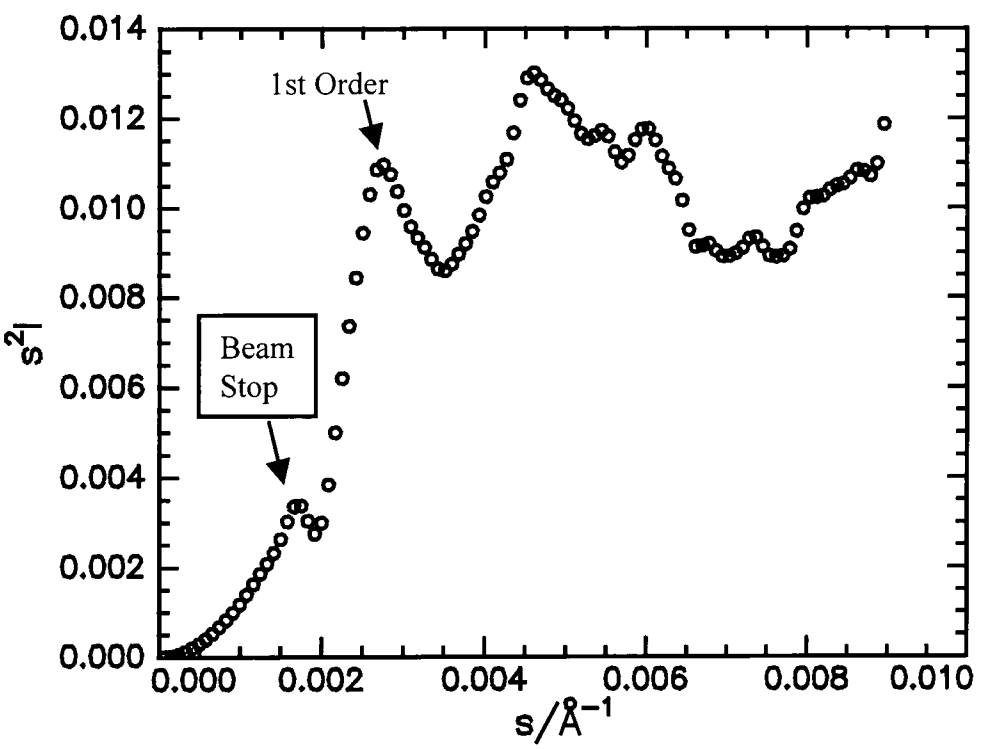

Figure 4.2a Lorentz corrected scattering curve for copolymer LS4

Characteristics of the uncross-linked spherical samples are summarised in table 4.2a where domain spacing values from Kratky camera and synchrotron SAXS values are compared to theoretical values[5,6].

Table 4.2a Spherical copolymer characteristics

BSB	MW (k)	Kratky SAXS Unannealed / Å	Synchrotron SAXS d spacing / Å		Theoretical d spacing / Å
			parallel	perpendicular	
LS1	35	150	-	-	160
LS2	40	200	-	-	180
LS3	60	220	-	-	250
LS4	120	355	390	375	400
LS5	240	410	440	420	470

Films of the uncross-linked spherical morphology copolymers were difficult to prepare for SAXS experiments due to processing problems encountered caused by the samples fluidity at room temperature. Therefore only limited data from the Kratky camera is available and no synchrotron data was obtained for the lower molecular weight polymer systems. Figure 4.2b summarises the spherical copolymer data in the form of a graph with error bars on the synchrotron domain spacing values. Materials that were possible to analyse with the Kratky camera and synchrotron radiation displayed a 1st order Bragg peak as in Figure 4.2a but subsequent peaks were difficult to justify. Domain spacing calculations for the spherical materials were possible, but structure characterisations were less straight forward and not pursued. Information from the data collected for the uncross-linked samples did not suggest whether the packing was of any of the known cubic forms[7].

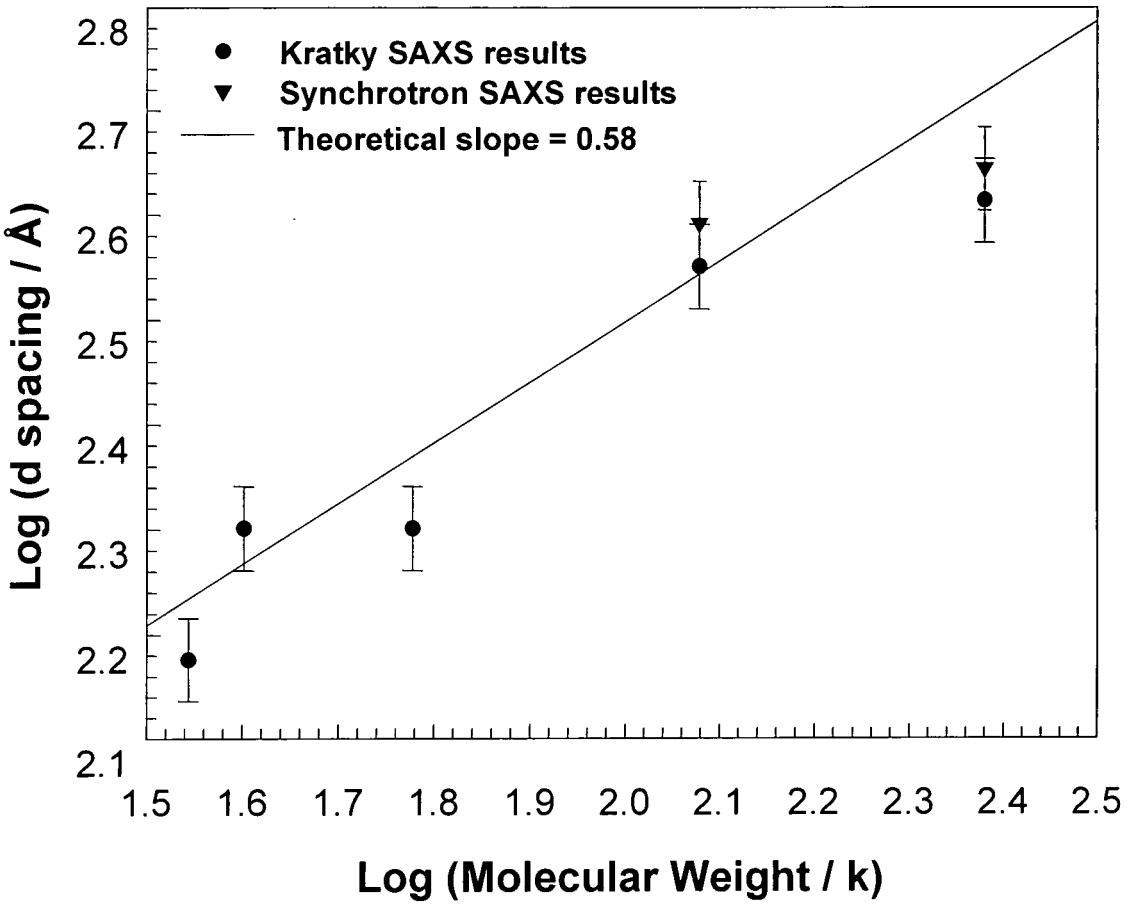

Figure 4.2b Spherical copolymer SAXS result comparison to theory

The results show that experimental data matches theoretical predictions within the predicted margin of error and for the limited results obtained from the materials. Spherical uncross-linked systems displayed similar behaviour to theoretical trends of the lamellar systems. Kratky camera SAXS results were similar to the predicted domain spacing values from the theoretical model by Helfand and Wasserman[1].

4.2.2 Cross-linked systems

4.2.2.1 Unstretched networks

Spherical morphology network samples have been studied using the Synchrotron SAXS and Kratky camera SAXS techniques. Sample preparation followed the same procedure as for the lamellar morphology systems. An example of a Lorentz corrected 2-D synchrotron scattering curve for a spherical morphology system is shown in figure 4.2c for network NS1. Tables 4.2b-d present characteristics of the spherical systems using SAXS analysis. Theoretical domain spacing values are based on the equivalent uncross-linked copolymer systems. The appearances of the spherical system scattering curves are very different from the lamellar systems. The main visible Bragg peak in the spherical morphology case is broader with lower scattering intensity. A decrease in scattering from the spherical morphology systems due to increased disorder is indicative that cross-linking has disrupted the formation of a cubic lattice.

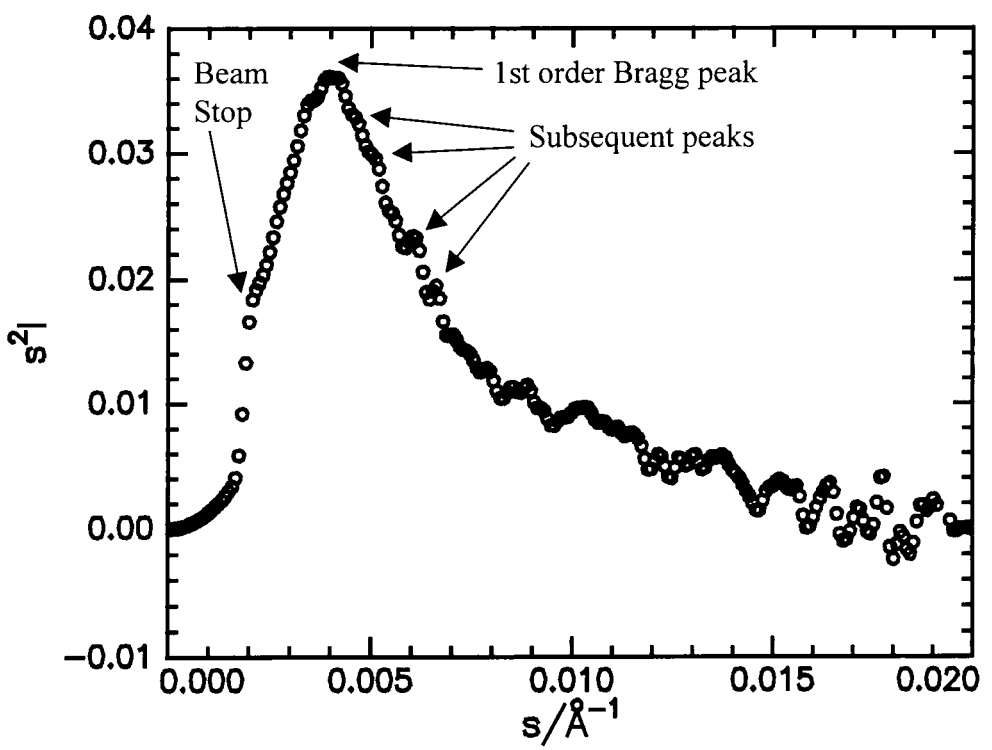

Figure 4.2c Lorentz corrected scattering curve for network NS1

The increase in width of the 1st order Bragg peak showed the spherical morphology system to be less ordered than the equivalent lamellar network system, due to lattice distortions of the first and second kinds[17] caused by cross-linking.

Cross-linking disrupts ideal crystal lattice formation limiting structure factor peaks from long range order and prevents the formation of perfectly shaped spherical domains which limits single particle form factor scattering. Some of the structure factor peaks are visible and can be identified but it is difficult to justify the packing present due to the irregularity of the peak ratios. Any number of peaks from figure 4.2c could be attributed to the structure factor. The subsequent peaks shown do not completely justify a case for any of the cubic crystal structures, but the possibility remains that structure factor peaks and form factor peaks are concurrently present in the scattering, cancelling each other out and disrupting structural analysis.

Table 4.2b Annealed spherical network characteristics

BSB Network	MW (k)	Kratky sphere radius / Å	Theoretical sphere radius / Å	Kratky d spacing / Å	Theoretical d spacing / Å
NS1	35	57	49	200	167
NS2	45	71	54	250	192
NS3	50	86	60	300	209
NS4	60	57	65	200	230
NS5	80	69	88	240	300
NS6	100	107	92	375	330
NS7	150	114	123	400	436

Theoretical calculations of values for the sphere radius of each network are made using a Fortran computer program written by Helfand and Wasserman[1]. Kratky sphere radius dimensions were also calculated using the computer program mentioned due to form factor peaks not being visible in the scattering traces.

Table 4.2c Domain spacing values in the spherical networks from Synchrotron SAXS

BSB Network	Parallel (d/Å)		Perpendicular (d/Å)	
	Annealed	Unannealed	Annealed	Unannealed
NS1	250	242	250	250
NS2	295	264	295	265
NS3	360	360	310	307
NS4	200	240	223	240
NS5	274	303	284	291
NS6	250	333	295	354
NS7	360	366	300	329

Table 4.2d Radius values in the spherical networks from Synchrotron SAXS

BSB Network	Parallel (d/Å)		Perpendicular (d/Å)	
	Annealed	Unannealed	Annealed	Unannealed
NS1	71	69	71	71
NS2	84	75	84	75
NS3	103	103	88	87
NS4	57	68	64	68
NS5	78	86	81	83
NS6	71	95	84	101
NS7	103	104	85	94

Further analysis of the peak ratios from scattering traces of the spherical morphology networks is presented in section 4.2.3 of this chapter, showing the possible structures deduced from the data available. Figure 4.2d graphically presents a comparison of domain spacing results from SAXS techniques with theoretical values[5,6] from the equivalent uncross-linked systems.

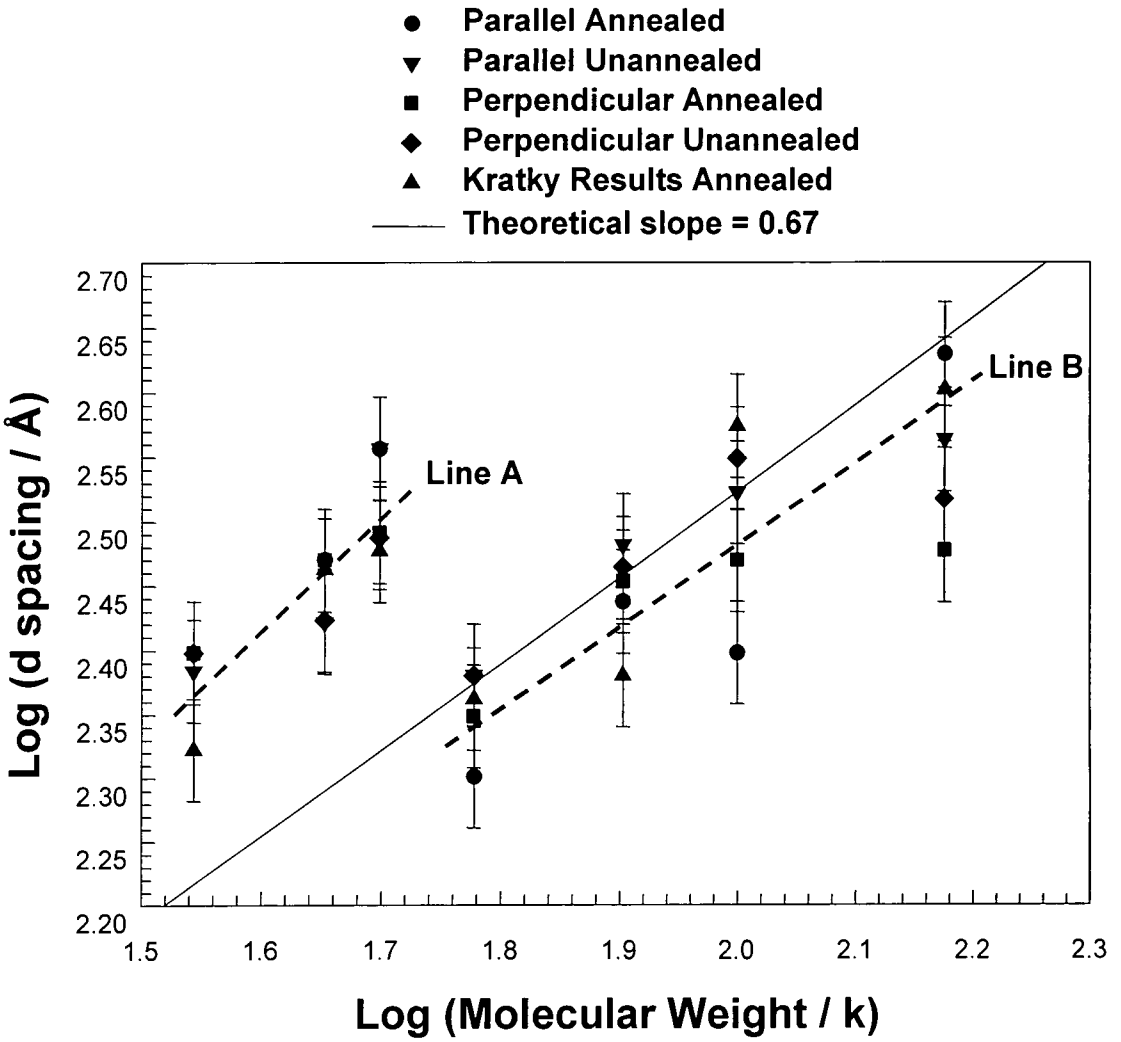

Figure 4.2d Network domain spacing values for spherical morphology systems

It can be seen in figure 4.2d that there are two lines that have similar slopes but different intercepts on the y-axis. Therefore it is assumed that line A corresponds to the 1st order Bragg peak domain spacing values of a spherically packed cubic structure, and line B to the 2nd order Bragg peak domain spacing values. If the packing of the system was to be body centred cubic or face centred cubic, the same plot can be redrawn to encompass these factors. Now it is assumed that line B arises from the 2nd order Bragg peak of the cubic structure as the 1st order one is hidden by the beam stop.

Figure 4.2e plots the graph with corrected domain spacing values. If the spherical structure is assumed to be body centred cubic (BCC), the main visible Bragg peak would be the second one, a ratio 1.41 times greater than the position of the first order Bragg peak. If the spherical morphology is assumed to be face centred cubic (FCC), the 2^{nd} order Bragg peak would be 1.15 times greater than the position of the first order Bragg peak. Therefore a comparison of the two possible cubic packing morphologies can be made. Figure 4.2e shows the corrected plot assuming BCC (a) or FCC (b) packing, that demonstrates the most likely spherical morphology of the network structures.

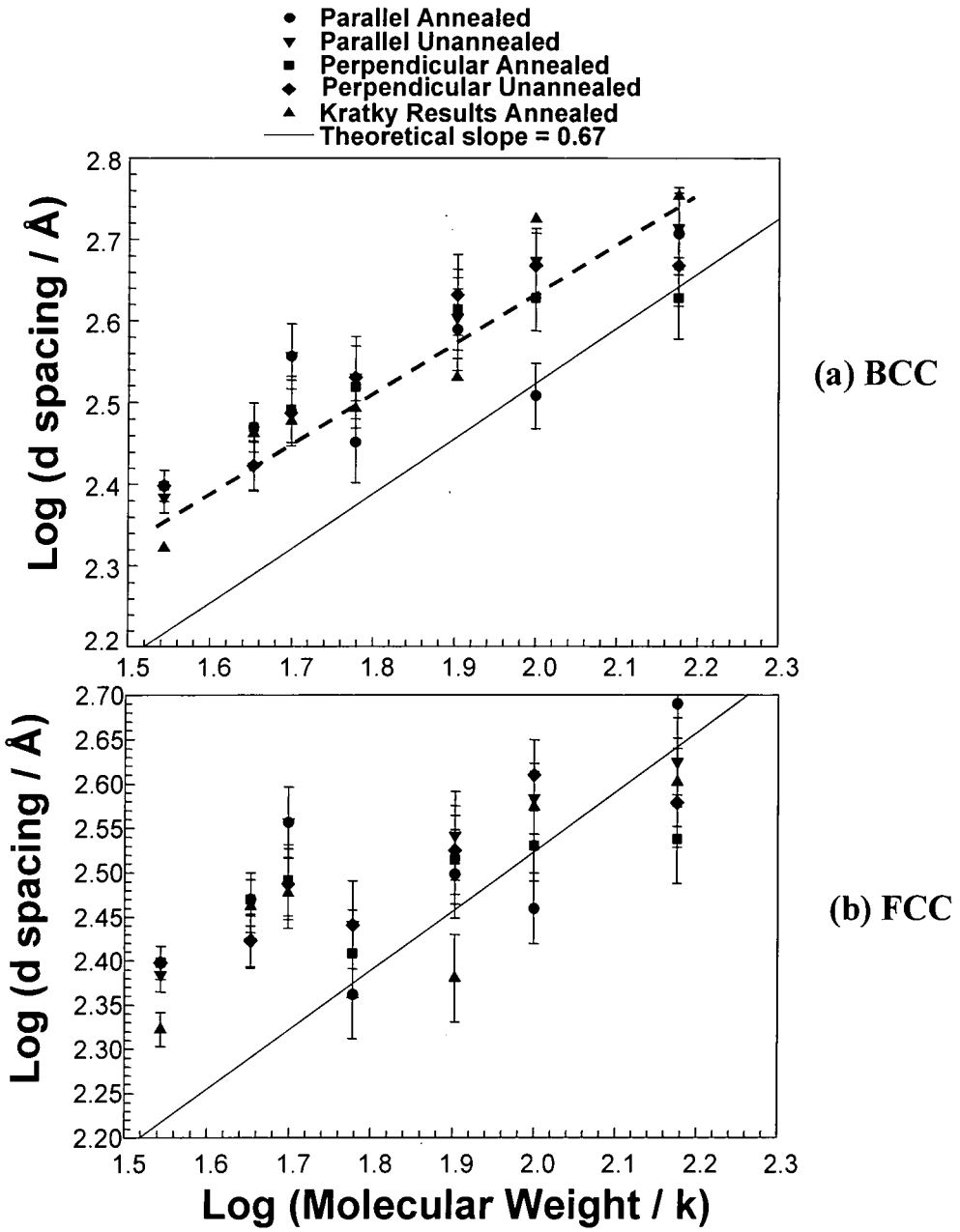

Figure 4.2e Corrected log-log spherical morphology plot

Once the correction has been made it is evident that domain spacing values are greater than the theoretical trend of uncross-linked equivalents. This behaviour has been seen to occur in certain networks systems where a block copolymer and equivalent networks have been synthesised and domain spacing values compared[18]. The packing of the network systems is assumed to be BCC due to the domain spacing values falling closer to the theoretical slope than the FCC packing case.

4.2.2.2 Stretched

Time resolved synchrotron and Kratky camera SAXS data were recorded for the spherical morphology networks using the same conditions as the lamellar systems at room temperature. Samples were stretched to a maximum extension ratio of four at a rate of 1cm/min. Examination of the scattering curve as the sample was stretched enabled the structure to be monitored under nominal stress. Table 4.2e shows 2-D synchrotron SAXS results obtained from a stretched spherical morphology sample.

Table 4.2e Synchrotron SAXS analysis of spherical network sample NS1 stretched

Frame	Extension		Annealed (d/Å)		Unannealed (d/Å)	
	Mm	ratio	Parallel	Perpendicular	Parallel	Perpendicular
0	0.00	1.00	250	250	240	250
1	1.66	1.17	267	250	235	245
2	3.33	1.33	291	245	245	240
3	5.00	1.50	311	237	256	237
4	6.66	1.66	320	230	271	228
5	8.33	1.83	307	225	281	221
6	10.00	2.00	307	225	295	213
7	11.66	2.17	324	219	311	213
8	13.33	2.33	329	213	303	213

Plots for the remaining force-extension curves and SAXS extension ratios of the spherical samples are listed in appendix 2. Figure 4.2f demonstrates the variation of scattering for network NS1 parallel to the direction of stretch and figure 4.2g perpendicular to the direction of stretch.

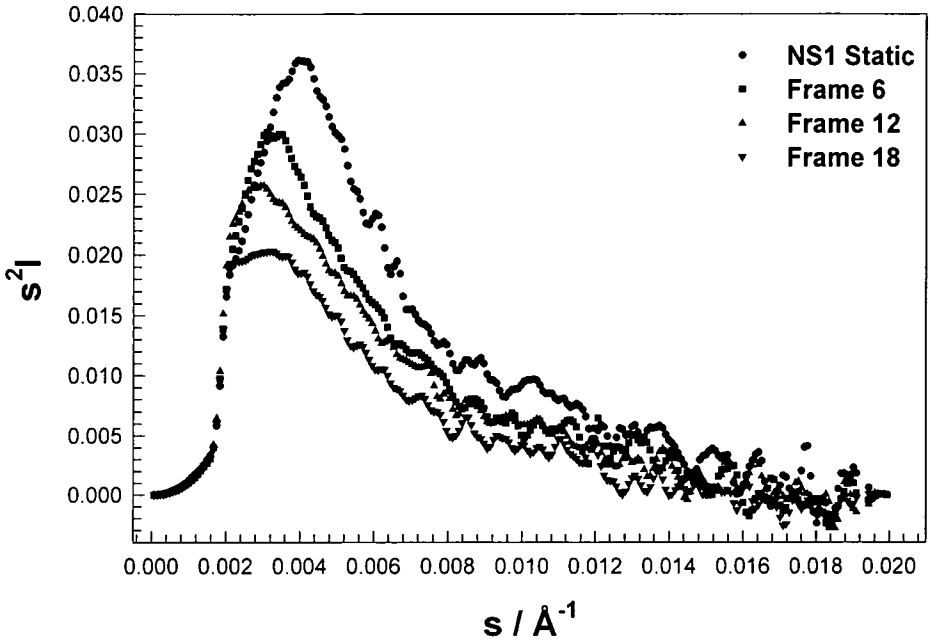

Figure 4.2f Scattering curves parallel to the direction of stretch for a spherical morphology network

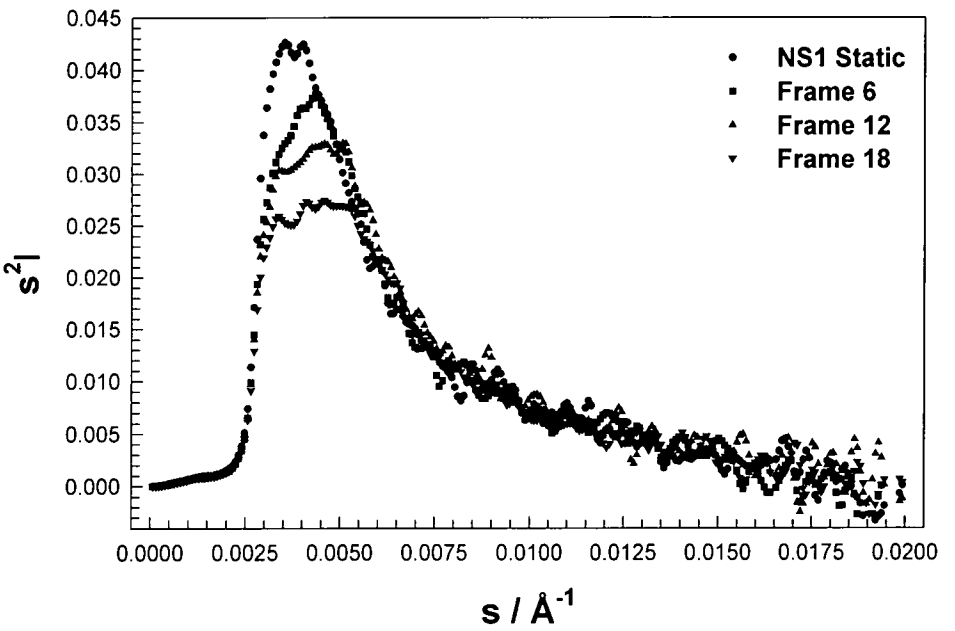

Figure 4.2g Scattering curves perpendicular to the direction of stretch

When the spherical network samples are stretched in the parallel direction (figure 4.2f) there is an increase in domain spacing, the symptom being the approach of the 1st order Bragg peak to the beam stop. In the perpendicular direction there is a steady decrease in domain spacing, indicating that samples perpendicular to the uniaxial stretch direction narrow when stretched uniaxially. The behaviour suggests that domain spacing values vary in a similar way to the parallel and perpendicular dimensions of the sample as stretching occurs, due to the uniform manner in which the scattering pattern changes.

There is a decrease in the scattering intensity as sample stretching occurs in both parallel and perpendicular directions, indicating an increase in sphere disorder as the main Bragg peak broadens out. The observation of peak broadening is restricted in the parallel direction due to the beam stop obscuring the view of the peak. If the main visible Bragg peak was sharp, there would be evidence of a narrow variation of domain spacing values, however the perpendicular scattering displays an increase in peak broadening showing that there is a greater variation of domain spacing in network samples. The two plots show that cross-linking disrupts long and short-range order in spherical systems and as stretching occurs, the order of each sample is further disrupted. As there will be no deformation of the glassy polystyrene domains, the elastic polybutadiene lattice deforms as the sample stretches - changing the domain spacing with parallel and perpendicular directions of stretch.

The 1st order Bragg peak height of the scattering curves from these systems decrease in a monotonic manner as the sample is stretched to the maximum extension ratio. Due to the increased amount of polybutadiene in the systems, the behaviour of the spherical systems is different at room temperature to the lamellar systems, and so they change at a monotonic rate.

Force-extension curves (figure 4.2h) for the spherical morphology networks conform more to affine deformation predictions than those for lamellar morphology networks. This can be seen from the scattering curves as stretching occurs, scattered intensity decreases at the same rate as sample extension increases which compliments the effect of the force extension curve. The increase in the SAXS domain spacing extension ratios are not affine, but the main Bragg peak is obscured by the beam stop in the parallel direction as the uniaxial extension ratio, λ, approaches four. Data taken after the Bragg peak is obscured will be misleading and not indicate the real domain spacing, therefore explaining the behaviour of the SAXS extension ratio.

The spherical morphology scattering trace (figures 4.2f-g) changes at a uniform rate when compared to the stress-strain of the material, showing continual 1st order Bragg peak movement through to an extension ratio, $\lambda = 4$. At room temperature lamellar samples do not possess the property of a continual increase in the SAXS extension ratios due to yielding of the sample at an early stage. Spherical morphology systems extend more affinely and tend not to yield as much as the lamellar ones. Figure 4.2h shows the SAXS extension ratio in the parallel direction compared to uniaxial deformation for spherical morphology network NS1.

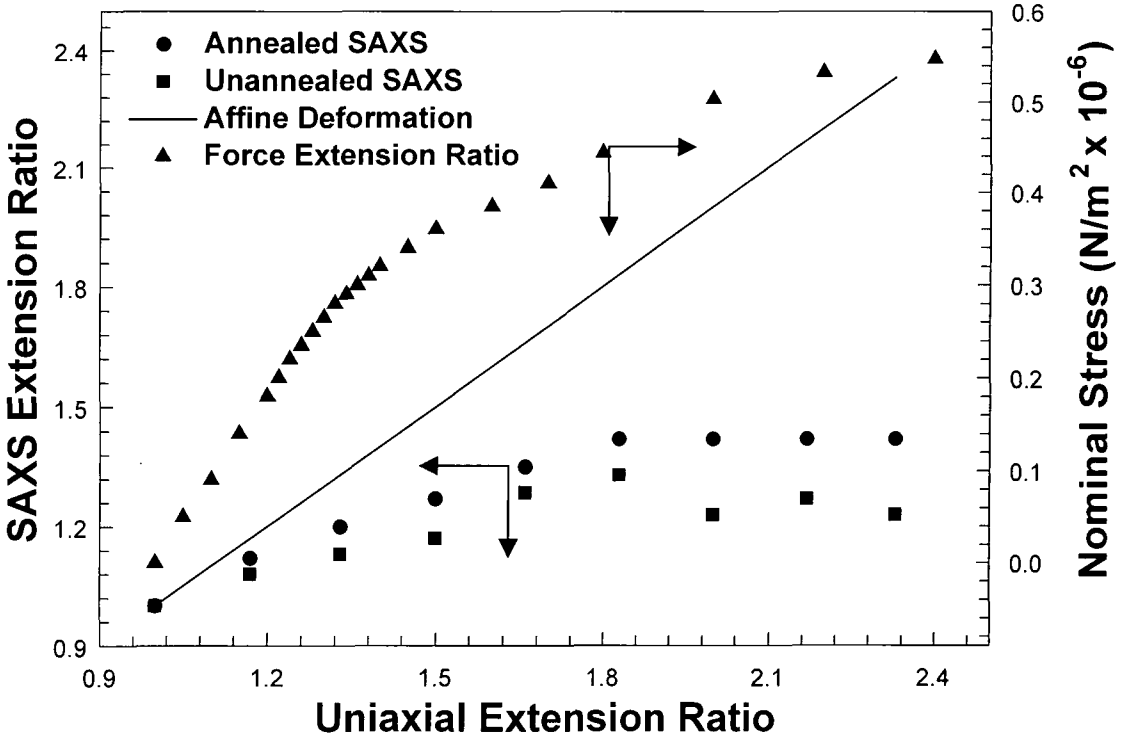

Figure 4.2h Force extension data for network parallel to the direction of stretch

The extension ratios calculated from the domain spacing values of the stretched networks, have a qualitatively similar shape to the force-extension curve observed for the material. Force-extension plots for the spherical morphology systems analysed display little evidence of yielding within the extension ratio range of these experiments, due to their elastomeric nature. The force-extension curve shown in figure 4.2h can be assumed to be the same for both annealed and unannealed network samples in this comparison. This behaviour has been observed in the literature for S-I and S-I-S block copolymers[19]. The SAXS extension ratio from the domain spacing behaved as a function of the sample uniaxial extension ratio. This result is observed above in figure 4.2h. The elastomeric properties of the block copolymers are associated with the initial increase in interdomain distance, followed by the formation of localised regions of lower density, and subsequently microvoids.

Figure 4.2i shows the SAXS extension ratio in the perpendicular direction for sample NS1, compared to the uniaxial extension ratio and with the predictions of affine deformation of the sample.

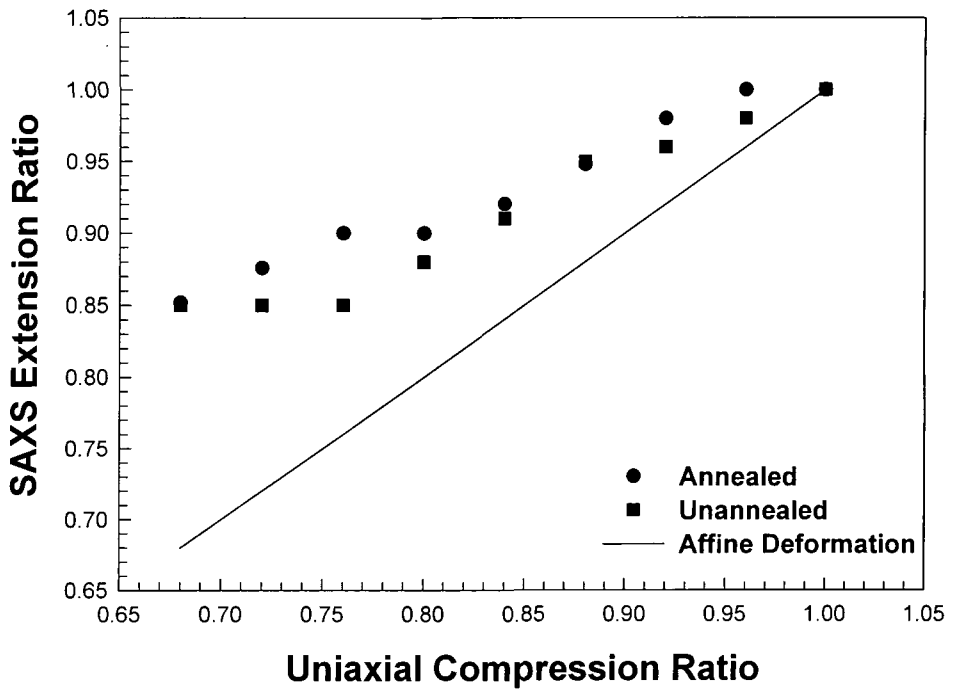

Figure 4.2i SAXS extension ratio data for network NS1 perpendicular to the direction of stretch

SAXS extension ratio curves for the spherical morphology samples were very similar to each other, none of them increasing or decreasing in an affine manner. Data parallel to the direction of stretch behaves similarly to the force extension curve with sample extension. Data perpendicular to the direction of stretch shows that sample compression decreases the domain spacing in a monotonic manner. Initially SAXS extension ratios increase at a rate similar to the affine extension but as the sample extension increases

further, the domain spacing values and therefore SAXS extension ratios plateau, a similar behaviour to the force-extension curve.

Data obtained from the Kratky SAXS camera were collected from samples stretched in the direction parallel to the detector. Examination of the visible diffraction peaks to determine the SAXS extension ratios allowed comparisons to the force extension data to be made. Table 4.2f shows results from spherical network systems stretched at extension ratios, λ, of 1.25, 1.50, 1.75 and 2.0.

Table 4.2f Spherical networks stretched to an extension ratio of 2.0

BSB Network	Kratky domain spacing	Predicted domain spacing	Extension Ratio 1.25 (d/Å)	Extension Ratio 1.50 (d/Å)	Extension Ratio 1.75 (d/Å)	Extension Ratio 2.0 (d/Å)
NS1	200 Å	167 Å	240	245	255	275
NS2	250 Å	192 Å	275	285	290	290
NS3	300 Å	209 Å	340	380	380	380
NS4	200 Å	230 Å	-	-	-	-
NS5	240 Å	300 Å	250	260	230	240
NS6	375 Å	330 Å	-	-	-	-
NS7	400 Å	436 Å	415	430	460	480

The results in table 4.2f show an immediate increase in domain spacing extension ratios as stretching begins – along the trend of affine deformation. After this initial change of the 1st order Bragg peak position, the beam stop obscures the 1st order Bragg peak, only by analysing subsequent Bragg peaks is the calculation of further domain spacing values possible. Network samples NS4-7 used estimations of the 1st order Bragg peak from subsidiary order peaks as the domain spacing values could not be calculated initially due to the beam stop position obscuring the 1st order Bragg peaks. Figure 4.2j plots SAXS extension ratio results from the spherical morphology systems against the uniaxial extension ratios, comparing curves with a typical force extension result for the systems concerned.

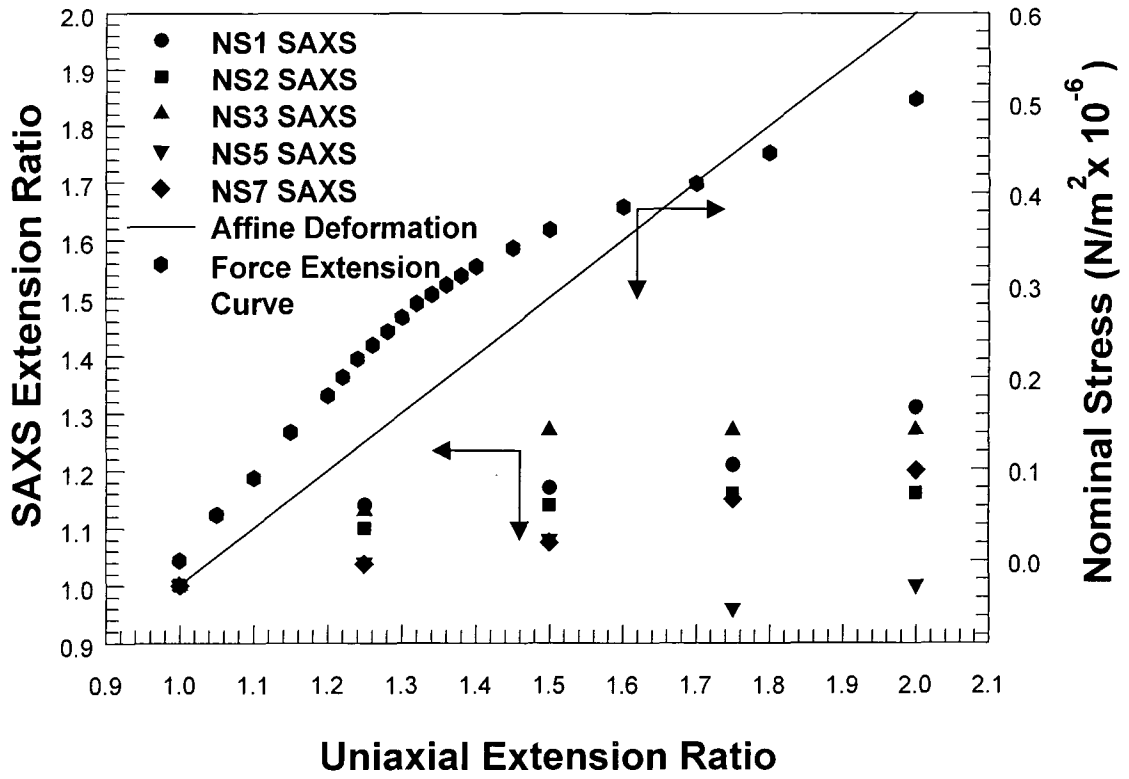

Figure 4.2j Spherical morphology scattering traces from Kratky SAXS extension curves of network samples

As the samples stretch the main Bragg peak approaches the beam stop at a lower rate than affine deformation predicts, but possesses a similar shape to the stress-strain extension curve shown on the same plot. The results show similar trends to the equivalent synchrotron data. Figure 4.2k shows the analysis from the Kratky equivalent plot to figure 4.2f depicting domain spacing variation as the network sample is extended parallel to the direction of stretch.

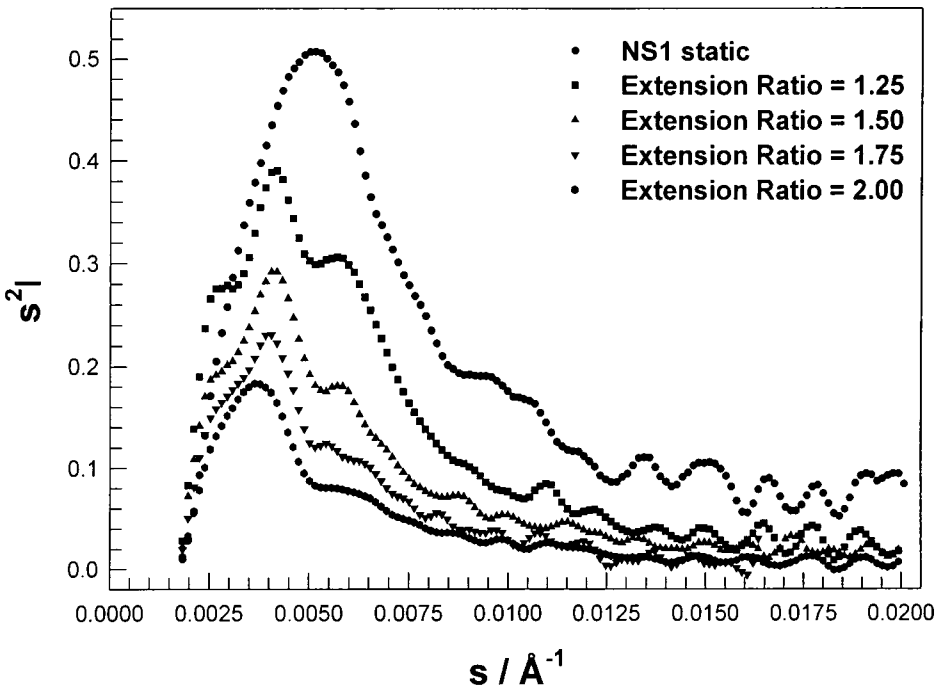

Figure 4.2k Kratky camera SAXS analysis of spherical morphology system NS1

Figure 4.2k shows that data from both Kratky camera and synchrotron SAXS behaves in the same manner i.e. a good match. Sample stretching decreases the intensity of the scattering in each network analysed, therefore increasing the disorder of the system. Results from the Kratky camera SAXS analysis of the spherical morphology systems are very different from the lamellar systems, there are peaks present after the first order peak in the data indicating that a cubic structure can be determined from the peak ratios, this is discussed in section 4.2.3.

4.2.3 Discussion of spherical morphologies

The ratio of initial Bragg peak separations observed in scattering curves from the spherical morphology systems suggests the existence of cubic packing. However, it is not clear which form of packing is present. Body centred cubic ratios seem to match most closely the ratios observed from experimental results. Table 4.2g is a summary of the results obtained from the Kratky SAXS data for the spherical morphology systems, obtained from the Bragg peak ratios of the scattering curves. Data in table 4.2g are only included if 1st, 2nd and 3rd order Bragg peaks were identifiable from the scattering curves.

Table 4.2g Bragg peak spacing ratios from spherical morphology systems

Kratky Camera data	**Bragg peak ratio**					
BSB	**1st Order**		**2nd Order**		**3rd Order**	
Network	**Un**	**An**	**Un**	**An**	**Un**	**An**
NS1 (1st Order)	1.0		0.75	0.71	0.67	0.65
NS2 (1st Order)	1.0		0.74	0.75	0.50	0.51
NS3 (1st Order)	1.0		0.68	0.69	0.57	0.53
BCC ratio (1st Order)	1.0		0.707		0.577	
FCC ratio (1st Order)	1.0		0.866		0.612	
SC ratio (1st Order)	1.0		0.707		0.577	
NS4 (2nd Order)	1.0		-	0.82	-	0.68
NS5 (2nd Order)	1.0		0.69	0.78	0.60	0.63
NS6 (2nd Order)	1.0		0.72	0.86	0.53	0.62
NS7 (2nd Order)	1.0		0.73	0.83	0.61	0.63
BCC ratio (2nd Order)	1.0		0.816		0.707	
FCC ratio (2nd Order)	1.0		0.707		0.603	
SC ratio (2nd Order)	1.0		0.816		0.707	

1st Order – Assumes main visible Bragg peak is the 1st order peak

2nd Order – Assumes main visible Bragg peak is the 2nd order peak

The majority of the results in table 4.2g suggest the presence of body centred cubic lattices in the network systems. It is possible to analyse the higher molecular weight

network systems in a similar way by assuming that the 1st order Bragg peak is hidden behind the beam stop. Therefore the observed peak is actually the 2nd order one. As the body centred and simple cubic systems have the same ratios for the first order peaks the difference between them is negligible. Simple cubic packing is included as a possible packing structure together with body centred packing but is highly unlikely because of the flimsy nature of its structure. Together with Bragg peak results from the synchrotron data the packing of the spherical morphology network systems appears to be body centred.

Ratios of the Bragg peaks in the spherical morphology systems analysed using synchrotron SAXS are reported in table 4.2h. Scattering peaks or shoulders were visible for some of the networks and could be assigned as diffraction peaks of a cubic packed spheres.

Table 4.2h Bragg peak spacing ratios from spherical network systems

Synchrotron SAXS data	**Bragg peak ratio**					
BSB	**1st Order**		**2nd Order**		**3rd Order**	
Network	**Un**	**An**	**Un**	**An**	**Un**	**An**
NS1 (1st Order)	1.0		0.74	0.69	0.69	0.63
NS2 (1st Order)	1.0		0.82	0.78	0.72	0.67
NS3 (1st Order)	1.0		0.68	0.83	0.57	0.65
BCC ratio (1st Order)	1.0		0.707		0.577	
FCC ratio (1st Order)	1.0		0.866		0.612	
SC ratio (1st Order)	1.0		0.707		0.577	
NS4 (2nd Order)	1.0		-	-	-	-
NS5 (2nd Order)	1.0		0.79	0.82	0.71	0.70
NS6 (2nd Order)	1.0		-	-	-	-
NS7 (2nd Order)	1.0		0.73	-	0.67	-
BCC ratio (2nd Order)	1.0		0.816		0.707	
FCC ratio (2nd Order)	1.0		0.707		0.603	
SC ratio (2nd Order)	1.0		0.816		0.707	

1st Order – Assumes main visible Bragg peak is the 1st order one

2nd Order – Assumes main visible Bragg peak is the 2nd order one

Systems that were not possible to analyse possessed scattering traces in which subsequent Bragg peaks could not be identified because of the weak scattering obtained from the system. Synchrotron data obtained from the spherical morphology systems displayed a variety of Bragg peak ratios for static data. Evidence from the results lead to the conclusion that systems are packed in a body centred cubic manner because values of the 2nd order Bragg peak are rarely near 0.866, this value would suggest FCC packing. Network systems NS4-NS7 are assumed to possess a 2nd order Bragg peak as the main visible domain spacing identification point. Results from the bottom section of the table (NS4-NS7) above suggest the structure adopts a BCC packing. Due to cross-linking of the spherical systems Bragg peak identification was not obvious, and any further analysis from the scattering curves of the static samples such as form factor scattering information was not possible.

Diagrams of the spherical packing systems are shown in figure 4.21 predicting what the packing would be like if the cubic lattices were packed without any distortions present.

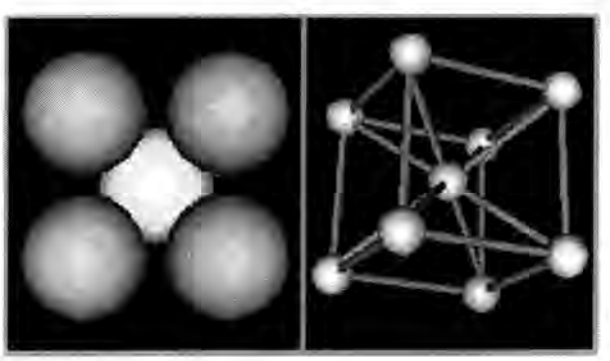

(a) Body Centred Cubic Packing (**BCC**)

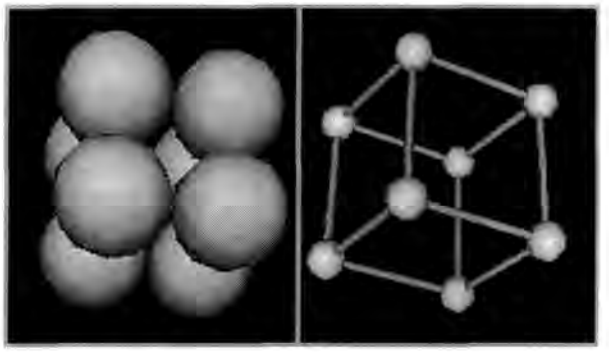

(b) Simple Cubic Packing (**SC**)

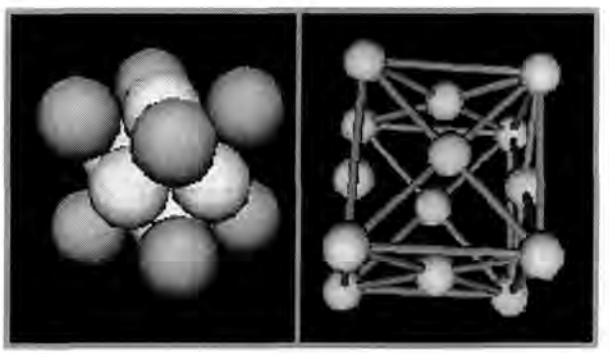

(c) Face Centred Cubic Packing (**FCC**)

Figure 4.2l Possible spherical morphology network packing structures

It is possible to predict the packing of a cubic structure from the domain spacing and radius values of the spherical systems. A comparison will be made of theoretical and experimental domain spacing values to calculate the form of cubic packing.

Simple cubic packing forms rows, columns and layers: they sit at the corners of stacked cubes and are rarely observed, mostly because they are floppy and tend to distort. Body centred cubic (BCC) packing of atoms tends to be most stable at temperatures higher than face centred cubic (FCC) packing in order to have room to vibrate, where one atom

sits in the centre of each cube. Face centred cubic (FCC) crystals are common among metals at low temperatures because the atoms pack well where one atom sits in each 'face' of the cube. Any one of the three systems is possible in the networks synthesised in the work presented here.

Table 4.2i includes results of the predicted domain/radius dimensions, experimental calculations of these values and expected volume fractions in the network systems. The results from this investigation suggest that these systems could be face centred or body centred cubic structures.

Table 4.2i Spherical morphology network cubic structure analysis (pt.1)

Network	Domain spacing	Domain radius	Unit cell length (SC)	Unit cell volume	Sphere volume	Spherical volume fraction
	Å	Å	Å	$Å^3$ (x 10^{-6})	$Å^3$ (x 10^{-6})	
NS1	200	57	200	8.00	0.776	0.097
NS2	250	71	250	15.63	1.499	0.096
NS3	300	86	300	27.00	0.266	0.099
NS4	360	103	360	46.67	4.577	0.098
NS4	240	69	240	13.82	1.376	0.099
NS6	375	107	375	52.73	5.131	0.097
NS7	400	114	400	64.00	6.203	0.097

SC denotes treatment for a system that has simple cubic packing.

Analysis involves taking the domain spacing values obtained experimentally and assuming that the packing is of a simple cubic structure, by calculating volume fractions for the simple cubic structures it is then possible to calculate values for Body Centred Cubic and Face Centred Cubic structures. The volume fractions are then compared to those calculated from the chemistry of the materials, analysed using solution ^{1}H NMR

data. The packing model with the closest match to the experimental results from NMR analysis is assumed to be that in the spherical structures. Values of the domain radius obtained experimentally from SAXS data were calculated using a Fortran computer program[1] based on the domain spacing values obtained from the scattering curves.

Table 4.2i Spherical morphology network cubic structure analysis (pt.2)

	Volume Fraction from X-ray data		**Spherical fractions obtained from ^{1}H NMR analysis**		**Theoretical Volume Fractions**	
Network	**BCC**	**FCC**	**Volume**	**Weight**	**BCC**	**FCC**
NS1	0.126	0.137	0.205	0.18	0.137	0.150
NS2	0.124	0.135	0.134	0.12	0.120	0.131
NS3	0.129	0.140	0.162	0.14	0.129	0.140
NS4	0.127	0.139	0.147	0.13	0.122	0.134
NS5	0.129	0.141	0.199	0.17	0.138	0.150
NS6	0.126	0.138	0.143	0.13	0.118	0.128
NS7	0.126	0.137	0.152	0.13	0.122	0.133

Experimental results obtained in the analysis indicate a cubic packing form that is nearer to face centred cubic than body centred, but neither conclusively predict a definite packing form. Volume fraction values obtained from solution state ^{1}H NMR analysis are higher in some of the cases presented in table 4.2i, indicating that neither packing model (BCC or FCC) is suitable for the network structures analysed. The fact that domain radius values have to be predicted from the 1st order scattering maximum as opposed to being identified from the trace itself introduces error in the accuracy of the predictions.

Scattering from the network systems is not conclusive in the identification of the packing form in the systems and indicates possible FCC or BCC formation. Results describing the lattice peak ratios (tables 4.2g-h) suggest that packing is body centred

cubic rather than face centred cubic, but there is difficulty in giving any definite answer due to the wide spread of results for the Bragg peak ratios in the network systems. Network cross-linking has disrupted the identification of long-range order peaks that describe the crystal structure of the spherical morphology systems. Therefore no full identification of the network structures is possible.

4.3 References

[1] Helfand, E.; Wasserman, Z. R. *Macromolecules* **1978,** *11*, 361

[2] Helfand, E.; Wasserman, Z.R. *Dev. Block Copolym.* **1982,** *1*, 99

[3] Helfand, E. *Acc. Chem. Res.* **1975,** *8*, 295

[4] Helfand, E.; Wasserman, Z.R. *Polym. Eng. Sci.* **1977,** *17*, 535

[5] Helfand, E. *Macromolecules* **1975,** *8*, 552

[6] Helfand, E.; Wasserman, Z.R. *Macromolecules* **1976,** *9*, 879

[7] Haward, R.N. *The Physics of Glassy Polymers, Applied Science Polymers, London.* **1973**

[8] de Gennes, P.G. *J. Phys. Lett.* **1979,** *40*, 69

[9] Derouiche, A.; Bettachy, A.; Benhamou, M.; Daoud, M. *Macromolecules* **1992,** *25*, 7188

[10] Briber, R.M.; Bauer, B.J. *Macromolecules* **1988,** *21*, 3296

[11] Jinnai, H.; Hasegawa, H.; Hashimoto, T.; Briber, R.M.; Han, C.C. *Macromolecules* **1993,** *26*, 182

[12] Sakurai, S.; Iwane, K.; Nomura, S. **1993,** *26*, 5479

[13] Urayama, K.; Takigawa, T.; Masuda, T. *Macromolecules* **1993,** *26*, 3092

[14] Li, Y.; Hu, Z.; Li, C. *J. App. Polym. Sci.* **1993,** *50*, 1107

[15] Panyukov, S.; Rubinstein, M. *Macromolecules* **1996,** *29*, 8220

[16] Pakula, T.; Saijo, K.; Kawai, H.; Hashimoto, T. *Macromolecules* **1985,** *18*, 1294

[17] Balta-Calleja, F.J.; Vonk, C.G. *X-ray scattering of synthetic polymers, Elsevier,* **1989**

[18] Jones, J.J.; Burford. R.P. *Polymer International* **1991,** *26*, 163

[19] Inoue, T.; Moritani, M.; Hashimoto, T.; Kawai, H. *Macromolecules* **1971,** *4*, 500

CHAPTER 5

Solid State ^{1}H NMR investigations

5.1 Introduction

Solid state ^{1}H NMR provides a way of investigating the motional characteristics of polymers. It can give information about the motional heterogeneity present in most solid polymer samples, which is of importance in determining physical properties at the macroscopic level. It has the great advantage of requiring no special sample preparation and can be applied to solid polymers in most physical forms. The direct study of the NMR phenomenon of spin diffusion can yield valuable information about spatial heterogeneity of the block copolymer systems down to the molecular level. Solid state ^{1}H NMR is therefore a valuable tool for studying heterogeneities in heterophase copolymer samples.

Spin diffusion occurs via the energy conserving ('flip-flop') transitions of the homonuclear dipolar interaction. This is schematically described as term B in figure 5.1a.

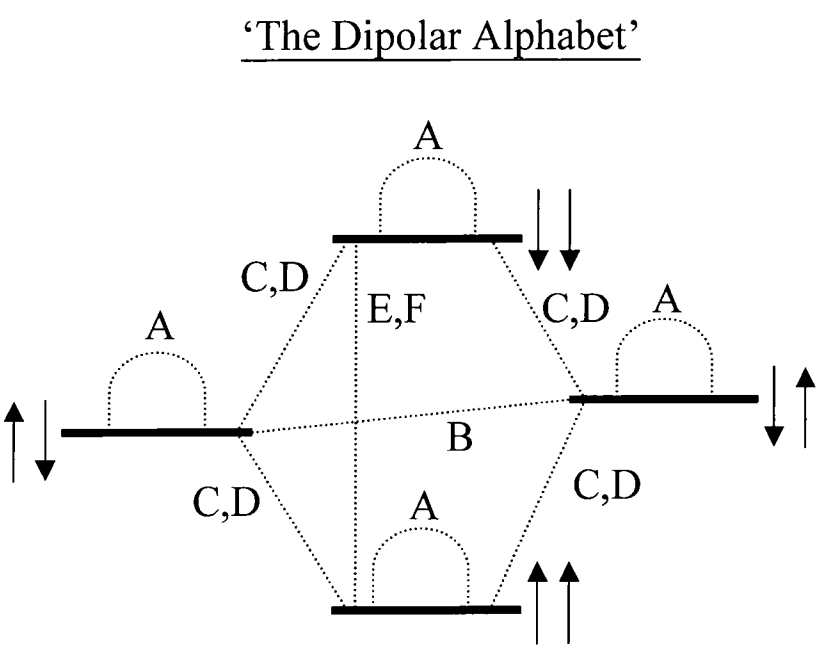

Figure 5.1a 'The dipolar alphabet' from dipolar interaction theory

The important term from dipolar interaction theory is the B term which couples spins of opposite polarisation enabling the exchange of polarisation states ('flip-flop'). Along with the B term the A term is an energy conserving term ('static' or 'secular') which does not change overall polarisation, and represents a field (frequency) shift at the nucleus. The remaining terms ('non-secular') involve a change in the polarisation and therefore are not energy conserving. They are only 'allowed' in the presence of suitable fluctuations in the magnetic field to compensate for the energy difference. The B term in the interaction is the mechanism by which spin diffusion occurs. If different states of polarisation occur in different parts of the system, the whole of which is strongly coupled by homonuclear dipolar interactions, the 'flip-flop' interaction allows transportation of polarisation from one part of the system to another. This evens out polarisation throughout the system. Spin diffusion coefficients are dependent on homonuclear dipolar coupling and can be calculated from the second moment of the NMR line shape. Spin diffusion can be described by a diffusion equation (5.1a).

$$\frac{dM}{dt} = Wa^2 \frac{d^2M}{dr^2} \qquad \text{eq.5.1a}$$

W is the 'flip-flop' transition probability

a is the inter-nuclear distance

M is the polarisation at position r

Wa^2 is the given the symbol D (spin diffusion coefficient)

In polymers, proton spin diffusion is an effective mechanism for polarisation transport. Therefore in heterogeneous polymers, observation of the evolution of the NMR signal following the creation of a polarisation gradient allows the deduction of spin diffusion behaviour. If the spin diffusion coefficients of the system concerned are known, the

dimensions of the heterogeneities can be deduced (and vice versa). Spin diffusion couples regions in a heterogeneous polymer system such that the observed spin-lattice relaxation behaviour differs from the intrinsic behaviour of the regions.

Goldman and Shen[1] developed a useful experiment that yields information about domain sizes in heterogeneous systems by means of spin diffusion. In organic materials spin diffusion is most efficient among protons since they possess a large gyromagnetic ratio and small average separations because of their high isotopic natural abundance. The principle behind the experiment is to observe the effects of spin diffusion directly and quantitatively to deduce the minimum domain dimensions of the system given that the spin diffusion coefficients of the two phases are known. Measurement of the combined spin diffusion and relaxation behaviour was carried out using the Goldman-Shen pulse sequence shown in figure 5.1b.

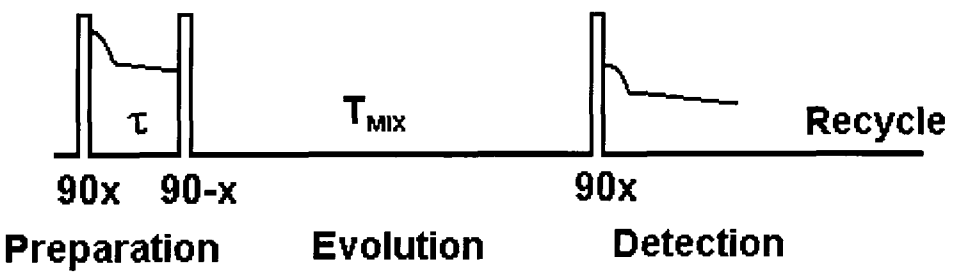

Figure 5.1b Pulse sequence used in the Goldman-Shen experiment

The basic experiment progresses in three phases. The time τ, is chosen, based on the FID analysis results, so that the rapidly decaying FID component decays to zero.

The three steps used in the experiment are described as follows. Firstly, the preparation phase where a spatial magnetisation profile is created based on the heterogeneity during an adequate time, such that $T_{2\,RIGID} < \tau < T_{2\,MOBILE}$. This ensures that the magnetisation

from the mobile region is selected in the preparation phase. The magnetisation in the rigid region will be lost by de-phasing, whilst the magnetisation in the mobile region is hardly affected. The second pulse, applied after time τ, begins an evolution phase (T_{MIX}) in which the magnetisation profile is allowed to evolve towards an equilibrium via spin diffusion, and simultaneously via T_1 relaxation bringing the magnetisation back to the +z direction. The mixing time, where evolution of the magnetisation profile takes place, is therefore under the influence of spin diffusion and T_1 relaxation. The third is a detection phase in which the state of the magnetisation profile is detected and monitored by flipping it from the z-direction back to the xy-plane for acquisition.

Simple analysis of the basic Goldman-Shen experiment only works exactly if spin-lattice relaxation has a negligible effect during the mixing time. A major problem associated with the experiment is that of spin lattice T_1 relaxation, which can change the total amount of magnetisation detected and the relative populations of the regions in a manner similar to spin diffusion effects. To solve this problem a complete analysis of the combined relaxation/spin diffusion behaviour must be done[2].

A useful modification to the basic experiment can be made by alternating the phases of the first 90° pulse in the sequence. The magnetisation is therefore alternately stored in the +z and –z directions during T_{MIX}. Spin lattice relaxation is thus made to affect both response curves in the same direction, whereas spin diffusion affects the magnetisation in opposite directions because of the alteration of the phases during the preparation period. Therefore subtraction of the two values of magnetisation and dividing by 2 should reduce the T_1 effect. This has been the basis of an experiment used by Spiess *et al*[3,4] in which T_1 effects are supposedly eliminated by suitable manipulation of the magnetisation. The experiment tends to eliminate bulk changes in the magnetisation due

to the T_1 process, but not the tendency of T_1 processes that flatten out the magnetisation profile in a manner that resembles the action of spin diffusion, Thereby replacing a known distortion of the data with an unknown one.

The modified Goldman-Shen experiment used in this project is based on a direct observation of the ^1H NMR signal from a static sample.

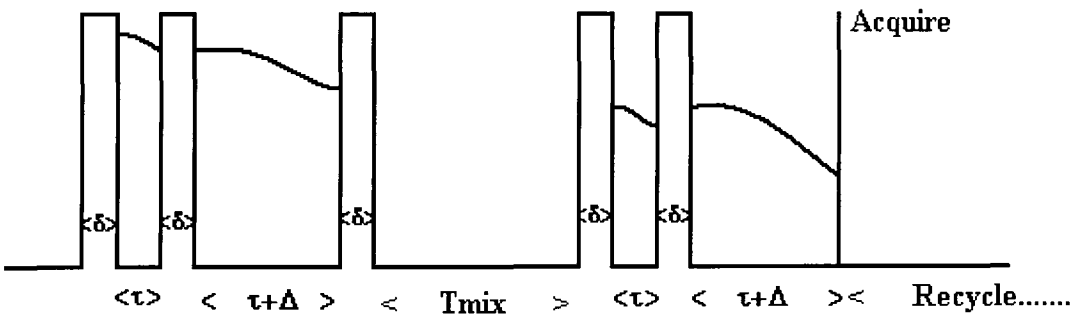

Figure 5.1c Pulse sequence used in the modified Goldman-Shen experiment

By observing the rate at which magnetisation is transported by spin diffusion from one region to another in a heterogeneous sample a characteristic time for diffusion can be obtained. This is proportional to l^2/d (where l is related to the repeat length and D is the spin diffusion coefficient). The pulses are of equal duration, δ, and correspond to 90° flip angles. The initial pulse then alternates using a 180° phase shift on the first pulse which provides storage in the +z and –z directions on alternate passes. A complex data point pair is acquired at the indicated point for each value of T_{MIX}. An important criteria for carrying out the experiment is that the signal at very short mixing times ($T_{MIX} \rightarrow 0$) should have as near as possible the same modulus of amplitude regardless of whether the magnetisation was stored along +z or –z during the mixing time. The use of solid echo pulses in both the preparation and detection phases was found to be important in this respect and helps to eliminate effects due to pulse imperfections.

In contrast to scattering techniques, solid state ^{1}H NMR does not rely on periodic structures in the sample. Therefore it is possible to deduce the domain spacing values in lamellae, cylinders and spherical heterophase systems using this technique. The numerical model used in the analysis has evolved from that described by Packer *et al*[5,6] and is based on numerical solution of the combined relaxation/diffusion equation. A two domain system consisting of a rigid phase of type A into a matrix of type B behaves with polarisation $P_{(r,t)}$ at position r at time t is described by equation 5.1b.

$$H_i\left(\frac{dP_{r,t}}{dt}\right) = r^{-q}\,\frac{d}{dx}\left(r^q D_i H_i \frac{dP_{r,t}}{dr}\right) + \left(P_e - P_{r,t}\right) R_i H_i$$

Spin-Diffusion Relaxation eq.5.1b

$P_{r,t}$ is the polarisation per spin at position r at time t

P_e is the thermal equilibrium value of polarisation per spin

D_i is the spin-diffusion coefficient in region i

R_i is the intrinsic relaxation rate in region i (the reciprocal of the intrinsic relaxation time)

H_i is the relative proton density of region i

q is an integer describing the morphology (0=lamellar, 1=cylindrical, 2=spherical)

Equation 5.1b is directly analogous to the equations for mass transport and heat transport. The method used to analyse the results is based on simulating the data by iterative optimisation of a numerical model. The model used is for a regular two-region system (lamellar, cylindrical or spherical morphology) in which each region is considered homogeneous. The behaviour is considered along a line from the centre of region A to the centre of region B. The equation is solved numerically subject to

suitable boundary conditions with a computer program which uses the Numerical Algorithms Group (NAG) FORTRAN Library subroutine D03PBF as its core[7]. In the computer program the magnetisation of each region is defined by a number of mesh points, plus one mesh point at the contact of two regions. Integration over these mesh points gives the observed magnetisation.

The numerical model consists of a series of cells along the direction of diffusion (i.e. perpendicular to the boundaries in the sample). Polarisation in a cell can change by spin diffusion from a neighbouring cell, spin diffusion to a neighbouring cell and relaxation to the lattice. This is described schematically in figure 5.1d.

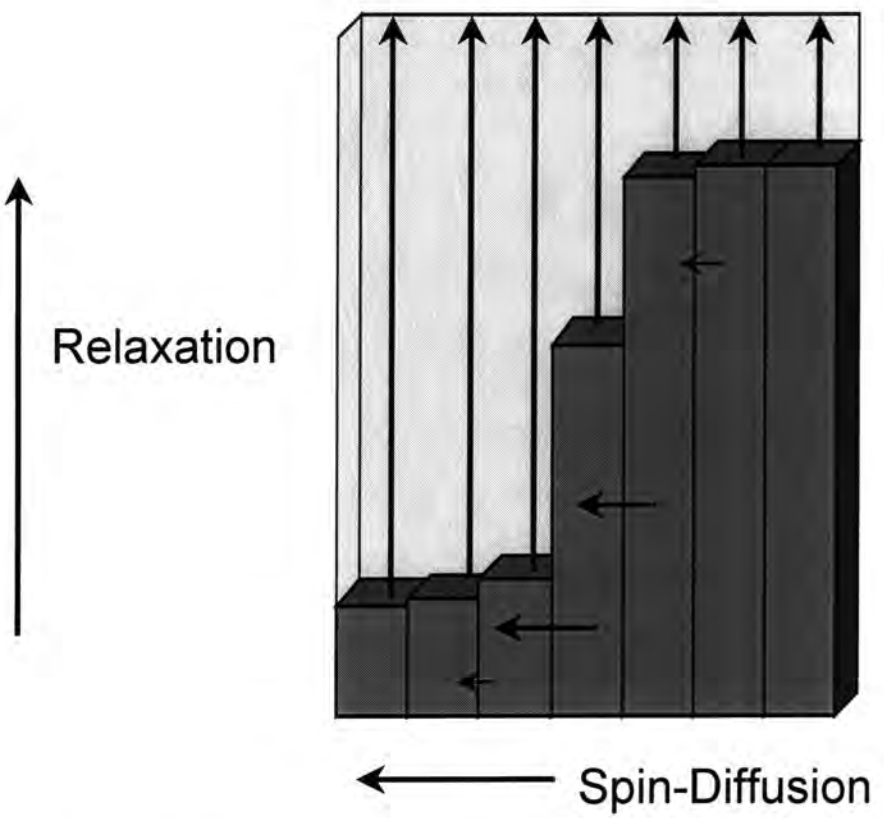

Figure 5.1d Schematic representation of relaxation and spin diffusion

At any instant the rate of spin-lattice relaxation is the sum over all cells of the relaxation rate constant for the cell times displacement from equilibrium. Spin diffusion present only redistributes the magnetisation between cells.

Information from complimentary experiments is used to derive good initial estimates for the variable parameters and, if necessary, to reduce the number of variable parameters used. Analysis of the Free Induction Decay (FID) shape provides information on the proportions of rigid-R (polystyrene) and mobile-M (polybutadiene) material in the copolymer system. The 'solid-echo' sequence in the modified Goldman-Shen experiment is used to overcome the problem of dead time. Figure 5.1e is a schematic that shows a typical 2-D FID analysis from the BSB copolymer systems.

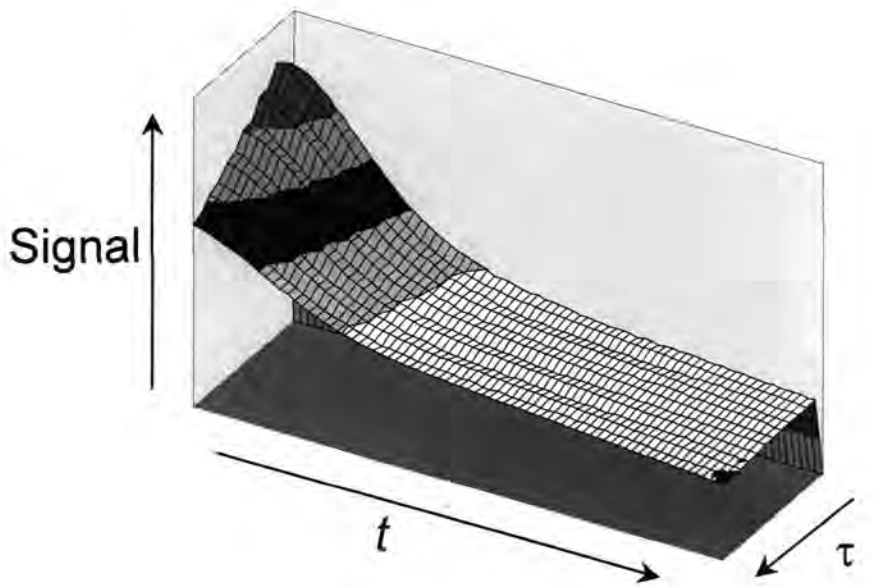

Figure 5.1e 2-Dimensional FID analysis of a block copolymer

It is known that the FID signal of the rigid component follows a Gaussian decay, while the mobile region follows a Weibullian function. Both components show a Gaussian decay as a function of the solid echo delay, τ. The measurements were carried out as a

function of τ, and the entire data set was analysed by a least squares optimisation[8] of equation 5.1b.

Equation 5.1b

$$S(\tau,t) = S_R(0,0)\exp-\left(\frac{2\left(\tau+\delta/2\right)}{T_{eR}}\right)^2 \exp-\left(\frac{t}{T_{2R}}\right)^2 + S_M(0,0)\exp-\left(\frac{2\left(\tau+\delta/2\right)}{T_{eM}}\right)^2 \exp-\left(\frac{t}{T_{2M}}\right)^n$$

Gaussian Weibullian

$S_{(\tau,t)}$ is the measured signal

S_Z (0,0) is the intrinsic signal due to region Z

T_{eZ} is the time constant for the decay of the "solid-echo" for region Z

T_{2Z} is the time constant for the FID

n is the Weibullian exponent

δ is the pulse duration

Values calculated for the ^1H populations of the two regions at τ=0 were taken as true ones, and were found to be in agreement with values derived from analysis of the solution state ^1H NMR spectra. Values for the bulk density of each component were taken from the literature[9] taking into account the microstructure of the polybutadiene. Therefore using the molecular formulae it is possible to calculate the ^1H density in each region (g ^1H cm^{-3}), and the volume proportions of the two regions. For a lamellar morphology the volume proportions translate directly into a length ratio for the two regions in the repeat unit, and reduces the number of unknown parameters for lengths in the system.

The instantaneous rate of change of magnetisation for the whole sample depends on the distribution of magnetisation and the intrinsic relaxation rates. Therefore the observed initial rate of change following inversion of the equilibrium magnetisation (i.e. the population-weighted rate average (PWRA) of the observed components) must be equal to the PWRA of the intrinsic components (same initial slope). Data analysis of the observed T_1 values was carried out using an iterative optimisation.

Knowledge of the PWRA reduces the number of unknown parameters in the relaxation/diffusion equation by one. Therefore for a given intrinsic relaxation rate for the mobile region, and knowing the populations of the rigid and mobile regions from FID analysis, the intrinsic relaxation rate of the rigid region can be calculated. The instantaneous rate of change of magnetisation depends not only on the displacement of the total magnetisation from its equilibrium value but also on the distribution of polarisation within the two-region system. Therefore the measured T_1 cannot be considered a good parameter of the system while the distribution of polarisation is non-uniform. This is why T_1 compensation schemes only work properly in Goldman-Shen type experiments at times longer than the characteristic spin diffusion time.

5.2 Data Analysis

Data resulting from the storage of magnetisation in the +z and –z directions was treated as a single data set for which the model was optimised. Data were analysed using a seven-parameter fit. The number of variable parameters was reduced on the basis of complementary measurements (FID and T_1 measurement and analysis), the actual variable parameters used were:

1. The intrinsic T_1 of the mobile region

2. The overall repeat length, d, of the model

3. The signal amplitude at thermal equilibrium

4. "T_2 up" – a parameter relating the observed signal at the end of the dephasing delay, Δ, to the signal amplitude at thermal equilibrium for magnetisation stored in the +z direction

5. Attenuation ratio - the ratio of the observed signal at the end of the dephasing delay, Δ, for magnetisation stored in the -z direction to that stored in the +z direction, this is initially set to unity

6. The population-weighted rate average (PWRA)

7. Fraction of the total signal due to the mobile component

Figure 5.2a shows how the experiment is used to estimate parameters directly from the data and other parameters from complimentary measurements.

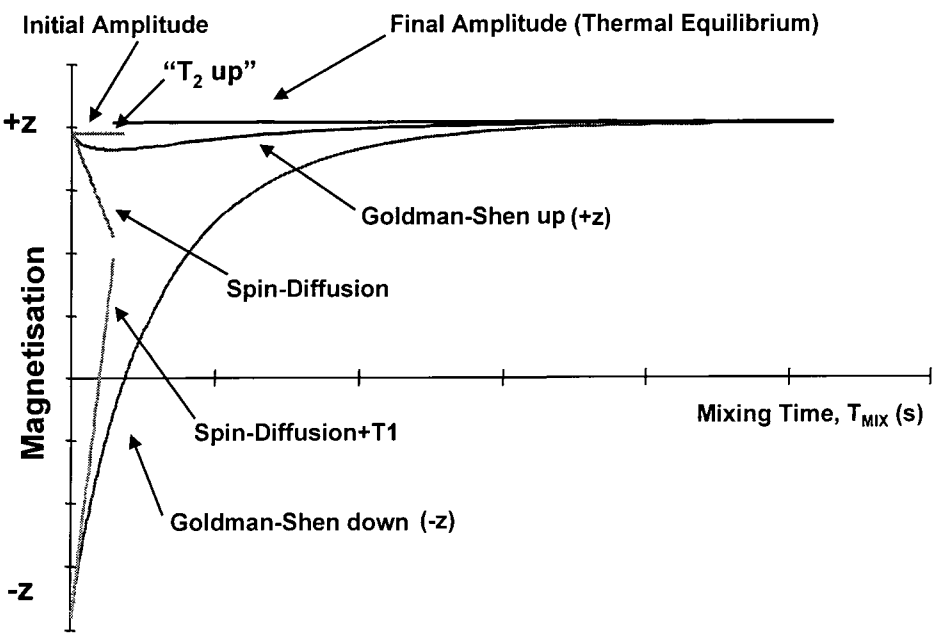

Figure 5.2a Schematic diagram showing the behaviour of the magnetisation arising from the modified Goldman-Shen experiment with initial estimates of parameters used in the fitting procedure

The method is used to derive spin diffusion coefficient values of the polymers when the samples domain spacing values, d, have been characterised using small angle x-ray scattering (SAXS). Otherwise values for the spin diffusion coefficients taken for example from the literature[3,4], could be used to determine domain spacings from the NMR analysis. Proportions of the rigid and mobile sections of the polymers were obtained from the free induction decay (FID) analysis and the PWRA of the intrinsic T_1 values are taken from observed T_1 data. The remaining parameters are derived directly from the analysis shown in figure 5.2a. Initial estimates of the variable parameters were derived as follows.

The mean of the last data points in the +z and –z directions was taken as the estimate for thermal equilibrium. The estimate for "T_2 up" was derived from the ratio of the first data point stored in the +z direction to the last data point (thermal equilibrium). Since the data for magnetisation stored in the +z direction starts off close to thermal equilibrium, effects due to T_1 relaxation will be small for short mixing times and the initial rate of change for this data will be due to spin diffusion. The initial rate of magnetisation transfer due to spin-diffusion can be used to derive an estimate of the overall repeat length, d, of the system[10] according to equation 5.2a.

$$d = \sqrt{20.3\, D\, T_{MIX}} \qquad \text{eq.5.2a}$$

D is the effective spin diffusion coefficient

T_{MIX} is the time taken to reach magnetisation level appropriate to full mixing

For the magnetisation stored in the –z direction, the initial rate of change as a function of mixing time (T_{MIX}) will have significant contributions from both spin diffusion and

the intrinsic T_1 of the mobile region, and hence an estimate of the intrinsic T_1 can be derived. The raw data from the Goldman-Shen experiment together with the behaviour predicted by the relaxation/diffusion model optimised using the seven parameter fit (plot A) are shown in figure 5.2b together with plots of the residuals (the difference between the model and the data – plot B).

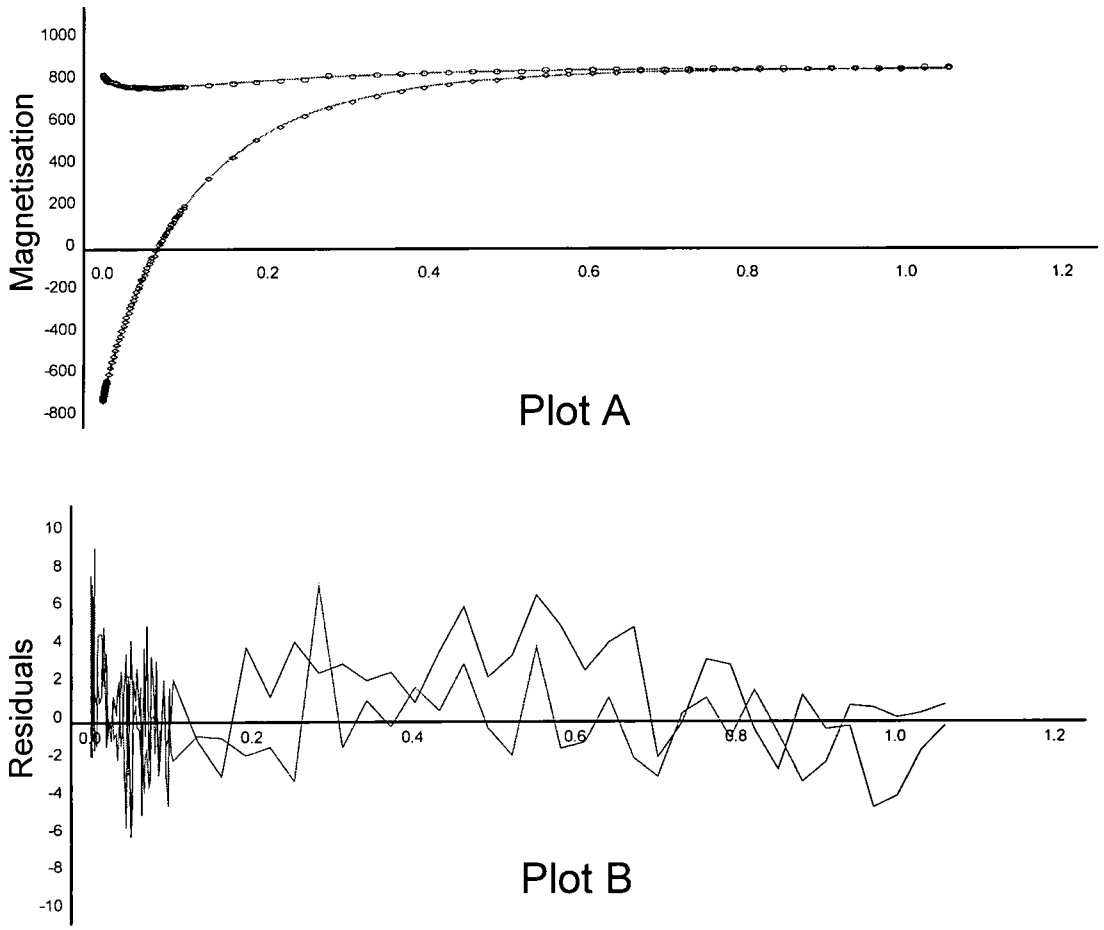

Figure 5.2b Comparison of the predicted behaviour from the optimised numerical model (7-Parameter fit) with the data from the Goldman-Shen experiment described in the text

The upper plot shows data from the Goldman-Shen experiment (circles) together with the predicted behaviour from the relaxation/diffusion model (solid line) optimised using seven variable parameters. The lower plot shows the corresponding residuals at a vertical scale expansion of 100 times. It can be seen that the model represents the data

well over the entire data set, even when population transfer due to spin diffusion is active over a time-scale that is comparable to T_1. The sum of squares of the deviations (SDSQ) after fitting was about the same as that measured for the imaginary signal component after phasing, which indicates that the residuals are due solely to the noise on the data. From the data fit it is now possible to measure the time taken for magnetisation transport across the repeat length of the block copolymer to derive a domain spacing value if the spin diffusion coefficients are known.

Figure 5.2c shows a visualisation for the overall relaxation/spin diffusion behaviour for one of the systems analysed.

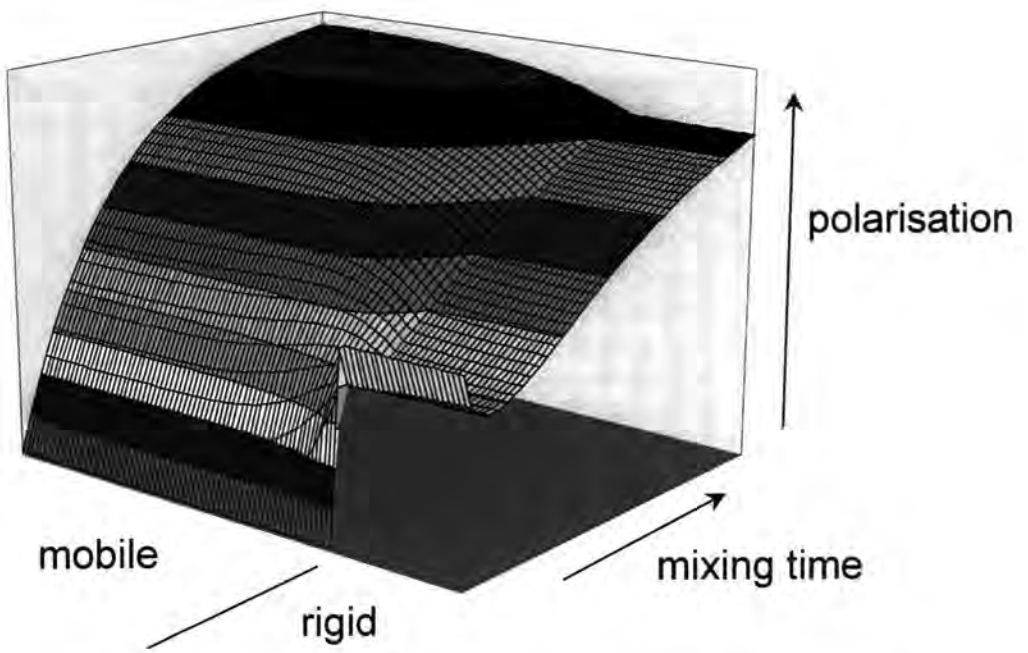

Figure 5.2c Relaxation/Spin diffusion picture for PS/PB lamella system

The surface shows the evolution of polarisation as a function of mixing time (T_{MIX}) over the domain spacing used in the model (centre of rigid region to centre of mobile region) for storage in the –z direction. Initial loss of polarisation from the mobile region due to spin diffusion coupled with the abrupt change in polarisation gradient at the phase

boundary are due to the large difference in spin diffusion coefficients of the two regions.

5.3 Results

A summary of the results from data obtained using the seven-parameter fit compared to the optimised numerical model for copolymer LL1 are given in table 5.3a. Tables of data for the remaining lamella copolymer samples are shown in appendix 4 of the thesis.

Table 5.3a Results of the solid state ^{1}H NMR experiment for copolymer LL2

	Origin	**Results**
^{1}H density ratio Styrene : Butadiene	Literature	0.884
SD coefficient Styrene (m^2/s)	Literature	8.00e-16
SD coefficient Butadiene (m^2/s)	Literature	2.00e-16
Amplitude (a.u.)	Fitted	1160
Repeat Length (d/Å)	Fitted	250
Mobile T_1 (s)	Fitted	0.118
Mobile T_2 (ms)	Fitted	760
1/PWRA (s)	Fitted	0.171
Fraction Mobile	Fitted	0.636
Length of rigid (Å)	Derived	98
Length of mobile (Å)	Derived	152
Rigid T_1 (s)	Derived	0.86

Results obtained provide a complete description of relaxation/diffusion behaviour of the system along with information on the intrinsic T_1 relaxation behaviour of each region. Simulations from the analysis have shown that optimisation yields quite accurate results for the T_1 of the faster relaxing intrinsic component, with any inaccuracy showing in the slower relaxing intrinsic T_1. Therefore the values obtained for the faster relaxing intrinsic T_1 components can be regarded as a good approximation, while the values obtained for the slower relaxing intrinsic T_1 should be regarded more cautiously.

A good value for the spin diffusion coefficient in the rigid region ($\approx 8\times10^{-16} m^2 s^{-1}$) is relatively easy to obtain from the analysis (calculations and measurements by Spiess *et*

al[3,4]). Whilst a value for the spin diffusion coefficient in the mobile region is more of a problem. A suprisingly high value for similar polymers based on the proton linewidth has previously been obtained by Spiess *et al*[3,4]. So if we analyse the data obtained in this study using D_{MOBILE} (mobile spin diffusion coefficient) from Spiess *et al*, distances for the domain spacing in the copolymer are too small by about a factor of two as compared with results from synchrotron SAXS results. Conversly, if a value for the domain spacing derived from synchrotron SAXS measurements, and we analyse the proton NMR data to obtain a value for the D_{MOBILE}, an apparent value of $\approx 2\times10^{-16} m^2 s^{-1}$ is derived which is about a factor of four higher than reported by Spiess *et al*[3,4]. The same value for D_{MOBILE} has been obtained from measurements on other well characterised copolymer samples (e.g. TR41-1649) for which SAXS and Transmission Electron Microscopy (TEM) analysis has been done[11].

The high value obtained for D_{MOBILE} is probably due to a major contribution from bulk self-diffusion of the polymer chains in the mobile region. Bulk diffusion coefficient values have been produced from pulsed field gradient (PFG) NMR measurements on polymers that are well above the T_g value, and have shown to produce a value for the self-diffusion coefficient that could contribute to the measured 'spin diffusion' coefficient[12]. Therefore the observed diffusion behaviour is due to a combination of bulk diffusion and spin diffusion, where spin diffusion is the spatial transport of magnetisation via the 'flip-flop' regime and bulk diffusion is the spatial transport of magnetisation via polymer chain reptation.

The probable reason for the difference between D_{MOBILE} found in this project and D_{MOBILE} from Spiess *et al* measurements is because the experiments carried out by Spiess used Magic Angle Spinning (MAS) which tends to reduce the 'flip-flop'

contribution to the spin diffusion term. MAS is used in high resolution solid state ^{13}C detection, and apparent spin diffusion coefficient values are reduced due to narrowing of the ^{1}H line. The measurements carried out in this project were made with the polymer sample in a static state.

If a value of $2\times10^{-16}m^2s^{-1}$ is taken for D_{MOBILE} and we then fit all the data for the lamellar annealed copolymer samples to obtain values for the domain spacing, d, results are in reasonable agreement with theoretical predictions and the SAXS measurements. Table 5.3b and figure 5.3a presents a comparison of domain spacing results from NMR and SAXS techniques (average values), with theoretical repeat distances obtained using a computer program written by Helfand and Wasserman[13].

Table 5.3b Summary of the domain spacing results obtained from solid state NMR

BSB Copolymer	Molecular Weight (K)	Solid State ^{1}H NMR d (Å)	Kratky SAXS d (Å)	Synchrotron SAXS D (Å)	Theoretical d (Å)
LL1	40	214	280	254	200
LL2	60	250	340	275	270
LL3	100	451	380	302	390
LL4	150	548	520	428	490
LL5	250	546	680	605	620

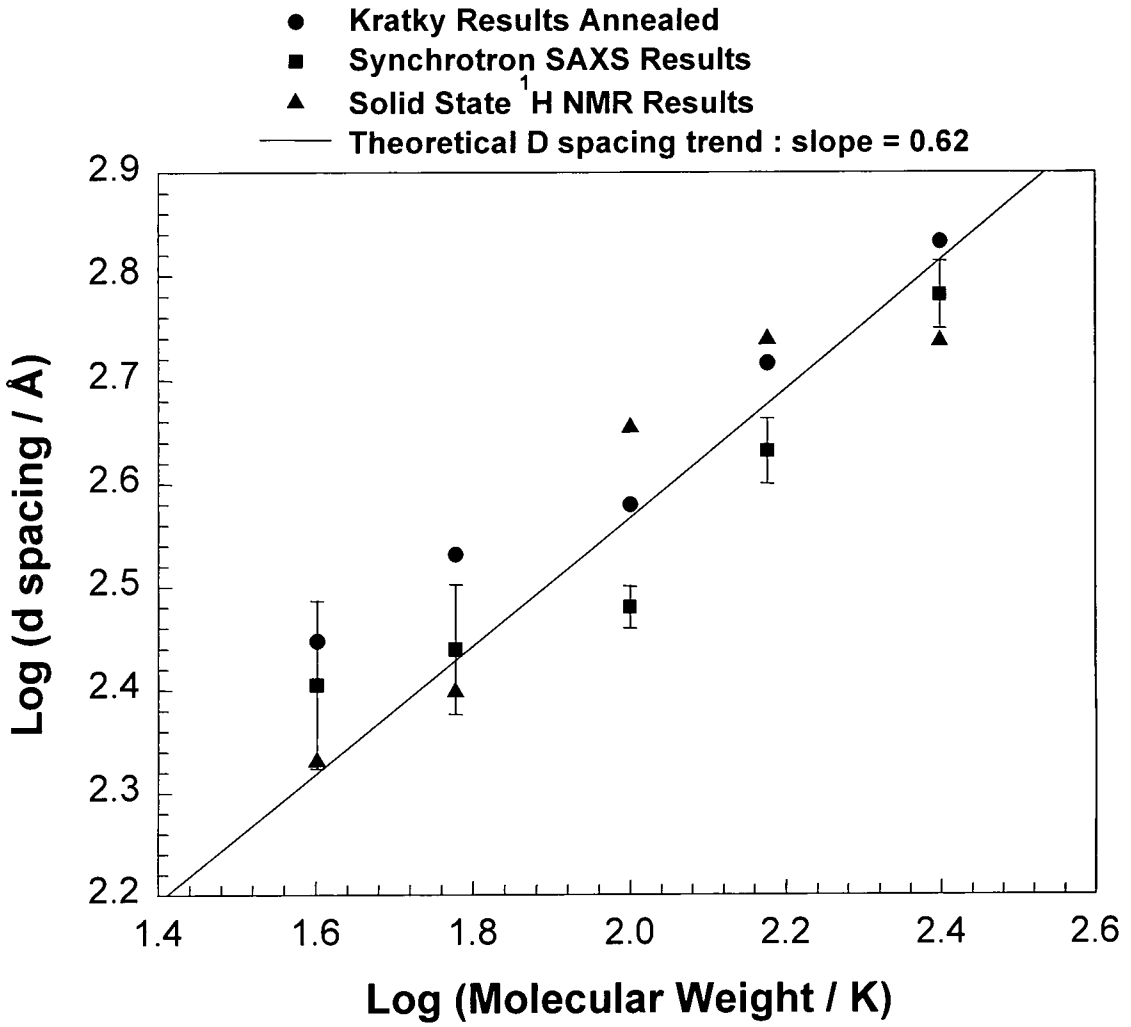

Figure 5.3a Comparison of solid state NMR data with SAXS analysis and theory

5.4 Conclusions

The investigation has shown that by using a set of relatively simple ^{1}H NMR measurements including the Goldman-Shen experiment, it is possible to produce a numerical model of a heterogeneous polymer system which can be optimised by varying a small number of parameters to fully represent the combined spin-diffusion and relaxation behaviour of the system. The method provides values for the region lengths (domain spacings) and for the intrinsic relaxation behaviour of BSB triblock copolymer systems. The results obtained display a high value for the apparent spin diffusion coefficient in the mobile region. We believe that the reason for this is that bulk self-diffusion of the polymer chain is a major contributing factor.

Direct ^{1}H detection gives high sensitivity, leading to a high signal to noise ratio (S/N) and comparatively short measurement times. Spectrometer requirements are relatively low-technological using only single channel and static sample analysis. Derivations made of the initial estimates directly from the raw data makes the technique suitable for routine use.

5.5 References

[1] Goldman, M.; Shen, L. *Phys. Rev.* **1966,** *144*, 321

[2] Kenwright, A.M.; Say, B.J. *Solid State Nuclear Magnetic Resonance* **1996,** *7*, 85

[3] Spiess, H.W.; Schmidt-Rohr, K.; Clauss, J. *Acta Polymer.* **1993,** *44*, 1

[4] Spiegel, S.; Schmidt-Rohr, K.; Boeffel, C.; Spiess, H.W. *Polymer* **1993,** *34*, 4567

[5] Packer, K.J.; Pope, J.M.; Yeung, R.R.; Cudby, M.E.A. *J. Polym. Sci., Polym. Phys. Ed.* **1984,** *22*, 589

[6] Kenwright, A.M.; Packer, K.J.; Say, B.J. *J. Magn. Res.* **1986,** *69*, 426

[7] Friebel, S.; Harris, R.K.; Kenwright, A.M. *Magnetic Resonance in Chemistry* **1997,** *35*, 290

[8] Kenwright, A.M.; Say, B.J. in Ibbet, R.B. (Ed.) *NMR Spectroscopy of polymers, Blackie, Glasgow* **1993** (and references therein)

[9] Brandrup, J.; Immergut, E.H. (Eds.) *Polymer Handbook, Wiley, Chichester,* **1974**

[10] Schmidt-Rohr, K.; Spiess, H.W. *Multidimensional Solid-State NMR and Polymers, Academic Press, London,* **1994**

[11] Hashimoto, T.; Fujimura, K.; Saijo, K.; Kawai, H.; Diamant, J.; Shen, M. *Advanced Chemical Series* **1979,** *176*, 257

[12] Griffiths, P.C.; Cosgrove, T.; Hollingshurst, J.; Richards, R.D.C.; Semlyen, J.A.; *Macromolecules* **1992,** *25*, 6761

[13] Helfand, E.; Wasserman, Z. R. *Macromolecules* **1978,** *11*, 361

CHAPTER 6

Discussion

6.1 Summaries and Conclusions

BSB copolymer networks with lamellar and spherical morphology and their analogous uncross-linked triblock materials have been prepared by anionic polymerisation of styrene and butadiene using an organolithium difunctional initiator. Cross-linking of the living polymerisation then proceeded by addition of a dilute solution of tetraethoxysilane in benzene. Both lamella and spherical morphology networks were found to contain a sol fraction of between 3-10%. These networks were characterised and analysed using a variety of techniques. Solution state ^{1}H NMR, size exclusion chromatography and differential scanning calorimetry were used to study the composition, molecular weight properties and glass transitions respectively of the linear copolymers and networks synthesised. It was found that polymers and network precursors possessed molecular weights and polydispersities were within the range expected from the criteria set when the synthesis of the materials was carried out.

Network mechanical properties were determined using stress-strain and swelling measurements on the materials. Stress-strain experiments were carried out at room temperature and at 393K. Room temperature analysis yielded unexpectedly low values for the molecular weight between cross-links ($\overline{M}_c$) of the networks. This is due to the glassy component (polystyrene) of the network distorting rubber-like elastomeric behaviour. Force-extension measurements performed at 393K made sure that both copolymer constituents were above their respective glass transition temperatures. The Mooney-Rivlin and Ball-Edwards models were used to fit the experimental force-elongation data to enable the calculation of network $\overline{M}_c$.

It has been shown that the Ball-Edwards slip-link model produces $\overline{M}_c$ values that are close to the molecular weight of the network precursor polymers. Swelling data and

Mooney-Rivlin stress-strain analysis yielded $\overline{M}_c$ values that departed from model network trends because they do not account for imperfections such as physical entanglements, loops and dangling chain ends. The Ball-Edwards model takes these parameters in to account when fitting the data to a theoretical function, producing values for chemical cross-link density, physical entanglement density and a parameter (η) describing the overall looseness of each network sample. Therefore the conclusion that the Ball-Edwards treatment is the most comprehensive method of network analysis can be made. Results from this section of the thesis evaluate structural changes in all the networks analysed whilst the samples possess rubber-elastic character at 393K.

Morphological properties of the uncross-linked copolymer systems, studied using small angle x-ray scattering (SAXS), yielded domain spacing values that were to be expected from theoretical predictions. Domain spacing values for each copolymer were comparable for different sample preparations of each film, and results from synchrotron SAXS traces compare favourably to Kratky camera data obtained. Bragg peak ratios determined from scattering traces of the materials with a 50:50 (PS/PB) composition give results that indicate predominantly a lamellar morphology. However, it was not possible to confirm the spherical packing morphology of the uncross-linked materials with a 15:85 (PS/PB) composition due to the poor experimental scattering traces obtained.

Morphological properties of the PS/PB cross-linked materials with a 50:50 composition showed the existence of phase separation within each material analysed. However, further subsidiary Bragg peaks were not observed indicating that long range order in the materials had been disrupted due to the presence of cross-links, limiting the formation of periodic domain structure. Domain spacing values obtained for each material varied

above and below theoretical predictions for each network system, indicating further structural disruption due to the cross-linking process. It is apparent that there is an increase in the domain spacing values as the cross-link density in each system is decreased, indicating that larger domain sizes are allowed to form as the cross-link density is lowered.

Stretching the lamellar morphology network systems at room temperature enabled the investigation of microstructure behaviour as samples were deformed in a uniaxial manner. Scattering traces from the materials in the direction parallel to that of stretching showed that domain spacing values increased with stretching until the sample yielded. After this point very little increase in the domain spacings of the material occurred. Initially domain spacings increased at an affine rate before sample yielding disrupted the microstructure of each system. During uniaxial stretching, the intensity of the 1st order Bragg peak decreased indicating an increase in disorder of the lamellar phases. The scattering curves measured perpendicular to the direction of stretching also decreased in intensity with sample stretching and decreased in domain size as expected. The scattering peak breadth at half height increases as stretching occurs indicating a decrease in lamellar grain size with stretching. After sample yielding the lamellar grains break up and form smaller grains before the system is totally disorders upon further stretching. A comparison of results obtained from Kratky camera and synchrotron data showed good agreement.

Cross-linked systems that possess a PS/PB composition of 15:85 show phase separation indicated by scattering traces that show a periodic two-phase spherical morphology structure. However, the scattered intensity maximum is considerably less than that of

the lamellar morphology systems, indicating a greater amount of disorder in the spherical morphology networks due to distortions of the first and second kind.

However, subsidiary Bragg peaks are visible on a number of the scattering traces indicating the possible formation of a body centred cubic structure. Unfortunately, no single particle form factor scattering was present to enable the calculation of individual domain dimensions of the systems. The domain spacing values of each system increased with molecular weight along the lines of theoretical trends, but only after a correction had been made to some of the values to account for the 1^{st} order Bragg peak being obscured by the beam stop. After correction, the values of domain spacing appear to be slightly higher than theory predicts. The reason for this behaviour maybe due to the influence of the cross-links on the periodic structure increasing the average separation of the phases.

Spherical morphology networks were analysed in both parallel and perpendicular directions to assess the behaviour of the microstructure with uniaxial stretching at room temperature. Scattering traces measured parallel to the direction of stretch, decrease in intensity at a monotonic rate with sample extension indicating increased disorder. Domain spacing values increase until sample yielding limits the observation of a definite Bragg peak. Scattering traces measured in the perpendicular direction also decrease in intensity as stretching occurs, indicating disorder in the microstructure. Domain spacing values decrease in this direction indicating sample compression. As stretching proceeds, long-range structural order ceases to exist indicated by the disappearance of subsidiary Bragg peaks on the scattering traces. Therefore no long-range cubic structures form as uniaxial stretching proceeds. The results obtained from synchrotron SAXS experiments were in reasonable agreement with data obtained from

the Kratky camera. SAXS data on both lamellar and spherical morphology systems has yielded important information with regards to sample morphology and microstructure during uniaxial deformation.

Solid state ^{1}H NMR investigations on lamellar copolymer systems have produced a set of results that indicate domain spacing values that are reasonably close to those obtained from SAXS techniques and theoretical predictions. Using the Goldman-Shen experiment, a numerical model of a heterogeneous polymer system has been optimised by varying seven parameters, to represent the combined spin-diffusion and relaxation behaviour of the system. Preliminary analysis on the lamellar morphology network systems has been carried out, and with further work, could be a good comparison to SAXS data. Networks analysed using SAXS techniques appear to possess morphologies with lamellar stacks sectioned in to grains, with orientations of the grains in all directions. However, the model used to determine the domain spacings in the NMR experiments is based on the classic lamellar model. Therefore, a comparison of domain spacing values from SAXS and NMR results for these systems would be an interesting experiment to carry out.

It has not been possible to calculate the domain spacing values of the spherical morphology materials because of the difficulty in analysing the spin diffusion from the rigid to mobile regions of the heterophase system. This is because the rigid phase has a volume fraction of 0.15, which is not sufficient to observe the effect of spin diffusion accurately between the two phases.

During the course of the project, most of the copolymer and network characteristics investigated have been assigned using the techniques of stress-strain analysis, SAXS,

and solid state ^{1}H NMR. A series of novel triblock copolymer networks have been synthesised, characterised and analysed, possessing properties that display equilibrium morphologies dictated by the cross-linking process of the precursor copolymers in solution. Networks that are synthesised from low molecular weight precursor polymers (25-40K) appear to cross-link most efficiently, possessing mechanical properties that would be most desirable for industrial application. As the network systems are stretched, the morphology of the system appears to be destroyed when sample yielding takes place. Domain spacing values for static network systems have been characterised using two SAXS techniques and solid state ^{1}H NMR. The values obtained are comparable with theoretical predictions.

6.2 Suggestions for future work

A logical continuation of the investigations carried out in this thesis could include the synthesis of a similar series of networks in which the polystyrene and/or polybutadiene was deuterated. Labelling of this nature could be useful in helping to determine some of the physical dimensions, e.g. radius of gyration (R_g) of the networks using techniques such as small angle neutron scattering (SANS). Network structures analysed could determine how cross-linking has affected the microphase separated structure. It would also be advantageous to determine how for example, the radius of gyration varied as the network structure is uniaxially deformed in order to pursue knowledge of network deformation upon stretching. Comparisons of chain statistics could be made between analogous uncross-linked systems.

The investigation of B-S-B network materials that possess deuterated or partially deuterated polybutadiene chains, using deuterium solid state NMR could investigate the relaxation dynamics of polybutadiene chains. The behaviour of the chains near the

junction cross-links could be compared to the behaviour in the middle of the polymer chains between the junction points. It is expected that chain relaxation proceeds most rapidly at chain sections furthest from the cross-link junctions, due to the constrained nature of the polymer in regions adjacent to cross-links constricting chain movement. Comparisons of relaxation behaviour could be made to analogous uncross-linked systems.

Further development of the solid state ^{1}H NMR technique could enhance the work carried out on the lamellar morphology B-S-B network systems. A comparison of domain spacing values with SAXS data would clarify the accuracy of any results that would be obtained. The development of the experiment has only been recent and therefore needs further attention to yield explanations for the complete diffusion behaviour within these heterophase systems.

Appendices

Appendix 1

Lamella network synchrotron scattering with uniaxial extension

Table 1. Network sample NL1 unannealed and annealed

Frame	Extension		Annealed (d/Å)		Unannealed (d/Å)	
	mm	ratio	Parallel	Perpendicular	Parallel	Perpendicular
0	0.00	1.00	228	213	240	195
1	1.66	1.17	237	211	250	195
2	3.33	1.33	237	200	270	195
3	5.00	1.50	250	193	300	190
4	6.66	1.66	258	191	300	190
5	8.33	1.83	288	187	300	190
6	10.00	2.00	310	183	315	190
7	11.66	2.17	330	180	315	190
8	13.33	2.33	330	180	315	190

Table 2. Network sample NL2 unannealed and annealed

Frame	Extension		Annealed (d/Å)		Unannealed (d/Å)	
	mm	ratio	Parallel	Perpendicular	Parallel	Perpendicular
0	0.00	1.00	200	185	223	195
1	1.66	1.17	210	180	226	198
2	3.33	1.33	220	180	258	193
3	5.00	1.50	220	180	280	183
4	6.66	1.66	230	180	280	188
5	8.33	1.83	225	180	307	195
6	10.00	2.00	230	180	303	193
7	11.66	2.17	230	180	305	195
8	13.33	2.33	235	180	305	195

Table 3. Network sample NL3 unannealed and annealed

Frame	Extension		Annealed (d/Å)		Unannealed (d/Å)	
	mm	ratio	Parallel	Perpendicular	Parallel	Perpendicular
0	0.00	1.00	260	250	250	240
1	1.66	1.17	280	235	256	242
2	3.33	1.33	295	210	256	237
3	5.00	1.50	307	210	256	228
4	6.66	1.66	360	210	264	223
5	8.33	1.83	360	210	303	219
6	10.00	2.00	360	210	333	213
7	11.66	2.17	360	210	360	213
8	13.33	2.33	360	210	360	213

Table 4. Network sample NL4 unannealed and annealed

Frame	Extension		Annealed (d/Å)		Unannealed (d/Å)	
	mm	ratio	Parallel	Perpendicular	Parallel	Perpendicular
0	0.00	1.00	240	250	246	250
1	1.66	1.17	291	242	264	240
2	3.33	1.33	349	242	315	242
3	5.00	1.50	370	250	324	250
4	6.66	1.66	370	250	324	250
5	8.33	1.83	370	250	333	250
6	10.00	2.00	370	250	333	250
7	11.66	2.17	370	250	333	240
8	13.33	2.33	370	250	333	240

Table 5. Network sample NL5 unannealed and annealed.

Frame	Extension		Annealed (d/Å)		Unannealed (d/Å)	
	mm	ratio	Parallel	Perpendicular	Parallel	Perpendicular
0	0.00	1.00	237	240	277	259
1	1.66	1.17	240	237	288	253
2	3.33	1.33	245	232	330	232
3	5.00	1.50	242	237	370	228
4	6.66	1.66	242	232	380	245
5	8.33	1.83	242	237	390	237
6	10.00	2.00	242	232	390	240
7	11.66	2.17	242	232	390	240
8	13.33	2.33	242	232	390	240

Table 6. Network sample NL6 unannealed and annealed

Frame	Extension		Annealed (d/Å)		Unannealed (d/Å)	
	mm	ratio	Parallel	Perpendicular	Parallel	Perpendicular
0	0.00	1.00	237	245	290	280
1	1.66	1.17	240	232	320	274
2	3.33	1.33	277	221	354	267
3	5.00	1.50	295	219	383	261
4	6.66	1.66	303	219	390	256
5	8.33	1.83	307	217	397	261
6	10.00	2.00	315	213	411	253
7	11.66	2.17	307	217	426	261
8	13.33	2.33	300	219	426	261

Appendix 2

Spherical network synchrotron scattering with uniaxial extension

Table 1. Network sample NS1 annealed and unannealed

Frame	Extension		Annealed (d/Å)		Unannealed (d/Å)	
	Mm	ratio	Parallel	Perpendicular	Parallel	Perpendicular
0	0.00	1.00	250	250	240	250
1	1.66	1.17	267	250	235	245
2	3.33	1.33	291	245	245	240
3	5.00	1.50	311	237	256	237
4	6.66	1.66	320	230	271	228
5	8.33	1.83	307	225	281	221
6	10.00	2.00	307	225	295	213
7	11.66	2.17	324	219	311	213
8	13.33	2.33	329	213	303	213

Table 2. Network sample NS2 annealed and unannealed

Frame	Extension		Annealed (d/Å)		Unannealed (d/Å)	
	mm	ratio	Parallel	Perpendicular	Parallel	Perpendicular
0	0.00	1.00	250	250	264	265
1	1.66	1.17	277	250	250	253
2	3.33	1.33	259	245	260	261
3	5.00	1.50	280	245	264	277
4	6.66	1.66	291	250	299	271
5	8.33	1.83	303	245	274	277
6	10.00	2.00	288	258	311	261
7	11.66	2.17	284	256	288	250
8	13.33	2.33	300	260	320	250

Table 3. Network sample NS3 annealed and unannealed.

Frame	Extension		Annealed (d/Å)		Unannealed (d/Å)	
	mm	ratio	Parallel	Perpendicular	Parallel	Perpendicular
0	0.00	1.00	360	310	360	307
1	1.66	1.17	349	299	366	307
2	3.33	1.33	377	299	383	307
3	5.00	1.50	377	299	377	307
4	6.66	1.66	372	299	360	307
5	8.33	1.83	383	299	370	307
6	10.00	2.00	390	299	370	307
7	11.66	2.17	390	299	366	307
8	13.33	2.33	390	299	383	307

Table 4. Network sample NS4 annealed and unannealed.

Frame	Extension		Annealed (d/Å)		Unannealed (d/Å)	
	mm	ratio	Parallel	Perpendicular	Parallel	Perpendicular
0	0.00	1.00	200	240	222	240
1	1.66	1.17	200	240	222	237
2	3.33	1.33	232	240	222	237
3	5.00	1.50	221	240	222	237
4	6.66	1.66	223	240	222	237
5	8.33	1.83	227	240	250	237
6	10.00	2.00	250	240	250	237
7	11.66	2.17	250	240	250	237
8	13.33	2.33	250	240	250	237

Table 5. Network sample NS5 unannealed and annealed

Frame	Extension		Annealed (d/Å)		Unannealed (d/Å)	
	mm	ratio	Parallel	Perpendicular	Parallel	Perpendicular
0	0.00	1.00	274	303	284	291
1	1.66	1.17	307	277	307	277
2	3.33	1.33	329	274	320	288
3	5.00	1.50	349	250	333	277
4	6.66	1.66	371	262	365	267
5	8.33	1.83	390	250	377	258
6	10.00	2.00	390	250	349	250
7	11.66	2.17	390	262	360	250
8	13.33	2.33	390	281	350	274

Table 6. Network sample NS6 annealed and unannealed

Frame	Extension		Annealed (d/Å)		Unannealed (d/Å)	
	mm	ratio	Parallel	Perpendicular	Parallel	Perpendicular
0	0.00	1.00	250	295	333	354
1	1.66	1.17	262	295	333	350
2	3.33	1.33	250	299	333	350
3	5.00	1.50	250	295	333	350
4	6.66	1.66	255	299	333	350
5	8.33	1.83	250	295	333	350
6	10.00	2.00	260	295	333	350
7	11.66	2.17	255	299	333	350
8	13.33	2.33	260	295	333	350

Appendix 3

Fortran computer program used to calculate theoretical domain spacings

```
$DEBUG
C     PROGRAM TO DETERMINE DOMAIN SIZE
C     IN A LAMELLAR, CYLINDRICAL OR SPHERICAL
C     BLOCK COPOLYMER SYSTEM
C     SI UNITS
C
      INTEGER BLANK,PA,PB,DIMEN,DOMTYP(4,3),UNIT1(3),UNIT2(3),UNIT3(3)
      REAL RHO(5),BETA(5),XM(5),B(5),MWA,MWB
      INTEGER POLYMR(5)
      DATA AVOGAD/6.02252E23/
      DATA BLANK /1H /,UNIT1/3H(/M,3H(/M,1H /,
     1 UNIT2/3H**2,1H),1H /,UNIT3/1H),2*1H /
      DATA DOMTYP/3H   ,3HLAM,3HELL,3HAR ,3HCYL,3HIND,3HRIC,
     12HAL,3H  S,3HPHE,3HRIC,2HAL/
10    DATA RHO/10100.,13600.,16500.,2*0./,
     1 XM/.10414,.06811,.05409,2*0./,
     1 B/.68E-9,.63E-9,.63E-9,2*0./,
     1 POLYMR/2HPS,2HPI,2HPB,2*1H /
      DATA NPOL/3/
      FUN(X)=-C1+X+X**3*(C3*(C2*X**2+C4)**C5+C7*(C6*X**2+C8)**C9)
C     INPUT SECTION
C     PA AND PB ARE THE NAMES OF THE POLYMER COMPONENTS. A
C     REFERS TO THE ONE WITH CYLINDRICAL OR SPHERICAL DOMAINS
C     DIMEN IS THE DIMENSIONALITY OF THE SYSTEM
C     J INDICATES THE TYPE OF BLOCK COPOLYMER
C     1 = DIBLOCK COPOLYMER.  A CYLINDERS OR SPHERES
C     2 = TRIBLOCK COPOLYMER BAB
C     3 = TRIBLOCK COPOLYMER ABA
C     MWA AND MWB ARE THE MOLECULAR WTS. OF THE A AND B BLOCKS
(KG)
C     T IS THE TEMPERATURE
C     BLANK LINE AS INPUT TERMINATES THE RUN
C
20    WRITE(6,999)
      READ (5,998)PA,PB,DIMEN,J,MWA,MWB,T
      PRINT*,PA,PB,DIMEN,J,MWA,MWB,T
      IF(PA.EQ.BLANK) STOP
      IF(DIMEN.GE.1.AND.DIMEN.LE.3) GO TO 30
      WRITE(6,990)
      GO TO 20
30    IF(J.GE.1.AND.J.LE.3) GO TO 40
      WRITE(6,997)
      GO TO 20
40    IA=0
      IB=0
      DO 50 I=1,NPOL
      IF(PA.EQ.POLYMR(I)) IA=I
```

```
      IF(PB.EQ.POLYMR(I)) IB=I
   50 CONTINUE
      IF(IA.NE.0.AND.IB.NE.0) GO TO 60
      WRITE(6,996) (POLYMR(I),I=1,NPOL)
      GO TO 20
C     PARAMETER ASSIGNMENT AND CALCULATION
   60 ALPHA=-900.+750000./T
      ZA=MWA/XM(IA)
      Z1=ZA
      IF(J.EQ.2) Z1=Z1*.5
      ZB=MWB/XM(IB)
      Z2=ZB
      IF(J.EQ.3) Z2=Z2*.5
      BETA(IA)=SQRT(RHO(IA)/6.)*B(IA)
      BETA(IB)=SQRT(RHO(IB)/6.)*B(IB)
      BETAAV=.5*(BETA(IA)+BETA(IB))
   70 GAMOKT=SQRT(ALPHA)*(BETAAV+(BETA(IA)-BETA(IB))
     1 **2/(12.*BETAAV))
      ZORA=Z1/RHO(IA)
      ZORB=Z2/RHO(IB)
      ZORS=ZORA+ZORB
      RXI=((ZORB/ZORA)+1.)**(1./DIMEN)-1.
      XI=1./RXI
      BTG=AMAX1(BETA(IA),BETA(IB))
      BTS=AMIN1(BETA(IA),BETA(IB))
      Y=(BTS/BTG)**2
      AJ=(BTG/SQRT(ALPHA))*(1.+.4630151*Y+.1077812*Y**2
     1 -(.2452727*Y+.0412496*Y**2)*ALOG(Y))
C     PARAMETERS OF THE DOMAIN FREE ENERGY
      GO TO (80,110,140),DIMEN
   80 IF(J.NE.2) GO TO 90
      ETAA1=.061
      ETAA2=.838
      ETAA3=2.64
      GO TO 100
   90 ETAA1=.0766
      ETAA2=.531
      ETAA3=2.57
      IF(J.NE.3) GO TO 100
      ETAB1=.061
      ETAB2=.838
      ETAB3=2.64
      GO TO 170
  100 ETAB1=.0766
      ETAB2=.531
      ETAB3=2.57
      GO TO 170
  110 IF(J.NE.2) GO TO 120
      ETAA1=.0166
      ETAA2=1.051
      ETAA3=2.86
      GO TO 130
```

```
120  ETAA1=.0274
     ETAA2=.202
     ETAA3=2.605
     IF(J.NE.3) GO TO 130
     ETAB1=.0659+.0357*RXI
     ETAB2=.757-.132*RXI
     IF(ETAB2.LT.0.) ETAB2=0.
     ETAB3=2.59-.147*RXI
     GO TO 170
130  ETAB1=.0792+.0412*RXI
     ETAB2=.539-.206*RXI
     IF(ETAB2.LT.0.) ETAB2=0.
     ETAB3=2.53-.152*RXI
     GO TO 170
140  IF(J.NE.2) GO TO 150
     ETAA1=.00810
     ETAA2=1.07
     ETAA3=2.87
     GO TO 160
150  ETAA1=.0123
     ETAA2=.384
     ETAA3=2.68
     IF(J.NE.3) GO TO 160
     ETAB1=.0705+.0578*RXI
     ETAB2=.596+.599*RXI
     ETAB3=2.55-.132*RXI
     GO TO 170
160  ETAB1=.0852+.0744*RXI
     ETAB2=.348+.220*RXI
     ETAB3=2.48-.123*RXI
170  C1=DIMEN*ZORA*GAMOKT
     C2=6./(B(IA)**2*Z1)
     C3=ETAA1*ETAA3*C2
     C4=ETAA2**2
     C5=ETAA3*.5-1.
     C6=(6./Z2)*(RXI/B(IB))**2
     C7=ETAB1*ETAB3*C6
     C8=ETAB2**2
     C9=ETAB3*.5-1.
C    CALCULATION OF THE FREE ENERGY MINIMUM
     A=C1
     EPS=1:E-15
     AS=.99*A
     FS=FUN(AS)
     F=FUN(A)
180  ANEW=A-F*(A-AS)/(F-FS)
     AS=A
     A=ANEW
     IF(A.NE.AS) GO TO 190
     WRITE(6,995)
     EPS=EPS*10.
     IF(EPS.LE.1.E-8) GO TO 190
```

```
      WRITE(6,994)
      GO TO 20
  190 FS=F
      F=FUN(A)
      IF(ABS(F).GT.EPS) GO TO 180
C     CALCULATION OF SYSTEM'S PROPERTIES
      SIGMA=DIMEN*ZORA/(A*AVOGAD)
      T1=(1.+RXI)**DIMEN
      IF(J.EQ.2) T1=SQRT(T1)
      IF(J.EQ.3) T1=SQRT(T1*(T1-1.))
      F=C1/A+ALOG(A*T1/(DIMEN*AJ))
     1 +ETAA1*(C2*A**2+C4)**(.5*ETAA3)-ETAA1*ETAA2**ETAA3
     1 +ETAB1*(C6*A**2+C8)**(.5*ETAB3)-ETAB1*ETAB2**ETAB3
     1 -ALPHA*ZORA*ZORB/ZORS
      DA=2.*A
      GO TO (200,210,220),DIMEN
  200 D=2.0
      XN=2.0
      GO TO 230
  210 D=1.904626
      XN=3.14159
      GO TO 230
  220 D=1.80940
      XN=4.188790
  230 D=D*(ZORS/ZORA)**(1./DIMEN)*A
      XN=XN*A**DIMEN*AVOGAD*RHO(IA)/ZA
C     OUTPUT
      IF(J.NE.1) GO TO 260
      GO TO (240,250,250),DIMEN
  240 WRITE(6,993)POLYMR(IA),POLYMR(IB),(DOMTYP(J,DIMEN),J=1,4)
      GO TO 320
  250 WRITE(6,993)POLYMR(IA),POLYMR(IB),(DOMTYP(J,DIMEN),
     1 J=1,4),POLYMR(IA)
      GO TO 320
  260 IF(J.NE.2) GO TO 270
      IOUT=IB
      IIN=IA
      GO TO 280
  270 IOUT=IA
      IIN=IB
  280 GO TO (290,300,300),DIMEN
  290 WRITE(6,992)POLYMR(IOUT),POLYMR(IIN),POLYMR(IOUT),
     1 (DOMTYP(J,DIMEN),J=1,4)
      GO TO 310
  300 WRITE(6,992)POLYMR(IOUT),POLYMR(IIN),POLYMR(IOUT),
     1 (DOMTYP(J,DIMEN),J=1,4),POLYMR(IA)
  310 F=2.*F
      XN=.5*XN
  320 WRITE(6,991)POLYMR(IA),MWA,POLYMR(IA),ZA,POLYMR(IA),DA
      WRITE(6,989)POLYMR(IB),MWB,POLYMR(IB),ZB,D
      WRITE(6,988)T,XI,F
      WRITE(6,987)UNIT1(DIMEN),UNIT2(DIMEN),UNIT3(DIMEN),XN,SIGMA
```

```
    GO TO 20
999  FORMAT(//41H PA,PB,DIMENSION,J,MOL. WT. A,MOL. WT. B,4HTEMP)
998  FORMAT((A2,1X),(A2,1X),I1,I1,F6.2,F5.2,F10.4)
997  FORMAT(19H J MUST = 1, 2 OR 3/)
996  FORMAT(35H0ILLEGAL POLYMER NAME - THE LEGAL
   1 11H NAMES ARE /20(3XA2))
995  FORMAT(19H0ACCURACY DECREASED)
994  FORMAT(12H NO SOLUTION)
993  FORMAT(/12X19H DIBLOCK COPOLYMER ,A2,1H-,A2,
   1 6H WITH 4A3,8HDOMAINS,A2)
992  FORMAT(/12X20H TRIBLOCK COPOLYMER ,A2,1H-,A2,1H-,
   1 A2,6H WITH 4A3,8HDOMAINS ,A2)
991  FORMAT(9H0MOL.WT.-,A2,5H (KG)F9.2,6X2HZ-A2,F10.2,6X
   1 13HDOMAIN DIAM.-,A2,4H (M)1PE11.4)
990  FORMAT(33H DIMENSIONALITY MUST BE 1, 2 OR 3)
989  FORMAT(9H MOL.WT.-A2,5H (KG)F9.2,6X2HZ-A2,F10.2,6X
   1 19HLATTICE SPACING (M)1PE11.4)
988  FORMAT(6H T (K)F19.2,6X2HXIF12.3,6X5HF/NKT1PE25.4)
987  FORMAT(3H N 2A3,A1,1PE15.4,26X13HSIGMA (/M**2)1PE17.4)
    END
```

Appendix 4

Solid State ^{1}H NMR results for lamella block copolymers

Table 1. Results of the solid state ^{1}H NMR experiment for copolymer LL1

	Origin	Results
^{1}H density ratio Sty:But	Literature	0.884
SD coefficient Styrene (m^2/s)	Literature	8.00e-16
SD coefficient Butadiene (m^2/s)	Literature	2.00e-16
Amplitude (a.u.)	Fitted	972
Repeat Length (d/Å)	Fitted	214
Mobile T_1 (s)	Fitted	0.105
Mobile T_2 (ms)	Fitted	680
1/PWRA (s)	Fitted	0.161
Fraction Mobile	Fitted	0.650
Length of rigid (Å)	Derived	81.2
Length of mobile (Å)	Derived	133.2
Rigid T_1 (s)	Derived	-125.0

Table 2. Results of the solid state ^{1}H NMR experiment for copolymer LL3

	Origin	Results
^{1}H density ratio Sty:But	Literature	0.884
SD coefficient Styrene (m^2/s)	Literature	8.00e-16
SD coefficient Butadiene (m^2/s)	Literature	2.00e-16
Amplitude (a.u.)	Fitted	785
Repeat Length (d/Å)	Fitted	451
Mobile T_1 (s)	Fitted	0.112
Mobile T_2 (ms)	Fitted	459
1/PWRA (s)	Fitted	0.178
Fraction Mobile	Fitted	0.812
Length of rigid (Å)	Derived	94
Length of mobile (Å)	Derived	358
Rigid T_1 (s)	Derived	-0.114

Table 3. Results of the solid state ^{1}H NMR experiment for copolymer LL4

	Origin	Results
^{1}H density ratio Sty:But	Literature	0.884
SD coefficient Styrene (m^2/s)	Literature	8.00e-16
SD coefficient Butadiene (m^2/s)	Literature	2.00e-16
Amplitude	Fitted	746
Repeat Length (d/Å)	Fitted	564
Mobile T_1 (s)	Fitted	0.119
Mobile T_2 (ms)	Fitted	818
1/PWRA (s)	Fitted	0.147
Fraction Mobile	Fitted	0.749
Length of rigid (Å)	Derived	155
Length of mobile (Å)	Derived	410
Rigid T_1 (s)	Derived	0.518

Table 4. Results of the solid state ^{1}H NMR experiment for copolymer LL5

	Origin	Results
^{1}H density ratio Sty:But	Literature	0.884
SD coefficient Styrene (m^2/s)	Literature	8.00e-16
SD coefficient Butadiene (m^2/s)	Literature	2.00e-16
Amplitude	Fitted	892
Repeat Length (d/Å)	Fitted	548
Mobile T_1 (s)	Fitted	0.119
Mobile T_2 (ms)	Fitted	785
1/PWRA (s)	Fitted	0.160
Fraction Mobile	Fitted	0.707
Length of rigid (Å)	Derived	175
Length of mobile (Å)	Derived	372
Rigid T_1 (s)	Derived	0.983

Appendix 5

UNIVERSITY OF DURHAM

Board of Studies in Chemistry

COLLOQUIA, LECTURES AND SEMINARS FROM INVITED SPEAKERS

1994

October 5	Prof. N. L. Owen, Brigham Young University, Utah, USA Determining Molecular Structure - the INADEQUATE NMR way
October 19	Prof. N. Bartlett, University of California Some Aspects of Ag(II) and Ag(III) Chemistry
December 7	Prof. D. Briggs, ICI and University of Durham Surface Mass Spectrometry

1995

January 18	Dr G. Rumbles, Imperial College, London Real or Imaginary Third Order Non-linear Optical Materials
February 1	Dr T. Cosgrove, Bristol University Polymers do it at Interfaces
February 8	Dr D. O'Hare, Oxford University Synthesis and Solid-state Properties of Poly-, Oligo- and Multidecker Metallocenes
March 1	Dr M. Rosseinsky, Oxford University Fullerene Intercalation Chemistry
May 4	Prof. A. J. Kresge, University of Toronto *The Ingold Lecture* Reactive Intermediates : Carboxylic-acid Enols and Other Unstable Species
October 11	Prof. P. Lugar, Frei Univ Berlin, FRG Low Temperature Crystallography
October 25	Dr.D.Martin Davies, University of Northumbria Chemical reactions in organised systems
November 17	Prof. David Bergbreiter, Texas A&M, USA Design of Smart Catalysts, Substrates and Surfaces from Simple Polymers

November 22 Prof. I Soutar, Lancaster University
A Water of Glass ? Luminescence Studies of Water-Soluble Polymers

November 29 Prof. Dennis Tuck, University of Windsor, Ontario, Canada
New Indium Coordination Chemistry

1996

January 17 Prof. J. W. Emsley , Southampton University
Liquid Crystals: More than Meets the Eye

January 31 Dr J. Penfold, Rutherford Appleton Laboratory,
Soft Soap and Surfaces

February 7 Dr R.B. Moody, Exeter University
Nitrosations, Nitrations and Oxidations with Nitrous Acid

February 28 Prof. E. W. Randall, Queen Mary & Westfield College
New Perspectives in NMR Imaging

March 12 RSC Endowed Lecture - Prof. V. Balzani, University of Bologna
Supramolecular Photochemistry

October 22 Professor B.J. Tighe, Department of Molecular Sciences and Chemistry, University of Aston
Making Polymers for Biomedical Application - can we meet Nature's Challenge?
Joint lecture with the Institute of Materials

October 23 Professor H. Ringsdorf (Perkin Centenary Lecture), Johannes Gutenberg-Universitat, Mainz, Germany
Function Based on Organisation

November 6 Dr Melinda Duer, Chemistry Department, Cambridge
Solid-state NMR Studies of Organic Solid to Liquid-crystalline Phase Transitions

November 12 Professor R. J. Young, Manchester Materials Centre, UMIST
New Materials - Fact or Fantasy ?
Joint Lecture with Zeneca & RSC

November 20 Professor J. Earnshaw, Deptartment of Physics, Belfast
Surface Light Scattering: Ripples and Relaxation

November 27 Dr Richard Templer, Imperial College, London
Molecular Tubes and Sponges

December 4 Professor K. Muller-Dethlefs, York University
Chemical Applications of Very High Resolution ZEKE Photoelectron Spectroscopy

1997

January 22 — Dr Neil Cooley, BP Chemicals, Sunbury
Synthesis and Properties of Alternating Polyketones

January 29 — Dr Julian Clarke, UMIST
What can we learn about polymers and biopolymers from computer-generated nanosecond movie-clips?

February 12 — Dr Geert-Jan Boons, University of Birmingham
New Developments in Carbohydrate Chemistry

February 26 — Dr Tony Ryan, UMIST
Making Hairpins from Rings and Chains

March 11 — Dr A. D. Taylor, ISIS Facility, Rutherford Appleton Laboratory
Expanding the Frontiers of Neutron Scattering

Conferences attended

1995

January	IRC Polymer Physics Introduction Course, Leeds University
January	IRC Polymer Engineering Introduction Course, Bradford University
September	IRC Industrial Club Seminar, Durham University

1996

April	MACRO Group UK Family Meeting, Manchester University*
September	IRC Industrial Club Seminar, Bradford University*

1997

April	MACRO Group UK Family Meeting, Leeds University**

* indicates poster presentation by the author

** indicates oral presentation by the author

First Year Induction Courses

The course consists of ten one hour lectures on the services available in the chemistry department at Durham University

Examined Lecture Courses: October 1994 – April 1995

Three courses were attended.

1. X-ray Diffraction

Prof. J.A.K. Howard

Chemistry Department

2. FORTRAN Programming

Six two hour workshops

Geology Department

3. The Physics of polymers

Prof. R.W. Richards

Chemistry Department